Hypoxia in Gliomas: A Pathogenic Driver and Therapeutic Opportunity

By

Katherine Louise Eales

A thesis submitted to the University of Birmingham for the degree of DOCTOR OF PHILOSOPHY

UNIVERSITY OF BIRMINGHAM

IMSR
INSTITUTE OF METABOLISM AND SYSTEMS RESEARCH

Institute of Metabolism and Systems Research

College of Medical and Dental Sciences

University of Birmingham

September 2018

Abstract

Gliomas are highly malignant brain tumours characterised by extensive areas of hypoxia which significantly contribute to therapy-resistance and reduced survival. Therapies that address the hypoxic microenvironment are therefore likely to significantly improve patient outcomes. Hypoxic regulation of Yes-associated protein (YAP) and its paralog TAZ – transcriptional co-activators whose increased activity enhance tumour survival – was investigated and observed to increase both YAP/TAZ expression and transactivation activity in glioma. Furthermore, YAP/TAZ were identified to be important for glutamine metabolism – an interesting finding since glutamine is heavily relied upon in hypoxic tumour cells to sustain anabolic growth. Suppressing YAP/TAZ activity could represent a novel means of targeting hypoxic gliomas and thus the effect of YAP inhibitor, verteporfin was investigated. Treatment of primary and immortalised glioma cell lines with verteporfin resulted in cell death but strikingly only under hypoxic conditions (1% O_2). This investigation discovered that cell death occurs through a YAP-independent mechanism, predominately involving binding of free iron and production of reactive oxygen species. This results in disruption of normal cellular processes and death in cells already under oxidative stress – such as those in hypoxia. Overall, this study suggests that repurposing verteporfin represents a novel means of treating highly therapy-resistant, hypoxic cells in glioma.

Acknowledgments

First and foremost I wish to thank my supervisor, Dr Daniel Tennant for his invaluable mentorship, advice, patience and encouragement during this project. His support is very much appreciated and I feel that I have truly developed both scientifically and professionally from the great opportunities and challenges I have encountered during the time spent in his group. I very much look forward to continuing this scientific collaboration as a post-doctoral fellow over the next few years.

I would like to acknowledge collaborators Professor Garth Cruickshank and his neurosurgical team as well as the glioma patients at the Queen Elizabeth Hospital Birmingham for providing primary tissue for this project. Glioma is an incredibly difficult disease and it has been a constant source of motivation during this PhD. I would also like to thank Alpesh Thakkar of the Tennant Lab for the running and analysing of the GC-MS samples as well as Ed Wilkinson and Professor Jim Tucker from the School of Chemistry, for their insight and performing the verteporfin mass spectrometry for this project.

I would also like to personally thank past Tennant Group members, in particular Kate Hollinshead, Debbie Williams, Giulio Laurenti and Robert Murren as well as the current members Cristina Escribano, Haydn Munford, Katarina Kluckova and Alpesh Thakkar for their valued friendship, continued support, patience and endless entertainment during my masters and PhD. I would also like to thank recent addition to the group Becky Westbrook, for helping me accept our fates as Metabolism Detectives. It's a difficult job but I look forward to continuing this partnership over the next few years.

I also wish to thank the IMSR for being such an excellent and welcoming department to work in. A special thanks goes to the IMSR crew, who have provided many a laugh through our lively lunch time discussions, endless games of Coup and the creation of many a dubious film plot. It has truly been a pleasure to get to know and work alongside you all.

Finally I would like to thank Kate Wickers, who from day one at Warwick Uni 10 years ago, has always been there for me; she is a truly inspiring friend and the best I could

ever ask for. Much love and thanks go to my family who have given their endless support and love and I am forever grateful to have such a supportive family who have always believed in me every step of the way. Last but by no means least, a huge thank you to Simon, from the bottom of my heart. You have been there for me throughout, providing many an insightful comment to my research and I cannot put into words how much it means to me to have had your incredible support during this PhD and in life.

I would also like to thank the many others who I have not been able to mention by name and to the University of Birmingham and the Medical Research Council for funding this PhD.

Chapter 1 provides a review of the literature behind this project and includes elements from the published review 'Hypoxia and the metabolic adaptation of cancer cells' (https://www.nature.com/articles/oncsis201550). Data from Chapter 3 and 4 have also been included in the published article 'Verteporfin selectively kills hypoxic glioma cells through iron-binding and increased production of reactive oxygen species' (https://www.nature.com/articles/s41598-018-32727-1). All experiments presented in this paper was conducted by myself with exception of the GBM tissue provided by Prof. G. Cruickshank and the mass spectrometry data (Supplementary Figure S4f), which was conducted by E. Wilkinson.

Table of Contents

CHAPTER 1: REVIEW OF THE LITERATURE 1

1.1. Introduction 2

1.1.1. The burden of cancer 2

1.2. Gliomas 3

1.2.1. Glioma classification 3

1.2.2. Glioma heterogeneity and genetic profiling 5

1.2.3. Glioma treatment strategies 10

1.3. Tumour hypoxia 15

1.3.1. Hypoxia inducible transcription factors 15

1.3.2. HIF and cancer 17

1.3.3. Tumour hypoxia and glioma 18

1.4. The Hippo pathway as a therapeutic target 20

1.4.1. Origins and physiological function 20

1.4.2. Mechanism of YAP and TAZ 21

1.4.3. Regulation of YAP/TAZ activity 25

1.4.4. Dysregulation of YAP/TAZ activity 28

1.4.4.1. Association with cancer 28

1.4.4.2. YAP/TAZ in glioma 30

1.5. Therapeutic targeting of YAP/TAZ signalling 32

1.5.1. Discovery of verteporfin as a YAP inhibitor 32

1.5.2. Clinical use of VP 33

1.5.3. Effect of VP as a YAP inhibitor on cancer growth 34

1.6. Metabolic-rewiring in cancer 36

1.6.1. Introduction to cancer metabolism 36

1.6.2. Glucose metabolism in cancer 38

1.6.3. Glutamine metabolism in cancer 39

1.6.4. Role of YAP/TAZ signalling in cancer metabolism 40

1.6.5. Hypoxia-induced alterations to cancer metabolism 42

1.6.6. Oxidative and endoplasmic reticulum stress in cancer 44

1.7. Thesis aims 48

CHAPTER 2: MATERIALS AND METHODS 49

2.1. Cell culture 50
2.1.1. Immortalised cell lines 50
2.1.2. Cell lines derived from patient tumours 52
2.1.2.1. Patient information 52
2.1.2.2. Primary cell line generation 53
2.1.3. Spheroid culture 54
2.1.3.1. VP treatment of spheroids (Chapter 4) 55

2.2. Chemicals 55

2.3. Sulforhodamine B assay 57
2.3.1. Cell proliferation assay (Chapter 3) 57
2.3.2. Determining VP dosage and treatment time (Chapter 4) 57
2.3.3. Cell viability following treatment with porphyrins (Chapter 4) 58
2.3.4. Cell viability following VP treatment when exposed to light (Chapter 4) 58
2.3.5. Cell viability following VP and DMOG treatment (Chapter 4) 59
2.3.6. Cell viability following treatment with VP and cell death inhibitors (Chapter 4) 59
2.3.7. Cell viability following VP and anti-oxidant treatment (Chapter 4) 59

2.4. Cell proliferation assay (Chapter 4) 60

2.5. Quantitative polymerase chain reaction (qPCR) 60

2.6. Protein analysis of cells under hypoxia (Chapter 3) 61

2.7. Western blotting 61
2.7.1. Protein preparation 61
2.7.2. SDS-PAGE gel electrophoresis, protein transfer and antibody incubation 62
2.7.2.1. Western blot antibodies 62

2.8. Co-immunoprecipitation 64
2.8.1. Preparing cell lysates 64
2.8.2. Co-immunoprecipitation 64

2.9. Immunocytochemistry (ICC) 65
2.9.1. Immunochemistry antibodies 65
2.9.2. Hypoxic YAP expression (Chapter 3) 66
2.9.3. VP timecourse (Chapter 4) 67
2.9.4. p62 (Chapter 4) 67

2.9.5. Z-VAD-FMK (Chapter 4) 67
2.9.6. Calreticulin (CRT)(Chapter 4) 68
2.9.7. Eeyarestatin-1 (Eer1)(Chapter 4) 68
2.9.8. 8-OHdG (Chapter 4) 68
2.9.9. Analysis of nuclear fluorescence 68

2.10. Gene Silencing 69
2.10.1. Knockdown of YAP and TAZ 69
2.10.2. Knockdown of YAP and TAZ for metabolic analysis (Chapter 3) 70
2.10.3. VP treatment following YAP/TAZ knockdown (Chapter 4) 70
2.10.4. Knockdown of HIF-1α (Chapter 4) 71

2.11. Protein over-expression 71

2.12. Metabolic tracing analysis 71
2.12.1. Addition of tracer 72
2.12.2. Metabolite extraction 73
2.12.3. GC-MS (in collaboration with Dr. A. Thakkar, UoB) 73
2.12.3.1. Sample derivatisation 73
2.12.3.2. GC-MS analysis 74

2.13. Flow Cytometry 75
2.13.1. Cell treatment 75
2.13.2. Annexin V/ Propidium Iodide viability assay 75

2.14. DCFDA assay 77

2.15. Binding Assays 78
2.15.1. VP absorption spectra 78
2.15.2. Metal cation binding 78
2.15.3. Mass Spectrometry (in collaboration with Prof. J.H.R. Tucker, UoB) 79

2.16. Statistical analysis 79

CHAPTER 3: INVESTIGATING THE HYPOXIC REGULATION OF YAP/TAZ AND THEIR RELATIONSHIP WITH GLIOMA METABOLISM 80

3.1. Introduction 81

3.2. Results 83
3.2.1. Glioma cell lines exhibit differential sensitivity to hypoxia 83

3.2.2. YAP1 and YAP1-target gene transcription is increased under hypoxic conditions 84
3.2.3. YAP1 protein expression is increased under hypoxic conditions 89
3.2.4. Increased YAP1 nuclear localisation suggests hypoxia amplifies YAP1 activity in glioma cells 95
3.2.5. Knockdown of YAP/TAZ reduces glioma cell proliferation 97
3.2.6. Investigating the importance of YAP/TAZ in cancer cell metabolism 99
3.2.6.1. YAP/TAZ support *de novo* serine synthesis 99
3.2.6.2. Knockdown of YAP/TAZ alters pyruvate metabolism 103
3.2.6.3. Knockdown of YAP/TAZ compromises oxidative glutamine metabolism 112
3.2.6.4. YAP/TAZ support glutamine-derived proline biosynthesis 119
3.2.6.5. Total carbon contribution from glutamine into TCA metabolites is significantly attenuated upon YAP/TAZ knockdown 121

3.3. Discussion 124
3.3.1. Glioma lines, U87 and U343, exhibit differential growth sensitivity to pathophysiological hypoxic conditions 124
3.3.2. Hypoxia upregulates YAP/TAZ expression and transcriptional co-activator activity in glioma cell lines 125
3.3.3. Glioma cell proliferation is significantly reduced upon YAP/TAZ knockdown 130
3.3.4. YAP/TAZ knockdown induces significant alterations in glucose and glutamine metabolism 131
3.3.4.1. YAP/TAZ act to support normoxic *de novo* serine synthesis in glioma 133
3.3.4.2. Pyruvate metabolism is altered in YAP/TAZ deficient cells 135
3.3.4.3. YAP/TAZ support oxidative glutamine metabolism 138

3.4. Summary 143

CHAPTER 4: ASSESSING THE POTENTIAL OF REPURPOSING VERTEPORFIN AS A NOVEL TREATMENT FOR GLIOMA 145

4.1. Introduction 146

4.2. Results 148
4.2.1. VP reduces proliferation of glioma cells 148
4.2.2. VP induces cell death under hypoxic conditions 151
4.2.3. VP reduces spheroid volume and causes destabilisation over time 157
4.2.4. VP rapidly induces changes in cell morphology 160
4.2.5. Exposure to ambient light during VP treatment increases sensitivity 164
4.2.6. Global expression of tumour suppressor and YAP binding partner, p73 is increased following VP exposure 166

4.2.7. VP-induced hypoxic cell death is YAP-independent 169
4.2.8. Stabilisation of HIF-1α only partially sensitises glioma cells to VP in normoxia 173
4.2.9. VP-mediated hypoxic cell death is partially preventable by pharmacological inhibitors of cell death 176
4.2.10. Cellular vacuolisation is a prominent characteristic of VP-induced cell death 183
4.2.11. Increased ROS production and DNA oxidation suggests VP significantly increases cellular oxidative stress 188
4.2.12. VP avidly binds ferric iron 192

4.3. Discussion 200
4.3.1. VP suppresses glioma cell proliferation 200
4.3.2. VP induces cell death under hypoxic conditions 201
4.3.3. VP induces rapid changes in cell morphology and is sensitive to ambient light 205
4.3.4. Expression of YAP-binding partner p73 is increased upon VP exposure but does not lead to increased YAP-p73 interaction 207
4.3.5. VP-induced hypoxic cell death is YAP-independent 208
4.3.6. VP-mediated hypoxic cell death is HIF-1α independent 210
4.3.7. Traditional cell death inhibitors only partially prevent VP-mediated hypoxic cell death 212
4.3.8. Hypoxia exacerbates VP-induced cellular vacuolisation and ER stress 214
4.3.9. VP induces significant cellular stress through increased production of ROS 216
4.3.10. VP can bind intracellular iron for use in potential Fenton-like chemistry to exacerbate ROS production 218

4.4. Summary 222

CHAPTER 5: CONCLUDING REMARKS 223

5.1. Significance and aims of investigation 224

5.2. Hypoxia influences YAP/TAZ signalling in glioma 225

5.3. YAP/TAZ support glucose and glutamine metabolism in glioma 227

5.4. VP induces hypoxia specific cell death showing potential as a novel therapeutic for glioma 229

LIST OF REFERENCES 234

APPENDICES……..255

List of Illustrations

Figure 1.1 Simplified schematic depicting the classification of gliomas and the common mutations associated with each category. 5

Figure 1.2 Genetic mutations defining primary GBM subtypes. 7

Figure 1.3 Cellular functions of IDH enzymes. 9

Figure 1.4 HIF-1α regulation by hydroxylation. 17

Figure 1.5 Overview of Hippo pathway regulation and regulation of transcription by YAP/TAZ transcriptional co-activators. 24

Figure 1.6 Chemical structure and absorption spectra of VP. 34

Figure 1.7 Cancer cells alter their metabolism to support anabolic growth. 37

Figure 1.8 Hypoxia-induced changes in cancer metabolism. 44

Figure 1.9 Interplay between oxidative stress and ER stress. 47

Figure 2.1 Expression of EGFR and IDH1 R132H in glioma cell lines. 51

Figure 2.2 MRI scans from GBM patient showing progression of therapy-resistant foci A but not of therapy-responsive foci B. 53

Figure 2.3 Examples of single and double stain controls for flow cytometry. 76

Figure 2.4 Simplified schematic depicting distinct cell populations generated through intensity of Annexin V and PI staining. 76

Figure 3.1 Glioma cells exhibit differential sensitivity to hypoxia. 83

Figure 3.2 Hypoxia increases YAP1 and YAP1-target gene expression in U87 and U343 cell lines. 85

Figure 3.3 Mutation in IDH1 does not influence hypoxia-induced YAP1 and YAP1-proliferative gene expression. 86

Figure 3.4 Hypoxia induces expression of HIF-1 target genes in U87 and U343 cell lines. 87

Figure 3.5 Hypoxia induces expression of HIF-1 target genes in HOG IDH1 WT and MUT cell lines. 88

Figure 3.6 YAP1 protein expression is increased under hypoxic conditions. 90

Figure 3.7 Hypoxia induces YAP1 protein expression in the HOG cells. 91

Figure 3.8 Hypoxia increases YAP/TAZ expression and transcriptional co-activator activity in established and primary GBM cell lines. 94

Figure 3.9 YAP1 nuclear localisation is increased under hypoxic conditions. 96

Figure 3.10 Knockdown of YAP1 and TAZ significantly reduces glioma cell growth. 98

Figure 3.11 YAP/TAZ support *de novo* serine synthesis under normoxic conditions. . 101/102

Figure 3.12 U343 cells exhibit altered serine-glycine metabolism..... 103

Figure 3.13 Knockdown of YAP and TAZ increases glycolysis in U343 cells. 105

Figure 3.14 Knockdown of YAP and TAZ alters pyruvate metabolism in U343 cells. 107

Figure 3.15 U343 cells showed reduced ^{13}C incorporation into alanine with knockdown of YAP/TAZ. 108/109

Figure 3.16 Knockdown of YAP/TAZ results in increased anaplerotic pyruvate metabolism. 110

Figure 3.17 PC activity is increased following YAP/TAZ knockdown and is sustained under hypoxia. 112

Figure 3.18 YAP/TAZ supports glutamine metabolism in glioma cells. 114/115

Figure 3.19 Knockdown of YAP/TAZ significantly increases reductive glutamine metabolism in hypoxia. 117

Figure 3.20 Knockdown of YAP/TAZ compromises oxidative glutamine metabolism. 119

Figure 3.21 YAP/TAZ supports glutamine-derived proline synthesis. 120

Figure 3.22 Knockdown of YAP/TAZ significantly alters glutamine contribution into TCA metabolites. 122/123

Figure 4.1 VP reduces cell proliferation of glioma cell lines. 149

Figure 4.2 Determining VP dosage and treatment time. 150

Figure 4.3 VP causes significant cell death under hypoxic conditions. 152

Figure 4.4 Porphyrin family members do not exhibit the same hypoxic cell-killing effect as VP. 154

Figure 4.5 VP significantly reduces cell viability in IDH1 and IDH2 WT and MUT cells. 156/157

Figure 4.6 VP reduces proliferation and formation of glioma spheroids. 158

Figure 4.7 Destabilisation of glioma spheroids occurs following long-term VP treatment... 159

Figure 4.8 VP induces morphological changes in glioma cells. 161/162

Figure 4.9 YAP1 expression is increased in hypoxia and reduced upon VP treatment. 163

Figure 4.10 YAP1 protein expression is unchanged upon VP treatment..... 164

Figure 4.11 VP sensitises cells to death if exposed to ambient light during treatment. 166

Figure 4.12 Expression of p73 is significantly increased following VP treatment. 168

Figure 4.13 YAP1 does not bind partner p73 upon VP treatment in hypoxia, despite increased expression..... 169

Figure 4.14 Hypoxic VP-induced cell death is YAP-independent..... 170

Figure 4.15 VP reduces p62 expression..... 172

Figure 4.16 Normoxic glioma cells are sensitised to VP upon stabilisation of HIF-1α. 174

Figure 4.17 VP-induced hypoxic cell death despite knockdown of HIF-1α..... 175

Figure 4.18 VP-induced cell death cannot be inhibited by Z-VAD-FMK in U87 cells..... 177

Figure 4.19 VP-induced cell death cannot be inhibited by Z-VAD-FMK in U343 cells..... 178

Figure 4.20 Z-VAD-FMK can partially rescue VP-induced death in U87 cells over 24 hours. 179

Figure 4.21 VP-induced changes in glioma cell morphology could not be prevented upon addition of Z-VAD-FMK. 180/181

Figure 4.22 Hypoxic VP-induced cell death of glioma cells could not be prevented by alternative inhibitors of cell death..... 182

Figure 4.23 Inhibiting p53-mediated cell death and autophagy did not prevent VP-induced cell death in hypoxia. 183

Figure 4.24 VP induces cytoplasmic vacuolisation. 184

Figure 4.25 ER stress is significantly increased upon VP treatment and is enhanced in hypoxia. 185

Figure 4.26 ERAD inhibitor Eer1 causes partial rescue of cell viability following VP treatment in hypoxia. 187

Figure 4.27 VP causes a significant increase in DNA oxidation. 189

Figure 4.28 VP increases ROS which can be prevented upon treatment with TEMPOL. 191

Figure 4.29 VP- induced cell death in hypoxia can be significantly reduced upon co-treatment with TEMPOL. 192

Figure 4.30 VP absorption spectra profile. 193

Figure 4.31 VP rapidly binds ferric chloride. 194

Figure 4.32 VP does not bind ferrous chloride as rapidly as ferric chloride. 196

Figure 4.33 VP does not immediately bind metal chlorides, magnesium and zinc. 197

Figure 4.34 VP can bind ferrous and zinc chloride but only over time. 199

Figure 4.35 Chemical additions to VP. 204

List of Tables

Table 2.1 Glioma cell line characteristics. 50

Table 2.2 Details of reagents used in this investigation. 56

Table 2.3 Primary antibodies used for western blotting. 63

Table 2.4 Secondary antibodies used for western blotting. 63

Table 2.5 Details of primary antibodies used for ICC. 66

Table 2.6 Secondary antibody and additional stains used for ICC. 66

List of Abbreviations

2-HG	2-hydroxyglutarate
3-PG	3-phosphoglycerate
3-PHP	3-phosphohydroxypyruvate
3-PS	3-phosphoserine
5-ALA	5-aminolevulinic acid
8-OHdG	8-hydroxydeoxyguanosine
α-KG	α-ketoglutarate
ACLY	ATP citrate lyase
ACO	Aconitase
ADP	Adenine diphosphate
ALT	Alanine transaminase
AMD	Age-related macular degeneration
AMPK	AMP-activated protein kinase
AREG	Amphiregulin
ARNT	Aryl hydrocarbon receptor nuclear translocator
ARTX	ATP-Dependent Helicase ATRX
ATP	Adenosine triphosphate
BBB	Blood-brain barrier
BBC3	BCL2 binding component 3
BCA	Bicinchoninic assay
BMP	Bone morphogenic protein
BNIP3	BCL2 interacting protein 3
BSA	Bovine serum albumin
C-TAD	C-terminal transactivation domain
ccRCC	Clear cell renal cell carcinoma
CDKN2A	Cyclin dependent kinase inhibitor 2A)
CIC	Capicua transcriptional repressor)
CNS	Central nervous system
CoA	Coenzyme A
CQ	Chloroquine
CRT	Calreticulin
CsA	Cyclosporin A
CSCs	Cancer stem cells
CTGF	Connective tissue growth factor
CTNF	Corrected total nuclear fluorescence
CyP-D	Cyclophillin D
CYR61	Cysteine-rich angiogenic inducer 61
DCFDA	2',7'-Dichlorofluorescin Diacetate

DFS	Disease-free survival
DMEM	Dulbecco's Modified Eagle Medium
DMOG	Dimethyloxalylglycine
DMSO	Dimethyl Sulfoxide
dNTP	Deoxyribonucleotide triphosphate
ECM	Extracellular matrix
Eer1	Eeyarestatin-1
EGFR	Epidermal growth factor receptor
EMT	Epithelial-mesenchymal transition
ER	Endoplasmic reticulum
ERAD	ER-associated protein degradation pathway
ETC	Electron transport chain
F-actin	Filamentous actin
FA	Fatty acid
FBS	Foetal Bovine Serum
FDA	Food and Drug Administration
FDG-PET	^{18}F-deoxyglucose-positron emission tomography
FH	Fumarate hydratase
FIH	Factor inhibiting HIF-1
FUBP1	Far upstream element-binding protein 1
G6P	Glucose 6-phosphate
GABRA1	Gamma-aminobutyric acid receptor 1
GAPDH	Glyceraldehyde 3-phosphate dehydrogenase
GBM	Glioblastoma
GC-MS	Gas chromatography-mass spectrometry
GFAP	Glial fibrillary acidic protein
GLDH	Glutamate dehydrogenase
GLS	Glutaminase
GLUL	Glutamine synthetase
GOT1	Glutamate-oxaloacetate transaminase
GPCR	G-coupled protein receptor
GSH	Glutathione
GSSG	Oxidised glutathione
HBRC	Human Biomaterials Resource Centre
HCC	Hepatocellular carcinoma
HGG	High-grade glioma
Hh	Hedgehog
HIF	Hypoxia-inducible factor
HOG	Human OligodendroGlioma
HP	Hematoporphyrin

HRE	Hypoxia response element
HRP	Horseradish peroxidase
ICC	Immunocytochemistry
IDH1/2	Isocitrate dehydrogenase 1/2
IP	Immunoprecipitation
KPS	Karnofsky performance status
LATS1/2	Large tumour suppressor kinase 1/2
LDH	Lactate dehydrogenase
LDL	Low-density lipoprotein receptors
LGG	Low-grade gliomas
MCT	Monocarboxylate lactate transporter
MET	Met proto-oncogene
MGMT	O^6-methylguanine DNA methyltransferase
MID	Metabolite isotopomer distribution
MM	Multiple myeloma
MOB1A/1B	MOB kinase activator 1A/1B
MPC	Mitochondrial pyruvate carrier
mPTP	Mitochondrial permeability transition pore
MRI	Magnetic resonance imaging
mRNA	Messenger RNA
MST1/2	Mammalian Ste2-like kinases
MTBSTFA	N-tertbutyldimethylsilyl-N-methyltrifluoroacetamide
MUT	Mutant
MYC	v-myc avian myelocytomatosis viral oncogene homology
NAD^+	Oxidised nicotinamide dinucleotide
NADH	Reduced nicotinamide dinucleotide
NADPH	Reduced nicotinamide adenine dinucleotide phosphate
Nanog	Nanog homeobox
NEAA	Non-essential amino acid
Nec-1	Necrostatin-1
NEFL	Neurofilament light polypeptide
NF1	Neurofibromin 1
NGS	Next-generation sequencing
NICE	National Institute of Health and Care Excellence
NSCLC	Non-small cell lung cancer
OAA	Oxaloacetate
OCT4	Octamer-binding transcription factor 4
ODDD	Oxygen-dependent degradation domain
OS	Overall survival
p-YAP	Phosphorylated YAP

P5CS	Delta-1-pyrroline-5-carboxylate synthetase
p73	Tumour protein 73
PARP	Poly (ADP-ribose) polymerase
PBS	Phosphate buffered saline
PBS-T	Phosphate buffered saline-Tween
PC	Pyruvate carboxylase
PDGFRA	Platelet derived growth factor receptor alpha
PDH	Pyruvate dehydrogenase
PDK1	Pyruvate dehydrogenase kinase1
PDT	Photodynamic therapy
PEP	Phosphoenolpyruvate
PFA	Paraformaldehyde
PFK1	Phosphofructokinase 1
PFT-α	Pifithrin-α
PHD	Prolyl hydroxylase
PHGDH	Phosphoglycerate dehydrogenase
PI	Propidium iodide
PKM2	Pyruvate kinase M2
pO_2	Partial oxygen pressure
PPIX	Protoporphyrin IX
PPP	Pentose phosphate pathway
PS	Phosphatidylserine
PSAT1	Phosphoserine aminotransferase
PSPH	Phosphoserine phosphatase
PTEN	Phosphatase and tensin homolog
pVHL	Von Hippau-Lindau protein
PYCR1/2	Pyrroline-5-carboxylate reductase 1/2
QEHB	Queen Elizabeth Hospital Birmingham
qPCR	Quantitative polymerase chain reaction
R5P	Ribose 5-phosphate
RASSF1A	Ras association domain-containing protein 1A
RB1	Retinoblastoma 1
RIPK	Death domain receptor interacting protein kinase
ROS	Reactive oxygen species
RT	Room temperature
RUNX1/2	Runt-related transcription factor 1/2
S.D	Standard deviation
S.E.M	Standard error of the mean
SAV1	Salvador homolog 1
SDH	Succinate dehydrogenase

SDS-PAGE	Sodium dodecyl sulphate polyacrylamide gel electrophoresis
SHMT1/2	Serine hydroxymethyltransferase 1/2
SIAH2	Seven in absentia homolog 2
siRNA	Small-interfering RNA
Smad1	Mothers against decapentaplegic homolog 1
SOD	Superoxide dismutase
Sox2/9	Sex determining region Y box 2/9
SQSTM1	Sequestosome 1
SRB	Sulforhodamine B
SSP	Serine synthesis pathway
TAZ	Transcriptional co-activator with PDZ-binding motif
TBDMSCl	Tertbutyldimethyl-chlorosilane
TCA	Tricarboxylic acid cycle
TCGA	The Cancer Genome Atlas
TEAD	TEA domain
TEMPOL/TPL	4-Hydroxy-TEMPO
THF	Tetrahydrofolate
TMZ	Temozolomide
TP53	Tumour protein p53
TTF	Tumour treating fields
UoB	University of Birmingham
UPR	Unfolded protein response
VEGF	Vascular endothelial growth factor
VP	Verteporfin
WHO	World Health Organisation
Wnt	Wingless
WT	Wild-type
Wwox	WW-domain-containing oxidoreductase
YAP	Yes-associated protein
Z-VAD-FMK	Carbobenzoxy-valyl-alanyl-aspartyl-O-methyl- fluoromethylketone
ZnPP	Zinc protoporphyrin

Chapter 1:

Review of the literature

1.1. Introduction

1.1.1. The burden of cancer

Cancer is a highly complex disease characterised by the malignant transformation of cells. Currently, over 200 different types of cancer have been identified, each with its own aetiology, cellular identity and therapeutic regimes which renders designing successful cancer treatments a significant challenge for scientists and clinicians[1]. Cancer is one of the leading causes of mortality in the UK, equating to around 28% of all deaths in 2016[2]. Brain and central nervous system (CNS) tumours comprise around 3% of all newly diagnosed cancers in the UK, although despite this relatively low incidence, are one of the most deadly with a five-year survival rate of just 19%[3]. The most common type of brain and CNS tumour in adults is glioma, a class of diffuse tumours derived from glial cells that account for around 34% of all brain neoplasms[3]. Gliomas are locally invasive tumours, which makes effective treatment extremely difficult given that one of the most significant determinants of overall survival is extent of surgical resection[4,5]. It is therefore not surprising that gliomas are incurable, with patients suffering from high-grade gliomas (HGG; grade IV) having an extremely poor prognosis – average overall survival without treatment being less than one year post-diagnosis which is extended to approximately 15-18 months upon addition of multimodal treatment[6,7]. Despite the wealth of glioma research conducted over the years, there has been little progress in providing effective treatment options and thus more research is desperately warranted in order to uncover novel and effective therapeutics which are so urgently needed.

1.2. Gliomas

1.2.1. Glioma classification

Gliomas are initially histologically and immunocytochemically categorised as either being an astrocytoma or oligodendroglioma, which are subsequently classified according to the morphology of the suspected glial cell of origin[8]. Gliomas are then graded using a set of parameters outlined by the World Health Organisation (WHO)[9]. The tumour specimen is analysed for histological features such as the number of mitoses present, microvascular proliferation, nuclear atypia and the presence of necrosis[10]. Like all tumour grading systems, this means of stratifying patients is based on a subjective assessment of the tumour, which then affects the clinical management of the patient[9]. To improve diagnostic objectivity, the WHO classification of tumours of the CNS was recently revised to include some of the signature genetic markers which should now be combined with histological analysis to provide a more accurate diagnosis[11].

Low-grade gliomas (LGG) are classified as grade I or II and considered to be less aggressive due to their slower-growth rate. Grade I tumours exhibit a low proliferation potential and thought by many to be biologically benign[8,9]. Gliomas of a grade II nature, despite exhibiting low proliferative potential, are well-differentiated tumours with a diffusely infiltrative phenotype concomitant with cytological atypia[10,12]. Despite often occupying significant space within the cranium, they exhibit little to no contrast-enhancement on magnetic resonance imaging (MRI) scans, indicating these tumours have an intact blood-brain barrier (BBB) and a lack of tumour necrosis[13]. Variations in survival outcome has been noted between the two types of grade II glioma, with oligodendrogliomas demonstrating the best prognosis, compared with diffuse astrocytomas, which have the worst prognosis[14]. Patients who present with LGG are

generally younger in age (median age of 41 years) and survive for an average of seven years post-diagnosis, however unfortunately almost all grade II tumours eventually progress to a higher malignancy grade[9,12,15].

Once tumours have progressed to grade III or IV, they are considered HGG. Grade III lesions typically show anaplasia, nuclear atypia, increased mitotic activity and a more invasive and proliferative phenotype compared to grade II tumours[9]. Reduced overall survival is also observed in patients diagnosed with grade III tumours, with survival on average between two and three years[9]. Grade III neoplasms show continuous growth and can rapidly progress to the most malignant grade, IV. Compared with lower grades, grade IV tumours are cytologically malignant with high mitotic activity, microvascular proliferation and a highly-accelerated growth rate[9,13]. In addition, grade IV tumours are also seen to exhibit a large degree of necrosis[9]. Histologically, these tumours are highly invasive and widely disseminate into the surrounding brain tissue meaning that despite gross total resections regularly being achieved, the tumour can never entirely be removed and thus have a fatal outcome[9]. Grade IV astrocytomas are known as glioblastoma (GBM) and account for 82% of malignant gliomas with median survival of less than one year post-diagnosis[16]. When a patient presents clinically with a GBM, it is seen to have one of two aetiologies; either as primary GBM which arise *de novo*, without any clinical or histological evidence of tumour progression from a preceding lower grade, or as secondary GBM, which show evidence of tumour progression from a less malignant lesion[12,17,18] (Figure 1.1). Around 90% of malignant gliomas are primary GBMs and often occur within older patients, with the average age of diagnosis being 62 years[17]. These tumours often have a short clinical history as they are often presented late to the clinic.

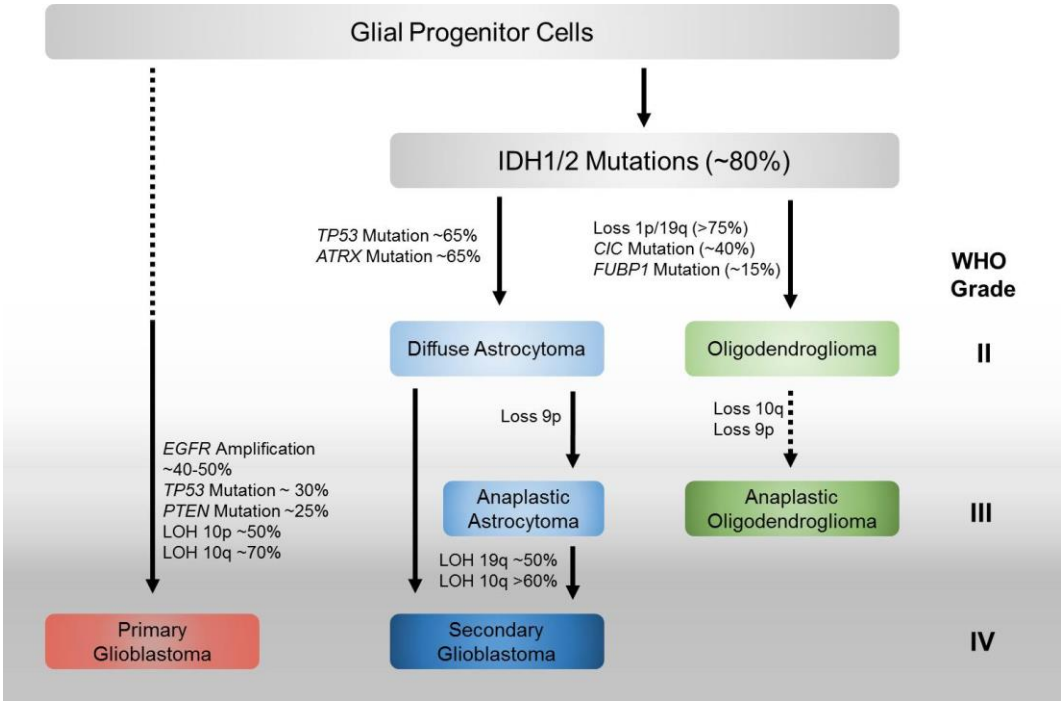

Figure 1.1 Simplified schematic depicting the classification of gliomas and the common mutations associated with each category. Image based upon Oghaki and Kleihues[17].

1.2.2. Glioma heterogeneity and genetic profiling

Over the past decade, genetic profiling of glial tumours has been used to attempt to better understand the underlying biology and heterogeneous behaviour of these tumours. Tumour heterogeneity is particularly important to consider in cancer treatment as tumours are not solely comprised of homotypic cells but rather a collective of diverse cell phenotypes that differ in their genetic landscape and/or microenvironment, ultimately leading to differential treatment sensitivity, invasiveness and survival outcome[19]. Cells obtained from different regions within the same tumour have been shown to exhibit diverse genetic profiles and even confer a different malignancy grade[20].

Advancements in next-generation sequencing (NGS) technologies have led to the identification of key mutations associated with the different histological subtypes. Many

genetic hallmarks have been identified within LGG and are distinguishable between morphological classes. Co-deletion of chromosomal arms 1p and 19q are associated with tumours of an oligodendroglial origin and are commonly observed in around 80% of grade II oligodendrogliomas[14,21]. Co-deletion of 1p/19q has been shown, independent of tumour grade, to be a significant predictor of increased survival in oligodendrogliomas, although the nature of the molecular driver of this phenotype is unclear[14].

Other mutations which have been uncovered in genomic characterisation of LGGs include mutations in *IDH1/2* (isocitrate dehydrogenase 1/2), *CIC* (capicua transcriptional repressor), *FUBP1* (far upstream element-binding protein 1) and *ARTX* (ATP-Dependent Helicase ATRX)[22]. HGG, predominately GBM, however have been shown to exhibit many additional mutations which are not apparent in LGGs. In 2010, The Cancer Genome Atlas (TCGA) research network outlined four genetic subtypes based on gene expression signature, according to the Verhaak classification system, which allowed for subsequent identification of different histological subtypes of GBM; proneural, classical, mesenchymal and neural[7,23,24] (Figure 1.2). The proneural subclass of GBM tumours is typically characterised by alterations in *PDGFRA* (platelet derived growth factor receptor alpha) and point mutations in *IDH1*, although the latter is highly observed in secondary GBM but rarely in primary GBM suggesting that these tumours may be the product of a different mechanism of pathogenesis[25-27]. Mutations in *TP53* (tumour protein p53; p53) are also a frequent occurrence in this class[24]. The classical subclass is predominantly defined by amplification or mutation (EGFRvIII truncation) of the epidermal growth factor receptor (EGFR) gene, which is apparent in approximately 40-50% of primary GBMs and a small fraction of secondary GBMs[18,28]. *TP53* mutations are rare in this class however homozygous deletion of *CDKN2A* (cyclin dependent kinase inhibitor 2A) is significantly

associated with the classical subtype[24]. Homozygous mutations or deletions in the neurofibromin 1 (*NF1*) gene typically defines the mesenchymal subclass of GBM, alongside other mesenchymal markers which classically correspond to a higher degree of necrosis and inflammation, which is generally observed within this class of tumours[24]. Alterations in *PTEN* (phosphatase and tensin homolog), *MET* (met proto-oncogene), and *RB1* (retinoblastoma 1) also occur more commonly in the mesenchymal subtype[24]. Finally, the neural subclass is generally classified by the expression of neuronal markers such as neurofilament light polypeptide (*NEFL*) and gamma-aminobutyric acid receptor 1 (*GABRA1*) and is most similar to normal neuronal tissue[24].

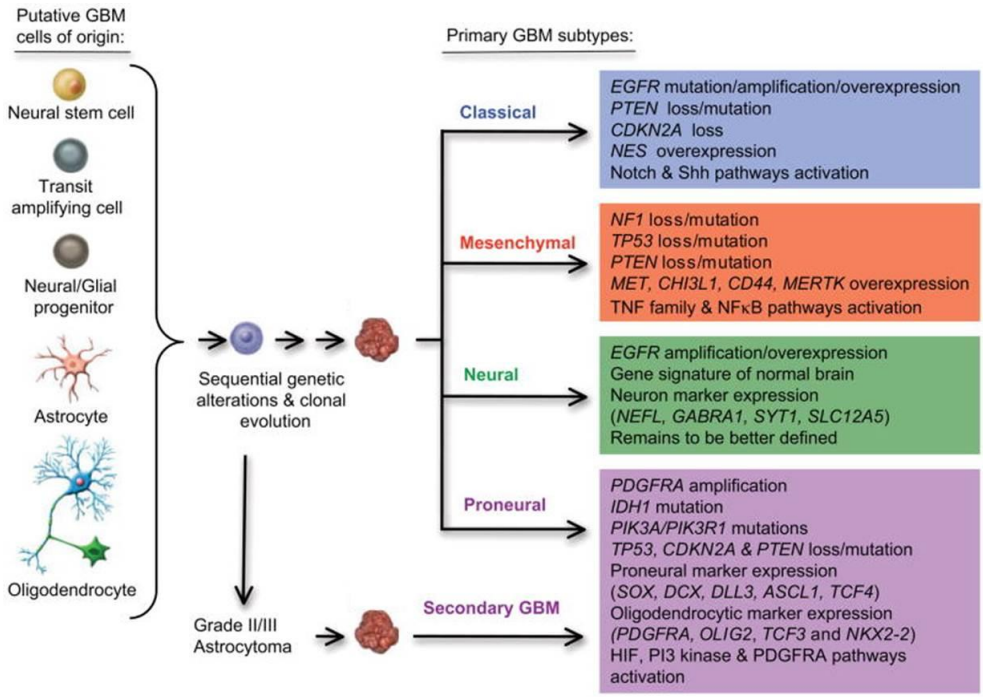

Figure 1.2 Genetic mutations defining primary GBM subtypes. Schematic showing four subtypes of GBM as defined by the Verhaak classification system and the corresponding gene amplifications, deletions, mutations and expression that characterise these subtypes. Secondary GBM are believed to arise from a pre-existing lesion of a lower malignancy grade and are generally characterised as proneural GBM. Image adapted from Van Meir *et* al[29].

The development of the Verhaak classification system of GBMs has allowed for objective molecular classification and therefore helped to overcome the limitations of morphological diagnosis. However, as previously mentioned, tumours are known to exhibit high intratumour heterogeneity, with cells from different areas in the tumour portraying diverse genetic profiles[30]. Interestingly, a study that collected multiple biopsies from spatially different areas within the same tumour showed that in 6 out of 10 tumours analysed, biopsies were classified into at least two different Verhaak subgroups[31]. Typically, molecular analysis is based upon a single tissue biopsy of the patient's tumour and is therefore likely to significantly underestimate the full genetic landscape of the tumour and potentially provide a misleading diagnosis[20,31]. Furthermore, different GBM subtypes have shown to respond differently to chemotherapy which may result in some areas of the tumour responding to treatment but other areas of the tumour being resistant and therefore perpetuating tumour growth[24]. As such, GBM treatment is yet to be stratified based upon Verhaak classification.

Despite the vast array of genetic markers identified, the only one of significant prognostic interest is the *IDH1* gene as heterozygous mutations have been strongly associated with increased patient survival from an average of 11.3 months to 27.1 months after combined surgery and radiotherapy, independent of the 1p/19q co-deletion[25,32]. A large-scale genomic study conducted by Parsons *et al.,* showed that IDH1 mutations were evolutionarily conserved at a key residue in the substrate-binding site at residue 132, where arginine (R) is converted to histidine (H; R132H), and was observed in around 80-90% of low-grade and secondary GBMs that possessed mutant-IDH1[33]. LGG that did not possess an IDH1 mutation were occasionally observed to possess a mutation in the

analogous residue, R172, of mitochondrial IDH2; although these mutations were only seen in around 3% of diffuse gliomas[34].

Physiologically, IDH1/2 isozymes are involved in a number of metabolic processes associated with lipid synthesis and the tricarboxylic acid (TCA) cycle, where IDH1 catalyses the oxidative decarboxylation of isocitrate to α-ketoglutarate (α-KG)[35]. Mutant IDH1 however loses the ability to catalyse this conversion but instead acquires a gain-of-function, converting α-KG to the (R)-enantiomer of 2-hydroxyglutarate (2-HG), which has since been described as an 'oncometabolite'[36] (Figure 1.3). This oncometabolite may influence gliomagenesis since excessive 2-HG production has been shown to increase risk of brain tumour formation in individuals who have mutations in 2-HG metabolism[21,37].

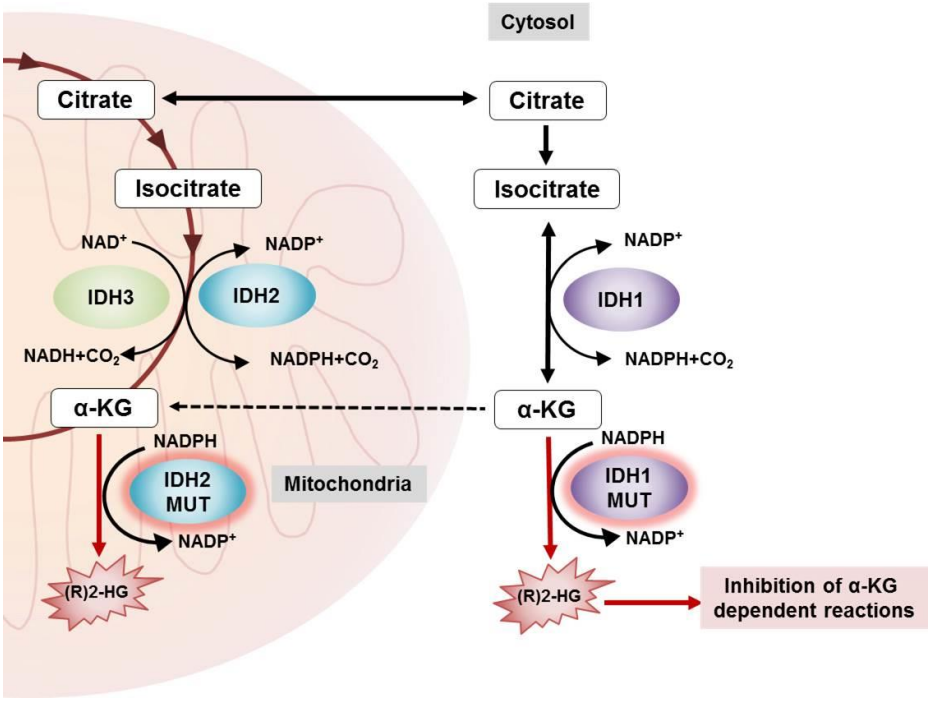

Figure 1.3 Cellular functions of IDH enzymes. In the cytosol, IDH1 catalyses the oxidative decarboxylation of isocitrate to α-KG, which is used within the TCA cycle. IDH1 (R132H) and IDH2 (R172K) mutant enzymes however gain neomorphic enzymatic activity, producing 2-HG from α-KG. Increased 2-HG production inhibits α-KG dependent reactions and has been linked to tumorigenesis. Image based upon Mondesir *et al*[38].

1.2.3. Glioma treatment strategies

Management of glioma are particularly problematic due to the tumour's extensive infiltration into surrounding healthy parenchyma meaning that complete surgical resection is not possible without significant damage to healthy brain tissue[39]. Dandy and Gardener, pioneers of neurosurgery in the early twentieth century, noted that even complete hemispherectomies of glioma patients were not sufficient for patients to be cured[40]. This concept has more recently been supported by research conducted using patient-derived xenograft models, demonstrating that primary GBM cells are capable of invading significantly into the contralateral hemisphere[41].

Tumour resection is however still the first line of treatment for gliomas wherever possible. Previously, there has been a lack of consensus as to the optimum treatment strategy, with some surgeons adopting a 'watch and wait' policy for the management of LGG. However, it has since been strongly argued due to the high percentage of LGGs that rapidly progress in malignancy, that these tumours should not be managed as a 'GBM in waiting'[22,42]. Therefore, in order to standardise glioma treatment across the UK, the National Institute of Health and Care Excellence (NICE) have recently published a set of guidelines (NICE guideline NG99) for healthcare professionals now advocating complete tumour resection (wherever possible) as part of initial management, with the assistance of the imaging agent, 5-aminolevulinic acid (5-ALA), to maximise total resection in HGG[43]. 5-ALA is an endogenous porphyrin based molecule which is metabolised within the cell to form haem[44]. As 5-ALA is metabolised, the photoactive precursor molecule protoporphyrin IX (PPIX) is produced and when light activated, is capable of exhibiting fluorescence in the red end of the visible spectrum[44]. Previous studies have indicated that tumours exhibit a selective uptake and accumulation of PPIX in the range of 50:1 for

malignant brain tissue compared with normal tissue[45]. As such, surgeons have exploited this biological pathway by orally administering exogenous 5-ALA to patients, which is then subsequently converted to PPIX and photo-activated during surgery, thereby allowing the surgeon to more accurately visually identify the brain-tumour interface as well as improving the extent of resection[44]. Consequently, trials have shown that fluorescence-guided surgery with 5-ALA significantly improved 6-month progression-free survival of glioma patients to 41% versus 21% when surgery was performed under white-light alone[45,46].

In addition to surgical intervention, radiotherapy remains the cornerstone of treatment for glioma, aiming to improve local control of the tumour as well as helping to preserve brain function and increase overall survival through destruction of residual tumour cells following tumour resection[47,48]. Historically, clinical trials have demonstrated a significant benefit of post-operative radiotherapy over supportive care, extending GBM patient survival by 3-6 months, as well as significantly improving quality of life[49-51]. This small, but significant increase in patient survival is further improved upon the addition of concurrent and adjuvant chemotherapy, extending median GBM patient survival to 14.6 months when compared to 12.1 months with radiotherapy alone and as such, become the standard of care for newly diagnosed GBM[6,52]. Over the past few decades, there have been significant advancements in radiotherapy treatment and imaging technologies, such as stereotactic fractionated radiotherapy, which allow for more precise delineation of treatment volumes as well as the ability to deliver conformal radiation doses. This thereby maximises treatment efficacy while restricting toxicity to adjacent normal tissue, which is particularly pertinent in the brain, and is likely to further contribute towards extending overall patient survival and improving quality of life[47,52].

Conventional radiotherapy doses and schedules for treatment of glioma are typically determined by patient diagnosis as well as prognostic factors such as age, Karnofsky performance status (KPS) and the extent of surgical resection[47]. As such, for radiotherapy treatment of LGG a standard dose of 50.4 Gy in 28 fractions of 1.8 Gy over six weeks is accepted practice in both the UK and internationally[53]. The standard radiotherapy dosage and schedule adopted for GBM patients who are perceived to have a better prognosis and are under 70 years old with a KPS of >70, is 60 Gy delivered in 30 fractions (1.8-2 Gy per fraction) over six weeks[47,52]. For management of GBM in elderly patients (>70 years old), it has recently been proposed that despite one of the significant negative prognostic factors for GBM being increased age, there is a significant benefit of treating elderly patients who have a higher KPS (>70) with radiotherapy, increasing median overall survival to 29.1 weeks compared to patients who received supportive care post-surgery, who had a median survival of 16.9 weeks[52,54]. Furthermore, it has also been suggested that for elderly GBM patients who exhibit a poor KPS and are considered unsuitable for chemoradiation treatment, a course of hypofractionated radiotherapy (30 Gy in six fractions over two weeks) may be an option for palliative treatment[53].

As previously mentioned, radiotherapy is now combined with successive rounds of chemotherapy, where tolerable by the patient. The current chemotherapy reagent of choice is the alkylating agent Temozolomide (TMZ), which is typically administered concomitantly during radiotherapy at 75 mg/m^2 per day followed by up to six cycles of adjuvant TMZ which consists of 150-200 mg/m^2 for 5 days during each 28 day cycle[6]. Although this can be successful in some tumours, unfortunately others can have resistance mechanisms against TMZ-induced cell destruction. Repair of the TMZ-

induced DNA adducts can be achieved by expression of the DNA repair enzyme O^6-methylguanine DNA methyltransferase (MGMT)[55]. However, epigenetic silencing of the MGMT gene promoter by methylation has been documented in between 45-50% of GBMs, successively restoring TMZ sensitivity in tumour cells and therefore increasing overall survival of those patients[56-58].

Bevacizumab, a monoclonal antibody targeting vascular endothelial growth factor (VEGF), is one of the four treatments alongside alkylating agent TMZ and the nitrogen mustards carmustine and lomustine, that are systemically administered for GBM[59]. However, while effective at controlling oedema in GBM patients, it has unfortunately shown no overall impact on patient survival for newly diagnosed GBM patients[59-61]. Erlotinib, a small molecule inhibitor of EGFR and EGFRvIII, has been effective in some cancers such as non-small cell lung cancer (NSCLC), but was again less effective in glioma patients, exhibiting limited clinical efficacy[62,63]. Some recent developments have changed tactics and employed different strategies such as electrical stimulation. Tumour treating fields (TTF) uses alternating electric fields set at specific frequencies to disrupt mitosis in dividing cancerous cells, leading to mitotic arrest[64]. Whilst clinical trials have shown some benefit to overall survival when combined with TMZ treatment (20.5 months compared to 15.6 months with TMZ alone), TTFs can cost in excessive of £18,000 per month and therefore based on a cost-benefit analysis, NICE do not currently advocate TTF for HGG treatment in the UK[43,64].

It is well known that tumours actively influence the host's immune system to avoid detection, of which gliomas are no exception[65]. The CNS was once believed to be immune privileged due to the presence of the BBB and absence of conventional

lymphatic drainage[65,66]. However, current evidence suggests that the CNS in fact exhibits its own form of immune surveillance different to that of other tissues, and is as such now identified as an immunologically specialised area[67]. The success of immunotherapy in the treatment of a wide range of cancers has thereby provided some hope in the search for effective therapeutics for glioma. GBM are known to induce a highly immunosuppressive microenvironment through secretion of immunosuppressive cytokines which can suppress natural killer cell activity, inhibit T-cell activation and growth, downregulate major histocompatibility complex expression and induce regulatory T-cells[65,67]. As such, current research has focused on discovering ways to modulate the glioma tumour microenvironment to prevent immune escape or to prime immune cells to target tumour-specific antigens[65]. Currently, only two phase III clinical trials have been completed – the EGFRvIII targeted vaccine rindopepimut and the checkpoint inhibitor nivolumab – however unfortunately neither have shown any benefit in extending patient survival[65]. Further clinical trials are being conducted investigating the effect of checkpoint inhibitors, adoptive T-cell therapies such as CAR-T, oncolytic viruses and dendritic cell vaccines[65-67]. Although many of these trials are still ongoing, early interim reports have been mixed but overall largely encouraging[65,68]. Future treatments are however, likely to require combination therapies in order to address the full complexity of the tumour-immune system interaction.

Novel therapies for glioma are therefore continually being sought after due to their high-therapy resistance and complications with drug delivery due to the BBB. The BBB is known to be highly disrupted or ‘leaky’ in GBM allowing some therapeutic access to the tumour. However, the BBB can remain intact across significant proportions of the tumour, resorting in large areas not receiving adequate therapy[69]. Studies are therefore being

conducted investigating methods of manipulating the BBB to allow efficient drug delivery[60]. Further investigations should also be conducted into how the tumour microenvironment, as well as the tumour metabolism, can be influenced as these also play a crucial role in the generation of therapy-resistance.

1.3. Tumour hypoxia

The significant demand for biomass production required to sustain the rapid and uncontrolled proliferation of cancer cells often leaves tumour cells in challenging environments. Proliferating cells are known to consume oxygen up to five times faster than quiescent cells and so the tumour avidly exhausts nutrients and oxygen from the surrounding vasculature, quickly resulting in cells being forced to survive under low oxygen conditions known as hypoxia[70]. As a biological consequence, pro-angiogenic factors are upregulated, stimulating neovascularisation of the tumour. However these newer vessels are often both structurally and functionally abnormal[71,72], leading to perpetuation of tumour hypoxia throughout the mass, with resulting mild to severe oxygen and nutrient deprivation[71]. To adapt to the surrounding hostile environment, physiological mechanisms are quickly instigated to maintain cell survival, many of which are mediated through the family of hypoxia-inducible factors (HIFs)[72].

1.3.1. Hypoxia inducible transcription factors

HIFs are a family of heterodimeric transcription factors comprised of a constitutively expressed β subunit (encoded by the aryl hydrocarbon receptor nuclear translocator, ARNT) and one of three oxygen-regulated subunits, HIF-1α, HIF-2α or HIF-3α. In the presence of oxygen, HIF-α subunits are targeted for degradation via hydroxylation of two prolyl residues situated in the oxygen-dependent degradation domain (ODDD) by a

family of dioxygenases, the prolyl hydroxylases (PHDs)[73-75]. PHDs require both oxygen and α-KG for their function; using one oxygen atom to hydroxylate the prolyl residue, with the other used to oxidatively decarboxylate α-KG to succinate and CO_2 for subsequent use in the TCA cycle[73]. Increased prolyl hydroxylation permits binding of the α subunit to the von Hippau-Lindau protein (pVHL), which is part of an E3 ubiquitin ligase complex that polyubiquitinylates and targets the subunit for proteasomal degradation[76] (Figure 1.4). HIF activity is further controlled through the oxygen-dependent factor inhibiting HIF-1 (FIH), which hydroxylates a specific asparaginyl residue in the C-terminal transactivation domain (C-TAD), consequently blocking interaction with p300; a co-activator required for HIF to exhibit full transcriptional activity[72,77,78]. Intriguingly, FIH has a considerably lower oxygen affinity compared to the PHDs, thereby permitting a graded response to hypoxia and ability to fine-tune the HIF transcriptional response by allowing differential expression of target genes at varying levels of hypoxia[71,79].

Reduced availability of oxygen consequently inactivates both PHDs and FIH, stabilising the α subunit which consequently relocates to the nucleus to form a heterodimer with the HIF β subunit[80]. This heterodimerisation subsequently triggers association with p300 and initiates transcription through binding to hypoxia response elements (HREs) – which contain the core sequence 5'-RCGTG-3' – in HIF-target genes[73,81] (Figure 1.4). Both HIF-1α and -2α can recognise the same HRE sequence although they can elicit different transcriptional responses, most likely dependent on tissue context; HIF-1α is ubiquitously expressed, while HIF-2α has a more restricted expression profile limited to certain cell types such as vascular endothelial cells and liver parenchymal cells[82]. Little is known about the influence of HIF-3α on the biological response to hypoxia as it lacks a C-TAD, but it is thought it might have a negative regulatory function[76]. Hundreds of HIF-regulated

genes have been identified, with genome-wide analysis uncovering over 600 binding sites of HIF-1α, HIF-2α or both factors[83]. Some of the main HIF targets are heavily involved in processes such as angiogenesis, cell survival, migration and metastasis, as well as mediating the switch from oxidative to glycolytic metabolism[71-73], which will be discussed in further detail in section 1.6.

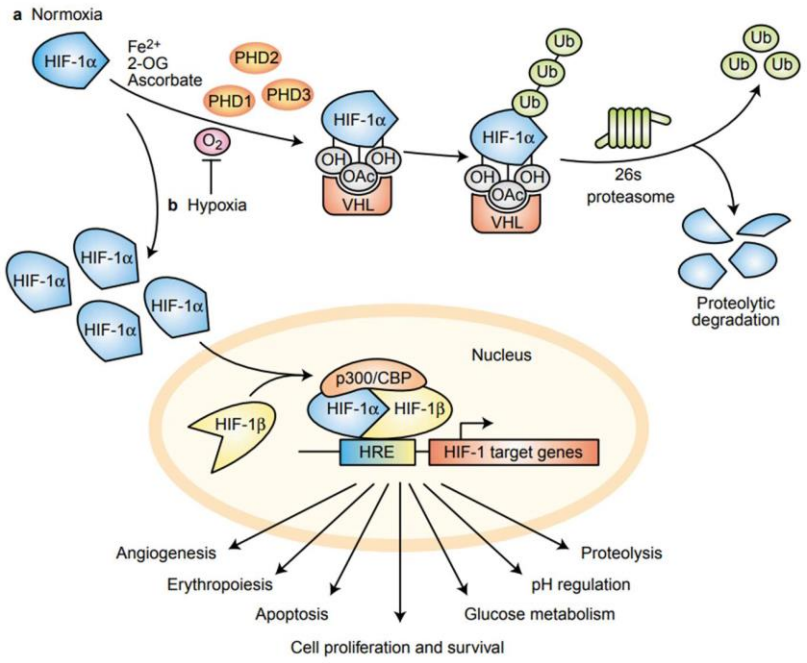

Figure 1.4 HIF-1α regulation by hydroxylation. (A) In the presence of oxygen, iron, 2-oxoglutarate (2-OG) and ascorbate, PHDs hydroxylate HIF-1α subunits subsequently permitting binding of pVHL. Part of an E3 ubiquitin ligase complex, pVHL assists in the polyubiquitination of HIF-1α subunits, thereby targeting subunits for degradation. (B) Under hypoxic conditions, PHDs are inactive allowing HIF-1α to accumulate and translocate to the nucleus where it dimerises with HIF-1β subunits. This triggers association with p300, initiating transcription of HIF-1 target genes which are implicated in a wide variety of biological processes. Image from Carroll and Ashcroft[84].

1.3.2. HIF and cancer

Tumours that exhibit high levels of hypoxia (intratumoural partial oxygen pressure (pO_2)<10 mmHg) have been associated with an increased risk of mortality, independent of prognostic factors such as malignancy grade, histology, nodal status and size of the

tumour[71]. Primary tumour biopsies from numerous cancers such as breast, lung, skin, pancreas, stomach, bladder and colon have all shown high expression levels of HIF-1α or HIF-2α[71,85,86]. Both animal and clinical models have shown that increased HIF expression correlates with increased tumour vascularisation, invasion and promotes epithelial-mesenchymal transition (EMT), therefore increasing the risk of metastasis and mortality[87,88]. Furthermore, xenograft studies have indicated that loss of HIF expression can result in a reduction in overall tumour mass, in VEGF expression and also tumour growth rate, thus providing evidence that HIF activity is crucial for cancer progression[89-91].

In addition to intratumoural hypoxia, there are other factors that can regulate HIF expression and activity such as loss of VHL, as reported in clear cell renal cell carcinoma (ccRCC), which results in constitutive HIF-α activity[92,93]. Additionally, HIF activity can be increased by oncogenes such as p53 and v-myc avian myelocytomatosis viral oncogene homology (MYC) which also influences cell metabolism[71]. Furthermore, mutations in the genes encoding the TCA enzymes succinate dehydrogenase (SDH) and fumarate hydratase (FH) can also affect HIF stability. Loss of enzymatic function blocks TCA cycle activity resulting in accumulation of either succinate or fumarate respectively, which can competitively inhibit PHD activity and result in stabilised HIF expression[94]. Interestingly, these mechanisms can all influence HIF stability independent of oxygen availability; a phenomenon known as pseudohypoxia, which is observed in many cancers[94,95].

1.3.3. Tumour hypoxia and glioma

Gliomas are highly hypoxic tumours as a result of both a rapid growth rate outstripping the bloody supply and the extensive cerebral oedema exhibited through breakdown of

the BBB. Intratumoural oxygen measurements recorded *in vivo* by Rampling *et al*., in the 1990's characterised the extent of hypoxia in gliomas, with tumours exhibiting a median pO_2 of a 7.4 mmHg (1% O_2). Tumour oxygen levels were observed to be highly heterogeneous, with some HGG also exhibiting areas under 2.5 mmHg O_2 (0.3% O_2), which is in stark contrast to normal brain tissue which has a pO_2 of around 35 mmHg (4.6% O_2)[96,97]. As mentioned above, elevated HIF expression has been associated with increased tumour progression. A substantial factor contributing to this is that poorly oxygenated/hypoxic tumour cells are highly resistant to both chemotherapy and radiotherapy (both dependent and independent of HIF)[97]. Intratumoural oxygen content is particularly important for radiotherapy since oxygen is a potent radiosensitiser[98]. Molecular oxygen has a particularly high affinity for electrons and following absorption of energy from ionising radiation, participates in chemical reactions that lead to generation of reactive oxygen species (ROS), which cause subsequent DNA and cellular damage[99]. As such, radiosensitivity rapidly declines when tumour pO_2 is <25-35 mmHg[100]. Furthermore, HIF-1 mediated upregulation of downstream pathways involved in cell survival, proliferation, angiogenesis and metabolism also significantly contribute towards chemo- and radioresistance under hypoxic conditions[100]. As a result of this oxygen-enhancement effect, the dose of ionising radiation necessary to attain the equivalent cell survival fraction is 2-3 times higher in hypoxia than compared with normoxia[97]. Furthermore, hypoxia can also support the development and survival of both neural and glioma stem cells, which have been characterised to exhibit high drug resistance as well as a high tumorigenic potential[101]. This well-established association between hypoxia (increased HIF expression) and therapy resistance has resulted in the search for therapeutics that act to either reduce or exploit tumour hypoxia. An extensive number of treatments have been investigated including inhibitors targeting HIF expression and

stability, approaches to normalise tumour vasculature as well as therapeutics to induce radiosensitisation[72,88]. Despite these efforts, drugs targeting the tumour hypoxia such as bevacizumab have shown limited clinical efficacy in GBM, which may be due aspects of clinical trial design (use of single-agents rather than rational combinations), inefficiency at completely inhibiting HIF activity or unacceptable off-target effects[72]. Further investigations into targeting the hypoxic microenvironment as well as identifying hypoxia-interacting signalling pathways which contribute towards promoting tumour progression and therapy resistance are critically warranted in the hope to identify novel glioma therapeutics.

1.4. The Hippo pathway as a therapeutic target

1.4.1. Origins and physiological function

A pathway that has stimulated interest in the search for new glioma therapeutics is the Hippo pathway. First elucidated from genetic mosaic screens and loss-of-function studies in *Drosophila melanogaster,* this core pathway has emerged to regulate many cellular processes underpinning tissue homeostasis and regulation of organ size such as cell proliferation, survival and differentiation[102,103]. These studies identified a set of four core genes – *Hippo*, *Warts*, *Salvador* and *Mats* – which when mutated, caused organomegly resulting in a 'hippopotamus-like' phenotype characterised by increased cell proliferation and decreased cell apoptosis[102,104,105]. The core components of pathway were subsequently shown to be highly conserved in mammals; MST1/2 (mammalian Ste2-like kinases), LATS 1/2 (large tumour suppressor kinase 1/2), SAV1 (salvador homolog 1) and MOB1A/1B (MOB kinase activator 1A/1B) are orthologs of Hippo, Warts, Salvador and Mats respectively[106]. Downstream targets of this cascade – the transcriptional co-activator Yes-associated protein (YAP; ortholog of Yorkie) and its close paralog TAZ

(transcriptional co-activator with PDZ-binding motif; also known as WWTR1) – were also identified and found to be the dynamic effectors of this pathway as they orchestrate binding to various different transcription factors to initiate transcription of various downstream target genes involved in cell growth and survival[103,107,108].

1.4.2. Mechanism of YAP and TAZ

YAP is a highly evolutionarily conserved 65 kDa protein expressed in all mammalian cells, with the exception of leukocytes[109]. The human YAP1 gene is located on chromosome 11 at position q22.1 and can be alternatively spliced into 11 different splice variants, nine of which are protein coding[110]. YAP1 splice variants are subsequently divided into 2 main categories, YAP1-1 or YAP1-2 (also referred to as YAP2), depending on whether the variant contains one or two WW domains respectively[104]. Characterisation of YAP isoforms has also determined the presence of an N-terminal TEA domain (TEAD)-interacting motif which is followed by either one or two WW domains, whose function is to mediate protein complexes containing a PPxY motif[104,111]. Within the C-terminal domain of YAP resides a PDZ-binding domain that has been proposed to orchestrate YAP cellular localisation[112]. YAP paralog TAZ, has been found to have 46% amino acid sequence homology, although TAZ has only been discovered in vertebrates and much less is known about this protein[104].

The core mechanism of the mammalian Hippo cascade is instigated through activation of the serine/threonine kinases MST1/2 by homodimerisation, triggered by various upstream regulators[113]. Once activated, MST1/2 function to phosphorylate the downstream kinase LATS1/2. Scaffold protein SAV1 acts to facilitate this interaction by forming a complex with MST1/2, bringing MST1/2 and LATS1/2 into close spatial

proximity in the cell[114]. Activation of LATS1/2, whose kinase activity is enhanced by forming a complex with the adaptor protein MOB1A/1B, subsequently continues the cascade and phosphorylates the downstream targets YAP and TAZ, which become inactivated upon phosphorylation at serine 127 and serine 89 respectively[106,114,115]. This inactivation of YAP/TAZ inhibits their function as transcriptional co-activators thus preventing transcription of various downstream targets involved in cell proliferation and survival. These inactive proteins are sequestered by 14-3-3 binding proteins and retained in the cytoplasm where they are subsequently degraded by ubiquitin proteasomes, therefore preventing cell proliferation and tissue growth[102]. Conversely, upon inactivation of the Hippo pathway, the kinase cascade is inhibited which results in YAP protein remaining un-phosphorylated and able to freely translocate to the nucleus, thereby co-activating transcription of its target genes[114].

In mammalian cells, YAP protein acts as a transcriptional co-activator but despite possessing strong transcriptional activity within the C-terminus, YAP does not possess DNA binding ability. Transactivation of downstream genes therefore requires a transcriptional binding partner, of which the most well-described are the TEAD family of transcription factors (TEADs 1-4)[114,116]. These transcription factors individually are not able to activate transcription of target genes, but when YAP is nuclear localised, a heterodimer is formed with a TEAD family protein[117,118]. Once forming this complex, YAP-TEAD can then activate expression of direct downstream genes such as connective tissue growth factor (*CTGF*), cysteine-rich angiogenic inducer 61 (*CYR61*) and amphiregulin (*AREG*), which have been implicated in cellular migration, proliferation and anti-apoptosis, resulting in the proliferative phenotype commonly associated with YAP activation[103,104,107].

Interestingly, additional transcription factors have been identified to interact with the WW domains of YAP/TAZ proteins such as Smad1 (mothers against decapentaplegic homolog 1), RUNX1/2 (runt-related transcription factor 1/2), and p73 (tumour protein 73), which exhibit pro-apoptotic effects in cells – an outcome seemingly at odds with the well-defined role of YAP supporting proliferation and survival of cells[107,114]. As a result, there has been much debate over the true role of YAP within the Hippo pathway, and whether it is a *bona fide* tumour suppressor or potential oncogene. It is currently believed that YAP has a dual function exhibiting pro- or anti-apoptotic downstream effects depending on the cell and tissue context, supporting its physiological function in the precise regulation of organ size[119,120].

Since signalling pathways are arranged more as networks than linear cascades, it implies that these pathways are dynamic and can alter depending on cellular context and differential regulation of the upstream components[121] (Figure 1.5). This is likely the case for YAP, as it has been shown that activation of the pathway through different upstream regulators leads to diverse downstream effects. It has been shown that activation of the Hippo pathway through the Ras association domain-containing protein 1A (RASSF1A), promotes association of YAP1 with pro-apoptotic protein p73 and limited association with TEAD transcription factors, therefore exerting an overall tumour suppressor effect[122]. This was further investigated by knocking down RUNX2 expression, which functions as a tumour suppressor gene. The reduction in RUNX2 expression consequently caused an enhanced association of YAP1 and TEAD transcription factors demonstrating that competition may exist between these factors depending on availability and/or upstream regulation[122]. It is therefore important to further investigate and fully understand the

differential upstream regulation of the Hippo pathway and how this contributes to YAP function in a variety of cell contexts.

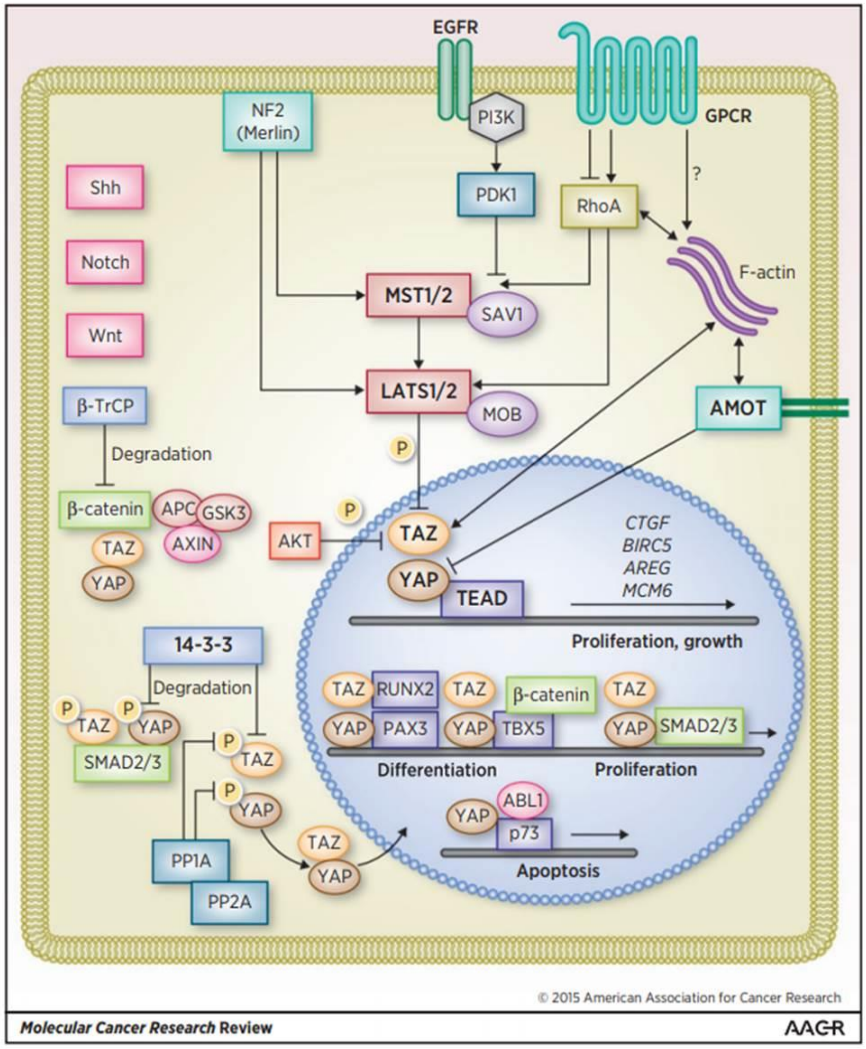

Figure 1.5 Overview of Hippo pathway regulation and regulation of transcription by YAP/TAZ transcriptional co-activators. Upstream activation of the Hippo pathway results in phosphorylation of downstream mediators YAP/TAZ. This phosphorylation inhibits their function as transcriptional co-activators thus preventing transcription of various downstream targets. Upon inactivation of the Hippo pathway or direct activation of YAP/TAZ, the co-activators remain un-phosphorylated and are consequently able to freely translocate to the nucleus, thereby co-activating transcription of its target genes involved in cell proliferation, growth, differentiation and even apoptosis. Image from Ehmer and Sage[123].

1.4.3. Regulation of YAP/TAZ activity

Regulation of YAP/TAZ activity can be either achieved through exerting direct effects on YAP/TAZ proteins or through indirect mechanisms that mediate the activity of the upstream Hippo pathway (Figure 1.5). Consistent with the distinct role of Hippo and YAP in regulating organ size, the majority of established regulators discovered were mechanical and physical cues involved in controlling tissue architecture. Cell-cell contact in particular has been prominently implicated in the direct and indirect regulation of YAP/TAZ, with high cell density inactivating YAP/TAZ activity[124]. The cadherin α-catenin, an important sensor of cell density which functions to integrate signals from neighbouring cells through the construction of adherens junctions, has been shown to interact directly with YAP by forming a complex with 14-3-3 proteins, thereby inhibiting YAP activation through sequestration at the plasma membrane[125]. This consequently prevents YAP dephosphorylation, thus blocking its nuclear translocation and subsequent activation of downstream transcription targets[126]. Other structural components that have been identified to influence YAP/TAZ activity include filamentous (F-) actin, which is important for a variety of cell functions such as cell mobility, division, establishment of cell junctions as well as integrating various mechanical and hormonal cues from neighbouring cells and the extracellular matrix (ECM)[102,127]. Actin destabilising proteins such as F-actin capping and severing protein cofilin, have been observed to directly assist in the cytoplasmic retention and therefore inactivation of YAP/TAZ, whereas stabilisation of F-actin instigates downstream activation of YAP/TAZ proteins[112,128]. Actin cytoskeleton dynamics are known to be influenced by a family of GTPases, the Rho GTPases, which transduce upstream cues from G-coupled protein receptors (GPCRs), and are consequently another important upstream regulator of the Hippo pathway[112]. As GPCRs are the largest family of cell surface molecules involved in signal transduction, it

highlights the huge amount of potential cross-talk between various hormonal signalling pathways, in addition to mechanical regulatory pathways, and YAP/TAZ to directly or indirectly influence their activity[129].

Since the Hippo pathway is not regulated by a specific and unique receptor/ligand interaction, it heavily relies on integration with other signalling networks to both regulate its own activity as well as influencing the downstream function of the interacting pathway[130]. Consequently, significant reciprocal cross-talk between Hippo/YAP/TAZ signalling and Wingless (Wnt), Notch, Hedgehog (Hh) and bone morphogenic protein (BMP) signalling pathways have already been identified[124,130]. Furthermore, microenvironmental cues have been recognised to be extremely important in regulating the output of YAP/TAZ signalling network, with stress responses such as AMP-activated protein kinase (AMPK) activation, DNA damage and hypoxia also being identified to influence Hippo/YAP/TAZ signalling activity[130].

The relationship between hypoxia and regulation of YAP/TAZ activity has been recently exposed in a handful of investigations, partially uncovering some of the complex interactions that mediate the pro-survival response to such hostile conditions. Previous research has demonstrated in MDA-MB-231 breast cancer cells, that hypoxia can negatively regulate the Hippo pathway through the ubiquitin E3 ligase, SIAH2 (seven in absentia homolog 2)[131]. SIAH2 is recognised as an essential component of the hypoxia response pathway as it targets PHDs for degradation via the ubiquitin-proteasome pathway thereby resulting in increased HIF-1α stabilisation and activity in hypoxia[132]. Additionally, SIAH2 was previously identified to directly interact with LATS2, instigating its proteasomal degradation and thus reducing LATS2-mediated YAP S127

phosphorylation[131]. As a result, enhanced YAP nuclear localisation was observed alongside increased protein and messenger RNA (mRNA) expression of the direct YAP target genes, CYR61 and CTGF[131]. Furthermore, direct interaction between YAP and HIF-1α was confirmed and shown to be significantly enhanced under hypoxic conditions, again implicating that the potential purpose of integrating these signalling networks is to ensure continuous cell growth and survival under hypoxic conditions[131].

This hypothesis was further corroborated by research showing that hypoxic induction of HIF-1α, but not 2α, was able to mediate both increased TAZ expression as well as nuclear localisation, inducing the breast cancer stem cell phenotype[133]. It was found that HIF-1α and TAZ acted as reciprocal co-activators, with the bi-directional crosstalk synergistically driving the expression of downstream target genes under hypoxic conditions[134]. This pro-survival hypoxic-YAP/TAZ regulation was also shown to perpetuate treatment resistance as hypoxia-induced YAP activity in hepatocellular carcinoma (HCC) cells was suggested to contribute towards chemoresistance against Topoisomerase I inhibitor SN38[135]. Interestingly, this study also demonstrated hypoxia-induced YAP activity in HCC cells to be HIF-1α independent as depletion of HIF-1α was insufficient to impair nuclear translocation of YAP[135]. This again highlights the complex nature of YAP under different cellular and tissue contexts and indicates that additional hypoxia-responsive regulatory mechanisms other than HIF-1α activity can also play a role in influencing YAP/TAZ activity. Hypoxic regulation of YAP/TAZ therefore warrants further investigation, and could be of particular interest within gliomas since they exhibit extensive areas of hypoxia which contribute significantly towards treatment resistance.

1.4.4. Dysregulation of YAP/TAZ activity

1.4.4.1. Association with cancer

Strict control of the Hippo pathway is imperative to healthy tissue development and it is therefore of no surprise that dysregulation of YAP/TAZ signalling has been strongly linked with tumorigenesis[136]. Despite this, naturally occurring mutations in Hippo pathway core components are extremely rare with only 0.2% of cancer tissue sections exhibiting homozygous deletion of YAP1[137]. Additionally, it has been presented that knockout of YAP results in embryonic lethality in mice[137]. Amplification and epigenetic silencing of Hippo pathway components however are more common and frequently observed within human cancers[115,116]. YAP/TAZ amplification and increased transcriptional activity has been observed in numerous cancers (reviewed in Zanconato *et al*.,[138]) and is detected in as high as 85% of colorectal tumours, 60-70% of astrocytomas and around 20% of breast neoplasms[104,116,139]. A wealth of studies have since demonstrated that increased YAP/TAZ expression and sustained activation can significantly promote aberrant tumour growth, induce EMT as well as enhance tumour migration, invasiveness and metastasis[104,138]. Supporting this, experiments using mouse xenograft models have shown that *in vivo* knockdown of YAP1 can significantly suppress tumour growth of cancers in organs including the oesophagus, lung and bone[140-142]. Nevertheless, in some breast cancer models, tumour growth of mouse mammary glands cannot be solely induced by YAP overexpression, suggesting that under some circumstances additional lesions are required to assist in the oncogenic transformation of these cells[114]. The status of YAP as a true oncogenic driver remains under debate since research has also shown YAP to act as a tumour suppressor in several haematological cancers such as multiple myeloma (MM), lymphoma and leukaemia[136]. It has been suggested that in these cancers YAP could induce expression of pro-apoptotic genes through interaction with the

transcription factor p73, thereby suppressing cancer formation[143]. These observations provide further evidence that YAP/TAZ signalling is incredibly complex and the functional output is heavily dependent upon the cell and tissue context.

Enhanced YAP/TAZ activation has also been identified as a prognostic indicator for patient survival in cancers in which YAP drives oncogenesis[114]. A recent meta-analysis has shown both YAP amplification and increased nuclear localisation to be statistically associated with both decreased overall survival (OS) and disease-free survival (DFS)[144]. Furthermore, additional studies have also highlighted the strong association between increased YAP/TAZ expression and both higher tumour malignancy grade and progression in several cancers[114,145,146]. Interestingly, a novel subclass of ovarian cancers have been identified that exhibit an independent prognostic gene signature reflecting YAP1 activation[147]. This expression signature corresponded with a poorer prognosis and was able to predict response to taxane-based treatment, stratifying patients who were likely to benefit from this therapy[147]. This provides new means of identifying tumours with high YAP activity through a defined gene signature and may prove to represent a novel method of stratifying patients for treatment.

In addition to influencing tumour growth and survival, increased YAP/TAZ activity has been demonstrated to confer chemoresistant properties on cancer cells[104]. In normal physiology, YAP/TAZ signalling has been associated with the maintenance and function of stem and progenitor cells, inducing the expression of genes such as *OCT4* (octamer-binding transcription factor 4), *Nanog* (Nanog homeobox), and *Sox2/9* (sex determining region Y box 2)[102]. Unsurprisingly, associations between aberrant YAP/TAZ signalling and regulation of cancer stem cells (CSCs) during tumorigenesis have been observed,

including that of high YAP and TEAD expression in CSCs of medulloblastomas[102]. CSCs are known to exhibit high chemoresistance and tumorigenic potential and are thought to be largely responsible for cancer initiation as well as recurrence and metastasis[102]. Interestingly, research has identified YAP1 to be a major determinant of bestowing CSC properties in both non-tumorigenic and oesophageal cancer cells through direct upregulation of Sox9[148]. Through genetic and pharmacological inhibition of YAP1, it was also shown that reduced YAP1 expression and activity significantly attenuated CSC tumorigenicity *in vivo* and tumoursphere formation *in vitro*[148]. Suppression of YAP/TAZ signalling may therefore be of inherent interest in the search for novel cancer therapies, as well as invaluable in overcoming therapy resistance to existing treatments.

1.4.4.2. YAP/TAZ in glioma

Despite the strong association between aberrant Hippo signalling and tumorigenesis, only a small number of studies have thus far focused their attention on elucidating the role of YAP/TAZ signalling in gliomas. YAP1 nuclear expression has been immunohistochemically characterised in both normal brain tissue and tissue from 198 glial tumours of varying WHO grades[149]. Non-neoplastic tissue was seen to exhibit YAP1 immunoreactivity exclusively in areas of the brain which were enriched with proliferating neural stem and progenitor cells, consistent with the established role of YAP/TAZ signalling in development[149]. Strikingly, nuclear YAP1 expression was also readily detected in 80-100% of grade II-IV glial tumours, although was considerably lower in grade I pilocytic astrocytomas (30%)[149]. These observations were corroborated in an additional glioma cohort, which showed significant amplification of both YAP/TAZ mRNA and protein expression to be associated with increasing malignancy grade[150]. Analysis of data from 564 gliomas from TCGA dataset also showed that amplified YAP/TAZ

expression positively correlated with a worse OS in glioma patients[150]. Expression levels of direct YAP target genes, *CYR61* and *CTGF* which are known to stimulate cell proliferation and migration as well as ECM formation, were also observed to be prognostic for both glioma progression and overall patient survival[151]. CYR61 and CTGF expression were analysed in tissue from 66 primary gliomas and observed to be significantly overexpressed in 48% and 58% of samples respectively when normalised to samples taken from normal brain tissue[151]. Furthermore, a significant association between increased tumour grade and worse OS with high CYR61 and CTGF expression was identified, again highlighting increased YAP/TAZ signalling to be associated with the advanced, more malignant stage of disease[151].

To date, only a few studies have investigated the molecular effect of YAP on glioma biology. Following the identification that nuclear YAP expression was significantly amplified in glial tumours, research demonstrated that by reducing YAP1 expression in GBM lines U87, U373 and neurosphere line HSR-GBM1, cell growth could be significantly attenuated[149]. In addition, it was recently demonstrated in established GBM lines (U251 and U87) and primary glioma cells, that YAP1 downregulation significantly impeded both cell migration and invasion whereas YAP overexpression significantly promoted these malignant phenotypes[152]. Together, these studies highlight the importance of aberrant YAP/TAZ signalling in glioma and how understanding this relationship could potentially unveil novel and effective therapeutic strategies.

1.5. Therapeutic targeting of YAP/TAZ signalling

1.5.1. Discovery of verteporfin as a YAP inhibitor

The idea of suppressing aberrant YAP/TAZ signalling to reduce malignant growth and cancer progression sparked the search for therapeutics which could directly or indirectly manipulate YAP/TAZ activity. Since the direct interaction between YAP and TEAD leads to transcription of pro-proliferative target genes, disrupting the YAP-TEAD complex could therefore provide an ideal drug target to selectively suppress YAP-induced tumorigenesis. Consequently, a previous study conducted a pharmacological drug screen of over 3300 small molecules contained in the John Hopkins Drug Library, with the hope of identifying YAP-TEAD interactors[153]. Three compounds that stood out amongst the top hits were interestingly all members of the porphyrin family; hematoporphyrin (HP), PPIX and verteporfin (VP)[153]. Further experimentation showed VP to be the most potent inhibitor of the YAP-TEAD interaction, with PPIX exhibiting much weaker activity and HP causing minimal effects at a concentration of 10 μM[153]. VP was shown to selectively bind YAP and alter its structural confirmation which as a result, abolished its ability to interact with TEADs[153]. However, it was unclear whether VP was able to inhibit the oncogenic ability of YAP *in vivo.* Using transgenic mouse models, it was observed that VP was able to suppress liver overgrowth induced by either YAP overexpression or increased activation, independently of light activation of the compound (see below). These data provided evidence to suggest that pharmacologically inhibiting the YAP-TEAD interaction could be a viable strategy for suppressing oncogenic YAP activity[153].

1.5.2. Clinical use of VP

VP is a benzoporphyrin derivative currently used in the clinic to treat age-related macular degeneration (AMD); a severe degenerative eye disease which is the leading cause of blindness in adults aged 65-74 years in Western countries[154,155] (Figure 1.6). Clinically-approved by the USA Food and Drug Administration (FDA), VP (trade name Visudyne) is commonly used as a photosensitiser in the application of photodynamic therapy (PDT)[155]. During PDT, VP is intravenously injected and activated using low-intensity light of between 685-690nm targeted at the area of interest to induce localised production of cytotoxic free radicals[155]. These radicals can subsequently inflict damage to the surrounding area and in the case of AMD, lead to thrombus formation and vascular occlusion which can improve or maintain visual acuity[155]. A major challenge when designing effect treatments is being able to precisely and specifically target the area of interest without damaging normal cell function and viability. Fortunately, VP is known to be selectively taken up by neovascular endothelial or malignant tumour cells via low-density lipoprotein receptors (LDLs) and is thus designed as a liposomal formulation[155]. Due to the strong preferential uptake in tumour cells, a few phase I/II clinical trials have examined VP efficacy in the use of PDT treatment in cancer such as in locally advanced pancreatic cancer[156]. Multiple applications of VP at a clinical dose of 6-12 mg/m^2 has been shown to be well-tolerated within patients causing minimal local and systemic side-effects, partially due to its rapid clearance from the body (plasma half-life around 5-6 hours)[154,155].

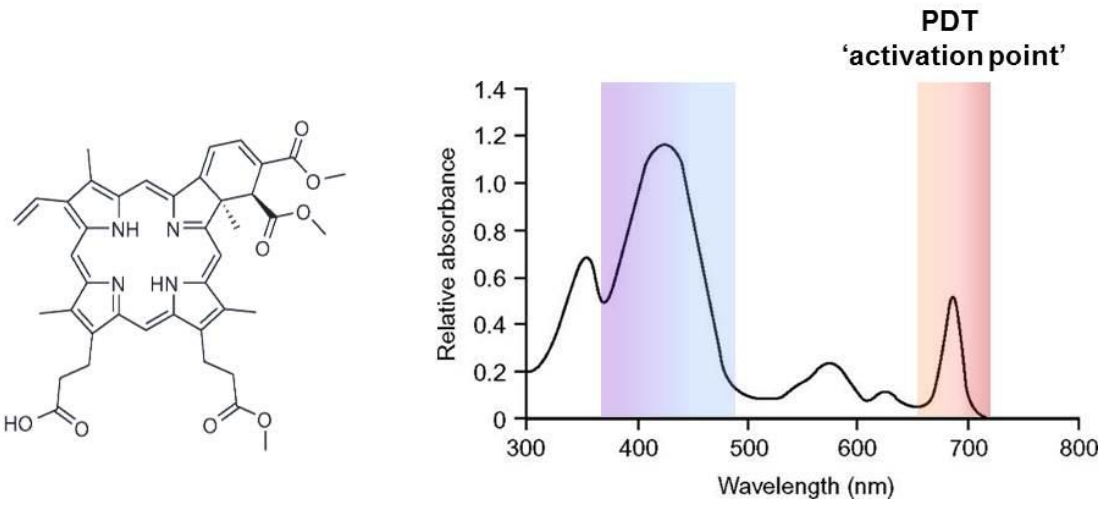

Figure 1.6 Chemical structure and absorption spectra of VP. VP is a benzoporphyrin derivative and characteristically strongly absorbs light. In addition to an absorption maximum in the UVA range (~430 nm; Purple/blue), VP offers an absorption peak between 685–690 nm (orange/red) which is used in the application of PDT. Image adapted from Ratkay *et al*[157].

Following the discovery that VP can also attenuate aberrant YAP-mediated signalling independent of light-activation, studies have recently focused their attention on the possibility of repurposing VP as a cancer therapeutic without the need for PDT.

1.5.3. Effect of VP as a YAP inhibitor on cancer growth

Several studies have previously demonstrated VP to significantly attenuate both tumour growth and proliferation in cancers such as retinoblastoma, pancreatic and ovarian through suppression of YAP-TEAD signalling[158-160]. More recently, VP has also shown to inhibit growth of LN229 and SNB19 glioma cell lines, again highlighting the importance of investigating YAP signalling in glioma[161]. Within these studies, VP was observed to directly reduce YAP expression as well as its direct targets CYR61, CTGF, survivin, axl and OCT4. Interestingly, VP has been shown to induce apoptosis and autophagy as a result of YAP-TEAD disruption however the mechanisms underlying how VP reduces tumour growth and progression remain elusive since some studies demonstrate VP to

reduce tumour mass through strict inhibition of cell proliferation and not through induction of cell death mechanisms[158-160].

A functional genomics screen previously identified YAP1 as a key determinant to overcome treatment resistance in lung cancer cells and it was consequently shown that treatment with VP was able to significantly sensitise PC9 cells to cisplatin, radiation and erlotinib treatment[162]. Research has also shown the ability of VP to both reverse YAP-induced paclitaxel resistance in colon cancer cells and overcome BRAF inhibitor resistance in melanoma respectively[163,164]. These studies provide further evidence that targeting aberrant YAP/TAZ signalling could be a valuable opportunity in the development of effective cancer therapeutics as well as in sensitising cancer cells to pre-existing treatments.

Despite pre-clinical studies highlighting the huge potential of YAP suppression by VP to attenuate tumour growth, research has also uncovered that under some circumstances VP can exhibit tumour suppressor activity independently of YAP. Two recent investigations have both demonstrated that despite significant YAP1 depletion, VP retains its ability to induce a significant reduction in both tumour cell proliferation and viability[165,166]. The tumour suppressive characteristics of VP are therefore complex and further investigation is warranted into the potential for repurposing VP as a new cancer therapeutic without the need for PDT.

1.6. Metabolic-rewiring in cancer

1.6.1. Introduction to cancer metabolism

Sustaining the high rates of cell proliferation in tumours requires cells to regularly duplicate their entire cellular contents including nucleotides, proteins, lipids and other macromolecules. This therefore places a significant energy demand on the cell, requiring increased uptake and use of key nutrients, production of adenosine triphosphate (ATP), as well as challenges in continuing to maintain cellular redox homeostasis. In the recent update to their seminal work in 2000 positing six hallmarks of cancer, Hanahan and Weinberg extended it to include two further emerging hallmarks: avoidance of immune destruction and deregulation of cellular bioenergetics[167]. This reprogramming can arise as a direct consequence of activation of various oncogenes (e.g., MYC, RAS) or mutations in tumour suppressors (e.g., TP53)[71,168]. Additionally, tumour metabolism can also be influenced by the surrounding microenvironment such as hypoxia, which as previously described, often leads to a more malignant phenotype[168].

Alterations in tumour metabolism were first identified almost a century ago in the 1920's, by Otto Warburg[169]. He discovered that unlike differentiated cells, which preferentially utilise mitochondrial oxidative phosphorylation for energy production, rapidly proliferating cancer cells significantly increase their rate of glycolysis to favour production of lactate from pyruvate[169,170]. This phenomenon termed 'the Warburg effect' (also referred to as aerobic glycolysis), at first seems counterintuitive since metabolising glucose to pyruvate and then lactate is far less efficient at producing ATP (per unit of glucose metabolised; ~2 moles ATP/mole glucose) as opposed to complete glucose catabolism through oxidative phosphorylation (~36-38 moles ATP/mole glucose)[171]. However, tumour cells have been observed to significantly increase their glucose uptake, predominately

through upregulation of cellular glucose transporters (GLUTs), to increase and sustain glycolytic rates which have been documented in some instances, to exceed ATP production from oxidative phosphorylation[172-175]. Although a specific functional rationale for this increased glycolysis and subsequent decrease in glucose oxidation remains elusive, a plausible justification could be for the cell to accumulate glycolytic intermediates such as 3-phosphoglycerate (3-PG), which can be diverted into various biosynthetic pathways to generate nucleotides and amino acids which are crucially required to facilitate sustained proliferation[176] (Figure 1.7).

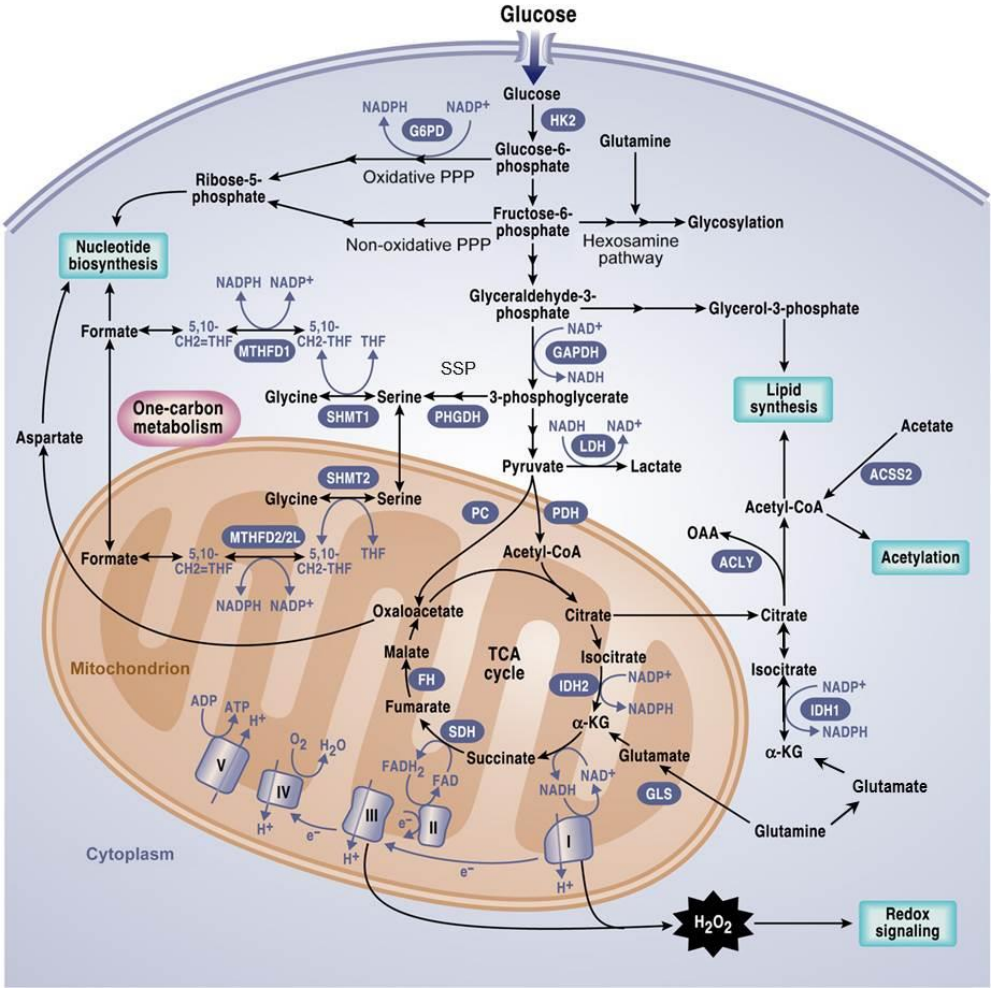

Figure 1.7 Cancer cells alter their metabolism to support anabolic growth.. Schematic highlighting some of the key metabolic pathways in central carbon metabolism which are heavily relied upon or altered in cancer to sustain uncontrolled proliferation and maintain cellular redox. Image adapted from DeBerardinis and Chandel[177].

1.6.2. Glucose metabolism in cancer

It has long been known that cancer cells rapidly consume glucose, demonstrating elevated rates of glycolysis. This phenotype is harnessed in the clinic through the use of ^{18}F-deoxyglucose-positron emission tomography (FDG-PET), the signal from which can be used to identify small, otherwise undetectable metastases and has been shown to significantly negatively correlate with patient survival in many cancers[172]. The plasma membrane is impermeable to glucose and thus glucose is mainly imported into the cell through the use of a family of plasma membrane transporters (GLUTs; SLC2A). Once imported, glucose is phosphorylated by hexokinase to produce glucose 6-phosphate (G6P). G6P can then be oxidatively used in glycolysis to produce ATP, culminating in generation of the end-product of glycolysis, pyruvate. Additionally, G6P can be diverted away from glycolysis into the oxidative arm of the pentose phosphate pathway (PPP) to generate reduced nicotinamide adenine dinucleotide phosphate (NADPH) and activated pentose units such as ribose 5-phosphate (R5P), for nucleotide synthesis[178]. Similarly, downstream glycolytic intermediate 3-PG can be shunted into the serine synthesis pathway (SSP) for *de novo* production of non-essential amino acids (NEAAs) serine and glycine which are utilised in biosynthetic production of nucleic acids, proteins and lipids[178].

Pyruvate has many metabolic fates within the cell, although in aerobic glycolysis a significant proportion is converted to lactate through lactate dehydrogenase (LDH). LDH is a ubiquitously expressed enzyme which reversibly catalyses the reduction of pyruvate to lactate coupled with the oxidation of reduced nicotinamide dinucleotide (NADH) to oxidised nicotinamide dinucleotide (NAD^+)[179]. This reaction is particularly important as the NAD^+ produced is critical for the continued activity of the glycolytic enzyme

glyceraldehyde 3-phosphate dehydrogenase (GAPDH) to facilitate ATP production and maintain glycolytic flux[179]. In addition to lactate production, pyruvate can also be transaminated by the enzyme alanine transaminase (ALT) to produce alanine for use in protein synthesis[179].

Once imported into the mitochondria through the mitochondrial pyruvate carrier (MPC), pyruvate can enter the TCA cycle to support ATP production through subsequent oxidative phosphorylation[179]. Pyruvate is first oxidatively carboxylated via pyruvate dehydrogenase (PDH) to form acetyl Coenzyme A (CoA), which subsequently condenses with oxaloacetate (OAA) to form citrate. Citrate is either isomerised to isocitrate and oxidatively decarboxylated via IDH enzymes to form α-KG for continued use in TCA cycle or exported to the cytoplasm where it is converted back to acetyl CoA via ATP citrate lyase (ACLY) for *de novo* lipid synthesis. Additionally, pyruvate carboxylase (PC), an enzyme traditionally associated with gluconeogenesis, can support alternative pyruvate entry into the TCA cycle through carboxylation of pyruvate to OAA. PC has been shown to be important for cancer cell proliferation in glutamine-deprived and hypoxic conditions, where PDH activity is reduced, through carboxylation of pyruvate to OAA supplying carbon for TCA intermediates as well as citrate for lipid synthesis[71,180]. OAA can also be transaminated to form aspartate, which has consequently been shown to be essential for tumour growth[181,182].

1.6.3. Glutamine metabolism in cancer

Since increased conversion of pyruvate to lactate in aerobic glycolysis is concomitant with decreased availability of pyruvate for oxidation in the mitochondria, cancer cells are known to become increasing reliant on glutamine both as a carbon and nitrogen source

for generation of TCA cycle intermediates and subsequent ATP production. In fact, some cancer cells cannot survive in the absence of exogenous glutamine and are described to be 'glutamine addicted'[183].

As with glucose, glutamine must first be imported into the cell through membrane transporters such as neutral amino acid transporter alanine-serine-cysteine-threonine transporter 2 (ASCT2/SLC1A5)[184]. Following its import, glutamine can either be directed towards use in nucleotide and protein synthesis or converted to glutamate through glutaminase enzymes (GLS). Glutamate has many uses within the cell including as an amino donor for nucleotide and NEAA synthesis, such as proline biosynthesis, as well as a crucial contributor towards glutathione (GSH) synthesis- a tripeptide produced from amino acids cysteine, glycine and glutamate, which acts as an essential endogenous antioxidant to reduce cellular damage incurred through cellular reactive oxygen species (ROS)[185,186]. Glutamate can also supply carbons into the TCA cycle for the production of anabolic substrates and reducing potential to generate ATP through its conversion to α-KG via glutamate dehydrogenase (GLDH) or transaminase activity.

1.6.4. Role of YAP/TAZ signalling in cancer metabolism

Aberrant YAP/TAZ signalling, as previously described, can induce tumour proliferation and survival and so it is possible that YAP/TAZ could directly regulate the metabolic pathways required to support this uncontrolled proliferation. Little is currently known about this emerging relationship, although it was recently shown that aerobic glycolysis could fine tune YAP/TAZ transcriptional activity in breast cancer[187]. When glucose metabolism was inhibited or diverted away from glycolysis in MDA-MB-231 and MCF10A cells, YAP/TAZ transcriptional activity was impaired, consequently attenuating cell

proliferation and clonogenic abilities[187]. Mechanistically, the authors showed that phosphofructokinase 1 (PFK1), an important regulatory enzyme in glycolysis, directly interacts with TEAD cofactors to stabilise their interaction with YAP/TAZ, thereby promoting increased transcriptional activity when glucose is being metabolised[187].

Further to the notion that metabolic pathways can exhibit cross-talk with YAP/TAZ signalling to support uncontrolled tumour growth, it has been demonstrated that YAP/TAZ can directly regulate expression of enzymes crucial for deoxyribonucleotide triphosphate (dNTP) biosynthesis[188]. This directly impacts dNTP metabolism as well as the pool of dNTP precursors available for DNA replication, consequently influencing cell proliferation. This was similarly demonstrated in a transgenic zebrafish model, where YAP was observed to directly induce expression and activity of glutamine synthetase (GLUL) to enhance glutamine production and thus increase steady-state glutamine levels[189]. This elevated glutamine was shown to enhance *de novo* nucleotide biosynthesis to fulfil the anabolic demands of rapid cell proliferation[189].

Finally, two recent studies have identified the importance of YAP/TAZ signalling in regulating glutaminolysis to drive both pulmonary hypertension and liver fibrosis[190,191]. Both studies came to the conclusion that YAP/TAZ activation regulated expression of metabolic enzyme GLS1, and was therefore crucial for replenishment of carbon intermediates in the TCA cycle to support biosynthesis of amino acids, such as aspartate, to continue cell proliferation[190,191]. It would therefore be of interest to investigate this relationship between YAP/TAZ signalling and glutaminolysis in cancer, since glutamine is heavily relied upon to sustain tumour growth.

1.6.5. Hypoxia-induced alterations to cancer metabolism

Cancer cells are known to modify their metabolism in response to hostile conditions, such as hypoxia, to switch towards oxygen-independent ATP production and maintain tumour cell proliferation and survival. Increased HIF-1 activity is believed to be the primary mediator of this response, enforcing increased glycolysis for ATP production in the face of reduced oxygen availability and consequent attenuated oxidative phosphorylation[86,192]. HIF-1 is known to directly stimulate increased transcription of glucose transporters GLUT1 and 3 to increase glucose uptake, as well as increasing the expression of nearly all glycolytic enzymes[192,193]. HIF-1 is also known to enhance expression of LDHA, increasing the pyruvate to lactate conversion rate in hypoxia to support continued glycolytic flux through regeneration of NAD^+ as well as maintaining the $NADH/NAD^+$ ratio in the absence of efficient mitochondrial oxidative phosphorylation[81]. Lactate must be rapidly excreted from the cell to prevent inhibition of glycolysis through lactate accumulation, which is supported by the HIF-1-dependent upregulation of monocarboxylate lactate transporters (MCTs)[194]. Not only does this prevent intracellular acidosis (which inhibits glycolysis), but it also acidifies the tumour microenvironment, which has been shown to be beneficial for the tumour by promoting tumour cell invasion and metastasis as well as immune evasion[71,179].

Another function of increased lactate production in hypoxia is to divert pyruvate away from undergoing oxidative phosphorylation in the absence of oxygen as the final electron acceptor in the mitochondrial electron transport chain (ETC), thereby limiting ROS accumulation. HIF-1 also mediates mitochondrial metabolic remodelling to limit carbon entry into the TCA cycle through transactivation of the gene encoding pyruvate dehydrogenase kinase1 (PDK1)[195]. PDK1 phosphorylates the E1α subunit of the PDH

enzyme complex, inactivating PDH and therefore the production of mitochondrial acetyl CoA from glucose[195,196]. This hypoxia-induced metabolic switch thereby supports increased glycolysis for ATP production as well as limiting inefficient mitochondrial pyruvate oxidation and ROS production[195]. However, this reduction in carbon entry into the TCA cycle alters the carbon incorporation intro citrate, thereby reducing the citrate to α-KG ratio. This reduction is believed to trigger altered glutamine metabolism as an alternative means to support production of citrate, which is required to generate acetyl CoA for fatty acid synthesis[197]. It was consequently demonstrated that cells under hypoxia almost exclusively rely on reductive carboxylation of glutamine-derived α-KG, mediated through IDH and aconitase (ACO) enzymes, to support *de novo* lipogenesis[198]. This mechanism additionally allows conservation of glucose for use in other biosynthetic pathways such as the PPP and SSP to generate molecules such as ribose and serine, thereby sustaining continued cell growth in conditions where nutrients are limiting, such as hypoxia[198] (Figure 1.8).

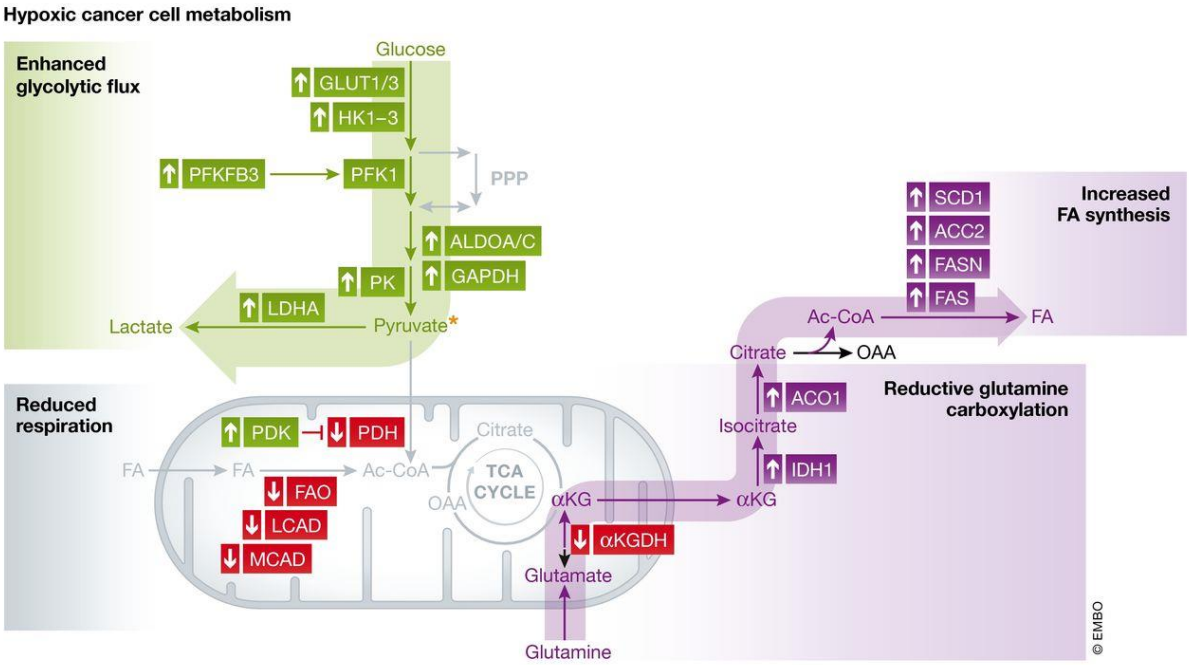

Figure 1.8 Hypoxia-induced changes in cancer metabolism. Hypoxia is known to enhance glycolytic flux through upregulation of glucose transporters GLUT1/3 as well as other glycolytic enzymes (green). As a result high levels of pyruvate are generated and converted to lactate by LDHA, which is also upregulated in hypoxia. Hypoxia is also known to decrease fatty acid oxidation and reduce glucose oxidation through the TCA cycle (grey). Glutamine oxidation is also reduced, diverting glutamine to reductive glutamine metabolism to produce citrate which is used to generate acetyl CoA for increased fatty acid (FA) synthesis (purple). Image from Wong *et al*[199].

1.6.6. Oxidative and endoplasmic reticulum stress in cancer

Metabolic rewiring not only acts to sustain tumour growth, it also prevents oxidative stress inflicted through toxic accumulation of ROS, which ultimately can result in cell death. Oxidative stress occurs when there are perturbations in the oxidant-antioxidant balance, in favour of excessive production of oxidants (ROS) alongside attenuated protective antioxidant mechanisms[200,201]. Tight regulation of cellular stress is therefore crucial for maintaining both healthy and malignant cell survival.

Under physiological conditions, ROS are a natural by-product of aerobic metabolism and at low levels, can act as signalling molecules stimulating and regulating various biological

processes in response to environmental changes, known as redox-signalling[202]. However, major and prolonged disturbances in this balance results in excessive ROS production causing subsequent destructive damage to the cell. The largest contributor to ROS production is through continuous leakage of electrons to oxygen from the mitochondrial ETC during ATP synthesis and it is believed that between 1-5% of oxygen consumed during aerobic metabolism gives rise to superoxide anions (O_2^-)[200]. ROS are subsequently known to be significantly increased in both cancer and under hypoxia, where the reduced availability of O_2 as an electron acceptor in the final stage of electron transport extends the time each electron spends in the chain, exacerbating their leak and therefore the generation of O_2^-[203,204]. ROS are also known to increase stabilisation and activity of HIF-1α, thereby perpetuating the malignant phenotype[200].

In a ploy to maintain cancer cell survival in the face of ROS production, enzymatic and non-enzymatic antioxidant mechanisms are employed to detoxify these reactive molecules such as superoxide dismutases (SODs), that convert superoxide anions to hydrogen peroxide, which is then further reduced to water by catalase and glutathione peroxidase[203]. Non-enzymatic molecules such as ascorbate, carotenoids and flavonoids also act to counteract the harmful effects of free radicals on the cell[203]. However, when the fine balance between oxidants and antioxidants is severely disrupted, H_2O_2 is a potent oxidising agent, capable of reacting with metal ions, such as ferrous iron (Fe^{2+}), to generate hydroxyl radicals (OH•); another highly reactive form of ROS species generated through Fenton chemistry[202,203,205]:

$$Fenton\ Reaction: Fe^{2+} + H_2O_2 \rightarrow Fe^{3+} + OH^- + OH\bullet$$

In addition to mitochondrial oxidative stress, the endoplasmic reticulum (ER) is also a large source of ROS due to the highly oxidised environment which is essential for successful oxidative protein folding and is strictly regulated by the redox state of the microenvironment. Hypoxia and nutrient deprivation are known to disrupt this, inflicting ER stress through impaired protein folding in the ER[205]. Accumulation of misfolded proteins consequently activates the unfolded protein response (UPR) in an attempt to resolve this defect. However, multiple attempts at correctly refolding proteins is a process known to increase ROS production since H_2O_2 is generated as a by-product of constant cycles of disulphide bond breakage and formation[206]. This increased ROS production is known to further exacerbate ER stress causing calcium release and a rise in cytosolic calcium concentration, which results in calcium-mediated calcium release from the second largest intracellular calcium store – the mitochondria. This, in turn, continues the feed-forward effect, further increasing mitochondrial ROS production[206]. This potent loop accentuates both ER and oxidative stress resulting in potentially catastrophic ROS levels in the cell[206]. All of the highly reactive ROS species, but particularly the OH•, can consequently attack and cause oxidation of DNA, protein and lipids, causing irreparable damage and ultimately induction of cell death mechanisms, such as apoptosis, necrosis or autophagy[202,206] (Figure 1.9).

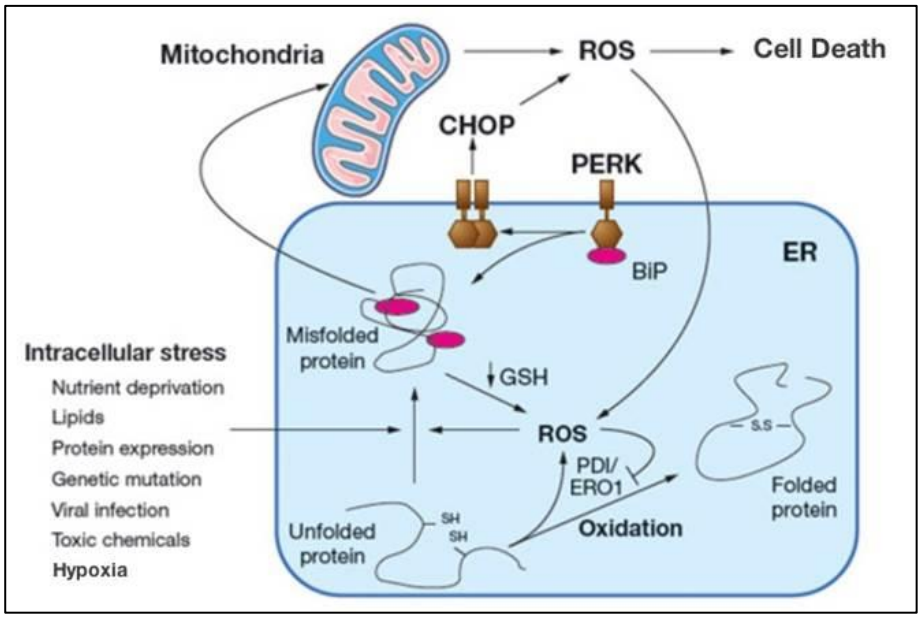

Figure 1.9 Interplay between oxidative stress and ER stress. Intracellular stresses such as hypoxia can generate ROS which can in turn disrupt protein folding in the ER. Protein misfolding can then produce ROS as H_2O_2 is generated as a by-product of protein refolding. This exacerbates ER stress causing Ca^{2+} release which ultimately results in Ca^{2+} release from the mitochondria, further increasing ROS production. ER stress is also known to activate CHOP expression which may lead to a further increase in ROS. This potent loop accentuates both ER and oxidative stress eventually resulting in cell death. Image adapted from Malhotra *et al*[207].

1.7. Thesis aims

Despite recent technological and surgical advancements, glioma patient survival remains incredibly poor. A large contributing factor to this abysmal survival is the severely hypoxic nature of gliomas, which bestows a highly aggressive and therapy-resistant phenotype. It is therefore imperative that pathways involved in gliomagenesis, as well as those that encompass the tumour microenvironment, are identified in the hope to discover more effective therapies to dramatically increase patient survival.

One signalling pathway of interest is YAP/TAZ signalling, with increased activity associated with enhanced cancer growth, invasion, metastasis and chemoresistance. Regulation of YAP/TAZ is incredibly complex, although hypoxia has recently been identified to influence signalling activity in breast cancer and could therefore potentially be observed in other cancers. This thesis therefore aims to investigate this potential hypoxic regulation of YAP/TAZ signalling in an established *in vitro* model of GBM. The challenging nature of the hypoxic tumour microenvironment is also known to contribute towards metabolic reprogramming in order to sustain uncontrolled proliferation and survival in this hostile environment. Integration of both hypoxic metabolism and YAP/TAZ signalling could potentially support this adaptation and so this thesis aims to investigate this potential relationship. Suppression of aberrant YAP/TAZ signalling has become an attractive target to develop novel cancer therapies. As such, the final objective of this thesis is to investigate the repurposing potential of VP – a recently identified YAP inhibitor – with the hope of identifying a potential new therapeutic for highly hypoxic and therapy-resistant gliomas.

Chapter 2:

Materials and Methods

2.1. Cell culture

2.1.1. Immortalised cell lines

Table 2.1 shows an outline of the four immortalised human glioma cell lines selected for this investigation.

Cell line	U87	U343	HOG IDH1 Wild-type (WT)	HOG IDH1 Mutant (MUT)
Representative Subtype/ Glioma Grade	Grade IV Glioblastoma	Classical; Grade IV Glioblastoma	Grade III anaplastic oligodendrogl-ioma	Grade III anaplastic oligodendrogl-ioma
Representative Mutation/ Characteristic	-	High EGFR expression	Expression of IDH1 WT enzyme	Mutation in IDH1 enzyme (R132H)

Table 2.1 Glioma cell line characteristics. Four main glioma cell lines were used throughout this investigation. U343 cells are known to exhibit amplified EGFR expression which is representative of the classical GBM subtype, as outlined by the Verhaak classification system[24]. The HOG cells have been engineered to express either wild-type (WT) or mutant (MUT; R132H) IDH1 enzyme.

U87 (300367) and U343 (300365) cell lines were obtained from CLS Cell Lines Service GmbH (Germany). U343 cells were known to have high EGFR expression, which is typical of the classical subtype of GBM (Figure 2.1A). The HOG (Human OligodendroGlioma) cells, kindly donated by Professor Hai Yan, were derived from a grade III human oligodendroglioma and infected with a lentivirus to stably express either wild-type (WT) or mutated (MUT) IDH1 (R132H)[208]. The cells were routinely assessed via western blotting to ensure stable expression of mutant IDH1 (Figure 2.1B).

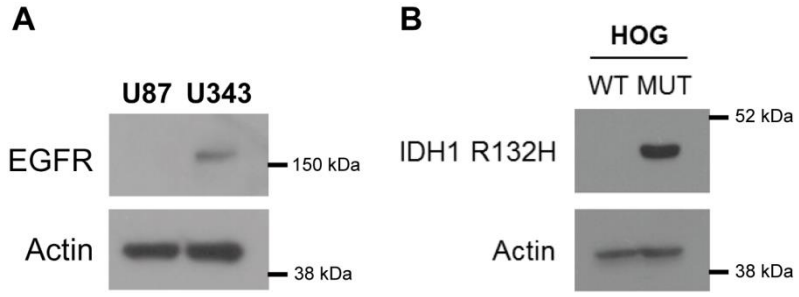

Figure 2.1 Expression of EGFR and IDH1 R132H in glioma cell lines.

Additional glioma lines U87 WT and MUT IDH1 (R132H), LN18 WT and MUT IDH1 (R132H) and LN18 WT and MUT IDH2 (R172K) were previously derived as outlined in Hollinshead *et al*[209]. Melanoma cell line, A375 (ATCC® CRL-1619™) was obtained from ATCC.

All cell lines were cultured under standard conditions (37°C, 5% CO_2) using Dulbecco's Modified Eagle Medium High Glucose with L-Glutamine (DMEM; Sigma Aldrich, D5796) supplemented with 10% Foetal Bovine Serum (FBS; Hyclone Thermo Scientific, SV30160.03). Cells were subject to routine mycoplasma testing using the EZ-PCR Mycoplasma Test Kit (Geneflow, K1-0210) to ensure no contamination.

For hypoxia studies, cells were cultured at 21% O_2 and then for each experiment transferred to the Whitley H35 Hypoxystations (Don Whitley Scientific) set to 1% and 0.3% O_2 for the stated amount of time, unless otherwise identified.

It should be noted that cell density is an important and defined regulator of YAP/TAZ, with high cell densities causing inactivation of YAP/TAZ activity[124]. As such, the *in vitro* cell densities used throughout this investigation were determined so that the cells were

approximately 50-70% confluent at the time of use, in order to minimise the risk of under- or over-stimulating YAP/TAZ activity during experiments.

2.1.2. Cell lines derived from patient tumours

2.1.2.1. Patient information

GBM cell lines, T1 and T2, were derived from a single surgical specimen excised in November 2014 from a 32 year old male diagnosed with GBM at the Queen Elizabeth Hospital Birmingham (QEHB) NHS Foundation Trust. The patient had previously undergone a right temporal craniotomy in March 2014 followed by cranial radiotherapy over 6 weeks to 54 Gy in 30 fractions with continuous oral TMZ. This was followed by a course of 5/30 adjuvant TMZ in July 2014. Immediate 'post-op' imaging showed two distinct areas/foci of residual tumour medial and lateral in the right temporal lobe (Figure 2.2). Follow-up MRI imaging in October 2014 showed that one area (labelled 'A'; from which T1 was derived) had increased in size, while the other (labelled 'B'; from which T2 was derived) was around the same size as when previously imaged suggesting a therapeutic response in one area but not the other. During reoperation in November 2014 samples were removed from sites 'A' and 'B' for derivation of cell lines – T1 (deemed more therapy-resistant due to its recurrent growth) and T2 (suggested more therapy-sensitive), respectively.

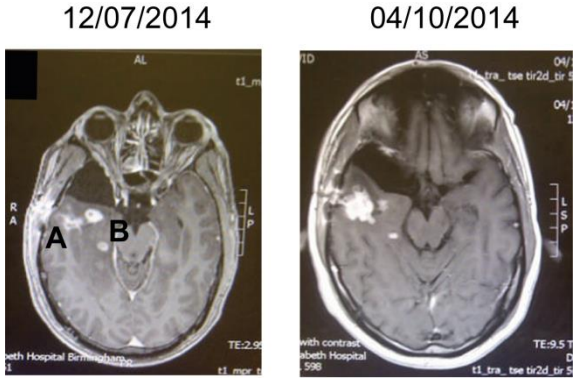

Figure 2.2 MRI scans from GBM patient showing progression of therapy-resistant foci A but not of therapy-responsive foci B. Images courtesy of Prof. G. Cruickshank.

The use of patient material was approved by the Human Biomaterials Resource Centre (HBRC) at the University of Birmingham (UoB; research project number 13-165) and the reference committee for ethical approval 15/NW/0079 (NRES Committee North West-Haydock). All patients provided full, informed, written consent as per the Declaration of Helsinki. Histopathological analysis of the tumour biopsy was conducted by the pathology department at QEHB and consequently given a tumour grade in accordance with the 2007 WHO classification system[9]. Following grading, the biopsies were processed and anonymised at the HBRC after which a piece of the biopsy was flash frozen. Primary cell lines were derived from the remaining biopsy through mechanical and enzymatic dissociation of the solid piece.

2.1.2.2. Primary cell line generation

Firstly, under sterile conditions, the tumour piece was placed into a petri dish and washed three times using 1x sterile phosphate buffered saline (PBS). Following washing, the tumour was dissected using a scalpel. The dissected pieces were transferred into a 50 ml Falcon tube, washed again with 1x PBS and then centrifuged (230 x g, 5 min) in 5 ml 1x PBS at room temperature (RT). The PBS was then carefully removed, ensuring

that the pieces were not disrupted, after which the washing and centrifugation was repeated. For enzymatic digestion, 5 ml of TrypLE ^{TM} Express (Gibco; 12605-10) was incubated with the pieces at 37°C for 10 min. Following digestion, the trypsin was neutralised with 10 ml of DMEM High Glucose with L-Glutamine (Sigma-Aldrich; D5796) and then centrifuged at 230 x g for 5 min at RT. The media was removed and the pieces were resuspended in 15 ml of DMEM with added antibiotics and fungicide (1% Penicillin/Streptomycin, 0.1% Gentamycin and 1% Amphotericin B; Sigma-Aldrich). The tumour pieces were mechanically dissociated by repeated pipetting until a homogenous solution was achieved. This cell suspension was then seeded onto flasks and cultured at the required oxygen tensions.

2.1.3. Spheroid culture

In addition to culturing the cells as adherent monolayers, U87 and U343 cells were grown in spontaneous cellular aggregates known as spheroids. This 3D culture method allows spatial and temporal organisation of cell growth, creating a metabolite, nutrient and oxygen gradient across the spheroid similar to that witnessed in *in vivo* tumours.

Spheroids were cultured on 0.5% agarose coated plates using the liquid-overlay method[210]. Firstly, 6-well plates were coated with a layer of 0.5% low-melting point agarose (Promega, V2111) in DMEM, which had been pre-heated to 60°C. Of this solution, 2 ml was added to each well of a 6-well plate and left to solidify at 4°C. Following plate preparation, $1.8x10^5$ cells were seeded onto each well with a total media volume of 2 ml, creating the aqueous overlay in which the spheroids formed. The plates were then incubated under standard conditions and left undisturbed until further use.

2.1.3.1. VP treatment of spheroids (Chapter 4)

To establish the effect of VP on spheroid formation and growth, spheroids were treated with vehicle (0.2% DMSO), 1, 3, 5 and 10 μM VP 2 h following cell seeding. The spheroids were left for 24 and 48 h undisturbed in the incubator. Images were then taken after the stated incubation time using the Leica DFC290 HD camera (20x objective). For quantitative analysis, spheroid images were imported into Image J (NIH) and two perpendicular diameters were measured and a mean diameter recorded for each complete, singular spheroid. It should be noted that an assumption has been made in the analysis that the spheroids were perfectly circular therefore two perpendicular diameters were recorded taking into consideration the smallest and widest parts of the spheroid. Any aggregated spheroids were excluded from analysis.

To assess long-term VP treatment, spheroids were also imaged following 1-10 μM VP treatment for 7 days. To investigate the effect of VP on fully formed spheroids, cells were seeded onto the agarose coated plates and left for 7 days to form, after which the spheres were treated with 5 μM VP and incubated for 24-168 h. Images were taken periodically every 24 h to assess spheroid morphology.

2.2. Chemicals

Unless otherwise stated, the following treatment conditions used during this investigation are summarised in Table 2.2. Drug concentrations were determined based upon dose-response curves (data not shown) and previous literature.

Drug	Abbreviation	Concentration	Product Information
ALLN	N/A	10 μM	VWR International, 208719
Chloroquine	CQ	10 μM	Sigma-Aldrich, C6628
Cyclosporin A	CsA	15 μM	Cayman Chemical, 12088
Dimethyloxalylglycine	DMOG	1 mM	Cayman Chemical, 71210
Dimethyl Sulfoxide	DMSO	Vehicle	Fisher, BP231-1
Eeyarestatin-1	Eer1	1 and 3 μM	Tocris Bioscience, 3922
Ferric Chloride Hexahydrate	$FeCl_3/Fe^{3+}$	3-500 μM	Sigma-Aldrich, F-2877
Hydrogen Peroxide	H_2O_2	50 and 100 μM	Sigma-Aldrich, 31642
Iron (II) Chloride Tetrahydrate (Ferrous Chloride)	$FeCl_2/Fe^{2+}$	3-500 μM	Honeywell Fluka, 44939
Magnesium Chloride	$MgCl_2/Mg^{2+}$	3-500 μM	Fisher, BP214-500
Methanol	MeOH	Vehicle	VWR Chemicals, 20847.307
Necrostatin-1	Nec-1	50 μM	Cayman Chemical, CAY11658-5
Pifithrin-α	PFT-α	30 μM	Tocris Bioscience, 1267
Protoporphyrin IX	PPIX	5 μM	Sigma-Aldrich, 258385
Verteporfin	VP	1-30 μM	Tocris Bioscience, 5305
Zinc Chloride	$ZnCl_2/Zn^{2+}$	3-500 μM	Alfa Aesar, A16281
Zinc Protoporphyrin	ZnPP	5 μM	Alfa Aesar, 32068
carbobenzoxy-valyl-alanyl-aspartyl-O-methyl-fluoromethylketone	Z-VAD-FMK/Z-VAD	20 μM	Sigma-Aldrich, V116
2',7'-Dichlorofluorescin Diacetate	DCFDA	20 μM	Sigma-Aldrich, D6883
4-Hydroxy-TEMPO	TEMPOL/TPL	3 mM	Sigma-Aldrich, 176141

Table 2.2 Details of reagents used in this investigation.

All experiments involving VP were conducted in the dark (by the use of aluminium foil).

2.3. Sulforhodamine B assay

Cells were fixed by adding 20% (v/v) ice-cold trichloroacetic acid (final concentration 25%; Sigma-Aldrich, T0699) directly to the media and incubated at 4°C for 30 min. The solution was then carefully removed and plates were washed three times with dH_2O and left to air-dry. Once dry, the intracellular protein was stained with 0.4% (w/v) sulforhodamine B (SRB; Sigma-Aldrich, 230162) in 1% acetic acid for 10 min at RT. SRB solution was removed and wells were washed three times with 1% acetic acid to reduce any non-specific staining. After drying at RT, SRB was dissolved using 50 mM Tris/HCL pH 8.8 and 100 µl per well was aliquoted into a 96-well plate. The absorbance was then quantified at 495 nm on FLUOstar OMEGA microplate reader (BMG LabTech). Absorbance values were corrected for background absorbance using 50 mM Tris/HCL pH 8.8 as a blank. Unless otherwise stated, final values were then normalised in each experiment to the vehicle for each oxygen tension.

2.3.1. Cell proliferation assay (Chapter 3)

U87 and U343 cells were seeded at $3x10^4$ cells on 24-well plates and left to settle overnight under standard conditions. The following day, the plates were either kept at 21% O_2 or moved to 1% or 0.3% O_2 and cultured for a further 24, 48 and 72 h. At each time point cells were fixed for SRB analyses. A time-zero plate was fixed when the plates were transferred into hypoxia to use as the control for all conditions. Data was normalised to the time-zero control plate.

2.3.2. Determining VP dosage and treatment time (Chapter 4)

For determining the dosage and treatment time of VP, U87 and U343 cells were seeded at $3x10^4$ cells on 24-well plates and left to adhere overnight under standard conditions.

The following day, cells were treated with either vehicle (control; 0.2% DMSO) or 1, 3, 5 and 10 μM VP and incubated under standard conditions. Cells were then fixed and processed via SRB assay 24, 48 and 72 h post VP-treatment. Cell number was recorded and normalised to the vehicle control for each time point.

For hypoxic cell viability, cells were seeded and treated as aforementioned before being incubated in 21% and 1% O_2 for 24 h. Cell viability was then measured via SRB and normalised to the vehicle control for each oxygen tension. Representative images were taken using the Leica DFC290 HD camera (20x objective).

2.3.3. Cell viability following treatment with porphyrins (Chapter 4)

To compare cell viability following VP treatment to other members of the porphyrin family, U87, U343 and A375 cells were seeded at $3x10^4$ cells on 24-well plates and left to adhere overnight under standard conditions. Cells were treated the next day with either vehicle (control; 0.1% DMSO) or 5 μM VP, PPIX or ZnPP in both 21% and 1% O_2 for 24 h. Primary GBM cell lines T1 and T2, HOG IDH1 WT and MUT, and LN18 IDH1 and IDH2 WT and MUT cells were also seeded onto 24-well plates at $3x10^4$ cells/well and treated with 5 μM VP for 24 h in 21% and 1% O_2. Cell viability was recorded using SRB assay. Data was normalised to vehicle control for each oxygen tension. For IDH1 and IDH2 WT and MUT cell lines, data was also normalised to the normoxic WT control.

2.3.4. Cell viability following VP treatment when exposed to light (Chapter 4)

U87 and U343 cells were seeded at $3x10^4$ cells on 24-well plates and left to adhere overnight under standard conditions. Cells were treated the next day with either vehicle (control; 0.1% DMSO) or 5 μM VP for 4 or 24 h in both 21% and 1% O_2. In the 4 h VP

condition, the media was removed and replaced with fresh DMEM for the remaining 20 h. For cells in the dark condition, the plates were kept obscured from ambient light as best possible during media replacement, whereas cells in the light condition were exposed to ambient light while the media was changed. Viability was measured using SRB assay.

2.3.5. Cell viability following VP and DMOG treatment (Chapter 4)

U87 and U343 cells were seeded at $3x10^4$ cells on 24-well plates and left to adhere for up to 8 h before being treated with 1 mM DMOG overnight under standard conditions. The following morning, cells were treated with either vehicle (control; 0.1% DMSO) or 5 μM VP for 4 h in both 21% and 1% O_2 before cell viability measured via SRB.

2.3.6. Cell viability following treatment with VP and cell death inhibitors (Chapter 4)

U87 and U343 cells were seeded at $3x10^4$ cells on 24-well plates and left to adhere overnight under standard conditions. Cells were treated the next day with either vehicle (control; 0.1% DMSO), 5 μM VP or 5 μM VP in combination with either 20 μM Z-VAD-FMK, 10 μM ALLN, 15 μM CsA, 50 μM Nec-1, 30 μM PFT-α, 10 μM CQ or 1 and 3 μM Eer1 for 24 h in both 21% and 1% O_2. Cells were also treated with inhibitor alone. Cells were pre-treated with the inhibitors for 1 h prior to VP addition. Cell viability was measured via SRB as aforementioned.

2.3.7. Cell viability following VP and anti-oxidant treatment (Chapter 4)

U87 and U343 cells were seeded at $3x10^4$ cells per 24-well plate and left to adhere overnight under standard conditions. The following day, cells were pre-treated with 3 mM

4-hydroxy-TEMPO (TEMPOL) for 2 h before being treated with 5 μM VP for 24 h in both 21% and 1% O_2. Cell viability was then measured via SRB.

2.4. Cell proliferation assay (Chapter 4)

U87 and U343 cells were seeded at $3x10^4$ cells in 24-well plates and left to settle for 4 h under standard conditions. VP (1-10 μM) was then added and the cells were cultured for up to 96 h. Cells were trypsinised (10 min, 37°C) and manually counted using chamber slides 24, 48, 72 and 96 h post VP-treatment. An average was taken from two cell counts for each VP concentration recorded at each time-point. Representative images were taken using the Leica DFC290 HD camera (20x objective).

2.5. Quantitative polymerase chain reaction (qPCR)

RNA was extracted using the RNeasy Mini Kit in accordance with the manufacturer's protocol (Qiagen, UK; 74104). A total of 1 μg RNA was transcribed using the Reverse Transcription System kit (Promega, UK; A3500). qPCR was performed on AB 7500 Real Time PCR System using the TaqMan® gene expression master mix (Applied Biosystems, UK). The following probes were used: *BBC3* (HS00248075_m1), *BNIP3* (HS00969291_m1), *CTGF* (HS01026927_g1), *CYR61* (HS00998500_g1), *SLC2A1* (GLUT1; HS00892681_m1), *VEGF-A* (HS00900055_m1) and *YAP1* (HS00902712_g1) (Thermo Fisher Scientific, UK). Gene expression levels were normalised to *ACTB* (Actin; HS01060665_g1). Relative expression levels were calculated using the $2^{-\Delta\Delta CT}$ method and compared to the relevant 21% O_2 control.

2.6. Protein analysis of cells under hypoxia (Chapter 3)

U87 and U343 cells were seeded at $2x10^5$ cells per 6-well and left to settle overnight under standard conditions. The following day, the cells were transferred to 1% or 0.3% O_2 for up to 24 h. Cells were lysed at the time-points 2, 4, 6, 8 and 24 h into 100 µl 1x Laemmli buffer (Sigma-Aldrich, S3401-1VL). Cells cultured under 21% O_2 for 24 h were used as a control. Samples were then stored at -20°C for western blotting.

To analyse TAZ expression under hypoxia, U87 and U343 cells were seeded at $6x10^4$ cells on 12-well plates and left to settle overnight. The following morning cells were either left under 21% O_2 or transferred to 1% O_2 for 24 h, after which cells were harvested for western blotting.

For analysis of protein expression of phosphorylated YAP (p-YAP) and YAP1 in T1 and T2 primary cells, protein was extracted from cells that had been cultured long-term under hypoxic conditions for four passages. Cells were seeded under hypoxic conditions at $3x10^5$ cells onto 10 cm plates and harvested 48 h later.

2.7. Western blotting

2.7.1. Protein preparation

To prepare samples for western blotting, cells were washed with 1x PBS and scraped directly into 100 µl 1x Laemmli buffer (Sigma-Aldrich, S3401-1VL) unless otherwise stated.

2.7.2. SDS-PAGE gel electrophoresis, protein transfer and antibody incubation

Extracted protein was heated to 95-100°C for 10 min and then placed on ice prior to loading on a polyacrylamide gel for sodium dodecyl sulphate polyacrylamide gel electrophoresis (SDS-PAGE). Proteins were resolved under reducing denaturing conditions at 120-150 V using the mini-PROTEAN Tetra System (BIO-RAD). Proteins were then transferred to 0.1 µm nitrocellulose membrane (GE Healthcare, 10600000) using either wet transfer at 100 V for 1.5 h or via dry transfer using the iBlot® gel transfer system (Invitrogen) and iBlot® gel transfer nitrocellulose stacks (Invitrogen, IB301001) for 7 min. Membranes were then blocked in 5% non-fat skimmed dried milk powder (Marvel) in 1x PBS-0.05% Tween (PBS-T) for 1 h at RT. All antibodies (Table 2.3) were diluted in either 5% milk PBS-T or 5% bovine serum albumin (BSA; Sigma-Aldrich, A7906) -PBS-T depending on antibody specification. Membranes were cut and incubated with the appropriate primary antibody overnight at 4°C (except for Anti-Actin which was incubated for 1.5 h at RT). Following incubation, membranes were washed three times with PBS-T and incubated with the appropriate Horseradish peroxidase (HRP)-conjugated secondary antibody for 1 h at RT (Table 2.4). The membranes were then washed three times for 15-30 min and developed using the EZ-ECL enhanced chemiluminescence detection kit (BI, 20-500-120). Proteins were visualised on High Performance Chemiluninescence Hyperfilm™ (Amersham, 28906836) using the Ecomax X-Ray film processor (Protec, 1186-3-4000).

2.7.2.1. Western blot antibodies

The following primary antibodies listed in Table 2.3 were used in this investigation.

Antibody	Dilution	Molecular Weight (kDa)	Species	Product Information
Anti-Actin	1:4000	42	Mouse	Sigma-Aldrich, A4700
Anti-β-Tubulin	1:5000	50	Rabbit	Cell Signaling, #2128
Anti-Connective Tissue Growth Factor (CTGF)	1:500	~38	Rabbit	Cusabio, CSB-PA09429A0Rb
Anti-Epidermal Growth Factor Receptor (EGFR)	1:500	170	Rabbit	Santa Cruz, sc-03
Anti-Glial Fibrillary Acidic Protein (GFAP)	1:1000	~55, 48	Rabbit	Abcam, ab7260
Anti-Glutaminase 1 (GLS1)	1:1000	~76	Rabbit	Abcam ab156876
Anti-HIF-1α	1:500	~120	Mouse	BD Transduction, 610959
Anti-Isocitrate Dehydrogenase 1 (IDH1) R132H	1:500	47	Mouse	Dianova, DIA H09
Anti-phosphorylated YAP (S127)	1:1000/1:2000	~65-75	Rabbit	Cell Signaling, #4911
Anti-YAP1	1:1000	~65-75	Mouse	Abcam, ab56701
Anti-YAP1 (EP1674Y)	1:25,000	~70	Rabbit	Abcam, ab52771
Anti-WWTR1 (TAZ)	1:1000	~50	Rabbit	Atlas Antibodies, HPA007415

Table 2.3 Primary antibodies used for western blotting.

The following secondary antibodies outlined in Table 2.4 were also used.

Antibody	Dilution	Molecular Weight (kDa)	Species	Product Information
Anti-mouse IgG HRP-Linked Secondary	1:4000	-	Mouse	Cell Signaling, #7076
Anti-rabbit IgG HRP-linked Secondary	1:4000	-	Rabbit	Cell Signaling, #7074

Table 2.4 Secondary antibodies used for western blotting.

Densitometry was performed using Fiji software[211]. Samples were normalised within each biological experiment and expressed as a percentage of the control.

2.8. Co-immunoprecipitation

2.8.1. Preparing cell lysates

U343 cells were seeded at $4x10^6$ cells/15 cm dish and cultured overnight. The following day, cells were treated with either vehicle (0.1% DMSO) or 5 μM VP in both 21% and 1% O_2 for 4 h. After treatment, the media was removed and cells were washed twice with ice-cold 1x PBS. The PBS was removed and 1 ml of immunoprecipitation (IP) buffer (50 mM Tris-HCl pH 7.4, 150 mM NaCl, 5 mM EDTA, 0.1% IGEPAL and 1x protease inhibitor cocktail (Sigma-Aldrich, P8340)) was added. Cells were then scraped into an Eppendorf before being placed on ice for 20 min and then centrifuged for 20 min at 13,000 RPM, 4°C. The supernatant was then aliquoted into a fresh tube and protein concentration was determined using a bicinchoninic assay (BCA) following the manufacturer's protocol (Thermo Fisher Scientific, 23227).

2.8.2. Co-immunoprecipitation

Primary antibody (YAP1, ab52771; 1:70 dilution) was added to 200 μg cell lysate per condition into an Eppendorf and incubated with rotation overnight at 4°C. A sample of the undiluted cell lysate was kept aside as the whole cell input for western blotting. Volumes were kept consistent between samples with addition of IP buffer.

Following overnight incubation, 30 μl of the 50% Protein G agarose bead slurry (Cell Signaling, #37478) was added to the lysate-antibody mix and incubated for 3 h under rotation at 4°C. Afterwards, samples were microcentrifuged for 30 sec followed by removal of the supernatant, which was kept in case of future use. The bead pellet was then washed five times on ice with 500 μl of IP buffer to remove any non-specific binding. Following washing, the bead pellet was resuspended in 20 μl of 2x Laemmli buffer and

heated to 95-100°C for 5 min before centrifugation for 1 min at 14,000 x g. Samples were then subjected to western blotting, as described previously, and probed for the protein of interest.

2.9. Immunocytochemistry (ICC)

Post treatment, cells were immediately fixed with 4% paraformaldehyde (PFA) for 15 min, followed by quenching with 0.1 M glycine-PBS for 5 min. Cells were then washed twice with 1x PBS and permeabilised with 0.1% Triton-X-100 for 5 min. Cells were then incubated with primary antibody (Table 2.5) for 1.5-2 h. Following incubation, cells were washed twice and incubated with secondary antibody (Table 2.6) for 1 h at 4°C. Afterwards, cells were washed twice and incubated with Hoechst 33342 for 20 min at RT to stain the nuclei. Cells were then washed and fixed onto microscope slides using Mowiol (Sigma, 81381). Images were then taken using a ZEISS LSM 780 confocal microscope using the Plan-Apochromat 100x/1.4 Oil DIC objective (1024 x 1024 pixels; 8-bit). The pinhole was set at 100 µm and the gain was adjusted for each cell line using the range indicator on the brightest sample for each channel. These parameters were then kept consistent across all samples and experiments using that antibody. Pseudo-colouring was applied to images using Zen 2012 SP1 software (ZEISS; black-edition, version 8.1): UV channel (blue), 488 channel (green) and 633 channel (red).

2.9.1. Immunochemistry antibodies

Table 2.5 lists the primary antibody and dilution used in this investigation. All primary and secondary antibodies were made in 5% BSA-PBS-T.

Antibody	Dilution	Species	Production Information
Anti-Calreticulin (CRT)	1:100	Rabbit	Cell Signaling, #12238
Anti-p73 (EPR18409(T)(MIX))	1:100	Rabbit	Abcam, ab189896
Anti-SQSTM1/Anti-p62	1:100	Rabbit	Abcam, ab91526
Anti-YAP1	1:100	Mouse	Abcam, ab56701
Anti-YAP1 (EP1674Y)	1:100	Rabbit	Abcam, ab52771
Anti-YAP1	1:100	Mouse	Abcam,ab56701
Anti-8OHdG	1:100	Rabbit	Abcam, ab62623

Table 2.5 Details of primary antibodies used for ICC.

The following secondary antibodies and additional stains used in this investigation are listed in Table 2.6.

Antibody	Dilution	Species	Excitation Laser	Fluorophore Spectral Range (nm)	Pseudo colour	Product Information
Alexa fluor® 488 goat anti-mouse IgG (H+L)	1:100	Mouse	488	Ex_{Max}- 500 Em_{Max}- 520	Green	Thermo Fisher, A-11001
Alexa fluor® 488 goat anti-rabbit IgG (H+L)	1:100	Rabbit	488	Ex_{Max}- 500 Em_{Max}- 520	Green	Thermo Fisher, A-11034
Anti-Hoechst 33342 (NucBlue® fixed cell stain ready probes™)	2 drops/ml	-	343	Ex_{Max}- 343 Em_{Max}- 483	Blue	Life Technologies, R37606
DyLight 649 horse anti-mouse IgG (H+L)	1:100	Mouse	633	Ex_{Max}- 655 Em_{Max}- 670	Red/ Magenta	Vector Laboratories, DI-2649
DyLight 649 horse anti-rabbit IgG (H+L)	1:100	Rabbit	633	Ex_{Max}- 655 Em_{Max}- 670	Red/ Magenta	Vector Laboratories, DI-1649

Table 2.6 Secondary antibody and additional stains used for ICC.

2.9.2. Hypoxic YAP expression (Chapter 3)

U87 and U343 cells were seeded at a density of $1.5x10^5$ per coverslip and left to settle overnight under standard conditions. Cells were then incubated the following day at

either 21% or 1% O_2 for 4 and 8 h. Cells were then fixed for ICC and stained for YAP1 expression.

2.9.3. VP timecourse (Chapter 4)

U87 and U343 cells were seeded at a density of $1.5x10^5$ per coverslip and left to settle overnight under standard conditions. Cells were then treated the following day with either vehicle (0.1% DMSO) or 5 μM VP and incubated at either 21% or 1% O_2 for 1, 2, 4, 6 and 8 h. Cells were then fixed for ICC and stained for YAP1 expression. Cells were also co-stained for p73 expression 4 and 8 h post VP-treatment.

2.9.4. p62 (Chapter 4)

U87 and U343 cells were seeded at a density of $1.5x10^5$ per coverslip and left to settle overnight under standard conditions. Cells were then treated the following day with vehicle (0.1% DMSO) or 5 μM VP for 4 h in both 21% and 1% O_2. Cells were then dual stained for both YAP1 and p62 expression.

2.9.5. Z-VAD-FMK (Chapter 4)

U87 and U343 cells were seeded at a density of $1.5x10^5$ per coverslip and left to settle overnight under standard conditions. Cells were then treated the following day with vehicle (0.1% DMSO), 5 μM VP, 5 μM VP and 20 μM Z-VAD-FMK or 20 μM Z-VAD-FMK only for 8 h in both 21% and 1% O_2. Cells were initially pre-treated with Z-VAD-FMK for 2 h prior to VP addition. Following treatment cells were processed for ICC and stained for YAP1 expression.

2.9.6. Calreticulin (CRT)(Chapter 4)

U87 and U343 cells were seeded at a density of $1.5x10^5$ per coverslip and left to settle overnight under standard conditions. Cells were then treated the following day with vehicle (0.1% DMSO) and 5 μM VP for 2 h at either 21% or 1% O_2. After treatment, cells were dual-stained as described above for YAP1 (mouse) and CRT for 1.5-2 h. Cells were then imaged using confocal microscopy as aforementioned.

2.9.7. Eeyarestatin-1 (Eer1)(Chapter 4)

U87 cells were seeded at a density of $1.5x10^5$ per coverslip and left to settle overnight under standard conditions. Cells were then treated the following day with vehicle (0.1% DMSO), 5 μM VP, 5 μM VP and 1 μM Eer1 or 1 μM Eer1 only for 4 h at either 21% or 1% O_2. Cells were pre-treated with Eer1 for 1 h prior to VP addition. Following treatment, cells were processed for ICC and stained for YAP1 expression.

2.9.8. 8-OHdG (Chapter 4)

U87 and U343 cells were seeded at a density of $2x10^5$ per coverslip and left to settle overnight under standard conditions. Cells were then treated the following day with vehicle (0.1% DMSO), 5 μM VP or 100 μM H_2O_2 for 2 h at either 21% or 1% O_2. Following treatment, cells were stained with Anti-8-hydroxydeoxyguanosine (8-OHdG) and imaged according to previously aforementioned.

2.9.9. Analysis of nuclear fluorescence

To analyse YAP1 nuclear expression, confocal images were imported into Image J (NIH). Using the freeform line tool, an outline was drawn around the nucleus and the following measurements taken; AREA, INTEGRATED DENSITY and MEAN GRAY

VALUE. Background fluorescence measurements were taken the same way by selecting three areas surrounding the cell. The following formula was then used to determine the corrected total nuclear fluorescence (CTNF) for each cell[212]:

CTNF= Integrated Density – (Area of selected cell X Mean fluorescence of background)

The integrated density determines the sum of all the pixels within a region to give a total fluorescence value, as opposed to an average fluorescence intensity. The CTNF further takes into account the area of the nucleus as smaller nuclei may appear to have higher levels of staining compared to a larger nucleus however this could be just down to its smaller size. To remove bias during cell imaging, areas of cells were selected at random using the Hoechst 33342 channel to discourage selecting for cells with the brightest YAP1 expression. During image analysis, only cells with complete nuclei present in each image were analysed for nuclear fluorescence.

2.10. Gene Silencing

2.10.1. Knockdown of YAP and TAZ

For experiments investigating the effect of knockdown of Hippo pathway genes YAP and TAZ, cells were seeded onto 12-well plates – U87 cells were seeded at a total density of $3x10^4$ and U343 at $4x10^4$ cells per well. Cells were cultured overnight under standard conditions and the following day were transfected with small-interfering RNA (siRNA). According to manufacturer's instructions, ON-TARGETplus SMARTpool human non-targeting RNA (siNT; Dharmacon, D-001810-10) and siRNA targeting YAP (siYAP; Dharmacon, L-012200-00), TAZ (siTAZ/siWWTR1; Dharmacon, L-016083-00) and both

YAP and TAZ together (siYAP/TAZ) were transfected at 25 nM using DharmaFECT 1 transfection reagent (Thermo Fisher Scientific, T2001). Target sequences for YAP1 and TAZ can be viewed in Appendix 1. The amount of DharmaFECT 1 reagent used per well had been optimised at 2 µl/ 12-well and 4 µl/ 6-well. Cells were then incubated at either 21% or 1% O_2 for 72 h post-transfection and subsequently processed for western blotting to assess protein knockdown and SRB analysis to assess cell proliferation.

2.10.2. Knockdown of YAP and TAZ for metabolic analysis (Chapter 3)

U343 cells were seeded at $2.5x10^5$ cells per 6-well and left to settle overnight under standard conditions. The following day, cells were transfected with siNT, siYAP, siTAZ and siYAP/TAZ as described above. Cells were left for 48 h before being used for metabolic tracing analysis.

2.10.3. VP treatment following YAP/TAZ knockdown (Chapter 4)

For experiments investigating the effect of VP on cell viability following YAP and TAZ knockdown, cells were seeded onto a 6-well plate (U87 at $3x10^5$ cells/well and U343 at $3.5x10^5$ cells/well) and cultured for 24 h. Cells were then transfected with siRNA as previously described and cultured under standard conditions. 24 h post-transfection, cells were re-plated onto 24-well plates at a density of $3x10^4$ cells per well and cultured for a further 24 h under standard conditions. The following day cells were treated with either vehicle (0.1% DMSO) or 5 µM VP and incubated at either 21% or 1% O_2 for 24 h. Post-treatment period, cells were then fixed and analysed using the SRB method.

2.10.4. Knockdown of HIF-1α (Chapter 4)

For knockdown of HIF-1α, cells were seeded at $3x10^4$ cells/12-well and left to settle overnight. The following day, cells were transfected with 25 nM siNT or siHIF-1α (Dharmacon, L-004018-00) according to manufacturer's instructions. Cells were then cultured for 48 h before being treated with either vehicle (0.1% DMSO) or 5 μM VP and incubated at either 21% or 1% O_2 for 24 h. Post-treatment period, cells were then fixed and analysed using the SRB method.

In all biological experiments, protein was harvested to ensure proper gene silencing.

2.11. Protein over-expression

Overexpression of a triple mutant form of HIF-1α (HIF1αTM)[213] was used which confers HIF-1α stabilisation under normoxic conditions, when the protein would normally be rapidly degraded. U87 cells were seeded at $4x10^4$ cells on 24-well plates and left to adhere. Cells were then transfected 24 h post-seeding with 3 μg of HIF1αTM plasmid using DharmaFECT kb transfection reagent (Dharmacon, T-2006-01) according to the manufacturer's protocol. Cells were then treated with 5 μM VP 24 h post-transfection for 4 h in 21% O_2. Cells were analysed 28 h post-transfection via SRB assay. Protein was also harvested to confirm HIF-1α expression in normoxia.

2.12. Metabolic tracing analysis

Metabolite labelling using stable isotope tracers is an effective technique to assess changes in metabolic pathway activity. ^{13}C-enriched tracers such as glucose and glutamine are added to the culture medium for a set period of time until isotopic steady state has been reached. For glycolysis this can typically be achieved in ~10 minutes,

TCA metabolites ~2-3 hours and nucleotides ~24 hours[214]. When a labelled substrate is metabolised by the cell, enzymatic reactions result in the rearrangement of carbon atoms incorporated in the downstream metabolites, resulting in a distinctive labelling pattern which can be used to infer the relative activity of metabolic pathways[215]. Analytical techniques such as gas chromatography-mass spectrometry (GC-MS), can determine the metabolite isotopomer distribution (MID) in each metabolite, which refers to the shift in mass of a metabolite as a result of the incorporation of ^{13}C isotopes. Typically, these are defined as M+0, M+1, M+2 to M+*n*, where M is the base mass of an ion fragment and the following number 0 to *n* refers to the mass shift from M as a result of the number of ^{13}C carbon atoms incorporated[216]. Consequently, the sum of all the fractions from M+0 to M+*n* is 100%[217]. For accurate labelling determination from ^{13}C isotopic tracers, the MIDs must also be corrected for natural isotope abundance.

2.12.1. Addition of tracer

Following transfection with siNT, siYAP, siTAZ and siYAP/TAZ for 48 h (outlined in section 2.10.2), the media was changed to basic formulation DMEM (Sigma-Aldrich D5030) containing 10% FBS and supplemented with the appropriate tracer; 10 mM uniformly labelled glucose ([U-$^{13}C_6$]-glucose; Sigma-Aldrich, 389373) or 2 mM uniformly labelled glutamine ([U-$^{13}C_5$]-glutamine; Sigma-Aldrich, 605166) and incubated at 21% or 1% O_2 for 24 h. Either unlabelled glucose (Sigma-Aldrich, G7021; 10 mM) or unlabelled glutamine (Sigma-Aldrich, G7513; 2mM) was supplemented to the media – depending on which tracer was being used – to ensure the cells were not deprived of glucose or glutamine.

2.12.2. Metabolite extraction

Following 24 h labelling, the media was quickly removed and the cells washed twice with 500 µl ice-cold 0.9% saline solution. The plate was then transferred onto dry-ice and 500 µl ice-cold methanol (HPLC grade; Fisher Scientific, 10093880) was added to rapidly quench cell metabolism. The cells were then scraped and transferred to a pre-chilled safe-lock Eppendorf tube where 500 µl ice-cold 1 µg/ml D_6-glutaric acid in dH_2O (C/D/N Isotopes Inc, D-5227) was added. Afterwards, 500 µl ice-cold chloroform (Sigma-Aldrich, 650498) was added and the tubes were rocked at full speed on ice for 15 min. Samples were then centrifuged at 14,000 RPM for 15 min at 4°C, after which 800 µl of the upper fraction containing the polar metabolites was aliquoted into a clean safe-lock Eppendorf and dried by speed vacuum at 45°C for 2-3 h. Once completely dried, samples were stored at -80°C until processing for GC-MS analysis.

2.12.3. GC-MS (in collaboration with Dr. A. Thakkar, UoB)

2.12.3.1. Sample derivatisation

For metabolite derivatisation for GC-MS analysis, the dried samples were first incubated at 95°C to remove any residual moisture. Next, the dried extracts were solubilised using 40 µl 2% methoxyamine hydrochloride (Sigma-Aldrich, 226904) dissolved in pyridine (Sigma-Aldrich, 270970) and incubated for 1 h at 60°C. Following incubation, 60 µl N-tertbutyldimethylsilyl-N-methyltrifluoroacetamide (MTBSTFA) with 1% (w/v) tertbutyldimethyl-chlorosilane (TBDMSCI; Sigma-Aldrich, 375934) derivatisation agent was added and incubated for 1 h at 60°C. Finally, samples were centrifuged (13,000 RPM, 5 min) and the supernatant transferred to a chromatography vial with glass insert (Agilent Technologies, 5188-6591) ready for GC-MS analysis.

2.12.3.2.GC-MS analysis

Derivatised polar extracts were analysed using an Agilent 7890B GC/MSD gas chromatograph equipped with a polydimethylsiloxane GC column (DB35MS; 30 m x 0.25 mm x 0.25 µm film thickness) coupled to an Agilent 5977A mass spectrometer (Agilent Technologies). 1 µl of sample was injected into the GC-MS in splitless mode with helium carrier gas at a rate of 1 ml/min. The inlet liner containing glass wool was set at 270°C and oven temperature at 100°C for 1 min before ramping to 280°C at a rate of 5°C/min. Temperature was further ramped to 320°C at a rate of 10°C/min held at 320°C for 5 min. Compound detection was carried out in full scan mode in the mass range 50 to 650 m/z, with 2-4 scans/sec and a source temperature of 250°C, a transfer line temperature of 280°C and a solvent delay time of 6.5 min. Before data was recorded, the injector needle was cleaned with acetonitrile three times as well as three times following every measurement thereafter.

Raw GC-MS data was converted to common data format using the acquisition software. Further data processing, including correcting for natural isotope abundance and MID determination was conducted using MetaboliteDetector software[218]. Metabolite ion counts were normalised to the internal standard D_6-glutaric acid and cell counts for each condition to account for any variation in derivatization and metabolite concentrations respectively. MID analysis and total carbon contribution from glucose and glutamine for each metabolite was calculated by Dr. Thakkar, UoB.

2.13. Flow Cytometry

2.13.1. Cell treatment

U87 and U343 cells were seeded $2x10^5$ onto 6-well plates and left to adhere overnight under standard conditions. The following day, cells were treated with vehicle (0.1% DMSO), 5 μM VP, 5 μM VP and 20 μM Z-VAD-FMK, or 20 μM Z-VAD-FMK alone in both 21% and 1% O_2 for 4 and 8 h. Cells were pre-treated with Z-VAD-FMK for 1 h prior to VP treatment.

2.13.2. Annexin V/ Propidium Iodide viability assay

After treatment, the cell media was collected separately for each condition following end of treatment. Cells were PBS washed, trypsinised and added to the appropriate collected media. Cell suspensions were then left for 20 min to allow for re-stabilisation of phosphatidylserine (PS) expression. Cells were centrifuged (230 x g, 5 min) and washed before the cell pellet was resuspended in 1x Annexin V binding buffer (BD Biosciences, 556454). Cells were then stained with FITC Annexin V (BD Biosciences, 556419; 5 μl per sample, Ex/Em 490/525 nm) and propidium iodide (PI; Life Technologies, V13242; 1 μl of 0.1 mg/ml solution, Ex/Em 535/617 nm) for 10 min at RT. Cells were then analysed on the BD LSRFortessa X-20 cell analyser (BD Biosciences) using BD FACSDiva Software. Forward scatter, side scatter and FITC and PE (laser channel to measure PI) signal intensities were recorded. The laser intensities for both channels were determined using the unstained control sample and set at 10^3. To check there was no signal bleed through across the channels, single stained cells were provided as a control (Figure 2.3). H_2O_2 treated cells was used as a positive control for both stains. 10,000 cells were analysed per sample and data was processed using FlowJo software (version 8.7.3, FlowJo, LLC, USA).

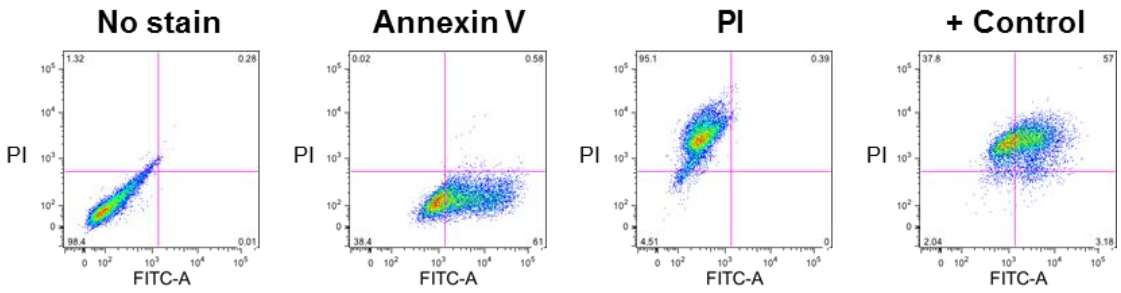

Figure 2.3 Examples of single and double stain controls for flow cytometry.

Firstly, FITC Annexin V signal was plotted against PI signal intensity for the vehicle control sample and gates were applied surrounding the viable population of cells. These gates were then kept consistent across the rest of the samples being analysed. From the gating, four different populations of cells can be determined (Figure 2.4).

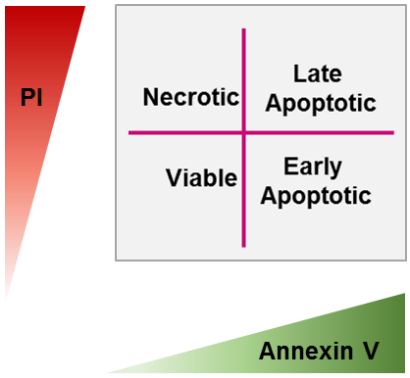

Figure 2.4 Simplified schematic depicting distinct cell populations generated through intensity of Annexin V and PI staining.

When cells are undergoing apoptosis, cells expose the membrane phospholipid PS on the outside of the plasma membrane. Annexin V can irreversibly bind to these residues and can therefore provide an estimation of cell apoptosis. During necrosis however, the plasma membrane integrity is disrupted allowing uptake of the cell-impermeable dye PI. Using these dyes in conjugation can therefore make a distinction between modes of cell death[219]. Consequently, the viable cell population is denoted by cells that are negative

for both Annexin V and PI staining (bottom left quarter). Cells which are undergoing early apoptosis generally have higher Annexin V but low PI staining (bottom right quarter). Late stage apoptosis is commonly represented by cells that stain highly for both Annexin V and PI (top right quarter) and finally, cells deemed to be necrotic largely have high levels of PI but low levels of Annexin V staining (top left quarter). To assess changes in viability upon VP treatment, the viable cell population for each sample was recorded.

2.14. DCFDA assay

2',7'-Dichlorofluorescin Diacetate (DCFDA) is a cell-permeable fluorogenic compound which is deacetylated by cellular esterases into a non-fluorescent intermediate which can subsequently be oxidised in the presence of ROS into the highly fluorescent compound DCF[220]. The fluorescence can then be measured using a plate reader (Excitation 485 nm, Emission 520 nm) and is directly proportional to the amount of oxidised DCFDA by hydroxyl, peroxyl and other ROS species[220].

U87, U343 and GBM T1 and T2 cells were seeded at $2.5x10^4$ cells per 96-well plate and left to adhere overnight under standard conditions. The following morning, to assess ROS, cells were treated with 5 μM VP or 5 μM PPIX (2 h, standard conditions) followed by overlay of 2x DCFDA (20 μM final concentration; Sigma-Aldrich, D6883) for the last 45 min of VP treatment. Wells were then washed with PBS and measured at 485 nm using the FLUOstar OMEGA microplate reader. To investigate whether VP-induced ROS production could be reduced, cells were co-treated with VP and free radical scavenger TEMPOL (TPL; 2 h pre-treatment, Sigma-Aldrich, 176141) and ROS levels assessed via DCFDA assay. H_2O_2 (50 μM) was used as a positive control. Fluorescence values were

corrected to the untreated cells for each experiment. For hypoxic measurements, the assay was conducted as described but in 1% O_2 before measurements read in normoxia.

2.15. Binding Assays

2.15.1. VP absorption spectra

VP was diluted to 75 μM in both dH_2O and methanol. The absorption spectra was then measured in the UV/Visible range (300-800 nm) using the FLUOstar OMEGA microplate reader.

2.15.2. Metal cation binding

To assess whether VP could bind metal ions, 3-500 μM of ferric chloride hexahydrate ($FeCl_3/Fe^{3+}$; Sigma-Aldrich, F-2877) Iron (II) chloride tetrahydrate ($FeCl_2/Fe^{2+}$; Honeywell Fluka, 44939), magnesium chloride ($MgCl_2/Mg^{2+}$; Fisher, BP214-500) and zinc chloride ($ZnCl_2/Zn^{2+}$; Alfa Aesar, A16281) was added to 30 μM VP diluted in methanol. The absorbance spectra were measured between 300-800 nm using the FLUOstar OMEGA microplate reader. For hypoxic measurements, 100 μM $FeCl_3$ was left under 21% or 1% O_2 for 4 h before 30 μM VP was added and absorbance read at 300-800 nm.

VP is activated during PDT around 685-690 nm (VP activation point). A shift in the VP absorption spectra from 686 nm towards 670 nm was seen upon addition of some of the metal cations indicating that the compounds could bind VP through altering the structure, inducing this shift. To determine binding therefore, first order binding kinetic graphs were generated by calculating the ratio of absorbance at 670/686 nm for all the metal chloride compounds. Absorbance values were read 1 min following addition of metal chloride to

VP (time-zero), and after 8 and 24 h. A specific binding nonlinear line of best fit was drawn for each metal chloride.

2.15.3. Mass Spectrometry (in collaboration with Prof. J.H.R. Tucker, UoB)

$FeCl_3$, $FeCl_2$, $MgCl_2$ and $ZnCl_2$ was added in excess to VP and dissolved using 99.8% methanol (extra-dry over molecular sieve; ThermoFisher, 10649492). Samples were then subject to low-resolution MALDI-TOF LD^+ mass spectrometry using the service provided by The Centre for Chemical and Materials Analysis in the School of Chemistry at UoB. Samples were prepared and analysed by E. Wilkinson from Prof. J.H.R Tucker's research group.

2.16. Statistical analysis

All statistical analysis was performed using GraphPad Prism v7 (GraphPad Software, La Jolla California, USA). Data is presented as mean ± standard error of the mean (S.E.M) or mean ± standard deviation (S.D) where stated. An unpaired T-test with Welch's correction (2 samples), one-way ANOVA (> 2 samples) or two-way ANOVA (>2 samples and oxygen conditions) with multiple comparisons post-hoc tests (Bonferroni and Tukey) were conducted as appropriate. A Shapiro-Wilk normality test was conducted where appropriate. Statistical significance was assigned at * $p<0.05$, ** $p<0.01$ and *** $p<0.001$. Sample sizes, reproducibility and statistical tests used are stated in the figure legends.

Chapter 3:

Investigating the hypoxic regulation of YAP/TAZ and their relationship with glioma metabolism

3.1. Introduction

Hippo signalling, in particular the main effectors YAP and its paralog TAZ, are known to be highly dysregulated in various cancers such as lung, breast, colorectal and liver to name a few[138]. Amplified expression and hyper-activated transactivational activity of YAP and TAZ have been strongly associated with the induction of a CSC phenotype, increased tumour growth and chemoresistance as well as increased metastases, as previously described. Studies conducted by Orr *et al*.,[149] and Zhang *et al*.,[150] have also highlighted the role of YAP and TAZ in glioma pathology, with amplified YAP expression observed in glioma tissues. In addition, YAP expression was seen to increase with histological grade in glioma, with the highest expression associated with grade IV (GBM)[149,150]. Patient prognosis is therefore also correlated with YAP1 expression, with high expression associated with a worse OS when compared with low expression, across all glioma grades[149,150]. Investigations into the underlying mechanisms as to how aberrant YAP1 expression influences tumour survival and therapy-resistance revealed a mechanistic relationship between hypoxia and aberrant Hippo/YAP signalling. It has previously been discovered that hypoxia influenced YAP activity in MDA-MB-231 breast cancer cells by deactivating upstream Hippo signalling which consequently led to increased YAP nuclear localisation and a concomitant increase in protein and mRNA expression of well-established YAP targets, *CYR61* and *CTGF,* contributing to a pro-survival role in hypoxic tumours[131]. Furthermore, these observations have been corroborated in breast cancer and HCC respectively, although this relationship has yet to be defined in glioma[133,135].

It is well known that cancer cells demonstrate an abnormal cellular metabolism, resulting in an altered, often increased requirement for nutrients to aid uncontrolled and

inappropriate cell proliferation[221]. Rapidly proliferating cells must accumulate biomass such as nucleotides, proteins, lipids and other cellular building blocks in order to generate new cells. The activity through the biosynthetic pathways underlying these processes has therefore been observed to be considerably altered in cancer. The challenging nature of the tumour microenvironment, which often includes hypoxia, also contributes to the metabolic reprogramming observed. Indeed, these alterations can support enhanced cell survival and proliferation, often resulting in a more malignant phenotype[80]. Despite many studies highlighting the oncogenic roles of YAP/TAZ in various cancers, little is known about how YAP/TAZ can potentially influence metabolism to support the increased cell proliferation observed with amplified YAP/TAZ expression and transactivational activity.

This chapter therefore aims to investigate the potential hypoxic regulation of YAP/TAZ in gliomas. Due to their complex hypoxic nature, aberrant YAP/TAZ activity is likely to be induced, which could ultimately contribute towards increased glioma growth and tumour progression. Furthermore, the metabolic implications of YAP/TAZ activity will be investigated using metabolic tracer-based analysis to assess whether YAP/TAZ can influence glioma metabolism, particularly under hypoxia, and whether YAP/TAZ could therefore be an attractive therapeutic target for glioma.

3.2. Results

3.2.1. Glioma cell lines exhibit differential sensitivity to hypoxia

Gliomas are known to be extremely hypoxic tumours due to their excessive growth and presence of oedema, as previously described. To assess whether hypoxia could influence the growth of the *in vitro* glioma cell lines used in this investigation, U87 and U343, cell proliferation was evaluated over a 72 hour period of hypoxia. Proliferation was seen to be significantly attenuated in the U87 cells after 48 hours in 1% and 0.3% O_2 when compared to cells grown under normoxia (21% O_2; Figure 3.1A). Conversely, proliferation of the U343 cell line was unaffected when the cells were cultured under hypoxic conditions (Figure 3.1B), indicating that these cells may harbour a specific characteristic or mutation which confers a growth advantage in hypoxia compared to the U87 cells.

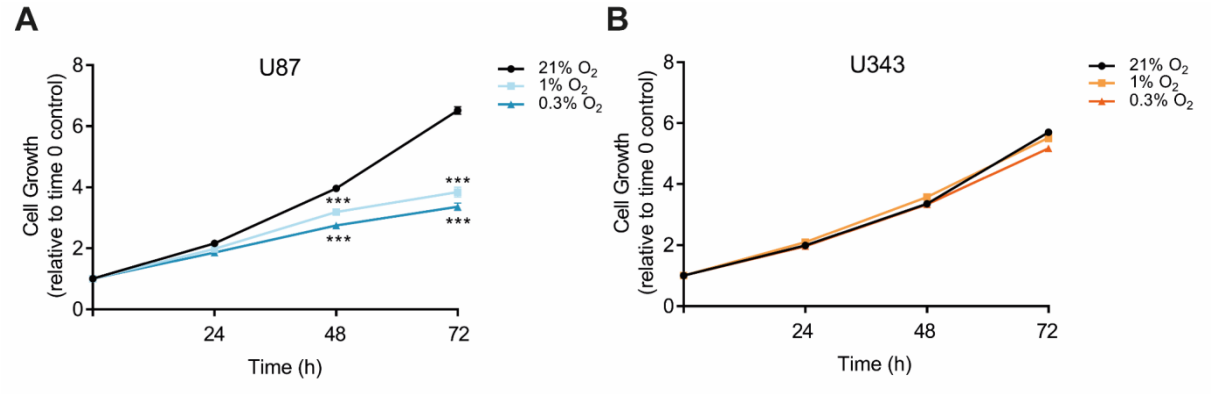

Figure 3.1 Glioma cells exhibit differential sensitivity to hypoxia. U87 (A) and U343 (B) cells were grown under normoxic (21% O_2) or hypoxic (1% and 0.3% O_2) conditions for up to 72 h. Cell growth was determined via SRB analyses every 24 h and normalised to the time-zero control. Although both cell lines proliferated under hypoxic conditions, growth was significantly reduced after 48 h in U87 cells whereas U343 cells remained unaffected. Data was performed in technical quadruplicate in 3 independent experiments. Error bars represent ± S.E.M. Significance determined using one-way ANOVA with Bonferroni post-hoc analysis. *** $p<0.001$.

3.2.2. YAP1 and YAP1-target gene transcription is increased under hypoxic conditions

YAP has been previously associated with increased growth and progression in numerous different tumour types including GBM, and thus its aberrant regulation in cancer must be deeper investigated. Due to tumours exhibiting a high degree of hypoxia, studies have now begun to focus on the potential relationship between hypoxia and YAP, however this association has yet to be characterised in glioma. Therefore, YAP1 mRNA expression was assessed in U87 and U343 (Figure 3.2A, E) as well HOG IDH1 WT and MUT (Figure 3.3A, E) glioma cell lines following 8 hours of hypoxia (1% O_2). At a transcriptional level, hypoxia was seen to increase YAP1 gene expression as well as amplifying YAP1 activity, which is implied through a concomitant increase in expression of YAP1-target genes *CYR61*, *CTGF* and *BBC3* (BCL2 binding component 3) due to YAP1's function as a transcriptional co-activator (Figure 2.4 and 2.5).

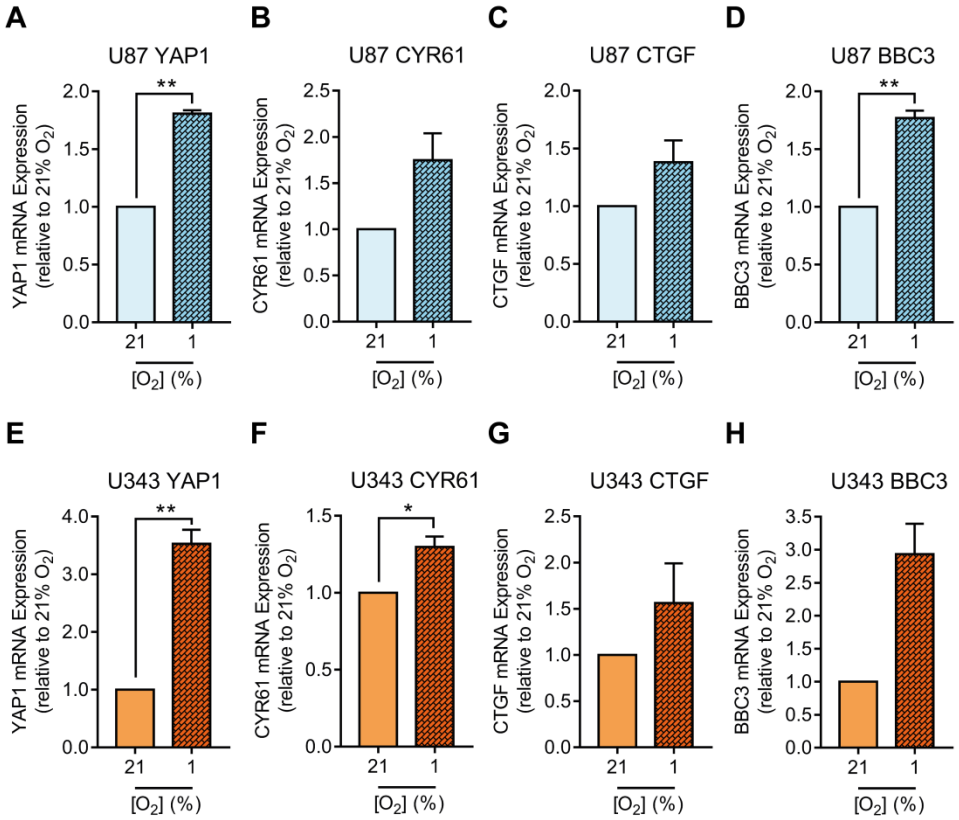

Figure 3.2 Hypoxia increases YAP1 and YAP1-target gene expression in U87 and U343 cell lines. Quantitative PCR was carried out on RNA harvested from U87 (A-D) and U343 (E-H) cells following 8 h in 21% or 1% O_2. YAP1 gene expression was seen to significantly increase under hypoxia in both cell lines compared to the 21% O_2 control (A and E). YAP1 activity was analysed through YAP1-target gene (*CYR61* (B and F), *CTGF* (C and G) and *BBC3* (D and H)) expression which suggested that hypoxia increased YAP1 activity due to increased expression of YAP1 target genes compared to the normoxic control. Samples were run in technical duplicate in 3 independent experiments. Error bars represent ± S.E.M. Significance determined using Welch's unpaired t-test. * $p<0.05$, ** $p<0.01$.

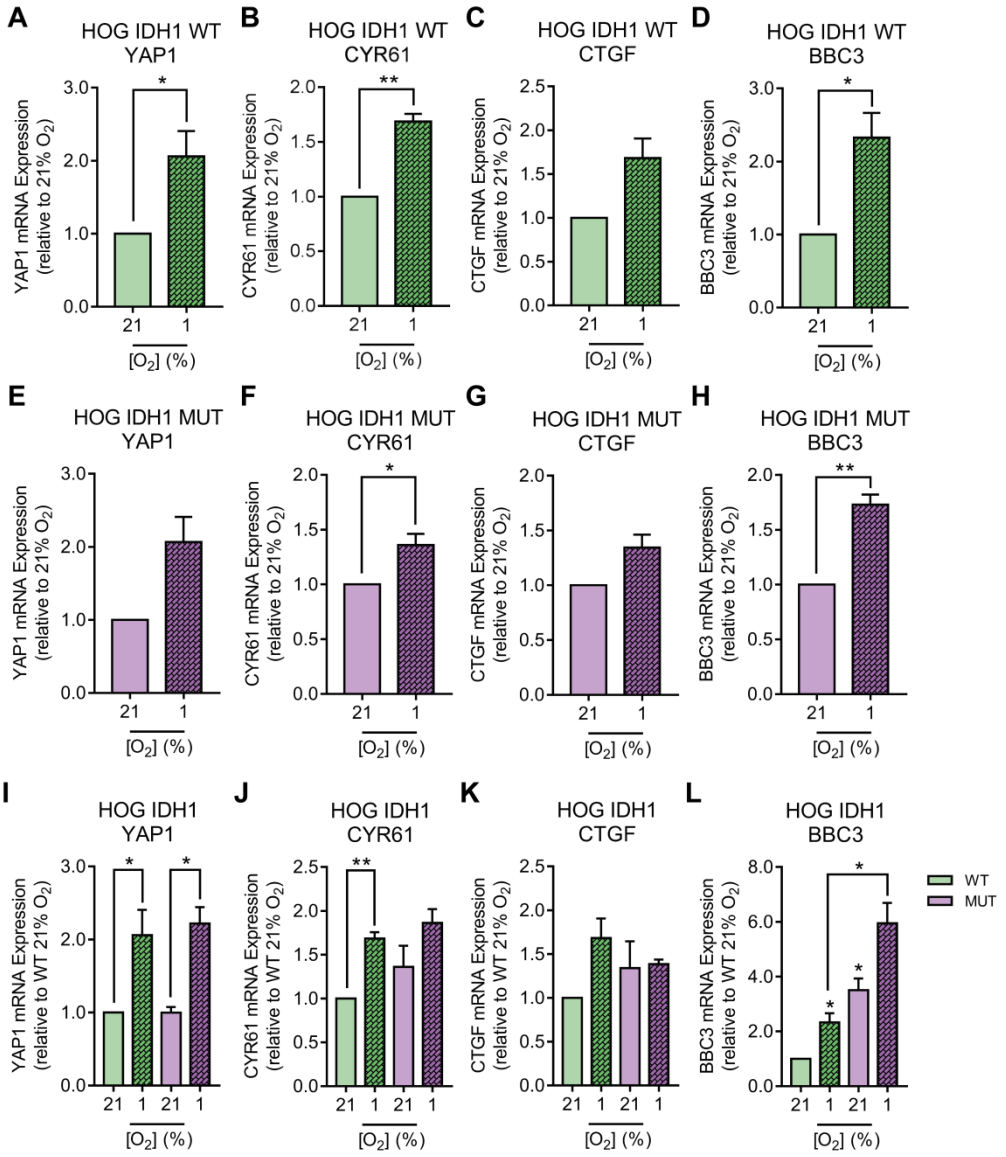

Figure 3.3 Mutation in IDH1 does not influence hypoxia-induced YAP1 and YAP1-proliferative gene expression. Quantitative PCR was carried out on RNA harvested from HOG IDH1 WT (A-D) and HOG IDH1 MUT (E-H) cells following 8 h in 21% or 1% O_2. YAP1 gene expression was seen to increase under hypoxia in both cell lines compared to the 21% O_2 control but was only significant in the WT cells (A and E). Expression of YAP1-target genes *CYR61* (B and F), *CTGF* (C and G) and *BBC3* (D and H) were also analysed and observed to be increased under hypoxic conditions. Gene expression of the HOG IDH1 MUT cells was normalised to the HOG IDH1 WT normoxic cells to observe the influence of the IDH1 R132H mutation (I-L). No significant differences in gene expression were seen between WT and MUT cells except in the expression of BBC3. HOG MUT cells were seen to have a significantly higher basal level of BBC3 compared to the 21% O_2 WT control which was also significantly increased under hypoxia when compared to hypoxic WT cells. Samples were run in technical duplicate in 3-5 independent experiments. Error bars represent ± S.E.M. Significance determined using Welch's unpaired t-test . * $p<0.05$, ** $p<0.01$.

To confirm cells were hypoxic, HIF-1α target genes *BNIP3* (BCL2 interacting protein 3*)*, *VEGF-A* and *SLC2A1* (otherwise known as *GLUT1*) were analysed across all cell lines and indeed found to be increased upon exposure to 1% O_2 (Figure 3.4 and 3.5).

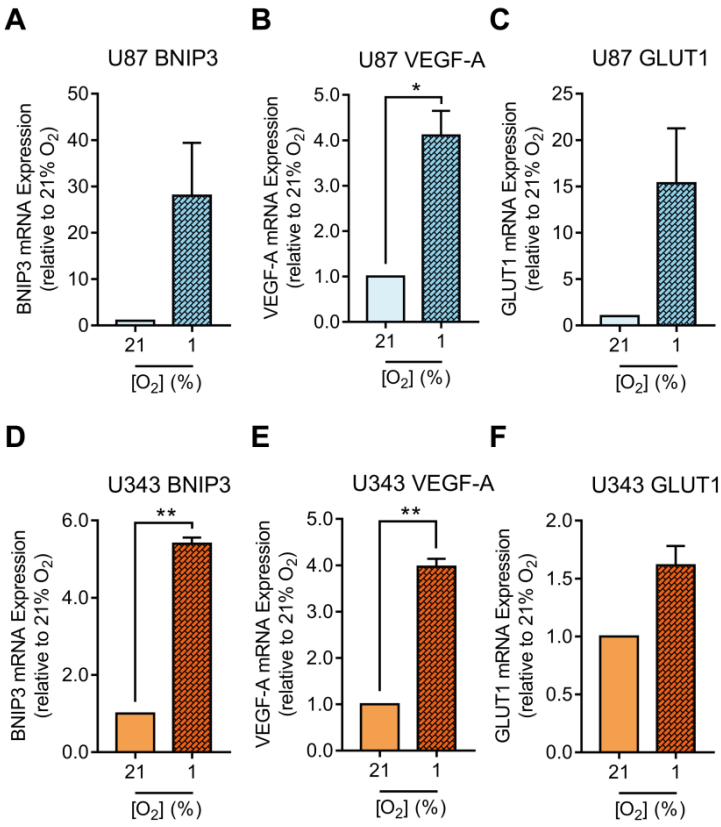

Figure 3.4 Hypoxia induces expression of HIF-1 target genes in U87 and U343 cell lines. To ensure glioma cells were hypoxic during gene analysis experiments, RNA was harvested from U87 (A-C) and U343 (D-F) cells following 8 h in 21% or 1% O_2. HIF-1 target genes *BNIP3* (A and D), *VEGF-A* (B and E) and *GLUT1* (C and F) were assessed via qPCR and were seen to increase under hypoxic conditions, with B, D and E deemed statistically significant. Samples were run in technical duplicate in 3 independent experiments. Error bars represent ± S.E.M. Significance determined using Welch's unpaired t-test . * $p<0.05$, ** $p<0.01$.

To assess the whether the presence of the R132H IDH1 mutation influenced YAP1 and YAP1-target gene expression, gene expression data from the HOG IDH1 MUT cells was normalised to their WT counterparts (Figure 3.3I-L and 3.5G-I). No significant differences were observed upon IDH1 mutation except in the expression of YAP1-target gene,

BBC3, in which a significant increase in mRNA expression was apparent under normoxic and hypoxic conditions (Figure 3.3L).

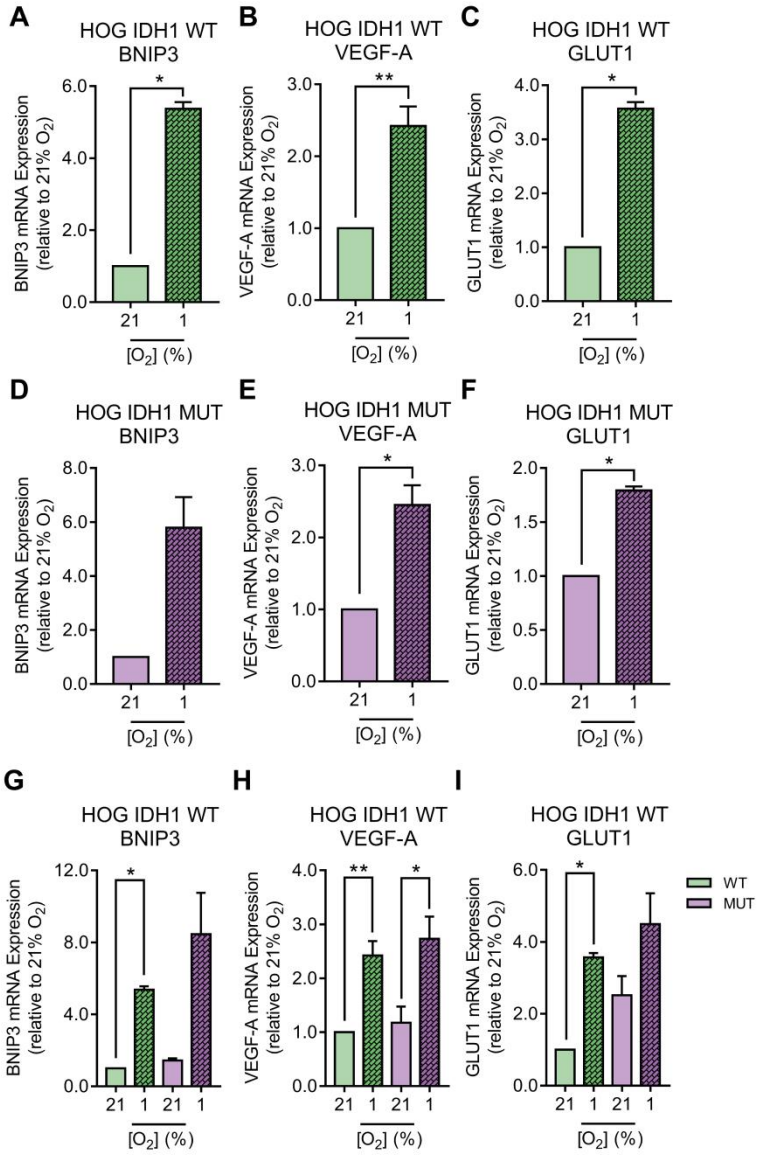

Figure 3.5 Hypoxia induces expression of HIF-1 target genes in HOG IDH1 WT and MUT cell lines. To ensure glioma cells were hypoxic during gene analysis experiments, RNA was harvested from HOG IDH1 WT (A-C) and HOG IDH1 MUT (D-F) cells following 8 h in 21% or 1% O_2. HIF-1 target genes *BNIP3* (A and D), *VEGF-A* (B and E) and *GLUT1* (C and F) were assessed via qPCR and were seen to increase under hypoxic conditions, with B, C, E and F deemed statistically significant. Gene expression of HOG IDH1 MUT cells was then compared to IDH1 WT cells (G-I), however no significant differences were observed between the two cell lines. HOG IDH1 MUT cells were seen to have a higher basal level of GLUT1 compared to WT cells however this was non-significant. Samples were run in technical duplicate in 2-5 independent experiments. Error bars represent ± S.E.M. Significance determined using Welch's unpaired t-test . * $p<0.05$, ** $p<0.01$.

3.2.3. YAP1 protein expression is increased under hypoxic conditions

To assess whether hypoxia could also increase YAP1 protein expression, U87 and U343 cells were exposed to hypoxia for 2-24 hours (Figure 3.6). While 1% O_2 was sufficient to induce a strong increase in YAP1 mRNA, only a minimal increase in YAP1 protein expression was apparent in the U87 and U343 cells after 8 hours hypoxia when compared to the normoxic control (Figure 3.6B, E). In fact, a lower oxygen tension of 0.3% O_2 was required to significantly increase YAP1 protein expression in the U87 cells (Figure 3.6B), whilst only a small difference was apparent in the U343 cell line (Figure 3.6E). Hypoxia was also able to induce a significant increase in YAP1 protein expression in the HOG IDH1 WT and MUT cells however only after exposure to the lower oxygen tension of 0.3% O_2 (Figure 3.7).

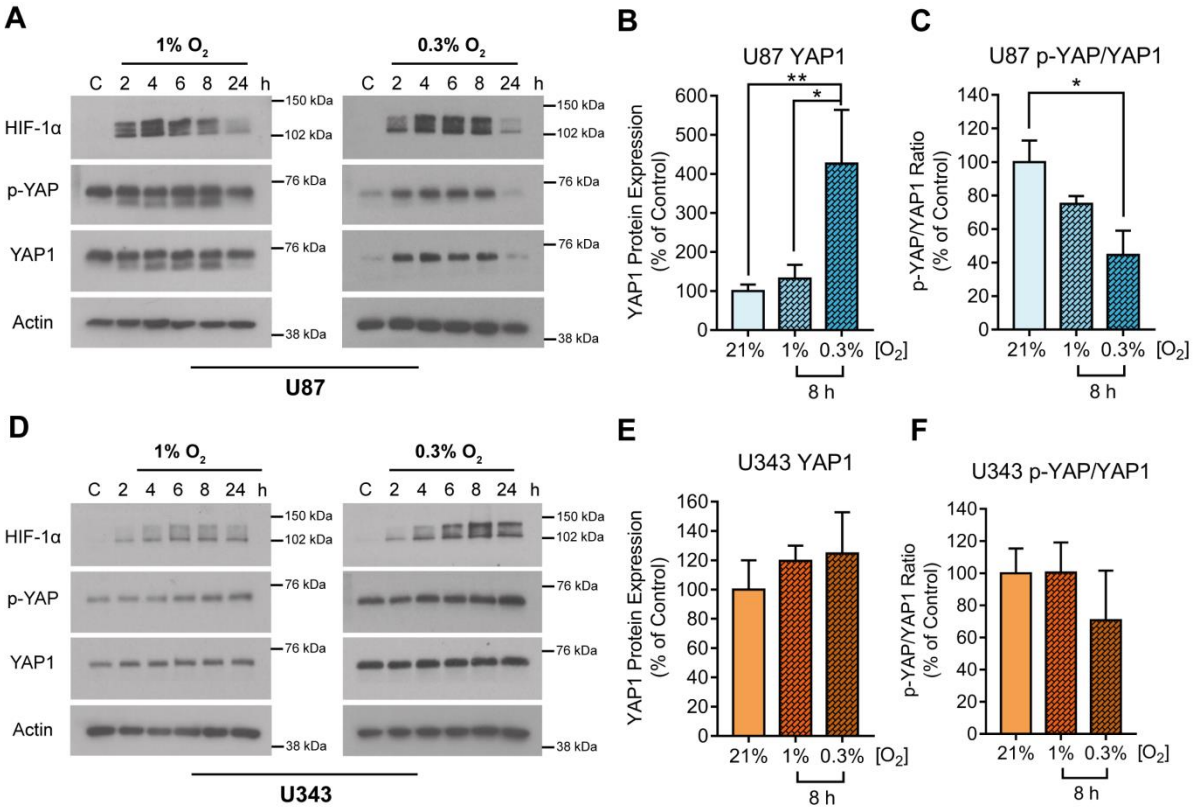

Figure 3.6 YAP1 protein expression is increased under hypoxic conditions. (A) Protein was harvested from U87 cells which had been under 1% and 0.3% O_2 for 2-24 h or 21% O_2 (C) for 24 h. HIF-1α (~120 kDa), phosphorylated-YAP (p-YAP, S127; ~65-70 kDa) and YAP1 (~65-70 kDa) expression was analysed through western blotting. As expected, HIF-1α expression was increased in hypoxic conditions, although was seen to reduce after 24 h. p-YAP and YAP1 expression increased however only under 0.3% O_2. (B) Densitometry analysis showed that YAP1 expression significantly increased under 0.3% O_2 for 8 h when compared to the control cells. Data is normalised to actin expression and expressed as a percentage of the control. (C) YAP1 activity was calculated as a ratio of the inactive p-YAP to the total YAP1 present. A reduction in p-YAP was observed under hypoxic conditions suggesting increased YAP1 activity. (D) Protein was harvested from U343 cells which had been under 1% and 0.3% O_2 for 2-24 h or 21% O_2 (*C*) for 24 h. Expression of p-YAP and YAP1 was seen to increase under 8 h hypoxia although was not significant from densitometry analysis (E). YAP1 activity was also increased under 0.3% O_2 (F), however was again non-significant. Actin (42 kDa) was used as a loading control. Data is from 3 (U343) and 4 (U87) independent experiments. Error bars represent ± S.E.M. Significance determined using Welch's unpaired t-test. * $p<0.05$, ** $p<0.01$.

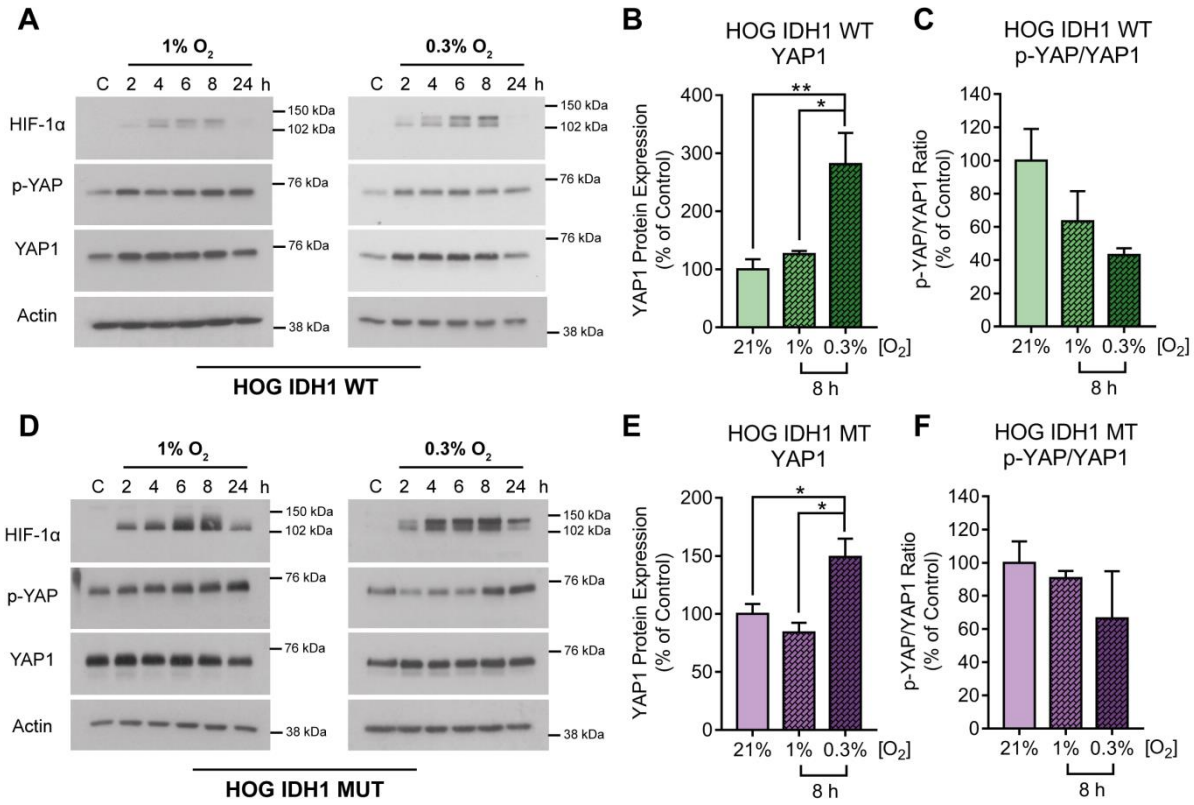

Figure 3.7 Hypoxia induces YAP1 protein expression in the HOG cells. (A) Protein was harvested from HOG IDH1 WT cells following 2-24 h under 1% and 0.3% O_2. Compared with the 21% O_2 control (*C*), p-YAP and YAP1 were induced under hypoxic conditions. Expression of HIF-1α was increased during hypoxic conditions, although undetected following 24 h. (B) Densitometry analysis showed a significant increase in YAP1 expression following 8 h 0.3% O_2. (C) A trend increased in YAP1 activity following 8 h hypoxia was observed from a decreased p-YAP/YAP1 ratio however was non-significant compared to the 21% O_2 control. (D) Protein was harvested from HOG IDH1 MUT cells following 2-24 h in 1% and 0.3% O_2. HIF-1α protein was seen to increase over time under hypoxic conditions. Expression of p-YAP was increased under hypoxic conditions compared to the 21% O_2 control cells. YAP1 expression also significantly increased but only under 0.3% O_2 which was confirmed by densitometry analysis (E). A trend decrease in p-YAP/YAP1 ratio was also observed suggesting increased YAP1 activity under hypoxic conditions, although was non-significant. Actin was used as a loading control. Data is from 2-5 independent experiments. Error bars represent ± S.E.M. Significance determined using Welch's unpaired t-test. * $p<0.05$, ** $p<0.01$.

YAP1 activity can also be inferred from determining the expression of phosphorylated YAP (p-YAP) compared to the total YAP1 expression. As previously described, YAP phosphorylation via upstream kinases renders the protein unable to enter the nucleus, thereby interfering with YAP's nuclear function as a transcriptional co-activator. Hence if less p-YAP is present in the cell, it can be suggested that more of the YAP present is

nuclear and thereby able to influence downstream target-gene transcription. YAP1 activity was thereby determined by calculating the ratio of p-YAP to total YAP1 protein in all four glioma cell lines and was seen to decrease upon exposure to hypoxia (Figure 3.6 and 3.7). Although a trend decrease in p-YAP/YAP1 ratio was apparent across all cell lines suggesting increased YAP1 activity in hypoxia, only 0.3% O_2 was able to induce a significant reduction in the U87 cell line when compared to the normoxic control (Figure 3.6C).

To further assess whether hypoxia influenced YAP1 transcriptional activity in addition to its expression, protein expression of YAP1-target gene CTGF was analysed and seen to be increased upon 6 hours of hypoxia, providing further evidence to suggest that hypoxia can amplify YAP1 transactivational activity (Figure 3.8A). In addition to YAP1, hypoxia elicited a strong upregulation in protein expression of its close paralog TAZ in both U87 and U343 cells following 24 hour exposure to 1% O_2 (Figure 3.8B). To confirm whether this response was also true in a more physiologically relevant model, p-YAP and YAP1 expression was analysed in two novel GBM cell lines, T1 and T2, which had been derived in-house from a single GBM patient biopsy (Figure 3.8C). Interestingly, the T1 cell line originated from an area of residual tumour which had progressed following the patient's initial craniotomy and chemoradiation treatment and thus deemed to be therapy-resistant due to its recurrent growth. The T2 cell line, on the other hand, was believed to be therapy-responsive as this area of the tumour did not increase in size over the follow-up period. From initial western blotting experiments, it was clear that both p-YAP and YAP1 expression were distinctly increased in the T1 therapy-resistant cell line (Figure 3.8C). Furthermore, culturing cells under hypoxia was able to induce a significant increase in YAP1 expression in both the T1 and T2 cell line when compared to their

normoxic counterparts, with the relative increase more exaggerated in the T2 line (Figure 3.8D). However, the initial YAP expression was lower in the T2 line, which may have resulted in the system being more sensitive to upregulation by hypoxia. The p-YAP/YAP1 ratio was calculated and small decrease was apparent in hypoxia suggesting potential increased YAP transcriptional co-activation activity (Figure 3.8E). In addition to differences in total YAP1 expression, distinct morphological differences were also apparent between the two cell lines (Figure 3.8F). Additionally, glial fibrillary acidic protein (GFAP) expression was assessed to confirm that the cell lines were derived from a tumour of glial origin and that the cells were astrocytic in nature (Figure 3.8G).

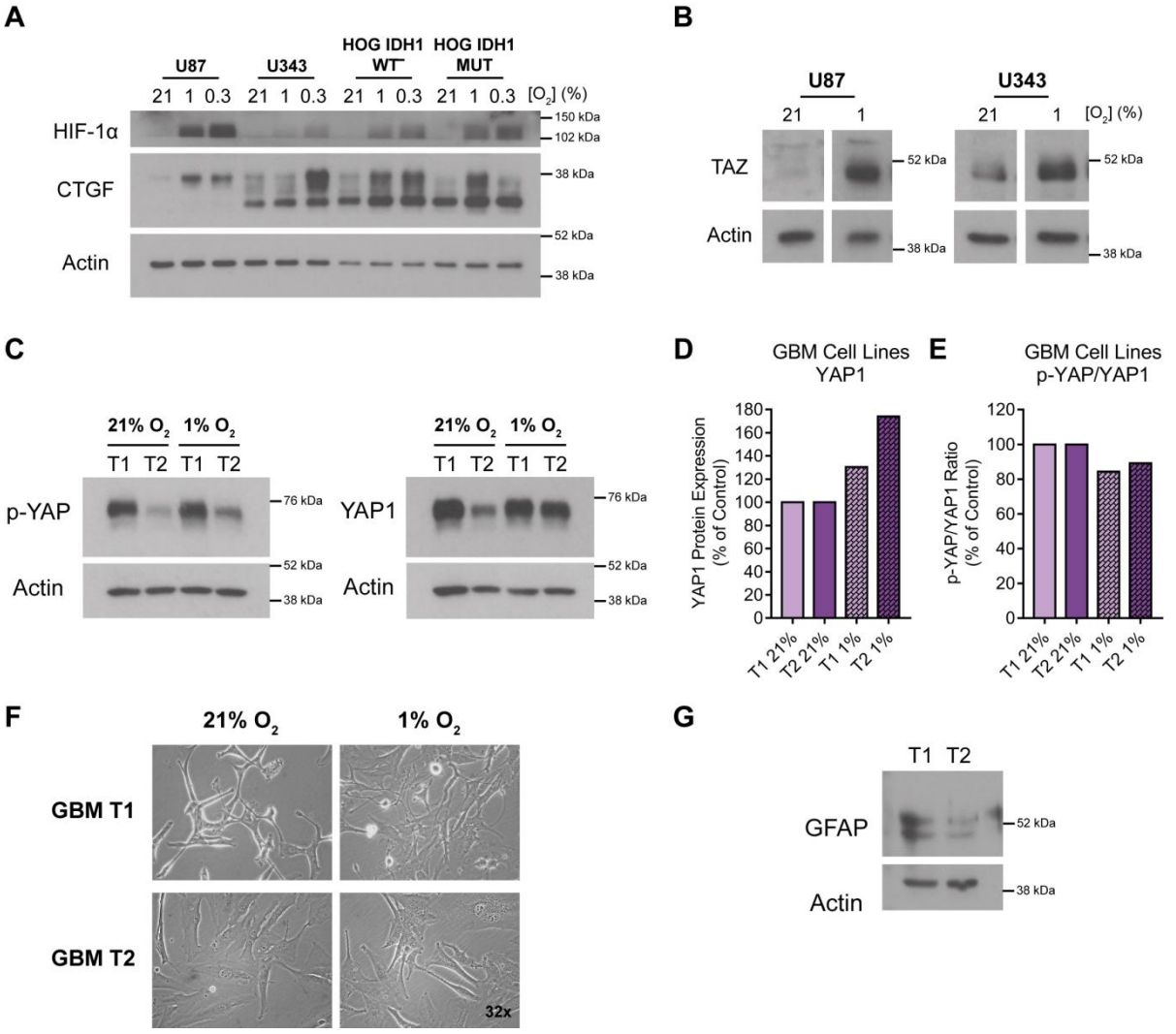

Figure 3.8 Hypoxia increases YAP/TAZ expression and transcriptional co-activator activity in established and primary GBM cell lines. (A) YAP1 target gene CTGF, expression was analysed via western blotting following 6 h under 1% and 0.3% O_2. Compared to control cells (21% O_2), hypoxia was seen to increase CTGF expression (38 kDa, upper band) in all four glioma cell lines. (B) Protein expression of YAP1 paralog TAZ (~50 kDa) was also analysed and seen to dramatically increase in 1% O_2 for 24 h when compared to normoxia. (C) Protein was harvested from cell lines T1 and T2, which were derived from a single GBM biopsy, in 21% and 1% O_2. p-YAP and YAP1 expression was seen to increase in the T2 therapy-sensitive line under hypoxic conditions however only a slight increase was observed in the T1 therapy-resistant cell line. (D) Densitometry analysis shows increased YAP1 expression in hypoxic conditions in both T1 and T2 cells compared to the normoxic control. (E) A slight decrease was observed in p-YAP/YAP1 ratio in both T1 and T2 cells indicating increased YAP1 activity when compared to the normoxic control. (F) Images showing the difference in cell morphology between the GBM T1 and T2 cell lines. Objective 32x. (G) Glial fibrillary acidic protein (GFAP; ~55, 48 kDa) expression confirms that T1 and T2 cells are of glial origin. Actin was used as a loading control.

3.2.4. Increased YAP1 nuclear localisation suggests hypoxia amplifies YAP1 activity in glioma cells

Cellular localisation of YAP is crucial for its function as a transcriptional co-activator as previously mentioned, and so YAP1 nuclear localisation was assessed by determining the CTNF for each cell, as outlined in section 2.2.9, upon exposure to hypoxia (Figure 3.9). Quantitative analysis of YAP1 nuclear staining showed that exposure to 1% O_2 for 4 hours significantly enhanced fluorescence indicating an increased presence of YAP1 in the nucleus and thus potentially increased transcriptional co-activator activity (Figure 3.9B, C). This nuclear enhancement was also present after 8 hours under 1% O_2 in the U87 cells although was not apparent in the U343 cells suggesting differential responses to hypoxia over time between the two glioma cell lines (Figure 3.9C).

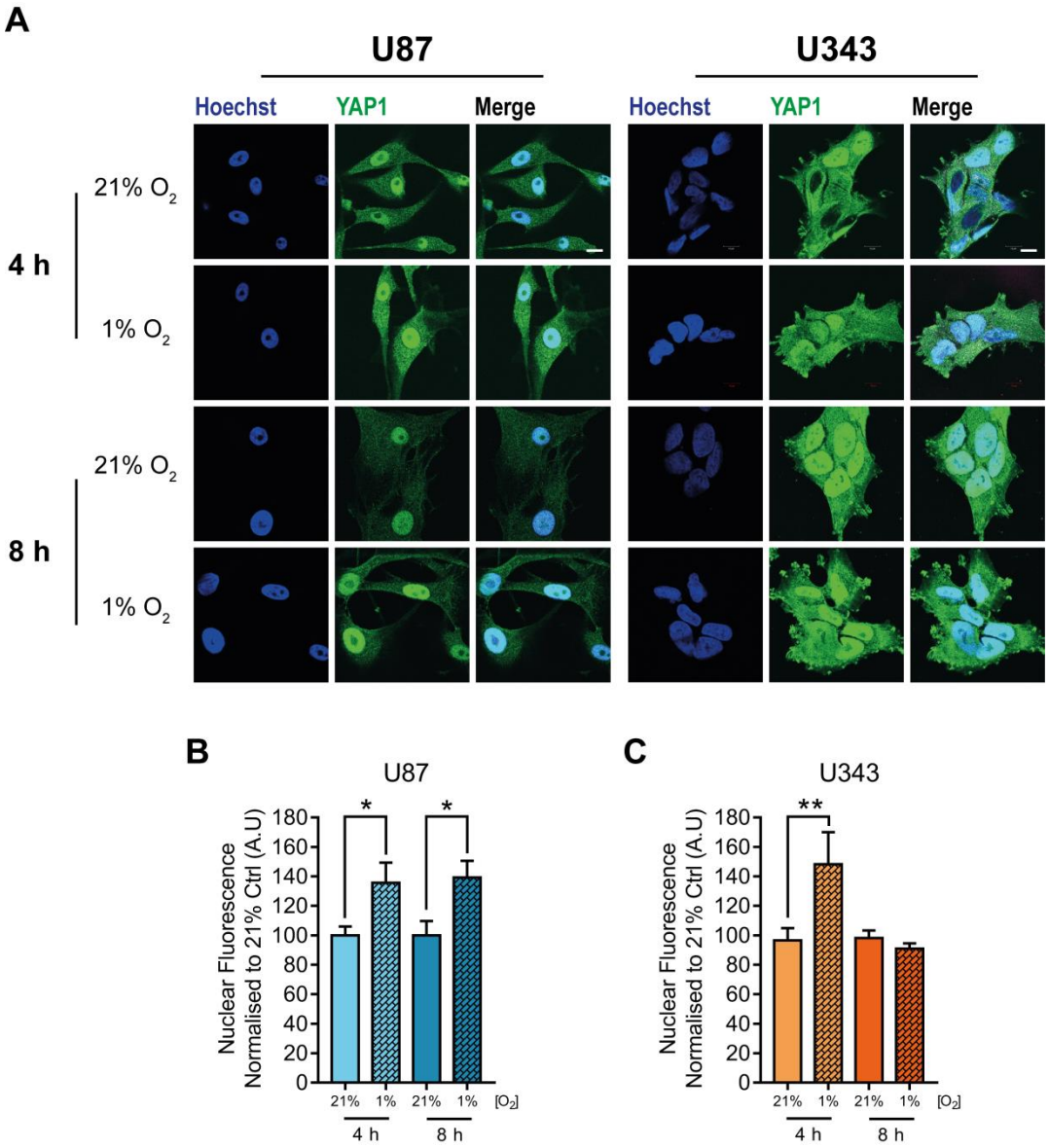

Figure 3.9 YAP1 nuclear localisation is increased under hypoxic conditions. (A) U87 and U343 cells were cultured under 21% and 1% O_2 for 4 and 8 h before being processed via ICC to visualise YAP1 localisation. Analysis of the nuclear YAP1 fluorescence was conducted and was seen to significantly increase following 4 h in 1% O_2 in the U87 (B) and U343 (C) cell lines when normalised to the normoxic control. Interestingly, YAP1 nuclear localisation was only seen to increase in the U87 and not the U343 cells following 8 h hypoxia. Scale bar represents 10 µm. All experiments were conducted in biological triplicate (except U343 4 h in biological duplicate). 2-4 images were analysed per condition, per experiment. Error bars represent ± S.E.M. Significance determined using one-way ANOVA, with Tukey post-hoc analysis. * $p<0.05$, ** $p<0.01$.

3.2.5. Knockdown of YAP/TAZ reduces glioma cell proliferation

Since enhanced YAP expression and activity have been associated with increased tumour progression and survival, it was questioned whether knockdown of YAP/TAZ would affect glioma cell survival; particularly under hypoxic conditions where YAP and TAZ expression were shown to be increased. Knockdown of YAP and TAZ using targeted siRNA was first validated in both U87 and U343 cell lines over a 96 hour time period (Figure 3.10A, B). Cell proliferation was then assessed in both normoxic (21% O_2) and hypoxic (1% O_2) conditions in both glioma cell lines following 72 hour knockdown of YAP, TAZ and YAP and TAZ together – to account for any potential compensation of the two proteins – compared to non-targeting siRNA control. Upon knockdown, cell proliferation was significantly reduced in the U87 cells, which was further increased under hypoxia (Figure 3.10C, E). On the other hand, only siTAZ and knockdown of both YAP and TAZ together was able to significantly reduce cell growth of the U343 cells and no additional reduction in cell growth under hypoxia was apparent (Figure 3.10D, E). To confirm that knockdown of YAP and TAZ was affecting the cell proliferation and not inducing cell death, images were taken showing that both cell lines were still viable upon knockdown (Figure 3.10F).

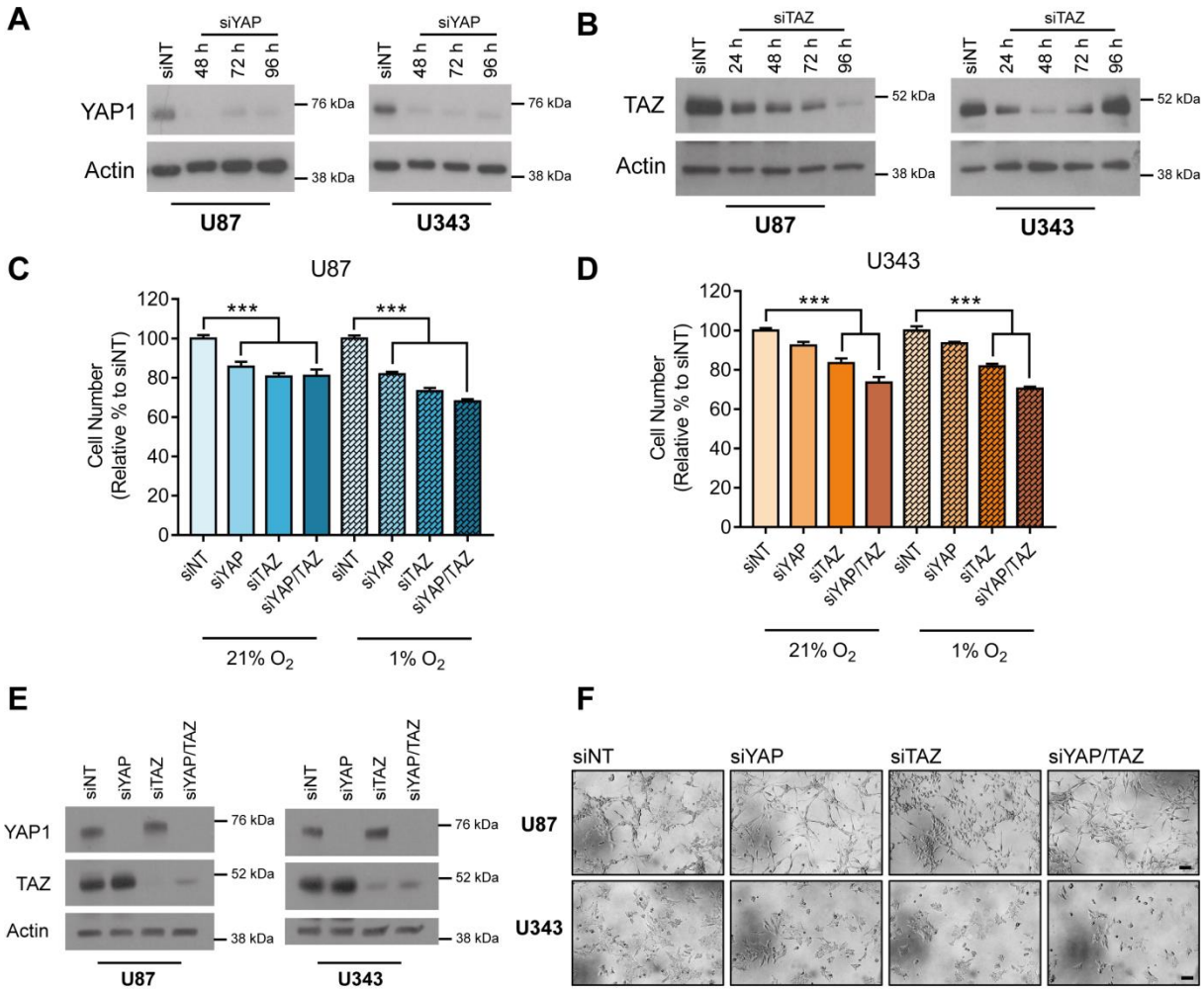

Figure 3.10 Knockdown of YAP1 and TAZ significantly reduces glioma cell growth. siRNA knockdown of YAP1 (A) and TAZ (B) was conducted over a 96 h time-course in both the U87 and U343 cell lines. 72 h post-transfection was subsequently chosen for all following experiments as this time point achieved the best knockdown for both proteins in both of the cell lines. (C and D) YAP, TAZ and both YAP and TAZ together were subjected to siRNA knockdown in the U87 and U343 cell lines. Cells were cultured under 21% and 1% O_2 for 72 h post-transfection and fixed for SRB analysis. Knockdown was seen to significantly reduce cell number in both cell lines in both normoxia and hypoxia however siYAP did not induce any significant reduction in growth of the U343 cell line. (E) Representative western blots confirming successful protein knockdown in the cell proliferation experiments. (F) Images showing that knockdown of YAP, TAZ and YAP/TAZ reduced U87 and U343 cell proliferation and was not a result of induced cell death. Actin was used as loading control. Scale bar 100 µm. Data is from 3 biological experiments, conducted in technical triplicate. Error bars represent ± S.E.M. Significance determined using two-way ANOVA, with Tukey post-hoc analysis. * $p<0.05$, ** $p<0.01$.

3.2.6. Investigating the importance of YAP/TAZ in cancer cell metabolism

Since cell metabolism is extensively altered in cancer to support increased tumour proliferation and survival in the often hostile microenvironment and as YAP/TAZ can play a significant role in these tumour phenotypes, it was investigated whether YAP/TAZ could influence aspects of metabolism. U343 glioma cells were incubated for 24 hours with either uniformly ^{13}C labelled glucose ([U-$^{13}C_6$]-glucose) or glutamine ([U-$^{13}C_5$]-glutamine) in normoxic (21% O_2) and hypoxic (1% O_2) conditions following siRNA knockdown of YAP, TAZ and YAP and TAZ together. The MIDs for each metabolite was conducted using GC-MS, and refers to the shift in mass of a metabolite as a result of the incorporation of ^{13}C isotopes. Typically, these are defined as M+0, M+1, M+2 to M+*n*, where M is the base mass of an ion fragment and the following number 0 to *n* refers to the mass shift from M as a result of the number of ^{13}C carbon atoms incorporated[216]. Consequently, the sum of all the fractions from M+0 to M+*n* is 100%[217].

3.2.6.1. YAP/TAZ support *de novo* serine synthesis

The NEAA serine is known to provide precursors for a variety of biosynthetic pathways which are vital for cell proliferation and survival[222]. Serine can either be imported from extracellular sources or synthesised *de novo* from a branch in glycolysis (Figure 3.11A). Importantly, serine can be converted into glycine via serine hydroxymethyltransferase 1/2 (SHMT1/2) to supply methyl units for one-carbon metabolism; an intricate network based upon the shuttling of carbon units via folate derivatives for the biosynthesis of crucial macromolecules such as proteins, lipids and nucleic acids for cellular proliferation as well as GSH for redox homeostasis[223] (Figure 3.11A).

Knockdown of YAP and TAZ was seen to significantly perturb serine metabolism in U343 cells under normoxic conditions, which is evident by a significant reduction in the percentage of ^{13}C incorporation into serine from [U-$^{13}C_6$]-glucose when compared to the siNT control (Figure 3.11B, C). Changes in the serine M+3 isotopomer are indicative of reduced *de novo* serine synthesis upon knockdown of YAP/TAZ. M+2 labelled serine on the other hand could arise from the conversion of glycine back into serine via SHMT 1/2, which again was significantly reduced upon YAP/TAZ knockdown. Interestingly, M+1 serine – which could potentially be generated through labelled glucose being utilised upstream through the oxidative and non-oxidative arms of the PPP – was also significantly reduced upon knockdown of YAP/TAZ. The majority of ^{13}C incorporation into serine was however unlabelled (M+0) suggesting that the U343 cells rely heavily on serine from extracellular sources rather than from *de novo* synthesis from glucose (Figure 3.11C, D). Knockdown of YAP and TAZ appeared to have no additional effect on serine metabolism in hypoxia, with a significantly reduced M+3 labelling observed across all conditions compared to normoxia suggesting a potential diversion from serine synthesis in these glioma cells under hypoxic conditions (Figure 3.11E).

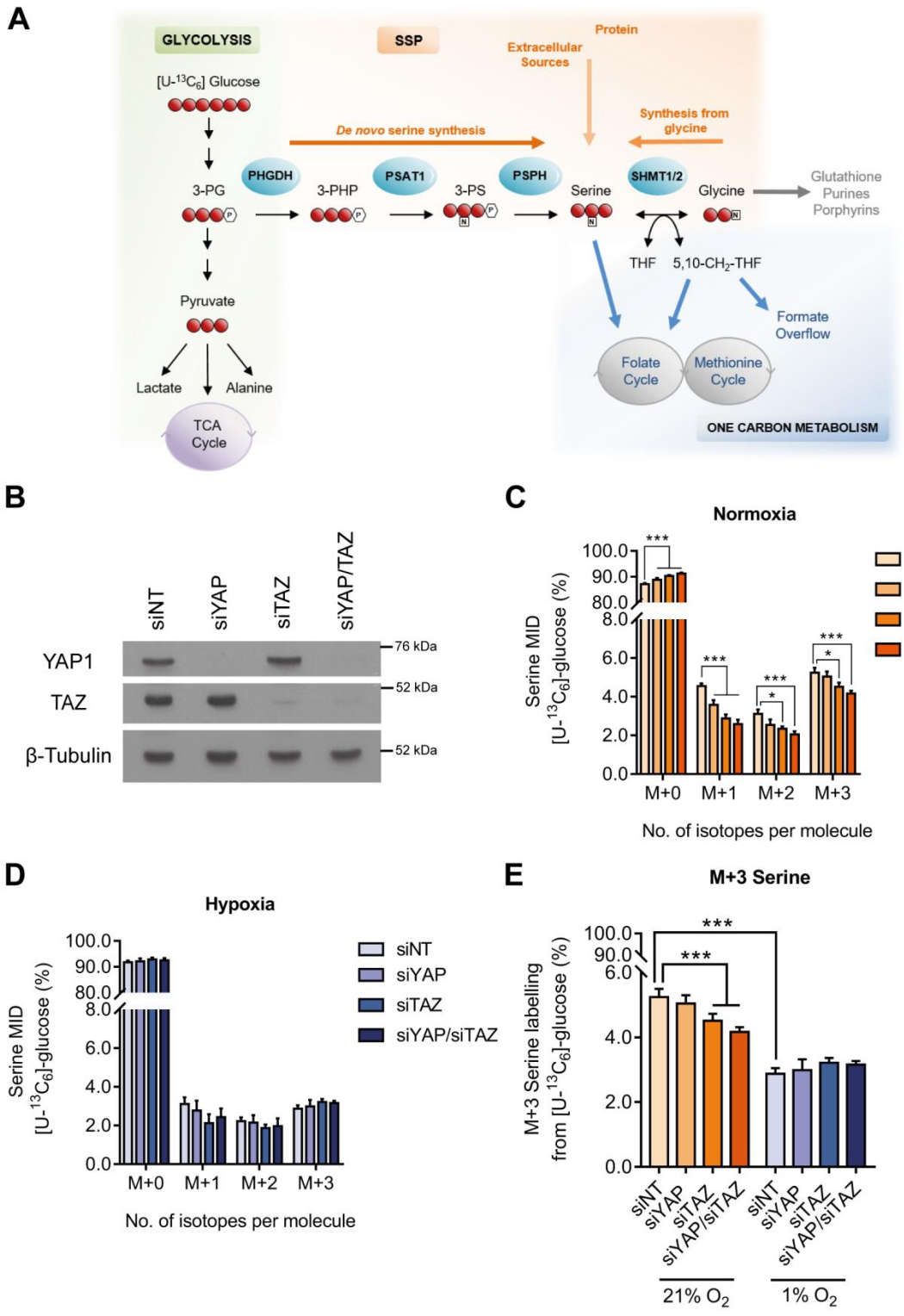
A
GLYCOLYSIS
SSP
Protein
Extracellular Sources
[U-13C6] Glucose
De novo serine synthesis
Synthesis from glycine
PHGDH
PSAT1
PSPH
SHMT1/2
3-PG
3-PHP
3-PS
Serine
Glycine
Glutathione
Purines
Porphyrins
THF
5,10-CH2-THF
Pyruvate
Formate Overflow
Lactate
Alanine
Folate Cycle
Methionine Cycle
TCA Cycle
ONE CARBON METABOLISM
B
siNT
siYAP
siTAZ
siYAP/TAZ
YAP1
TAZ
β-Tubulin
76 kDa
52 kDa
52 kDa
C
Normoxia
Serine MID [U-13C6]-glucose (%)
siNT
siYAP
siTAZ
siYAP/siTAZ
M+0
M+1
M+2
M+3
No. of isotopes per molecule
D
Hypoxia
Serine MID [U-13C6]-glucose (%)
siNT
siYAP
siTAZ
siYAP/siTAZ
M+0
M+1
M+2
M+3
No. of isotopes per molecule
E
M+3 Serine
M+3 Serine labelling from [U-13C6]-glucose (%)
siNT
siYAP
siTAZ
siYAP/siTAZ
21% O2
1% O2

Figure 3.11 YAP/TAZ support *de novo* serine synthesis under normoxic conditions. (A) Schematic showing an overview of the *de novo* SSP and pathways into one-carbon metabolism from glycolysis. Red circles denote the carbons in each metabolite which are incorporated from uniformly labelled ^{13}C glucose ([U-$^{13}C_6$]-glucose). (B) Successful knockdown of YAP, TAZ and YAP/TAZ was confirmed in U343 cells from glucose tracing experiments. (C) MIDs of serine following 24 h labelling of U343 cells with [U-$^{13}C_6$]-glucose and 72 h knockdown of YAP, TAZ and YAP/TAZ under normoxic conditions. M+0, M+1, M+2 etc. mass isotopomers correspond to the ion fragments containing 0, 1, 2 etc. ^{13}C atoms respectively. It is clear that knockdown of YAP, TAZ and YAP/TAZ significantly reduces the percentage of ^{13}C labelling into serine compared to the non-targeting siRNA (siNT). (D) Under hypoxic conditions however, the knockdown has no additional effect when compared to the siNT. (E) *De novo* serine synthesis can be denoted by the M+3 isotopomer, which is significantly reduced upon knockdown of TAZ and YAP/TAZ suggesting a potential role for YAP and TAZ supporting serine synthesis derived from glucose under normoxic conditions. Additionally, hypoxia was also seen to significantly reduce the percentage of M+3 serine derived from glucose. Abbreviations: 3-PG, 3-phosphoglycerate; 3-PHP, 3-phosphohydroxypyruvate; 3-PS, 3-phosphoserine; 5,10-CH_2-THF, N^5,N^{10}-methylene tetrahydrofolate; PHGDH, phosphoglycerate dehydrogenase; PSAT1, phosphoserine aminotransferase 1; PSPH, phosphoserine phosphatase; SHMT 1/2, serine hydroxymethyltransferase 1/2; TCA, tricarboxylic acid; THF, tetrahydrofolate. Data obtained was from 5 technical replicates. Error bars represent ± S.D. Significance determined using two-way ANOVA with Tukey post-hoc test. * $p<0.05$, *** $p<0.001$.

Despite a reduction in fully labelled M+3 serine suggesting reduced synthesis, it could also indicate that serine usage was increased upon YAP/TAZ knockdown, resulting in less detectable ^{13}C incorporation. Therefore, ^{13}C incorporation into glycine from [U-$^{13}C_6$]-glucose was analysed in both normoxic and hypoxic conditions (Figure 3.12). Surprisingly M+2 glycine, which is indicative of conversion from M+3 serine, was not detected in both normoxic (Figure 3.12A) or hypoxic conditions (Figure 3.12B) suggesting either disrupted *de novo* glycine production from serine or increased usage by the glycine-cleavage system for one-carbon metabolism. As the case for serine, the majority of glycine from glucose was unlabelled suggesting that U343 cells rely on extracellular sources to provide glycine for the cell, which could include serine (Figure 3.12).

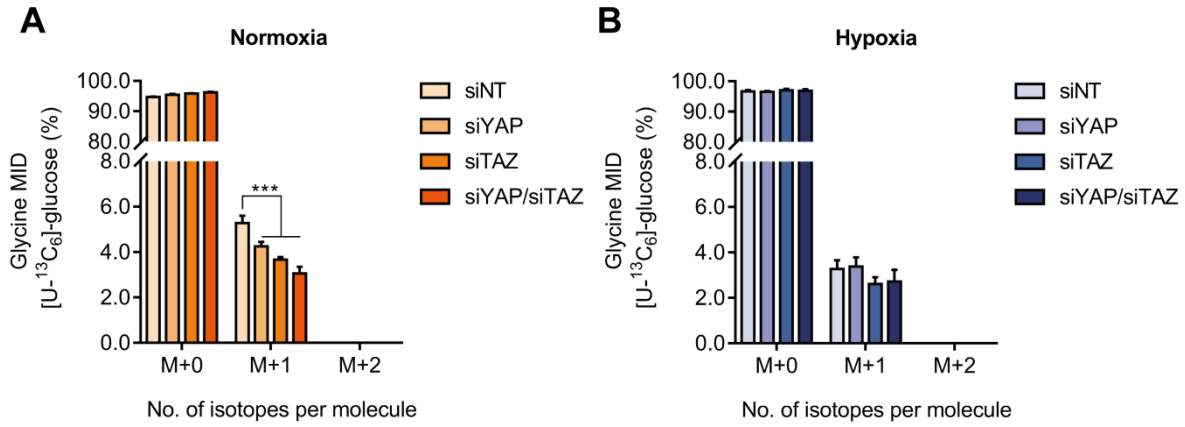

Figure 3.12 U343 cells exhibit altered serine-glycine metabolism. MIDs of glycine following 24 h labelling of U343 cells with [U-$^{13}C_6$]-glucose and 72 h knockdown of YAP, TAZ and YAP/TAZ under normoxic (A; 21% O_2) and hypoxic (B; 1% O_2) conditions. It is clear that knockdown of YAP, TAZ and YAP/TAZ results in reduced ^{13}C incorporation into glycine from glucose compared to the siNT under normoxic but not hypoxic conditions. Interestingly, no M+2 labelled glycine was detected in either condition, which would have been derived from M+3 serine. M+1 labelled glycine could be established by upstream processing of glucose through the oxidative and non-oxidative PPP resulting in differential labelling ^{13}C patterns of 3-PG which would then result in M+1 labelled serine. Data obtained was from 5 technical replicates. Error bars represent ± S.D. Significance determined using two-way ANOVA with Tukey post-hoc test. *** $p<0.001$.

3.2.6.2. Knockdown of YAP/TAZ alters pyruvate metabolism

At the end point of glycolysis, pyruvate is a critical metabolic node driving several crucial biosynthetic pathways as well as being one of the main entry points into the TCA cycle (Figure 3.13A). Alterations to ^{13}C incorporation into this important metabolite can therefore disclose information with regards to the cell metabolic function. Knockdown of YAP/TAZ was seen to significantly increase the percentage ^{13}C incorporation into fully labelled M+3 pyruvate from [U-$^{13}C_6$]-glucose when compared to the siNT control under both normoxic (Figure 3.13B) and hypoxic (Figure 3.13C) conditions. Under hypoxic conditions, ^{13}C incorporation into pyruvate was significantly increased with siYAP/TAZ compared to knockdown under normoxic conditions as well as the hypoxic siNT control (Figure 3.13D). Interestingly, upon knockdown of YAP/TAZ, unlabelled pyruvate was also significantly reduced suggesting increased reliance on pyruvate derived from glucose as

opposed to from other sources in these cells, particularly under hypoxic conditions (Figure 3.13C). These data thereby suggest that the glycolytic rate could be increased in the U343 cells upon knockdown of YAP/TAZ.

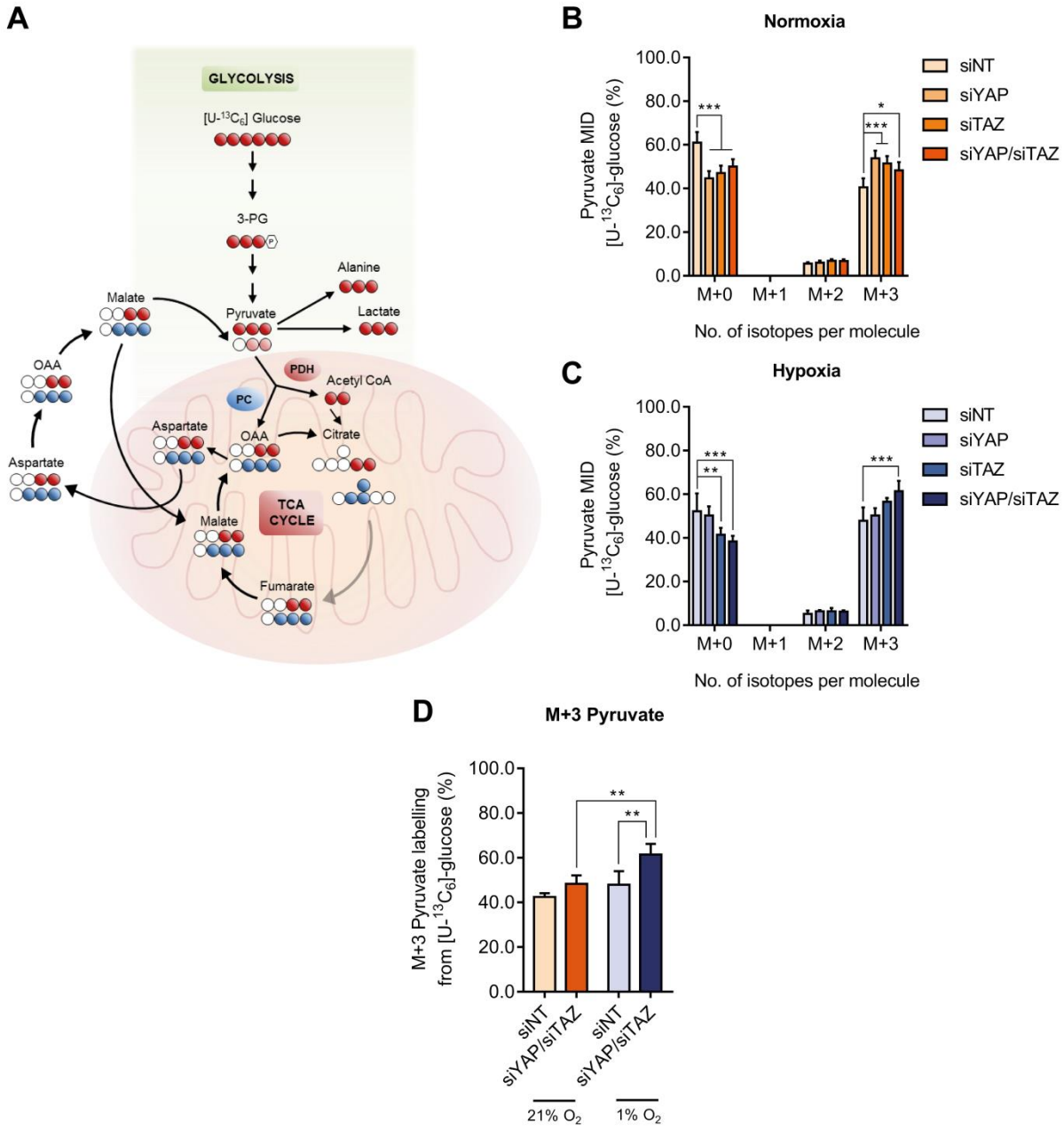

Figure 3.13 Knockdown of YAP and TAZ increases glycolysis in U343 cells. (A) Schematic showing an overview of pyruvate metabolism from glycolysis into the TCA cycle. Circles denote the incorporation of carbon from uniformly labelled ^{13}C glucose ([U-$^{13}C_6$]-glucose) through PDH (red) and PC (blue) activity in U343 cells. Upon YAP, TAZ and YAP/TAZ knockdown, fully labelled M+3 pyruvate is increased in both normoxic (B; 21% O_2) and hypoxic (C; 1% O_2) conditions. (D) Knockdown of YAP/TAZ is shown to significantly increase fully labelled M+3 pyruvate under hypoxia compared to normoxic conditions. Additionally, YAP/TAZ knockdown is seen to exacerbate M+3 labelled pyruvate when compared to siNT in 1% O_2 suggesting increased glycolysis. Abbreviations: 3-PG, 3-phosphoglycerate; OAA, oxaloacetate; PC, pyruvate carboxylase; PDH, pyruvate dehydrogenase, TCA, tricarboxylic acid. Data obtained was from 5 technical replicates. Error bars represent ± S.D. Significance determined using two-way ANOVA with Tukey post-hoc test.* $p<0.05$, ** $p<0.01$, *** $p<0.001$.

A significant proportion of glucose-derived pyruvate is reduced in the cytosol to form lactate via LDH; a reaction that is coupled with the oxidation of NADH to generate NAD^+ that can be subsequently recycled by GAPDH to maintain glycolytic flux[179]. Under hypoxic conditions, lactate production from pyruvate is substantially increased due to the decreased NADH oxidation by the mitochondrial ETC, thereby ensuring continued glycolytic flux for ATP production[179]. After knockdown of YAP and TAZ, percentage ^{13}C incorporation from [U-$^{13}C_6$]-glucose into lactate was seen to be slightly increased compared to the normoxic control (Figure 3.14A). Under hypoxic conditions however, knockdown of YAP, TAZ and YAP/TAZ all caused a significant reduction in M+3 lactate when compared to the siNT control (Figure 3.14B). Comparing the percentage incorporation from glucose into fully labelled (M+3) lactate, a significant increase was observed when cells were exposed to hypoxia, indicative of the cell maintaining increased glycolytic flux where conditions are limiting for ATP production through oxidative phosphorylation (Figure 3.14C). Interestingly, when the ratio of M+3 lactate from M+3 pyruvate was calculated (Figure 3.14D), a significant reduction was seen upon YAP and TAZ knockdown when compared to the siNT control in both normoxia and hypoxia suggesting that YAP and TAZ may influence pyruvate reduction to lactate. This would most often be through changes in mitochondrial NADH oxidation, so the fate of pyruvate in the mitochondria was also examined.

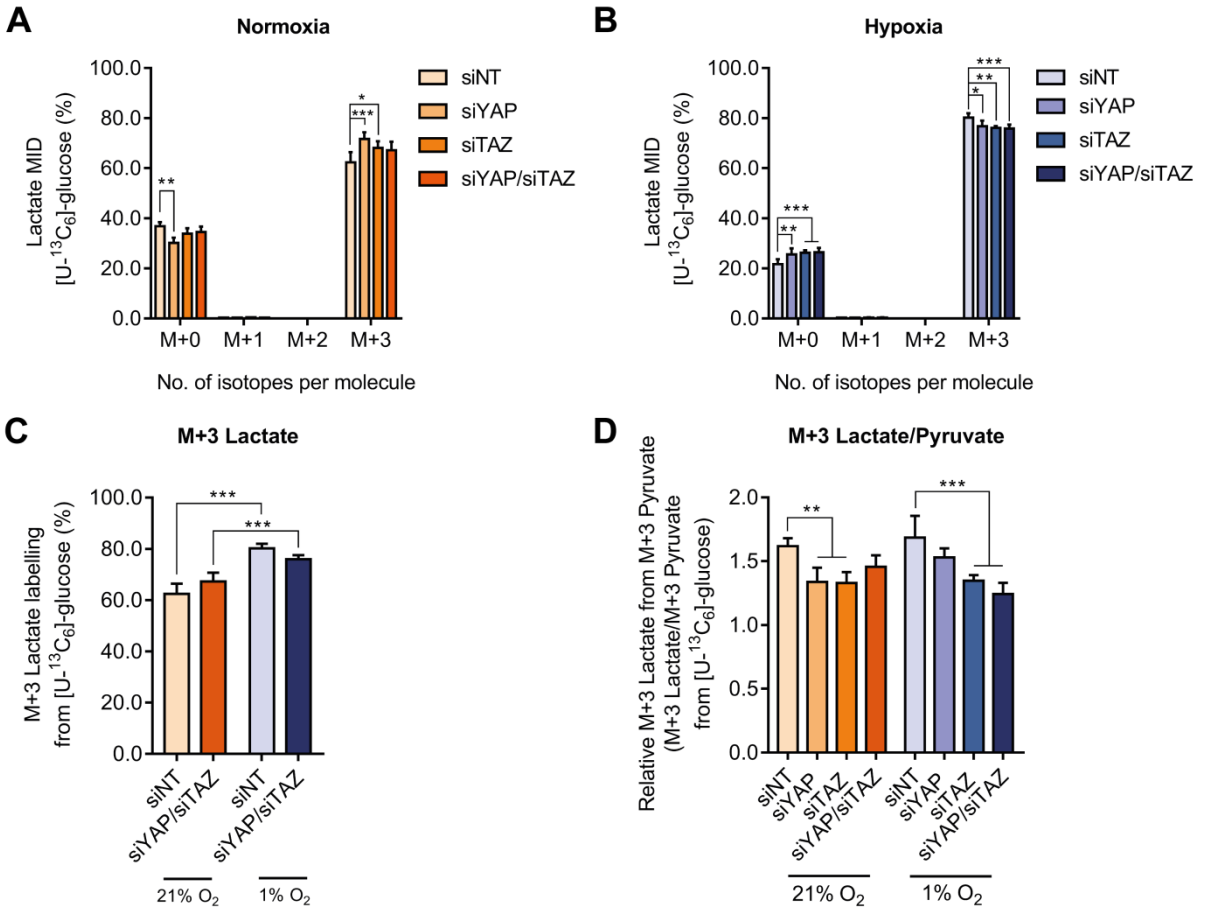

Figure 3.14 Knockdown of YAP and TAZ alters pyruvate metabolism in U343 cells. The percentage ^{13}C incorporation into lactate from [U-$^{13}C_6$]-glucose was increased following siYAP and siTAZ in normoxia (A; 21% O_2) but was decreased with siYAP, siTAZ and siYAP/TAZ under hypoxic conditions (B; 1% O_2) when compared to the siNT control. (C) M+3 lactate can be derived from fully labelled pyruvate and was seen to significantly increase under hypoxic conditions, which is indicative of increased aerobic glycolysis (D) The ratio of fully labelled lactate from fully labelled pyruvate was calculated and seen to significantly decrease upon knockdown with siYAP and siTAZ in normoxic and siTAZ and siYAP/TAZ in hypoxia when compared to the siNT for each oxygen tension. Data obtained was from 5 technical replicates. Error bars represent ± S.D. Significance determined using two-way ANOVA with Tukey post-hoc test.* p<0.05, ** p<0.01, *** p<0.001.

Transamination of pyruvate to alanine via ALT is thought to occur in the mitochondria for use in amino acid metabolism[179]. Metabolic analysis of ^{13}C incorporation from [U-$^{13}C_6$]-glucose into alanine revealed that knockdown of YAP/TAZ significantly reduced percentage incorporation in both normoxic (Figure 3.15A) and hypoxic conditions (Figure 3.15B). Furthermore, upon knockdown, the percentage incorporation which was unlabelled was significantly increased suggesting an increased reliance of carbon

incorporation into alanine from other sources. Hypoxia was seen to increase fully labelled M+3 alanine from glucose in both siNT and siYAP/TAZ cells however, percentage incorporation was significantly reduced upon siYAP/TAZ knockdown compared to the siNT in both normoxic and hypoxic conditions (Figure 3.15C). Analysis of the ratio of M+3 alanine from M+3 pyruvate (Figure 3.15D) showed that YAP/TAZ knockdown caused a significant reduction suggesting that pyruvate maybe being diverted elsewhere, such as increased entry into the TCA cycle.

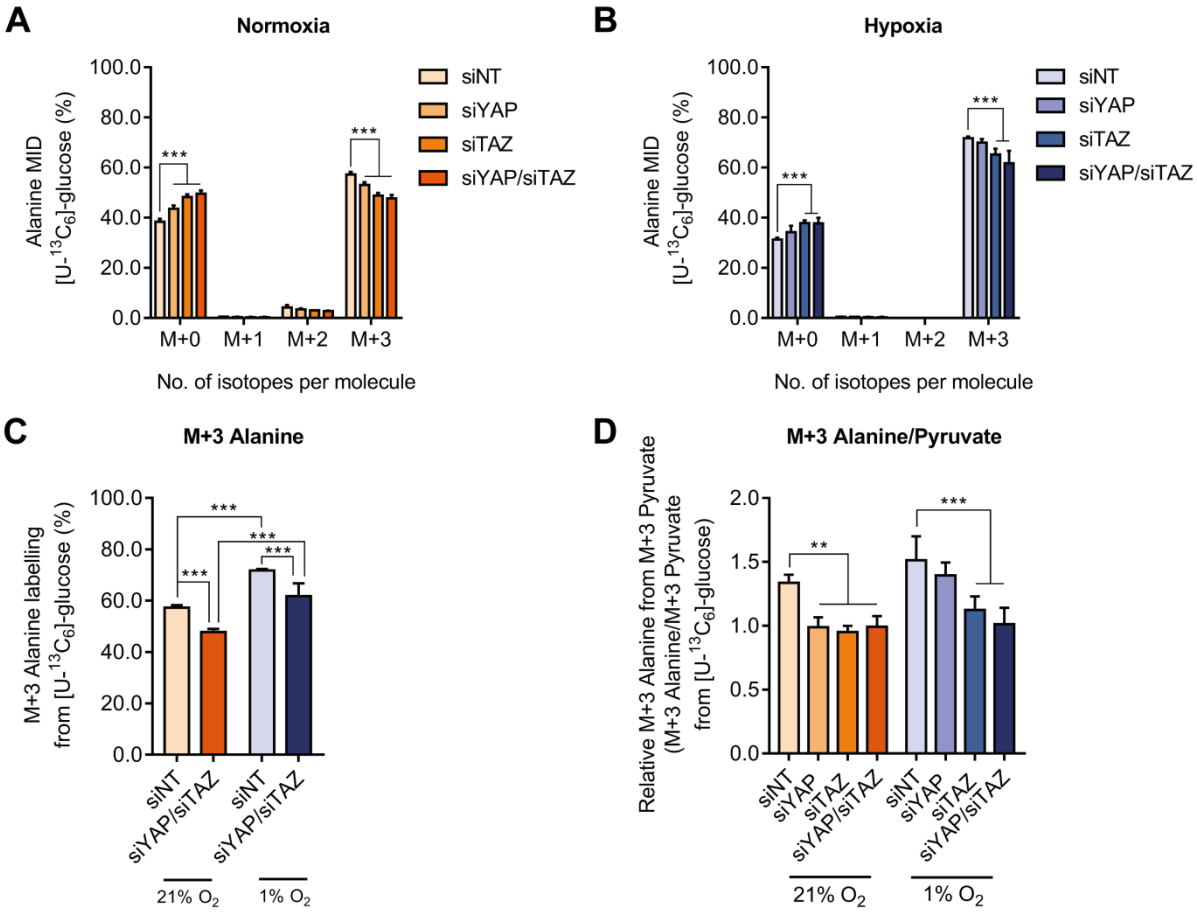

Figure 3.15 U343 cells showed reduced ^{13}C incorporation into alanine with knockdown of YAP/TAZ. The percentage ^{13}C incorporation into alanine from [U-$^{13}C_6$]-glucose was significantly decreased following knockdown of siYAP, siTAZ and siYAP/TAZ in normoxic (A; 21% O_2) and hypoxic conditions (B; 1% O_2) when compared to the siNT control. (C) Fully labelled M+3 alanine can be derived from fully labelled pyruvate and was seen to increase under hypoxic conditions in both the control cells and after knockdown of YAP/TAZ. However, when compared to the siNT control, YAP/TAZ caused a significant reduction in M+3 alanine in both 21% and 1% O_2. (D) Calculating the ratio of M+3 alanine derived from M+3 pyruvate showed a significant decrease upon knockdown of YAP and TAZ in both normoxic and hypoxic conditions. Data obtained was from 5 technical replicates. Error bars represent ± S.D. Significance determined using two-way ANOVA with Tukey post-hoc test. ** $p<0.01$, *** $p<0.001$.

Introduction of glucose carbons into the mitochondrial TCA cycle is through two different metabolic fates of pyruvate – oxidation to acetyl CoA by PDH, or carboxylation by PC to form OAA (Figure 3.13A). Due to a different number of carbons being incorporated from pyruvate into both acetyl CoA (M+2 labelled) and OAA (M+3 labelled), the resulting downstream TCA metabolites will demonstrate different labelling patterns from [U-$^{13}C_6$]-glucose depending on the relative enzymatic activity of PDH or PC (Figure 3.13A). Analysis of the TCA cycle (and related) metabolites aspartate, malate and fumarate showed significantly increased percentage ^{13}C incorporation in the M+3 isotopomer upon knockdown of YAP/TAZ in both normoxic and hypoxic conditions (Figure 3.16). Interestingly, there were no significant changes in the M+2 isotopomer in any of the metabolites upon knockdown compared to the siNT, indicating that upon knockdown of YAP/TAZ, downstream oxidative glucose metabolism remains relatively unchanged. On the other hand, an increase in M+3 labelled metabolites suggests that activity of PC is potentially increased and therefore favouring carboxylation of pyruvate to form OAA.

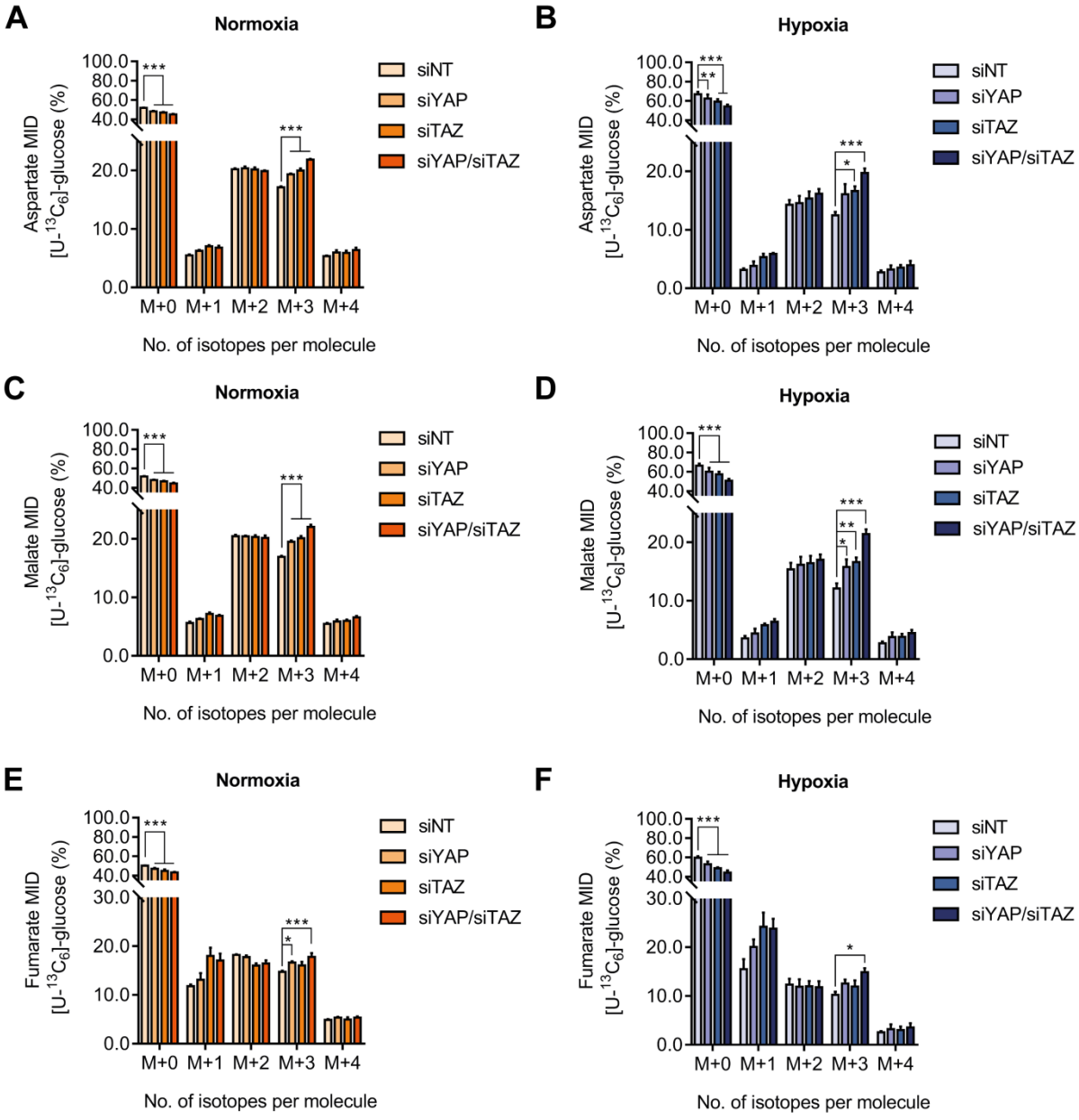

Figure 3.16 Knockdown of YAP/TAZ results in increased anaplerotic pyruvate metabolism. Upon knockdown of YAP, TAZ and YAP/TAZ, an increase in the M+3 labelling of metabolites aspartate (A, B), malate (C, D) and fumarate (E, F) was apparent in both normoxic (21% O_2) and hypoxic (1% O_2) conditions when compared to the siNT control. This increase in M+3 is indicative of increased pyruvate carboxylation by PC which subsequently generates M+3 labelled OAA from pyruvate and can therefore produce M+3 labelled aspartate, malate and fumarate. Little to no-change was apparent in the M+2 labelling which is a product of pyruvate being oxidatively decarboxylated via PDH to produce M+2 acetyl CoA, thus forming downstream M+2 labelled TCA metabolites. Data obtained was from 5 technical replicates. Error bars represent ± S.D. Significance determined using two-way ANOVA with Tukey post-hoc test. * $p<0.05$, ** $p<0.01$, *** $p<0.001$.

This observation can be further explored by investigating the MID of citrate, where carbons can arise both from acetyl CoA as well as OAA (Figure 3.17). Observations show that M+2 citrate was significantly reduced upon YAP/TAZ knockdown in both normoxic (Figure 3.17A) and hypoxic conditions (Figure 3.17B) which coincided with a significant increase in M+3 labelled citrate. Although, M+2 labelled citrate is most predominant isotopomer observed, these results suggest that YAP/TAZ knockdown can enforce a switch in pyruvate metabolism from oxidising glucose to anaplerotic pyruvate carboxylation to replenish TCA metabolites. Relative PC activity was therefore calculated through the ratio of M+3 citrate/M+2 citrate (Figure 3.17D) and observed to be significantly increased upon knockdown of YAP, TAZ and YAP/TAZ when compared to the siNT in both normoxic and hypoxic conditions. PC activity was seen to be significantly reduced under hypoxic conditions in the control cells which corresponds to an expected reduction in TCA activity, however knockdown of YAP/TAZ was able to sustain PC activity comparative to levels observed in normoxia (Figure 3.17D).

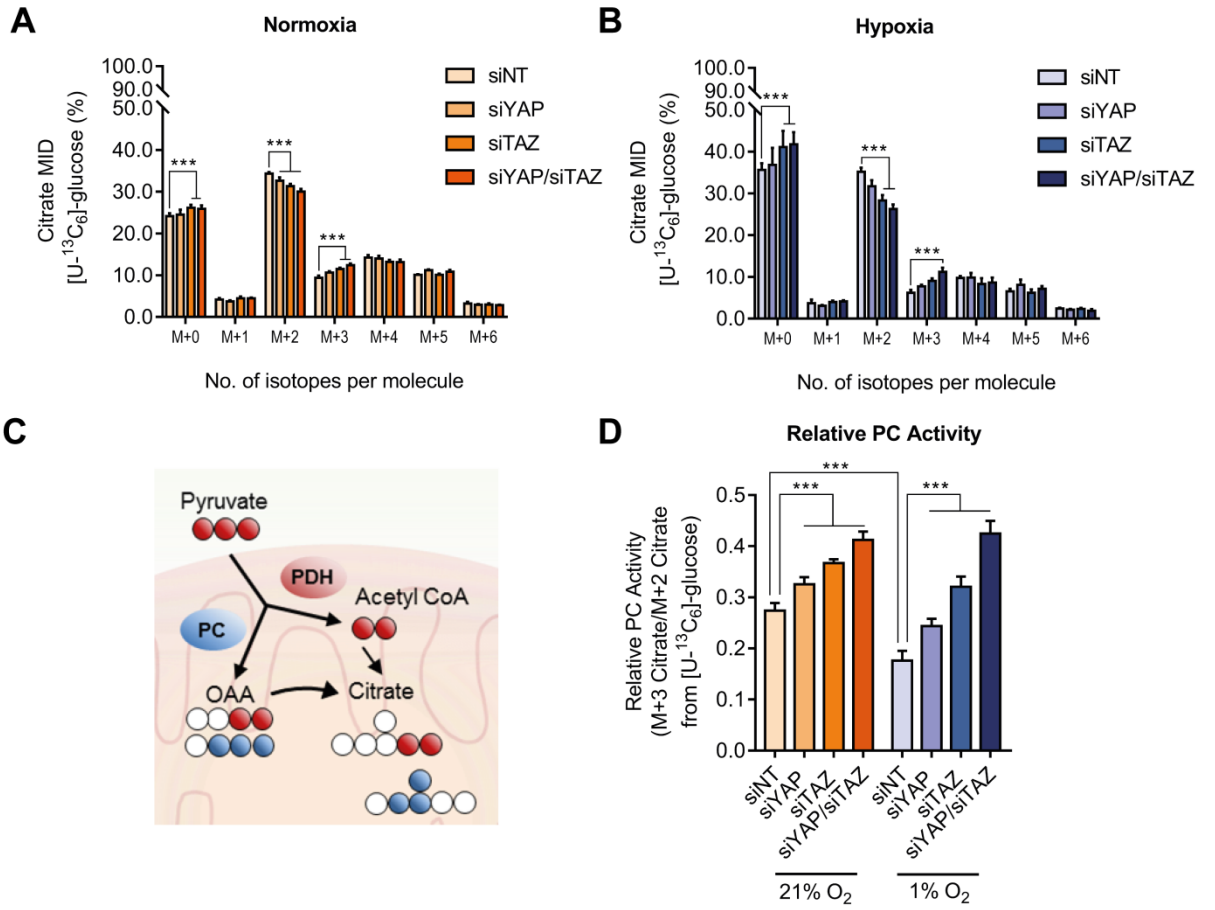

Figure 3.17 PC activity is increased following YAP/TAZ knockdown and is sustained under hypoxia. Knockdown of YAP/TAZ was seen to significantly reduce citrate M+2 labelling in both 21% (A) which was exacerbated under 1% O_2 (B). Additionally, a significant increase in citrate M+3 labelling was observed compared to the siNT control in both conditions. (C) Schematic showing the metabolic fate of pyruvate derived from [U-$^{13}C_6$]-glucose into the TCA cycle. Pyruvate oxidation via PDH (red pathway) results in M+2 citrate from [U-$^{13}C_6$]-glucose. Under certain conditions such as hypoxia, PDH activity can be reduced and an increase in PC activity is (blue pathway) observed which results in the carboxylation of pyruvate to OAA subsequently producing M+3 citrate. (D) The difference in the production of M+3 over M+2 labelled citrate can therefore imply the differential activity of these enzymes. It is clear that despite at a lower level than PDH activity, a switch from PDH to PC activity occurs upon knockdown of YAP, TAZ and YAP/TAZ which is significantly increased under hypoxic conditions when compared to the siNT control. Abbreviations: PC, pyruvate carboxylase; PDH, pyruvate dehydrogenase; OAA, oxaloacetate. Data obtained was from 5 technical replicates. Error bars represent ± S.D. Significance determined using two-way ANOVA with Tukey post-hoc test. *** $p<0.001$.

3.2.6.3. Knockdown of YAP/TAZ compromises oxidative glutamine metabolism

Cancer cells, in the absence of adequate glucose oxidation, are known to switch their reliance to glutamine as a carbon and nitrogen source to fuel nucleotide biosynthesis as

well as supply carbons into the TCA cycle to support the functioning of the ETC in the production of ATP[224]. Glutamine is known to be avidly consumed under hypoxic conditions to sustain rapid cell proliferation as well as becoming the major carbon source for fatty acid synthesis, as hypoxic cells shift their metabolism away from glucose oxidation through the TCA cycle towards increased glycolytic metabolism[197,198].

Since glutamine metabolism is crucial for rapidly proliferating cells and the oncogenic relationship between YAP/TAZ and malignant cell growth and survival, glutamine metabolism was investigated upon knockdown of YAP, TAZ and YAP/TAZ in U343 glioma cells under both normoxic and hypoxic conditions using [U-$^{13}C_5$]-glutamine. Following cellular uptake, glutamine can be deaminated to glutamate via GLS, which can subsequently be converted to α-KG by either GLDH or via transamination through transaminase activity (Figure 3.18A). Metabolic tracer analysis showed that upon knockdown of YAP/TAZ (Figure 3.18B), ^{13}C incorporation from [U-$^{13}C_5$]-glutamine into both glutamate and α-KG was significantly reduced under normoxic conditions (Figure 3.18C, E) and was seen to be amplified in hypoxia (Figure 3.18D, F), where glutamine usage is known to be increased. The ratio of fully labelled M+5 glutamate (Figure 3.18G) and α-KG (Figure 3.18H) from M+5 glutamine was significantly increased under hypoxic conditions as expected, however knockdown of YAP/TAZ caused a significant reduction in both normoxic and hypoxic conditions, with levels in hypoxia similar to those observed in normoxia upon knockdown (Figure 3.18G, H). These results fit with the increased anaplerosis from glucose through PC activity observed after knockdown of YAP and/or TAZ, as this would be required to 'top up' the TCA cycle when glutamine carbon entry is reduced.

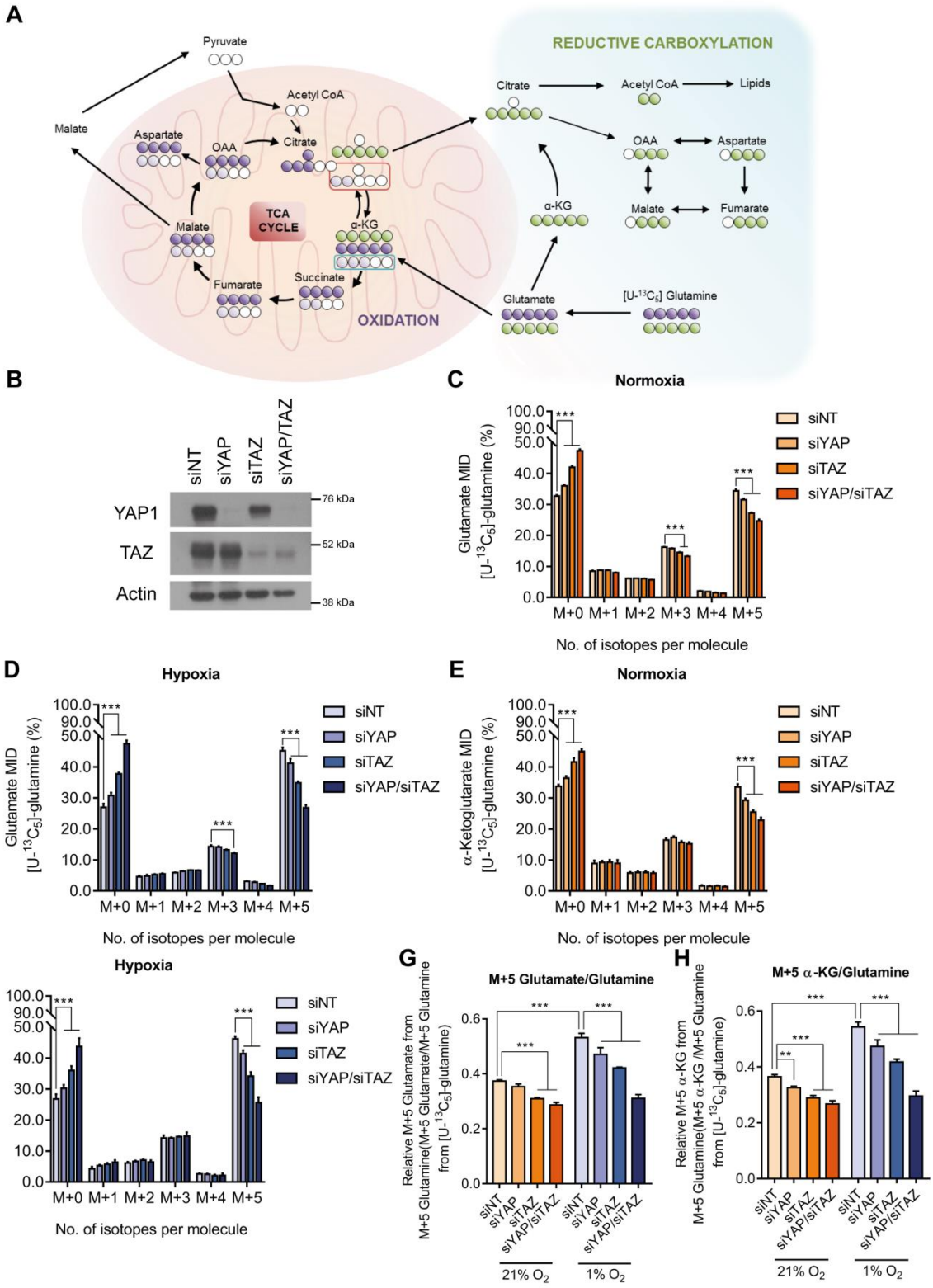
A
Pyruvate
Malate
Acetyl CoA
Aspartate
OAA
Citrate
TCA CYCLE
α-KG
Malate
Fumarate
Succinate
OXIDATION
REDUCTIVE CARBOXYLATION
Citrate
Acetyl CoA
Lipids
OAA
Aspartate
α-KG
Malate
Fumarate
Glutamate
[U-13C5] Glutamine
B
siNT
siYAP
siTAZ
siYAP/TAZ
YAP1
TAZ
Actin
76 kDa
52 kDa
38 kDa
C
Normoxia
Glutamate MID [U-13C5]-glutamine (%)
siNT
siYAP
siTAZ
siYAP/siTAZ
M+0 M+1 M+2 M+3 M+4 M+5
No. of isotopes per molecule
D
Hypoxia
Glutamate MID [U-13C5]-glutamine (%)
No. of isotopes per molecule
E
Normoxia
α-Ketoglutarate MID [U-13C5]-glutamine (%)
No. of isotopes per molecule
F
Hypoxia
α-Ketoglutarate MID [U-13C5]-glutamine (%)
No. of isotopes per molecule
G
M+5 Glutamate/Glutamine
Relative M+5 Glutamate from M+5 Glutamine(M+5 Glutamate/M+5 Glutamine from [U-13C5]-glutamine)
21% O2
1% O2
H
M+5 α-KG/Glutamine
Relative M+5 α-KG from M+5 Glutamine(M+5 α-KG /M+5 Glutamine from [U-13C5]-glutamine)
21% O2
1% O2

Figure 3.18 YAP/TAZ supports glutamine metabolism in glioma cells. (A) Schematic outlining the metabolic pathways of [U-$^{13}C_5$]-glutamine. Glutamine-derived α-KG can either be subjected to oxidative TCA metabolism (purple pathway) producing M+4 labelled TCA cycle intermediates or can undergo reductive carboxylation (green pathway) in conditions such as hypoxia, to generate M+5 labelled citrate and M+3 labelled TCA intermediates. Additionally a second round of the oxidative TCA cycle (light purple) can produce M+3 labelled α-KG (highlighted in blue) which generates M+2 labelled TCA metabolites and M+2 labelled citrate (outlined in red). (B) Successful knockdown of YAP, TAZ and YAP/TAZ was confirmed in U343 cells from [U-$^{13}C_5$]-glutamine tracing experiments. (C) M+5 labelled glutamate and α-KG (E) derived from [U-$^{13}C_5$]-glutamine was significantly reduced upon knockdown of YAP, TAZ and YAP/TAZ in 21% O_2 and was exacerbated in 1% O_2 (D and F). The ratio of M+5 glutamate (G) and M+5 α-KG (H) from fully labelled glutamine was calculated and seen to significantly decrease upon knockdown of YAP/TAZ in both normoxic and hypoxic conditions when compared to the siNT control. Additionally, significantly more M+5 labelled glutamate and α-KG from M+5 glutamine was observed under 1% O_2 which is indicative of metabolic changes seen in hypoxia. Abbreviations: α-KG, alpha-ketoglutarate; OAA, oxaloacetate; TCA, tricarboxylic acid. Data obtained was from 5 technical replicates. Error bars represent ± S.D. Significance determined using two-way ANOVA with Tukey post-hoc test. ** $p<0.01$, *** $p<0.001$.

Glutamine-derived α-KG is either metabolised oxidatively through glutaminolysis, supplying carbons into the TCA cycle for the production of anabolic substrates and reducing potential to generate ATP, or through reductive carboxylation to produce citrate to support *de novo* lipogenesis, the latter of which may be a major contributor to the anabolic drive in hypoxic conditions[198]. ^{13}C incorporation into citrate can therefore be used as evidence for the prevailing metabolic phenotype in a cancer cell. Upon knockdown of YAP/TAZ, a significant reduction in the citrate M+4 isotopomer was apparent under normoxic conditions, which is indicative of reduced contribution of glutamine oxidation through the TCA cycle to the citrate pool (Figure 3.19A). Under hypoxic conditions, an increase in M+5 labelling was seen compared to normoxia, however was reduced upon knockdown of YAP/TAZ, indicating that reductive carboxylation of glutamine was increased in hypoxia but attenuated in YAP/TAZ deficient cells (Figure 3.19B). A significant reduction in citrate M+4 labelling was also apparent in hypoxia upon YAP/TAZ deficiency, again suggesting that oxidative glutamine metabolism was severely compromised. The relative reductive/oxidative glutamine metabolism was

calculated using the ratio of M+5 citrate/M+4 citrate, which showed that despite reductive and oxidative glutamine metabolism being overall reduced in hypoxia with YAP/TAZ knockdown, the relative contribution of reductive glutamine metabolism was increased compared to glutamine oxidation under hypoxia (Figure 3.19C, D). These data suggest, in agreement with the literature on breast cancer, that YAP/TAZ activity supports glutamine oxidation in glioma – in both normoxia and hypoxia. This increased importance of YAP/TAZ to support glutaminolysis in hypoxia could be expected to sustain cell proliferation under these hostile conditions. Interestingly, knockdown of YAP/TAZ in U87 and U343 cells (Figure 3.10), significantly reduced cell proliferation in both normoxic and hypoxic conditions, supporting this potential association.

Due to the significant reduction in ^{13}C incorporation into glutamate and α-KG from [U-$^{13}C_5$]-glutamine coupled with attenuated glutamine oxidative and reductive metabolism, it was hypothesised that knockdown of YAP/TAZ could potentially interfere with glutamine processing such as through impeding glutaminase activity. Thus, GLS1 expression was analysed following knockdown of YAP, TAZ and YAP and TAZ together in both U87 (Figure 3.19E) and U343 (Figure 3.19F) cells. Despite considerable knockdown of these proteins, no differences were observed in GLS1 expression suggesting potentially that glutamine uptake could be reduced or that glutamine was being diverted elsewhere in the cell for use in other biosynthetic processes upon YAP/TAZ knockdown.

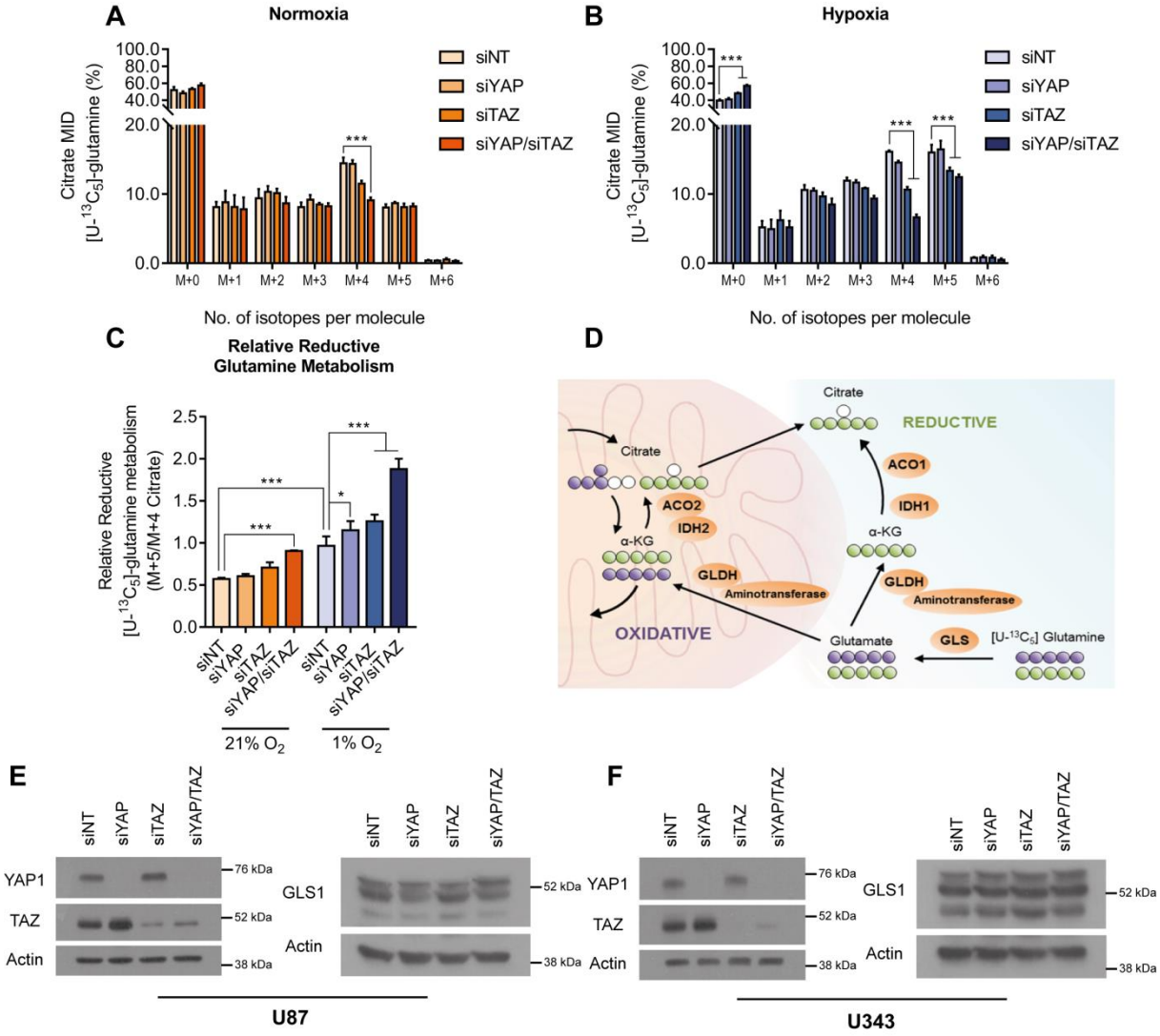

Figure 3.19 Knockdown of YAP/TAZ significantly increases reductive glutamine metabolism in hypoxia. (A) Knockdown of YAP/TAZ significantly decreased M+4 citrate from [U-$^{13}C_5$]-glutamine compared to siNT control. Under 1% O_2 (B), M+4 labelling was also decreased upon siTAZ and siYAP/TAZ however M+5 labelling was seen to increase, albeit at a reduced amount upon knockdown of TAZ and YAP/TAZ when compared to the siNT control. (C) The ratio of M+5 citrate to M+4 citrate was calculated to determine relative reductive glutamine metabolism and was observed to be significantly increased in hypoxic conditions compared to normoxic conditions which was further exacerbated upon knockdown of YAP/TAZ. (D) Schematic outlining the oxidative (purple) and reductive (green) glutamine metabolism including the relevant enzymes in orange. (E) Knockdown of YAP, TAZ and YAP/TAZ did not appear to cause any reduction in GLS1 expression in both the U87 and U343 cell lines. Abbreviations: α-KG, alpha-ketoglutarate; ACO1/2, aconitase 1/2; GLDH, glutamate dehydrogenase; GLS, glutaminase; IDH1/2, isocitrate dehydrogenase 1/2. Data obtained was from 5 technical replicates. Error bars represent ± S.D. Significance determined using two-way ANOVA with Tukey post-hoc test. * p<0.05, *** p<0.001.

The synthesis of glutamine-derived aspartate, a metabolite shown to be essential for tumour growth, was also observed to be affected upon YAP/TAZ knockdown[181,182]. Metabolic analysis showed that ^{13}C incorporation from [U-$^{13}C_5$]-glutamine was significantly reduced in normoxic (Figure 3.20A) and hypoxic conditions (Figure 3.20B). The aspartate M+4 and M+2 isotopomer was reduced, which corresponds to one and two rounds of oxidative glutamine metabolism respectively and corroborates previous data suggesting attenuated glutaminolysis upon YAP/TAZ deficiency. Interestingly, the M+3 isotopomer, derived from M+5 citrate through reductive carboxylation was also reduced suggesting the potential diversion of citrate and/or OAA – the latter of which cannot be detected due to very low steady-state levels being maintained in cells. Furthermore, the percentage of unlabelled (M+0) aspartate was significantly enhanced upon YAP/TAZ knockdown in both normoxia and hypoxia, suggesting an increased reliance on other carbon sources for aspartate production. Interestingly, in addition to unlabelled sources, a significantly increased carbon contribution from glucose to aspartate was observed upon YAP/TAZ knockdown in both normoxia and hypoxia (discussed later in Figure 3.22B). Nevertheless, some glutamine is still ultimately required to contribute the nitrogen in the amine group for aspartate synthesis via transamination of OAA. These observations may suggest that YAP/TAZ could influence transamination reactions since there is an overall reduction in the ^{13}C incorporation from glutamine.

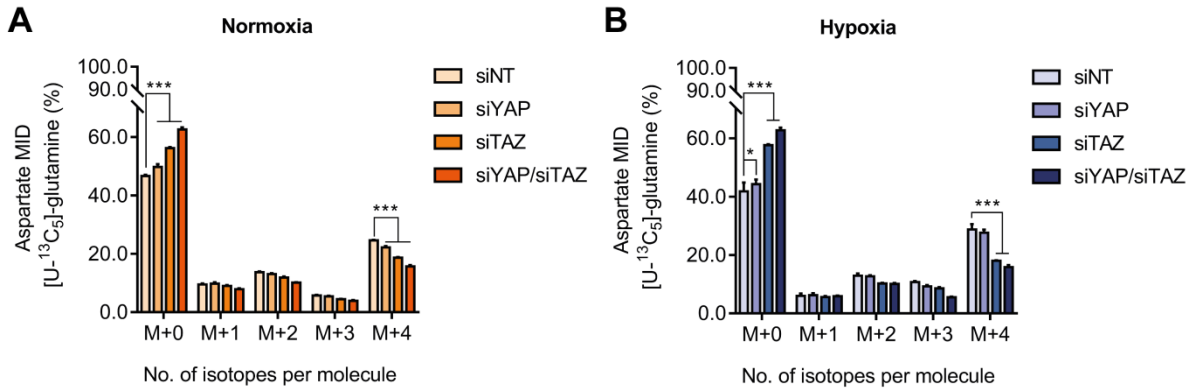

Figure 3.20 Knockdown of YAP/TAZ compromises oxidative glutamine metabolism. Knockdown of YAP/TAZ was seen to significantly decrease M+4 aspartate from [U-$^{13}C_5$]-glutamine compared to siNT control. Under 1% O_2 **(B),** M+4 labelling was also decreased upon siTAZ and siYAP/TAZ when compared to the siNT control. Data obtained was from 5 technical replicates. Error bars represent ± S.D. Significance determined using two-way ANOVA with Tukey post-hoc test. *** p<0.001.

3.2.6.4. YAP/TAZ support glutamine-derived proline biosynthesis

Glutamine is known to have a number of metabolic fates within the cell. In addition to amino acid and nucleotide synthesis, the biosynthesis of one of the many glutamine-derived NEAAs proline is particularly important for subsequent protein synthesis and cell proliferation[225] (Figure 3.21A). Metabolic tracing analysis showed a significant reduction in the percentage ^{13}C incorporation from [U-$^{13}C_5$]-glutamine into M+5 labelled proline in both normoxic (Figure 3.21B) and hypoxic (Figure 3.21C) conditions upon knockdown of YAP/TAZ. The relative ratio of fully labelled M+5 proline derived from M+5 glutamine was calculated and was seen to be significantly reduced upon YAP/TAZ knockdown when compared to the siNT control cells (Figure 3.21D). Hypoxia induced an increase in the ratio of M+5 proline from M+5 glutamine as a result of the enhanced hypoxic usage of glutamine. However with knockdown of both YAP/TAZ, this ratio was reduced to levels comparative to that observed in normoxia. This reduction in glutamine-derived proline synthesis could therefore suggest less glutamine uptake or the diversion of glutamine into other important biosynthetic processes such as nucleotide synthesis upon YAP/TAZ

deficiency in U343 cells. Alternatively, the data suggesting increased use of reductive glutamine metabolism could indicate that glutamine uptake remains the same but its use is changed. As GLS1 is mainly mitochondrial and did not appear to alter glutamine processing in this context upon YAP/TAZ knockdown, it could suggest that there are differences in glutamine cellular localisation.

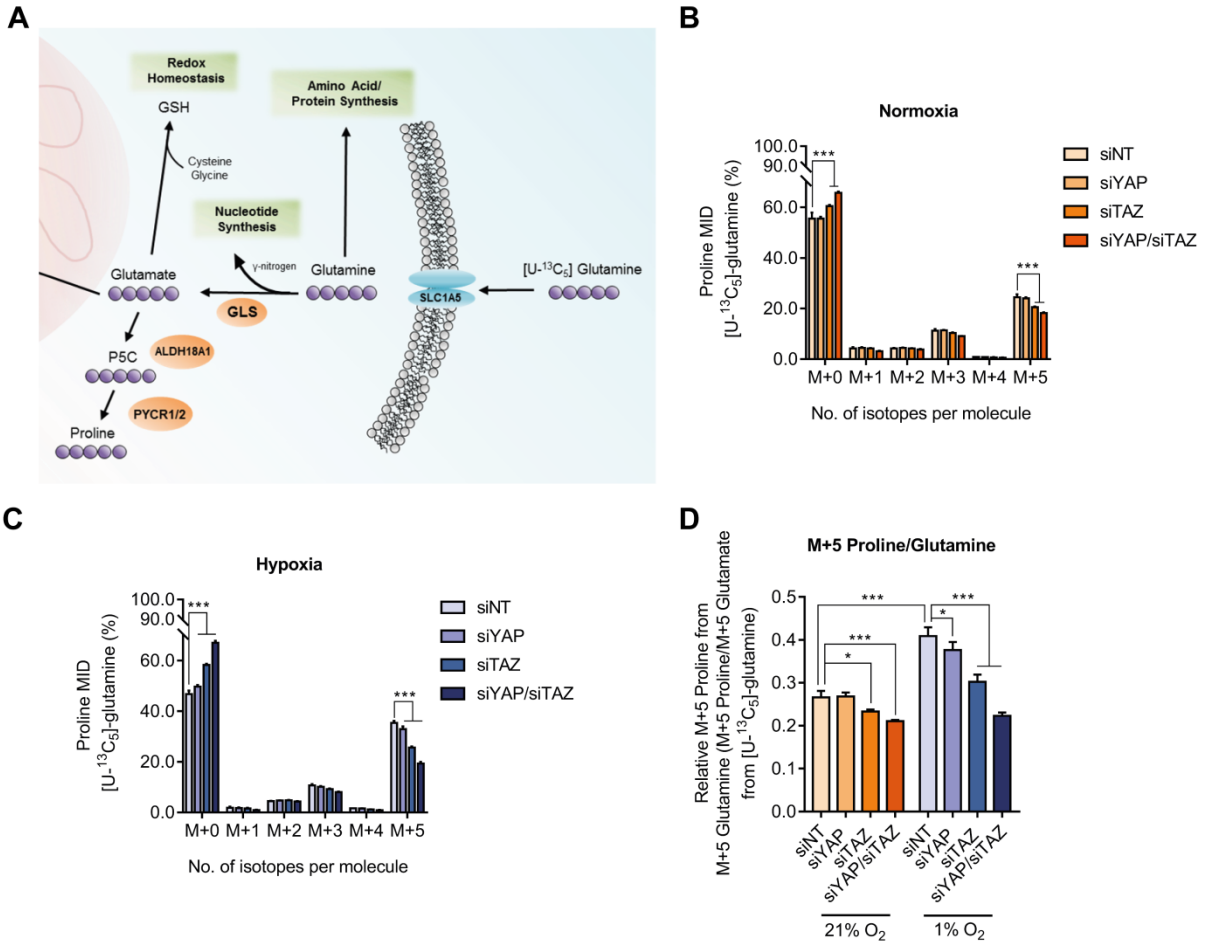

Figure 3.21 YAP/TAZ supports glutamine-derived proline synthesis. (A) Schematic outlining fates of glutamine following cellular uptake through glutamine transporter SLC1A5 including proline biosynthesis (purple pathway). Relevant enzymes are presented in orange. (B) siTAZ and siYAP/TAZ significantly reduced M+5 proline in 21% O_2 and was exacerbated under hypoxic (1% O_2) conditions (C). (D) Proline biosynthesis from M+5 glutamine was significantly increased in hypoxia in the siNT control cells. Interestingly, YAP/TAZ induced a significant reduction in glutamine-derived proline compared to the control. Additionally, despite hypoxia-induced increases in proline synthesis, no increase was seen in hypoxia upon siYAP/TAZ when compared to normoxia. Abbreviations: GLS, glutaminase; GSH, glutathione; P5C, pyrroline-5-carboxylate synthetase; P5CS, Delta-1-pyrroline-5-carboxylate synthetase; PYCR1/2, pyrroline-5-carboxylate reductase 1/2; SLC1A5, solute carrier family 1 member 5. Data obtained was from 5 technical replicates. Error bars represent ± S.D. Significance determined using two-way ANOVA with Tukey post-hoc test. *** p<0.001.

3.2.6.5. Total carbon contribution from glutamine into TCA metabolites is significantly attenuated upon YAP/TAZ knockdown

The percentage of ^{13}C enrichment from both [U-$^{13}C_6$]-glucose and [U-$^{13}C_5$]-glutamine into various TCA metabolites and amino acids was calculated to investigate the overall effect of knockdown of YAP/TAZ on central carbon metabolism (Figure 3.22). It is clear, that the percentage enrichment of glutamine into each metabolite was significantly reduced upon YAP/TAZ knockdown when compared to the siNT in both normoxia and hypoxia. Under hypoxia, ^{13}C enrichment from glutamine was increased consistent with the knowledge that glutamine is increasingly relied upon as a carbon source in hypoxic conditions. Interestingly, this increase was not apparent with YAP/TAZ deficiency and percentage enrichment into each metabolite remained similar to that of normoxia.

Glucose utilisation was consequently altered upon YAP/TAZ knockdown, with ^{13}C enrichment from glucose being increased in all metabolites except citrate (Figure 3.22). This effect was more prominent under hypoxic conditions where glucose contribution was reduced in the hypoxic control cells, corroborating reduced glucose oxidation under hypoxia. Knockdown of YAP/TAZ however, was able to retain levels of ^{13}C incorporation from glucose in hypoxia similar to that of control cells in normoxia.

Finally, it was implied that ^{13}C contribution from other carbon sources was increased upon YAP/TAZ knockdown, particularly under hypoxic conditions, which suggests that while ^{13}C enrichment from glucose is increased with YAP/TAZ deficiency, it is not enough to compensate for the significant loss of ^{13}C contribution from glutamine and so carbon must be incorporated from other sources such as lipids, breakdown of other amino acids or even from increased autophagy (Figure 3.22).

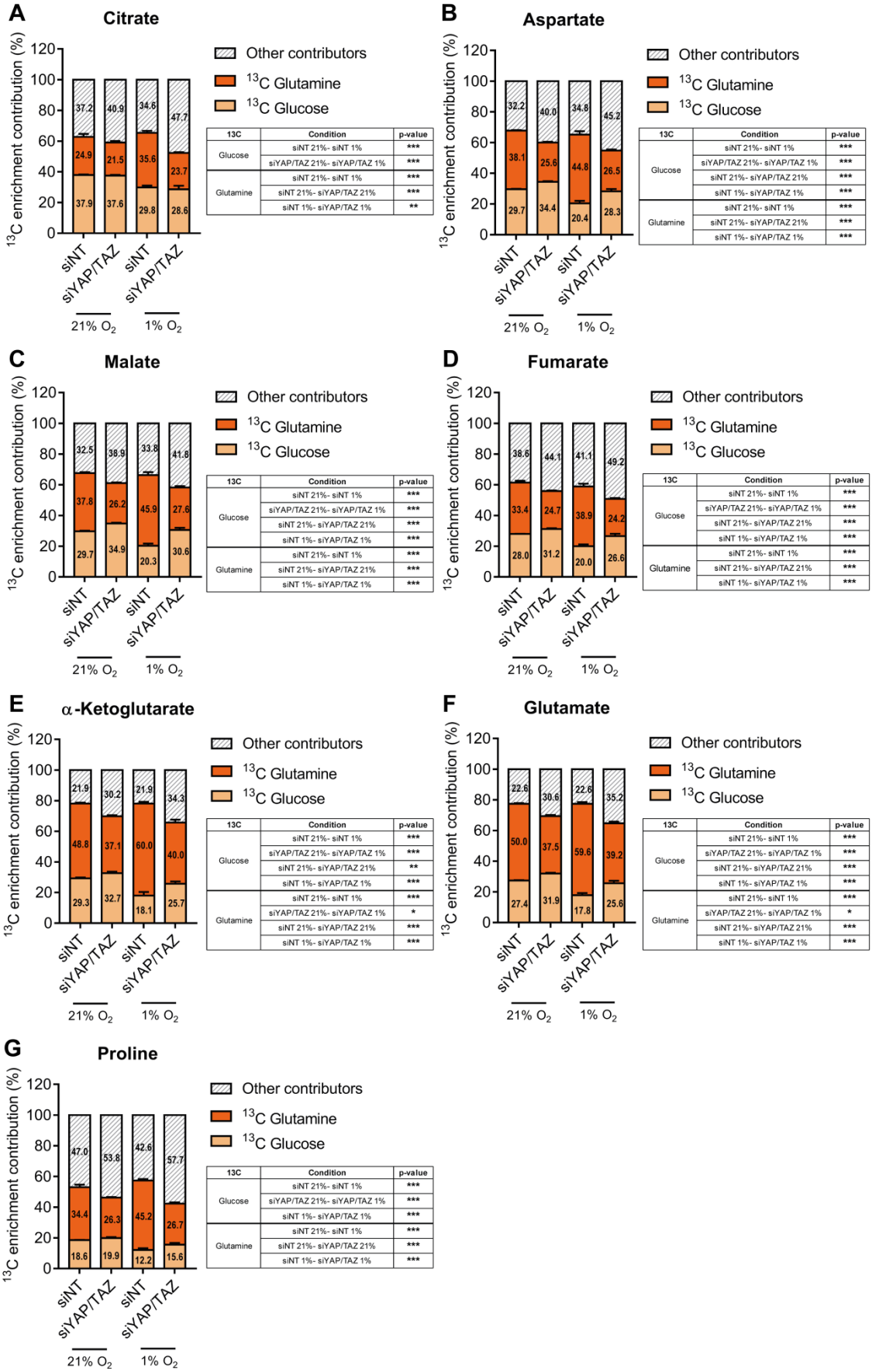
A
Citrate
B
Aspartate
C
Malate
D
Fumarate
E
α-Ketoglutarate
F
Glutamate
G
Proline
Other contributors
13C Glutamine
13C Glucose
13C enrichment contribution (%)
siNT
siYAP/TAZ
21% O2
1% O2
13C | Condition | p-value
Glucose | siNT 21%- siNT 1% | ***
siYAP/TAZ 21%- siYAP/TAZ 1% | ***
siNT 21%- siYAP/TAZ 21% | ***
siNT 1%- siYAP/TAZ 1% | ***
Glutamine | siNT 21%- siNT 1% | ***
siNT 21%- siYAP/TAZ 21% | ***
siNT 1%- siYAP/TAZ 1% | ***

Figure 3.22 Knockdown of YAP/TAZ significantly alters glutamine contribution into TCA metabolites. The total contribution of ^{13}C from glucose and glutamine was calculated for various metabolites; citrate (A), aspartate (B), malate (C), fumarate (D), α-KG (E), glutamate (F) and proline (G). The remaining percentage not derived from glucose or glutamine was deemed to be from other contributors such as from lipids or breakdown of amino acids. For all metabolites analysed there is a significantly reduced contribution from ^{13}C glutamine upon knockdown of YAP/TAZ when compared to the siNT control and is amplified in hypoxic conditions where the use of glutamine as a carbon source is preferred. To account for differences in glutamine use, the percentage ^{13}C contribution from glucose is increased upon YAP/TAZ knockdown, which is more apparent under hypoxic conditions. Furthermore, carbon contribution from other carbon sources is also increased upon YAP/TAZ knockdown to account for the significant reduction in glutamine usage. Data obtained was from 5 technical replicates. Error bars represent ± S.D. Significance determined using two-way ANOVA with Tukey post-hoc test. * $p<0.05$, ** $p<0.01$, *** $p<0.001$.

3.3. Discussion

Hypoxia is a major hallmark of solid tumours stemming from the rapid proliferation of malignant cells avidly exhausting nutrients and oxygen from the surrounding vasculature[71]. Pro-angiogenic factors such as VEGF are consequently upregulated, stimulating neovascularisation of the tumour. However, these newer vessels are often inefficient and 'leaky', subsequently leading to large areas of hypoxia throughout the tumour mass[72,226].The hypoxic tumour areas demonstrate increased treatment resistance and overall poorer patient survival due to the increased invasion and metastatic potential incurred as a biological response to hypoxia[97]. It is therefore crucial to investigate the underlying mechanisms of how hypoxia can influence tumour growth through aberrant regulation of various signalling pathways, as well as how hypoxia and the tumour microenvironment can be exploited therapeutically to enhance patient survival.

3.3.1. Glioma lines, U87 and U343, exhibit differential growth sensitivity to pathophysiological hypoxic conditions

Gliomas, as previously discussed, are particularly hypoxic tumours with a median pO_2 of a 7.4 mmHg (1% O_2), with some high-grade tumours shown to contain areas under 2.5 mmHg (0.3% O_2), as opposed to normal brain tissue which has a pO_2 of around 35 mmHg (4.6% O_2)[96,97]. Since *in vitro* cell culture is generally conducted at the supraphysiological oxygen concentration of 21% O_2, *in vitro* glioma cell lines were cultured at both 1% and 0.3% O_2 to investigate whether cell proliferation and/or survival was affected upon exposure to oxygen concentrations similar to that observed *in vivo*. Results showed that glioma cells were still viable and able to proliferate following chronic exposure to both 1% and 0.3% O_2, although hypoxia induced a significant reduction in U87 proliferation rate after 48 hours when compared to normoxia (21% O_2; Figure 3.1),

which is in agreement with previous studies[227]. Interestingly, U343 cell proliferation was completely unaffected when cells were cultured under 1% and 0.3% O_2 over 72 hours, highlighting the heterogeneous nature of the different glioma subtypes. According to the Verhaak classification system of gliomas, the U343 cell line is believed to be representative of the classical subgroup as it exhibits amplified expression of EGFR (Figure 2.1A), which is present in 40-50% of GBM[24,28]. Increased EGFR has been previously shown to confer a significant survival advantage under hypoxic conditions in many cancers such as breast, pancreas and NSCLC, with amplified EGFR signalling enhancing hypoxic induction of pathways promoting cell survival[228]. Hence, this growth advantage exhibited by the U343 cells under hypoxic conditions could be mediated through enhanced EGFR signalling and should thereby be investigated in further detail. Due to the difference in hypoxic growth between the two cell lines, future experiments were thereby normalised to the control for each oxygen tension, unless otherwise stated, to account for any reduced growth rate under hypoxia.

3.3.2. Hypoxia upregulates YAP/TAZ expression and transcriptional co-activator activity in glioma cell lines

Hypoxia has been previously shown to increase YAP/TAZ signalling in HCC[135], breast[131,133] and ovarian[229] cancer however as the activity and possibly control of YAP/TAZ is tissue-dependent, it is important to define whether a mechanistic link exists in gliomas. Glioma cells were therefore exposed to hypoxia (1% O_2) for 8 hours after which YAP1, and YAP1-target genes, *CYR61*, *CTGF* and *BBC3*, were assessed via qPCR. Hypoxia induced a significant upregulation of YAP1 mRNA expression in U87, U343 and HOG IDH1 WT cell lines, which coincided with an increase in YAP1-target genes (Figure 3.2 and 3.3). However, not all target genes were significantly upregulated

across all the glioma cell lines suggesting that a lower oxygen tension or longer period of hypoxia might be necessary to induce a significant difference in gene expression when compared to normoxic conditions. Interestingly, hypoxia was seen to induce both pro-proliferative (CYR61 and CTGF) and pro-apoptotic (BBC3) gene expression highlighting the complexity of YAP transcriptional regulation since it can bind with different transcription factor binding partners to transcribe different set of genes depending on the cell context[143]. In this circumstance, although BBC3 gene expression is increased potentially acting to induce cell death in response to a hostile environment such as hypoxia, other pro-survival mechanisms could be activated to counteract this increased expression since cell death was not induced under acute hypoxia. Interestingly, HOG IDH1 MUT cells were seen to significantly upregulate BBC3 expression in both normoxia and hypoxia when compared to HOG IDH1 WT cells (Figure 3.3L), which could potentially, despite an initial growth advantage (Figure 4.5), contribute towards the reduced cell proliferation observed upon R132H IDH1 mutation as previously reported[230].

Since enhanced gene transcription does not always necessitate increased protein expression, YAP1, as well as its inactive phosphorylated form (p-YAP), protein expression were analysed periodically over 24 hours. Interestingly, 1% O_2 induced a minimal increase in YAP1 protein levels, with even a slight decrease evident in the HOG IDH1 MUT cell line (Figure 3.6 and 3.7). This apparent difference between mRNA and protein expression could be due to differential post-transcriptional processing of YAP1 mRNA, differences in RNA stability or even protein translation. Importantly, there are data to show that the 2-HG produced by mutant IDH1 can alter RNA processing and translation through the inhibition of the 2-OG-dependent dioxygenases that play a

significant role in these processes, suggesting a potential reason for this differential protein expression[231,232].

Interestingly, protein expression of YAP paralog TAZ, was dramatically increased following exposure to 1% O_2 (Figure 3.8B), suggesting potential differential regulation and sensitivity to hypoxia. This concept has been previously suggested however due to limited evidence, further investigation is crucial to understand the complex relationship between the two co-activators[229]. To investigate whether a lower oxygen tension could evoke a stronger YAP protein response, p-YAP and YAP1 expression were analysed at a lower oxygen tension of 0.3% O_2, which is comparable to some *in vivo* oxygen measurements taken from GBM[96,97]. This more severe oxygen environment was observed to elicit a stronger response across the glioma cell lines – with the exception of the U343 cells – with YAP expression significantly increased compared to the normoxic control. This strongly upregulated YAP1 response under severe hypoxia (≤2.5 mmHg) could therefore confer a survival advantage under such extreme environments where cells struggle to survive. Hence, it could also explain why the highest YAP1 expression is found in grade IV gliomas, which are generally the most hypoxic[96]. The smaller increase in YAP1 expression after hypoxia in the U343 cells may be explained by their insensitivity to hypoxia-induced growth restriction (Figure 3.1B) – perhaps through a pre-existing enhanced basal YAP1 expression.

Increased YAP1 expression does not necessarily indicate increased transcriptional co-activation activity since YAP nuclear localisation is required for this role, and is controlled by its phosphorylation. Therefore, the ratio of cytosolically-retained p-YAP to total YAP expression was calculated, as well as analysis of the expression of downstream YAP1-

target, CTGF (Figures 3.6-3.8). A reduction was apparent in the p-YAP/YAP1 ratio in both the U87 and HOG IDH1 WT cell lines indicating that less of the YAP pool was inactive, although this alteration was more ambiguous in the U343 and HOG IDH1 MUT cell lines. CTGF expression on the other hand, was seen to increase across all glioma cell lines when exposed to both 1% and 0.3% O_2, implying increased YAP1 transactivational activity. To investigate whether hypoxia induced YAP1 expression in a more physiologically relevant model, p-YAP and YAP1 were also assessed in two novel cell lines which were derived from a single GBM patient biopsy. Interestingly, these two lines, despite originating from the same tumour specimen, had exhibited differential sensitivity to chemoradiation treatment. T1 cells were derived from an area of tumour recurrence that had progressed significantly post-treatment, and thus was believed to be therapy-resistant, whereas T2 cells were harvested from an area of the tumour which had not progressed post-treatment, and was therefore considered therapy-responsive. Initial investigations showed T1 cells express a higher level of both p-YAP and YAP1 protein compared to the T2 cells, suggesting that YAP1 signalling was amplified (Figure 3.8C). This amplified YAP1 expression could potentially contribute to the therapy-resistance exhibited by these cells, corroborating previous reports of YAP-induced chemoresistance[135,233]. However, this hypothesis would have to be appropriately tested in further experiments *in vitro*. Immediately following tissue dissociation, cells from the T1 and T2 tumour regions were transferred to hypoxia where they were subsequently cultured. YAP1 expression was characterised under these conditions and was seen to increase in both T1 and T2 cell lines, although the largest increase was seen in the T2 cells (Figure 3.8C-E), most likely due to the higher basal expression already observed in the T1 cell lines.

Finally, YAP1 expression was characterised in the U87 and U343 cell lines using immunocytochemistry to directly visualise whether hypoxia increased YAP1 nuclear localisation. Nuclear YAP1 fluorescence was investigated following cell exposure to 1% O_2 for 4 and 8 hours, and was seen to be significantly increased in U87 cells when compared to the normoxic control suggesting potential increased YAP1 co-activator activity (Figure 3.9B). Although YAP1 nuclear localisation was seen to be increased following 4 hour exposure in the U343 cells, interestingly YAP1 localisation was similar to that of normoxic cells after 8 hours (Figure 3.9C). As previously discussed, U343 cells have shown a lesser YAP1 response to hypoxia potentially due to their high basal YAP1 expression, which could be a result of their EGFR amplification. He *et al*., have previously shown that EGFR signalling can interact with the Hippo pathway to upregulate the proliferation of cervical cancer cells, specifically through transforming growth factor-α (TGF-α) and AREG, acting through EGFR, to increase YAP transcriptional activity[234]. Furthermore, they describe that this signalling is further amplified through an autocrine/paracrine feedback loop, in which enhanced YAP transcriptional activity causes a subsequent increase in TGF-α, AREG and EGFR, therefore perpetuating tumour progression[234]. This EGFR enhanced YAP signalling could therefore provide some explanation as to why hypoxia elicits a weaker YAP response in this glioma cell line compared to the others. Together, these data suggest that hypoxia can influence YAP1's activity as a transcriptional co-activator as well increasing its expression in glioma cells, supporting previous investigations in other cancers demonstrating hypoxia-enhanced YAP signalling[131,135]. To further validate these observations in glioma, expression of additional YAP1-targets should be investigated as well showing increased co-activator activity through promoter assays.

3.3.3. Glioma cell proliferation is significantly reduced upon YAP/TAZ knockdown

As YAP amplification and increased transcriptional co-activation have been associated with oncogenesis, it could therefore be suggested that suppression of YAP and its paralog TAZ expression and/or activity in malignant cells could be an attractive therapeutic option, particularly in hypoxia where cells are highly therapy-resistant.

This hypothesis was consequently investigated through knockdown of YAP, TAZ or both using siRNA in both the U87 and U343 cell lines (Figure 3.10). When cell proliferation was assessed 72 hours post-transfection, it was found to be significantly reduced in both cell lines, corroborating previous data demonstrating attenuated cell proliferation of both HCC and gastric cancer cell lines upon YAP silencing[235,236]. Knockdown of YAP individually however, did not induce a significant growth reduction in the U343 glioma cells, potentially due to its association with EGFR signalling, although it has been reported that TAZ can mitigate similar enhanced EGFR signalling[237]. Knockdown of YAP and TAZ together was seen to have the most effect on cell growth in both cell lines, suggesting a degree of redundancy between the two proteins. It appears that knockdown of YAP could induce TAZ expression resulting in a reduced effect of siYAP. Conversely, knockdown of TAZ may not influence YAP expression since knockdown of TAZ induced a greater reduction in cell proliferation than when YAP was silenced individually (Figure 3.10C-E). This hypothesis is supported by previous research which showed that silencing of YAP through shRNA resulted in a concomitant increase in TAZ expression and that YAP overexpression significantly decreased TAZ abundance[238]. Furthermore, the authors showed that this was specific to YAP with TAZ knockdown or overexpression inducing no changes in YAP expression. This further suggests that in addition to the

regulatory mechanisms shared by both proteins, TAZ expression is also modulated directly through YAP but not the other way around[238]. These findings could also potentially explain why YAP knockdown has an attenuated effect on reducing cell growth in the U343 cell lines since increased TAZ expression can also perpetuate EGFR signalling.

Hypoxia was found to have a minimal additional effect on the reduced proliferation seen upon YAP/TAZ knockdown in the U343 cells but did slightly enhance the effect of the knockdown in the U87 cells (Figure 3.10C, D). This again could potentially be due to the reduced effect hypoxia has on the growth of U343 cells. Although knockdown significantly attenuated glioma cell proliferation, the reduction was moderate suggesting that a longer knockdown period is probably required in these cell lines to induce a biologically significant effect.

Overall, knockdown of YAP, TAZ and YAP and TAZ reduced the proliferation rate of glioma cells, corroborating previous research in other cancers. Knockdown of YAP/TAZ expression could therefore represent a therapeutic target to reduce tumour proliferation, although these data suggest that targeting of both YAP and TAZ should be considered for maximum therapeutic benefit.

3.3.4. YAP/TAZ knockdown induces significant alterations in glucose and glutamine metabolism

It has long been established that cancer cells rewire their metabolism to fuel the increased energetic demand and generation of new biomass required to sustain the uncontrolled proliferation exhibited by tumours[239]. A key hallmark of cancer metabolism

first described by Otto Warburg in the 1920's, is the enigma that is aerobic glycolysis; where in the presence of oxygen, cells preferentially metabolise glucose through glycolysis to lactate, despite being a considerably less efficient pathway at producing ATP[169,170]. To this day, the purpose of this remains unclear however whilst endeavouring to understand this phenomenon, researchers have uncovered the full complexity of cancer metabolism and focus has now shifted towards cancer-induced metabolism of other nutrients and amino acids such as glutamine, serine, glycine and acetate in addition to glucose[240].

YAP and its paralog TAZ are known to play a central role in the tumorigenesis of various cancers, although it remains to be elucidated as to precisely how these signalling factors interact with metabolism – whether they directly alter metabolic enzyme expression to support a proliferative driver, or whether the changes in metabolism that have been previously reported are a downstream effect of the phenotypic changes directed by YAP/TAZ. In the last few years, aerobic glycolysis has been identified to regulate YAP/TAZ transcriptional activity through PFK1[187]. PFK1, a crucial enzyme in glycolysis, can interact with TEAD transcription factors to stabilise their binding to YAP/TAZ and thus, under conditions when cells are actively consuming glucose such as cancer, increase transcription of pro-proliferative target genes to support tumour growth. With this in mind, it was therefore hypothesised that YAP/TAZ could potentially associate with other metabolic and biosynthetic pathways in glioma to support tumour growth, in particular under hypoxic conditions, where YAP/TAZ activity is increased and metabolism is significantly altered to promote cell survival.

3.3.4.1. YAP/TAZ act to support normoxic *de novo* serine synthesis in glioma

Aberrant serine and glycine metabolism is indispensable for tumorigenesis, with hyper-activated *de novo* serine synthesis providing increased precursors for protein and nucleic acids synthesis, in addition to modulating cellular antioxidant capacity to promote tumour survival[221]. Conversion of serine to glycine is a major aspect of serine metabolism, and through the decarboxylation of serine, supplies carbon units for one-carbon metabolism which is essential for biosynthesis of proteins, nucleic acids and lipids as well as for DNA and histone methylation[223,241]. The use of metabolic tracers to investigate metabolism permit analysis of the changes induced in specific metabolic pathways (such as ^{13}C-glucose to study glycolysis) in different experimental conditions. After knockdown of YAP/TAZ, [U-$^{13}C_6$]-glucose labelling of cellular metabolites indicated that *de novo* serine synthesis was reduced and the large majority of serine was taken up by extracellular sources (Figure 3.11C). Interestingly in hypoxic conditions, ^{13}C incorporation into serine from glucose was significantly reduced across all conditions, which was unexpected since it has been documented that HIF-1 mediates increased flux through the SSP by inducing expression of SSP enzymes, PHGDH (phosphoglycerate dehydrogenase), PSAT1 (phosphoserine aminotransferase) and PSPH (phosphoserine phosphatase)[242,243]. One of the benefits of shunting 3-PG towards the SSP in hypoxia is to ultimately increase anti-oxidant capacity through the production of NADPH and GSH to subsequently combat increased hypoxia-induced ROS production[243]. A DCFDA assay could therefore be used to measure ROS levels following knockdown of YAP/TAZ to investigate whether ROS are increased as a result of reduced *de novo* serine synthesis. Additionally, the reduced GSH to oxidised glutathione (GSSG) could be biochemically quantified to assess any alterations in redox homeostasis and oxidative stress as a result of YAP/TAZ knockdown.

Intriguingly, the M2 isoform of pyruvate kinase (PKM2) may play a role in the regulation of serine synthesis in U343 cells exposed to hypoxia. PKM2, known to be upregulated in cancer, catalyses the last step of glycolysis, producing pyruvate and ATP from phosphoenolpyruvate (PEP) and ADP (adenine diphosphate)[223]. Serine is known to allosterically activate PKM2, increasing glycolytic glucose consumption in conditions when serine is abundant[244]. However, when serine is depleted PKM2 activity is reduced consequently causing accumulation of upstream glycolytic intermediates which are then diverted towards use in anabolic pathways such as the SSP, to sustain cell proliferation[244]. Interestingly, EGFR[245,246] and HIF-1[247] are known interactors of PKM2 both increasing PKM2 activity to promote aerobic glycolysis which could potentially provide an explanation as to why *de novo* serine synthesis is significantly reduced in hypoxia in U343 cells. Further investigations should be therefore be conducted to test this hypothesis such as by investigating PKM2 activity as well as conducting metabolic tracing analysis following knockdown of YAP/TAZ in other glioma cell lines, such as U87 and primary GBM lines, to assess whether these metabolic alterations are common to glioma or specific to the classical subtype.

Another possible interpretation of the serine/glycine data is that knockdown of YAP/TAZ increased serine usage, resulting in less being detected. Analysis showed that serine to glycine conversion was undetectable with no serine-derived glycine observed under both normoxic and hypoxic conditions (Figure 3.12). Together, these data could suggest increased flux through serine and glycine to shuttle more carbons into one-carbon metabolism or a diversion from this biosynthetic pathway, particularly under hypoxic conditions, towards increased usage through glycolysis for ATP production as described above.

Nonetheless, it has recently been observed that YAP/TAZ knockdown disrupted *de novo* serine synthesis in breast cancer cells through reducing both the mRNA and protein expression of one of the enzymes in the SSP, PSAT1, which converts 3-phosphohydroxypyruvate (3-PHP) into 3-phosphoserine (3-PS) in a transamination reaction that uses glutamate-derived nitrogen and produces α-KG[222,248]. Attenuated PSAT1 activity reduces both production of glutamate-derived α-KG required for anaplerosis, as well as decreasing one-carbon metabolism as a consequence of reduced serine and glycine synthesis. Together, this overall reduction could therefore contribute towards the reduced cell proliferation observed in these cells upon knockdown of YAP/TAZ (Figure 3.10). This investigation therefore provides evidence to suggest that YAP/TAZ actively support *de novo* serine synthesis in gliomas and since it has been shown that serine is essential for tumour growth[249,250], it could provide another benefit of attenuating YAP/TAZ activity in these tumours. To further support this hypothesis, enzyme expression of the SSP pathway should be checked upon YAP/TAZ knockdown in these cells.

3.3.4.2. Pyruvate metabolism is altered in YAP/TAZ deficient cells

Pyruvate is a critical metabolic node driving several crucial biosynthetic pathways as well as being one of the main entry points into the TCA cycle[179]. Metabolic tracing analysis showed that the percentage of ^{13}C incorporation into pyruvate from [U-$^{13}C_6$]-glucose was significantly increased upon YAP/TAZ knockdown consistent with increased glycolysis, which was further enhanced under hypoxic conditions (Figure 3.13). Unlabelled sources of pyruvate were also decreased suggesting that YAP/TAZ knockdown caused the cells to increase their reliance on glucose as a source for pyruvate. As previously discussed, Enzo *et al*., showed the ability of aerobic glycolysis to regulate YAP/TAZ transactivational

activity, with increased glycolysis amplifying YAP/TAZ pro-tumorigenic function through interaction with TEAD and PFK1[187]. Since labelling into pyruvate was increased upon YAP/TAZ knockdown, it therefore suggests that despite glycolysis regulating YAP/TAZ activity, glycolysis itself was not attenuated when YAP and TAZ activity was reduced.

Aerobic glycolysis is a hallmark of cancer metabolism, increasing pyruvate conversion to lactate through LDH coupled with the oxidation of NADH to NAD^+ that can be subsequently recycled by GAPDH to maintain cellular glycolytic flux[179]. Glycolysis can be further amplified under hypoxic conditions, substantially increasing lactate production to guarantee continued glycolytic flux for ATP production as well as diverting carbon entry into the TCA cycle thus reducing ROS production and oxidative damage[179,239]. As expected, metabolic tracer analysis showed an increased percentage ^{13}C incorporation into lactate from [U-$^{13}C_6$]-glucose when cells were exposed to hypoxia indicating increased aerobic glycolysis (Figure 3.14C). Intriguingly, the ratio of lactate derived from pyruvate was significantly reduced upon YAP/TAZ knockdown in hypoxic conditions suggesting potential increased lactate export out of the cell through MCTs and therefore less incorporation detected (Figure 3.14D). Lactate levels in the cell medium could therefore be measured to test this hypothesis. Alternatively, it could suggest that LDH activity was impaired upon YAP/TAZ knockdown. YAP/TAZ depletion has previously been shown to decrease the lactate/pyruvate ratio by decreasing LDHA expression, providing evidence that YAP/TAZ influences lactate production over exportation[190]. Upregulated LDHA expression and increased lactate production has been shown to be crucial for tumour growth and survival and therefore promoting LDHA expression and activity could be another approach that YAP/TAZ exploit to enhance tumour growth[179,251].

Knockdown of YAP/TAZ induced a significant decrease in ^{13}C incorporation into lactate and alanine from glucose suggesting that pyruvate was being preferentially shunted towards the TCA cycle (Figure 3.14 and 3.15). As previously described, once pyruvate is transported into the mitochondria, it can either undergo oxidative decarboxylation by PDH to acetyl CoA or carboxylation via PC to form OAA. Metabolic tracing analysis showed that although PDH activity was predominant, PC activity was significantly increased upon YAP/TAZ knockdown (Figure 3.17). As expected, hypoxia significantly attenuated PC activity due to hypoxia inducing reduced carbon entry into the TCA cycle in order to minimise ROS production. What was intriguing however was that cells were able to sustain PC activity in hypoxia to levels comparable to that of normoxia upon YAP/TAZ knockdown (Figure 3.17D). This therefore suggests that cells sustained PC activity regardless of oxygen presence. Previous research has shown that if LDHA activity is reduced, cancer cells revert to oxidative phosphorylation[252], which could explain the increased dependency on glucose as a carbon source upon YAP/TAZ knockdown when analysing the total ^{13}C contribution to TCA intermediates (Figure 3.22). Additionally, PDH activity is known to be reduced under hypoxia due to HIF-1-mediated upregulation of PDK1, which phosphorylates and inactivates the PDH complex[195,243]. Inactivation of PDH was induced upon YAP/TAZ knockdown in hypoxia, implied through significantly decreased citrate M+2 labelling, suggesting the relative increase in PC activity could be to continue using pyruvate for anaplerosis. However, this also suggests an alternative source of acetyl CoA is required in these conditions – the only sources other than glucose being exogenous acetate and lipids – and therefore requires further investigation.

3.3.4.3. YAP/TAZ support oxidative glutamine metabolism

Increased glycolysis in cancer – either aerobic, or when oxygen availability is limiting – is inefficient in terms of both energy production (per carbon used) and generation of anabolic precursors. Alternative pathways are therefore relied upon to compensate and sustain tumour proliferation. Glutamine is the most abundant amino acid in plasma, and tumour cells are known to consume it at much greater rate than any other amino acid, with some tumour cells believed to be 'glutamine-addicted'[253]. Glutamine is therefore used as an alternative carbon source for the TCA cycle and has been shown to be essential for *de novo* lipogenesis in these conditions[198].

Metabolic tracer analysis showed knockdown of YAP/TAZ to induce a significant reduction in glutamine-derived glutamate and α-KG when cells were labelled with [U-$^{13}C_5$]-glutamine (Figure 3.18). As expected, hypoxia significantly increased the percentage incorporation of ^{13}C into both glutamate and α-KG indicating their increased synthesis from glutamine under hypoxic conditions. However, this was not the case upon YAP/TAZ knockdown, with a significant reduction observed. Relative carbon incorporation from glutamine into glutamate and α-KG was the same in both normoxia and hypoxia upon knockdown of both YAP and TAZ suggesting that oxygen availability was an independent factor (Figure 3.18G, H). This therefore suggests a potential interference in glutamine conversion to glutamate via glutaminases and/or through transamination/dehydrogenation of glutamate to α-KG or possibly even differences in the cellular localisation of glutamine.

A-KG can be used oxidatively through glutaminolysis, replenishing metabolic intermediates through the TCA cycle to ultimately produce ATP. Conversely, α-KG can

undergo reductive carboxylation to produce citrate, which has been previously described as the major pathway for citrate production in hypoxic cells, to generate acetyl CoA for fatty acid synthesis[198]. Metabolic tracer analysis in this investigation corroborated these findings, as cells under hypoxia significantly increased M+5 labelled citrate, which is derived through reductive carboxylation (Figure 3.19). The data suggest that glutamine metabolism was severely affected upon YAP/TAZ knockdown as glutaminolysis was significantly reduced in both normoxia and hypoxia, implied through reduced M+4 citrate labelling, as well as reduced reductive carboxylation under hypoxic conditions (Figure 3.19). Interestingly, despite significant impairment in both pathways upon YAP/TAZ knockdown, cells were observed to likely switch to reductive glutamine metabolism as reductive carboxylation was significantly increased relative to oxidative glutamine metabolism in hypoxia (Figure 3.19C).

Since both oxidative and reductive glutamine metabolism was attenuated upon YAP/TAZ knockdown, it led to the idea that the cell's ability to utilise glutamine efficiently was hindered and so expression of GLS1, which mediates glutamine to glutamate conversion and is the rate-limiting enzyme for glutamine use, was assessed (Figure 3.19E, F). Surprisingly, no discernible differences in GLS1 expression were observed upon YAP/TAZ knockdown which was in contrast with two recent studies which both showed YAP/TAZ knockdown to suppress GLS1 expression[190,191]. However, these studies were conducted in pulmonary hypertension and liver fibrosis models and so there could be additional contributing factors in the context of cancer since GLS1 expression has been identified to be preferentially overexpressed in tumour cells[254,255].

As previously discussed, Yang *et al*., showed that YAP/TAZ not only influence glutamine-utilising transaminase PSAT1, but also the glutamate-oxaloacetate transaminase GOT1 (also known as aspartate aminotransferase), which transfers nitrogen from glutamate to OAA to produce both aspartate and α-KG[186,248]. This finding could provide evidence to support why carbon contribution from glutamine into α-KG was significantly reduced upon YAP/TAZ knockdown since Yang *et al*., also showed a positive association between YAP/TAZ and GOT1 and a negative correlation with GLDH, implying that YAP/TAZ act to promote transamination as opposed to oxidative deamination of glutamate to produce α-KG[248]. Knockdown of YAP/TAZ suppressing GOT1 expression could therefore also suggest why glutamine-derived carbon incorporation into aspartate was significantly reduced since the majority of carbon used for *de novo* aspartate synthesis is supplied by anaplerotic glutamine[256]. Furthermore, Garcia-Bermudez *et al*.,[182] and Sullivan *et al*.,[181] have both recently shown aspartate to be a limiting metabolite for tumour growth. Aspartate has poor cell membrane permeability and so cells generally rely on *de novo* synthesis from glutamine[176,181]. This could also explain the increasing reliance of U343 cells on carbon from glucose and other unlabelled sources to maintain aspartate production when glutamine-derived aspartate was reduced (Figure 3.22B). Cell proliferation was significantly reduced upon YAP/TAZ knockdown and so absolute aspartate levels could be measured to investigate whether YAP/TAZ knockdown influenced total aspartate synthesis, which could hence limit tumour cell proliferation. Furthermore, α-KG or aspartate could be supplemented to the cells to see whether exogenous α-KG or aspartate would restore oxidative metabolism and rescue cell proliferation in the presence of YAP/TAZ knockdown.

Like aspartate, proline is an amino acid important for tumour cell proliferation and metastasis, which can be derived from glutamine[225]. Interestingly, YAP/TAZ knockdown induced a significant reduction in glutamine-derived proline, which was exacerbated under hypoxic conditions suggesting that YAP/TAZ could also influence enzymes which mediate proline biosynthesis such as delta-1-pyrroline-5-carboxylate synthetase (P5CS encoded by ALDH18A1) or pyrroline-5-carboxylate reductase 1/2 (PYCR1/2; Figure 3.21D). Conversely, it could also suggest that glutamine may have been diverted towards nucleotide and amino acid synthesis in an attempt to compensate for reduced oxidative metabolism and therefore incorporating less ^{13}C from glutamine into proline. On the other hand, a reduction in carbon incorporation from glutamine into proline, as well as glutamate and α-KG, could ultimately suggest that glutamine uptake could be attenuated upon YAP/TAZ knockdown. Further experiments such as measuring glutamine consumption and excretion rate and the expression of the glutamine transporter SLC1A5 as well as investigating label incorporation into nucleotides could help to delineate the metabolic fate of glutamine upon YAP/TAZ knockdown.

Calculation of the total carbon contribution from both [U-$^{13}C_6$]-glucose and [U-$^{13}C_5$]-glutamine into various metabolites showed a significant reduction in glutamine-derived carbon into every metabolite upon YAP/TAZ knockdown corroborating the previous results highlighting a potential role for YAP/TAZ in glutamine metabolism (Figure 3.22). This reduction in glutamine contribution was amplified under hypoxia; a condition in which reliance on glutamine metabolism for anaplerosis is known to increase. Interestingly, ^{13}C enrichment from glutamine into various metabolites in hypoxia was at a similar level to that of normoxia with YAP/TAZ knockdown. To compensate for the loss in glutamate-derived carbon upon knockdown, ^{13}C enrichment from glucose was seen to

increase as well as from unlabelled carbon sources, most likely to be scavenged from lipids, breakdown of amino acids, increased rates of autophagy or in the case of proline, other precursors such as ornithine[257]. Interestingly, it has also recently been shown in rapidly proliferating mammalian cells, that amino acids are the major contributors of carbon to cell mass and surprisingly not glucose or glutamine which demonstrate the highest consumption rates[176]. These data in this study therefore indicate that long-term YAP/TAZ inhibition could potentially result in huge metabolic complications for the cell and consequently reduced tumour survival as cells would eventually run out of alternative carbon sources to sustain this inefficient cellular metabolism.

Together, these data highlight the importance of YAP/TAZ in glioma metabolism mainly through supporting oxidative glutamine metabolism for anaplerosis and subsequently promoting tumour proliferation and survival in hostile environments such as hypoxia. Further investigations are required to extensively delineate this relationship, however these data provide preliminary evidence to suggest that disrupting YAP/TAZ expression and transcriptional co-activator activity, particularly in hypoxia, could be a key target for therapeutic development since both pro-survival signalling and metabolism can be targeted in combination to reduce glioma growth and progression.

3.4. Summary

The data presented in this chapter established the role of hypoxia-induced regulation of YAP/TAZ signalling in gliomas. Hypoxia was seen to amplify YAP/TAZ expression as well as increase their activity as transcriptional co-activators across four established glioma cell lines and two novel GBM lines. Tumour hypoxia remains incredibly challenging in the design of therapeutics since hypoxic cells are generally therapy-resistant and poorly vascularised, limiting drug perfusion. Hypoxia-induced YAP/TAZ signalling may therefore contribute towards to this enhanced chemoresistance and cell survival. Thus, targeting YAP/TAZ signalling may be an effective therapeutic opportunity to target this highly-resistant hypoxic subset of cells in gliomas. Furthermore, due to the central role of YAP/TAZ in aberrant tumour growth, it was questioned whether YAP/TAZ signalling could influence glioma metabolism to subsequently support the production of biomass required to generate new cells. Interestingly, YAP/TAZ were identified to support *de novo* serine synthesis and potentially one-carbon metabolism which is required for nucleotide, lipid and protein synthesis. YAP/TAZ signalling was also seen to heavily influence glutamine metabolism, with YAP/TAZ knockdown severely attenuating glutaminolysis, which is an interesting finding since glutamine is heavily relied upon in hypoxic tumour cells to sustain anabolism for tumour growth. Together, the metabolomic data therefore suggest that YAP/TAZ activity plays an important role in sustaining cell proliferation both in normoxic, but more importantly hypoxic conditions and is potentially critical for supporting the hallmarks of cancer in hypoxia. Further investigations including metabolic tracer studies using other labelled carbon sources such as serine, palmitate and positionally labelled tracers such as [1,2-^{13}C]-glucose can help fully elucidate this complex relationship between cell metabolism and YAP/TAZ in gliomas. Together, these data provide an exciting basis highlighting how disrupting YAP/TAZ signalling could be

an attractive therapeutic opportunity for gliomas since targeting this pathway can disrupt both oncogenic growth and hypoxic cancer metabolism.

Chapter 4:

Assessing the potential of repurposing verteporfin as a novel treatment for glioma

4.1. Introduction

Gliomas are highly therapy-resistant tumours which have proved extremely challenging to treat effectively. Complications in the design of successful therapeutics have arisen from a number of hallmarks including their severe hypoxic nature, extensive invasion into the surrounding healthy brain as well as widespread genetic heterogeneity[101,258,259]. Despite considerable endeavours, glioma therapies have remained mostly stagnant since the development of TMZ in the 1990's, which remains first-line treatment over 20 years later[260]. Surgical and technological advancements have provided a small improvement in patient survival, but further significant improvements are desperately needed. It is therefore imperative that pathways involved in gliomagenesis, as well as those affecting the tumour microenvironment, are identified in the hope to discover better, more effective therapies.

As outlined in chapter three, disrupting abnormal YAP activity in malignant cells is of significant interest in cancer research and recently Liu-Chittenden *et al*., identified the benzoporphyrin derivative VP to be a potent YAP inhibitor[153]. VP is a second-generation FDA-approved photosensitiser, which in addition to its photochemical properties, has shown the ability to inhibit the pro-proliferative YAP-TEAD interaction through selective YAP binding[153,155]. This competitive interaction alters YAP protein confirmation thereby abolishing TEAD binding ability and consequently suppresses the oncogenic activity of YAP[153]. As a result, there has been a plethora of studies showing VP to have anti-tumour properties by reducing cell proliferation and viability in various cancers such as retinoblastoma[158], ovarian[160], colon[165] and pancreatic[159]. Recent research has also demonstrated VP to inhibit proliferation of glioma cell lines LN229 and SNB19 through suppression of the YAP-TEAD axis, again highlighting the importance of this signalling

pathway in gliomas[161]. Given the role of hypoxia in GBM and its ability to alter YAP activity, the activity of VP in hypoxia is an important aspect that has yet to be examined in gliomas. Furthermore, despite being identified to inhibit the YAP-TEAD interaction thereby suppressing proliferation, the exact mechanism as to how VP induces a reduction in cell viability has yet to be fully elucidated. Previous studies have shown VP to induce cell death in the absence of light-activation through various mechanisms including apoptosis[166,261,262], induction of proteotoxicity through impaired clearance of protein oligomers[165,263], and as an inhibitor of autophagy[264]. It has therefore become apparent that VP-induced cell death is largely dependent on cellular and microenvironmental context and thus should also be examined in the context of glioma.

Repurposing of clinically established drugs has become of significance in cancer research due to the incredibly low rate of less than 5% of novel cancer therapeutics passing through phase I trials to clinical approval[265]. Successful examples of drug reprofiling for cancer therapy include treatment of MM with derivatives of the anti-nausea agent Thalidomide as well as clinical trials proposing treatment of breast cancer patients with the type 2 diabetic drug Metformin[266,267]. VP therefore has significant repurposing potential as it is already used clinically in the treatment of neovascular AMD[155]. With its demonstrative ability to reduce cancer growth *in vitro*, this chapter aims to assess the effectiveness of VP to reduce glioma growth, with the hope that VP could be repurposed as a new and effective glioma therapy, which is so desperately needed for patients.

4.2. Results

4.2.1. VP reduces proliferation of glioma cells

VP has been identified as a YAP inhibitor as it disrupts the interaction between YAP and the TEAD family of transcription factors. This vital interaction is required to transcribe downstream target genes such as *CTGF* and *CYR61* which are subsequently involved in cell growth and survival[158]. Results from chapter three identify YAP to be an attractive therapeutic target for glioma and so the effect of VP on malignant cell growth and survival was therefore assessed, since if effective, VP could potentially be repurposed to treat gliomas and possibly other hypoxic cancers.

To assess growth characteristics, glioma cells were cultured in the presence of a range of VP concentrations (1-10 μM) for up to 96 hours. Proliferation was seen to be significantly reduced with all VP concentrations in both U87 and U343 cells (Figure 4.1A, B) by 96 hours, which is in agreement with previous studies[160,161]. To check that this VP-induced decline in cell number was a result of reduced proliferation and not from cell death, cells were imaged and seen to be viable in all conditions (Figure 4.1C).

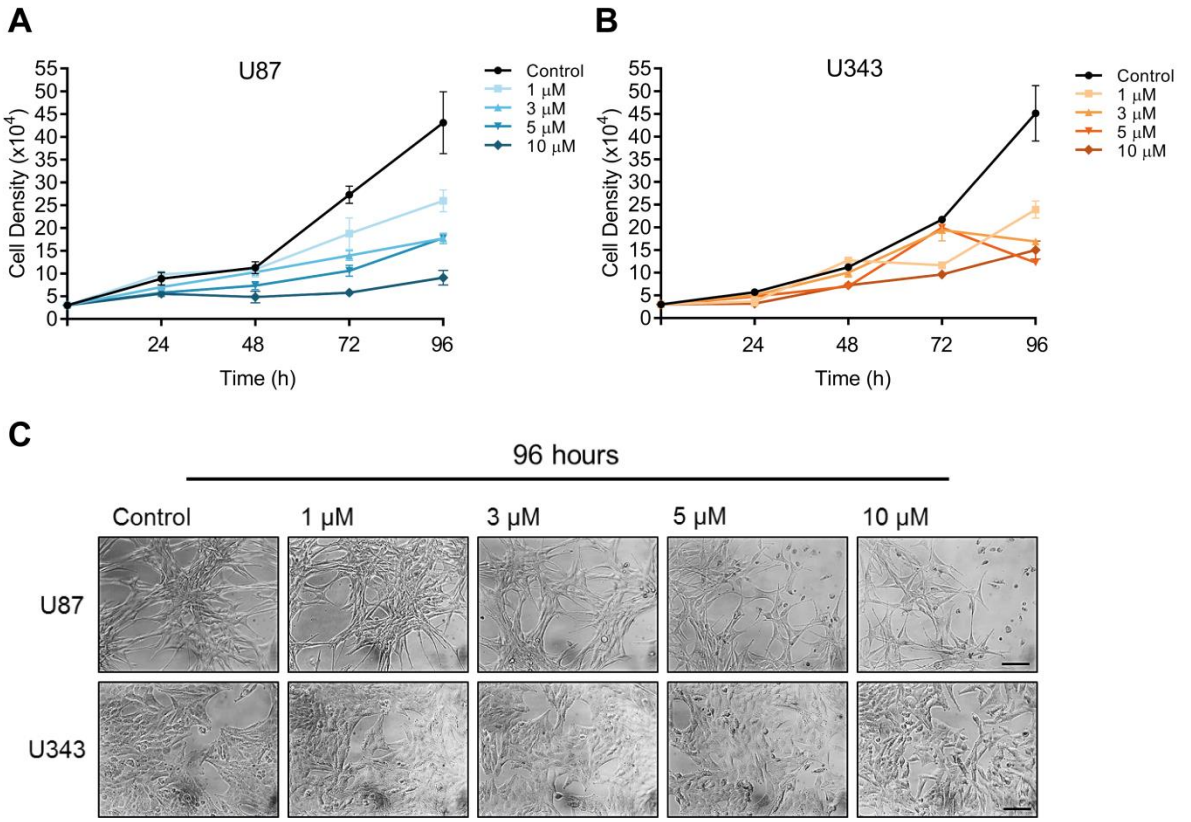

Figure 4.1 VP reduces cell proliferation of glioma cell lines. Cell proliferation assay of U87 (A) and U343 (B) cells treated with either vehicle (DMSO) or 1-10 µM VP for 24-96 h. Cell counts were taken by manual counting at the stated times. All concentrations of VP significantly reduced proliferation by 96 h in U87 (* 1 µM; ** 3 and 5 µM; *** 10 µM) and U343 (* 1 µM; ** 3, 5 µM and 10 µM) cell lines. (C) Representative images showing cell growth after 96 h treatment of either vehicle or increasing concentrations of VP. It is clear that the reduced cell density upon VP treatment is a result of a reduced proliferation rate and not from cell death. Images were taken at 20x objective and the scale bar represents 100 µm. Data is of 2 independent experiments. Error bars represent ± S.E.M. Significance is determined by one-way ANOVA, Tukey post-hoc analysis. * $p<0.05$, ** $p<0.01$, *** $p<0.001$.

To conduct further experiments investigating the effect of VP on glioma cell viability, the optimal dosage and treatment time was assessed. U87 and U343 cells were grown for 24 hours before being treated with a range of VP concentrations (1-10 µM) for 24-72 hours after which cell number was assessed via SRB analyses. It is evident that 10 µM VP caused a significant reduction in cell number in both U87 and U343 cells after 24 hours (Figure 4.2A, B). Consequently, 5 µM VP for 24 hours was chosen as the optimal dosage and treatment time as this was the highest dose that had the least effect on cell

number under normoxic conditions. It should be noted that there was a dose-dependent effect on reduction in cell number although this was only evident following 72 hour treatment. Cells were imaged 72 hours post-treatment which again confirmed that the cells were still viable, and the reduced cell number was due to reduced proliferation rate (Figure 4.2C).

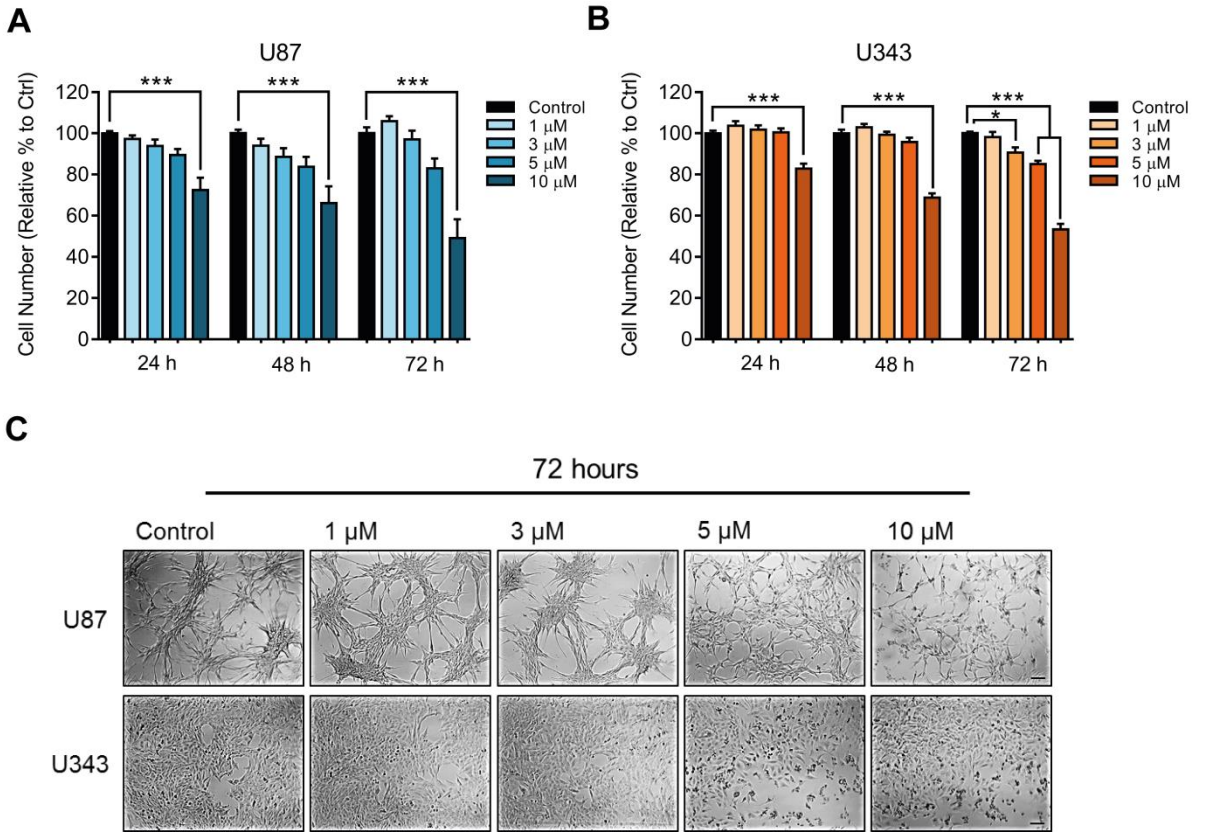

Figure 4.2 Determining VP dosage and treatment time. U87 (A) and U343 (B) cells were treated with either vehicle (DMSO) or 1-10 μM VP for up to 72 h. Cell number was determined using the SRB assay and normalised to the control at each time point. It is clear that 10 μM VP significantly reduced cell number in both cell lines following 24 and 48 h with lower concentrations not significantly reducing cell number until 72 h. (C) Representative images of U87 and U343 cells following 72 h treatment of either vehicle or increasing concentrations of VP. Cell number is seen to reduce with increasing concentrations of VP. Images were taken at 10x objective and the scale bar represents 100 μm. Analysis was performed in technical triplicate, in a minimum of 3 (U87) and 4 (U343) independent experiments. Error bars represent ± S.E.M. Significance determined using one-way ANOVA with Tukey post-hoc analysis. * $p<0.05$, *** $p<0.001$.

4.2.2. VP induces cell death under hypoxic conditions

Hypoxia is an important aspect of glioma biology and is a major determinant of treatment failure, as previously discussed. Since YAP expression and its activity has been shown to be upregulated under hypoxic conditions and that the YAP inhibitor VP can suppress proliferation of glioma cells, the effect of hypoxia on VP treatment was evaluated. U87 and U343 cells were cultured under either normoxic (21% O_2) or hypoxic (1% O_2) conditions for 24 hours in the presence of 1-10 μM VP before cell viability being assessed. As previously shown, only a high concentration of VP (10 μM) was able to significantly reduce cell number in normoxic conditions in both U87 and U343 cells (Figure 4.3A, B). Strikingly, when the cells were cultured under hypoxic conditions, VP significantly reduced cell viability. This was confirmed using brightfield imaging which showed that with increasing VP concentration the cells remained viable in normoxia but were dying and completely dead with 5 and 10 μM VP in hypoxia (Figure 4.3C, D).

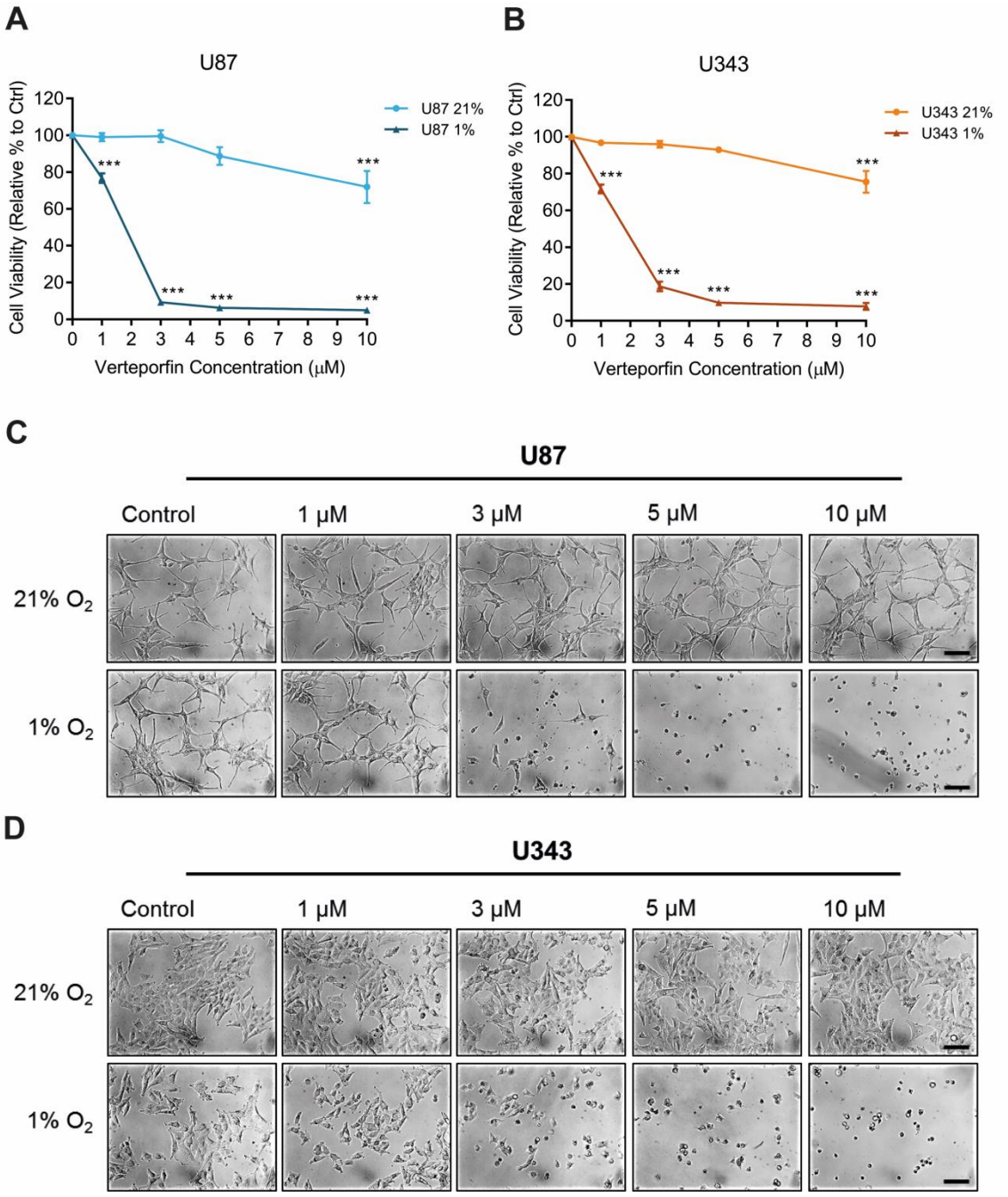

Figure 4.3 VP causes significant cell death under hypoxic conditions. U87 (A) and U343 (B) cell viability was measured using the SRB method following treatment with either vehicle (0.2% DMSO) or 1-10 μM VP for 24 h in both 21% and 1% O_2. Both cell lines remained viable with increasing concentrations of VP in normoxia (21% O_2) although 10 μM caused a significant reduction in cell number in both cells lines. In hypoxia, VP caused a significant reduction in cell viability under hypoxia (1% O_2) compared to the hypoxic control with all VP concentrations. Viability was normalised to the control for each oxygen tension. (C) Representative images of U87 and U343 cells showing that under normoxic conditions the cells remain viable however with 5 and 10 μM VP in hypoxia, the cells died. Images were taken at 10x objective and the scale bar represents 100 μm. Analysis was performed in technical duplicate/triplicate, in 4 independent experiments. Error bars represent ± S.E.M. Significance determined using one-way ANOVA, Tukey post-hoc analysis. *** $p<0.001$.

To investigate whether this effect was specific to VP, other porphyrin or porphyrin-related molecules – ZnPP and PPIX – were incubated with cells. Importantly, PPIX has also been previously identified as a YAP inhibitor[153]. Despite such similarity in structure (Figure 4.4A), when U87 and U343 cells were treated with the porphyrin compounds, only VP was observed to induce hypoxic cell death (Figure 4.4B, C). To investigate whether this VP-induced hypoxic cell death was unique to glioma, A375 melanoma cells were also treated with the different porphyrin compounds and again, only VP could significantly induce hypoxic cell death (Figure 4.4D). A pair of primary GBM cell lines derived in-house, T1 and T2, were also treated with VP for 24 hours in both normoxia and hypoxic conditions. T1 and T2 had been previously described by the pathologist upon tumour excision to have been derived from therapy-resistant and therapy-sensitive areas of the tumour respectively and therefore may vary in their response to cell death stimuli. Interestingly, VP induced hypoxia-specific cell death in both these novel primary glioblastoma lines while not affecting normoxic viability or growth (Figure 4.4E).

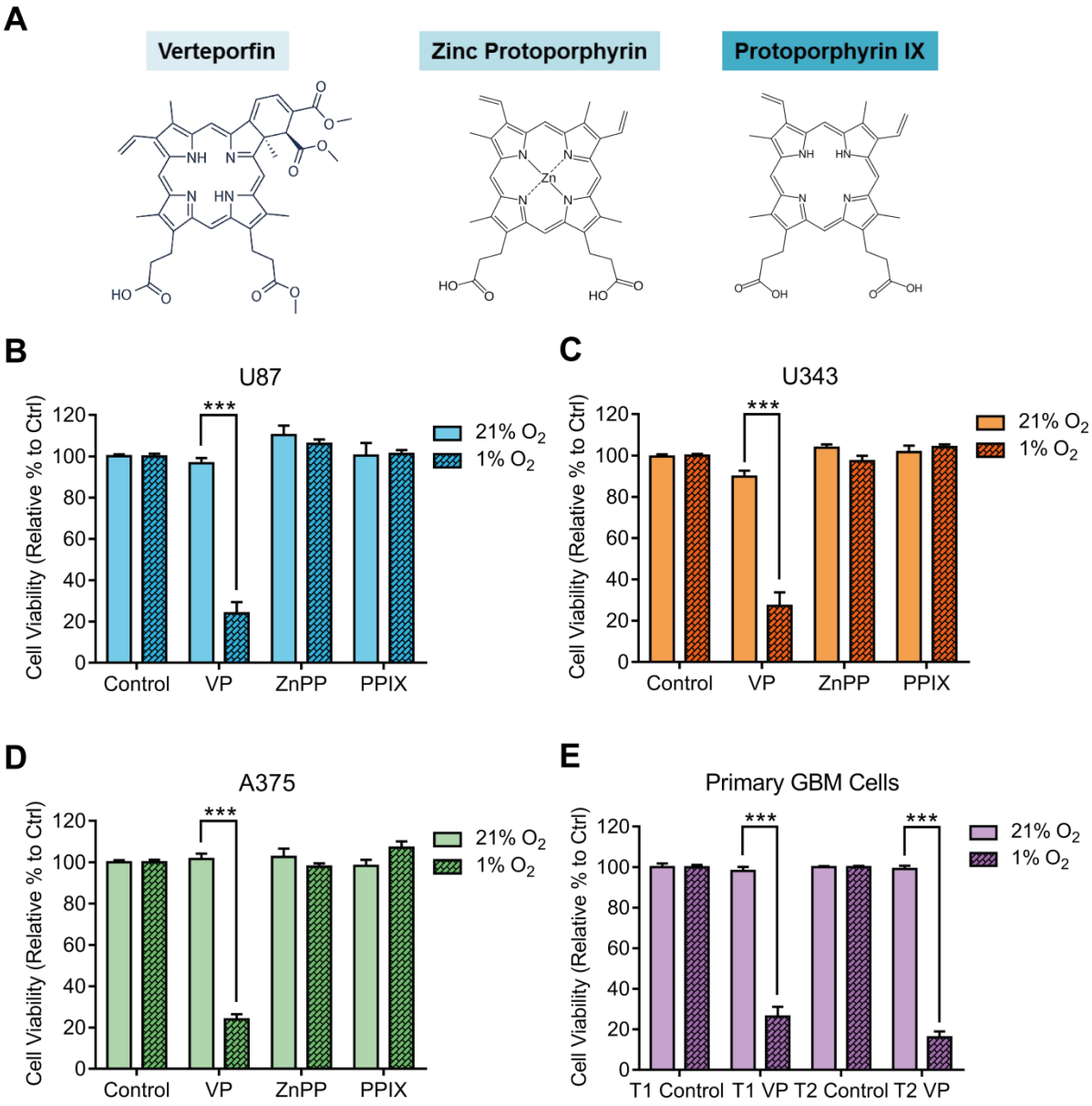

Figure 4.4 Porphyrin family members do not exhibit the same hypoxic cell-killing effect as VP. (A) Structures of porphyrin members VP, ZnPP and PPIX**.** U87 (B) and U343 (C) cells were treated with either vehicle (0.1% DMSO), or 5 μM VP, ZnPP or PPIX for 24 h in 21% and 1% O_2. Cell viability was then measured using the SRB assay. Of the porphyrin family members, only VP was seen to have a significant cell killing effect in hypoxia in both cell lines. (D) Viability of melanoma cell line A375 was also analysed and VP elicited the same hypoxic cell-killing effect as seen in the glioma cell lines. (E) Cell lines T1 and T2, which were generated from a GBM patient biopsy, were treated with either vehicle (0.1% DMSO) or 5 μM VP for 24 h in 21% and 1% O_2 after which the cell viability was analysed by SRB. Again, VP is seen to significantly reduce cell viability but only under hypoxic conditions. Treatments were normalised to the control for each corresponding oxygen tension. Analysis was performed in technical triplicate, in 3-4 independent experiments. Error bars represent ± S.E.M. Significance was determined by two-way ANOVA, Tukey post-hoc analysis. *** $p<0.001$.

Another important facet of glioma biology is the mutational status of the IDH enzyme, as previously mentioned. In order to assess whether there was a relationship between the mutational status of IDH and VP treatment, WT and MUT IDH1 and IDH2 cells were treated with VP for 24 hours, after which cell viability was assessed. Confirmation that the HOG and LN18 cells exhibited the R132H mutation in IDH1 was first achieved via western blotting (Figure 4.5A). The mutational status of the IDH2 cells (R172K) was previously confirmed as outlined in Hollinshead *et al*[209].

VP was seen to significantly reduce cell viability under hypoxic conditions in all cell lines regardless of IDH mutational status (Figure 4.5B-G). Interestingly, there seemed to be a little sensitisation to VP treatment in HOG IDH1 MUT cells under normoxic conditions (Figure 4.5B) as well as in both LN18 IDH1 WT and MUT cells (Figure 4.5D). When cell viability was normalised to the IDH1/2 WT control for both 21% and 1% O_2, it was evident that the mutation in IDH1 and IDH2 caused a significant increase in cell proliferation in both normoxic and hypoxic conditions (Figure 4.5C, E, G).

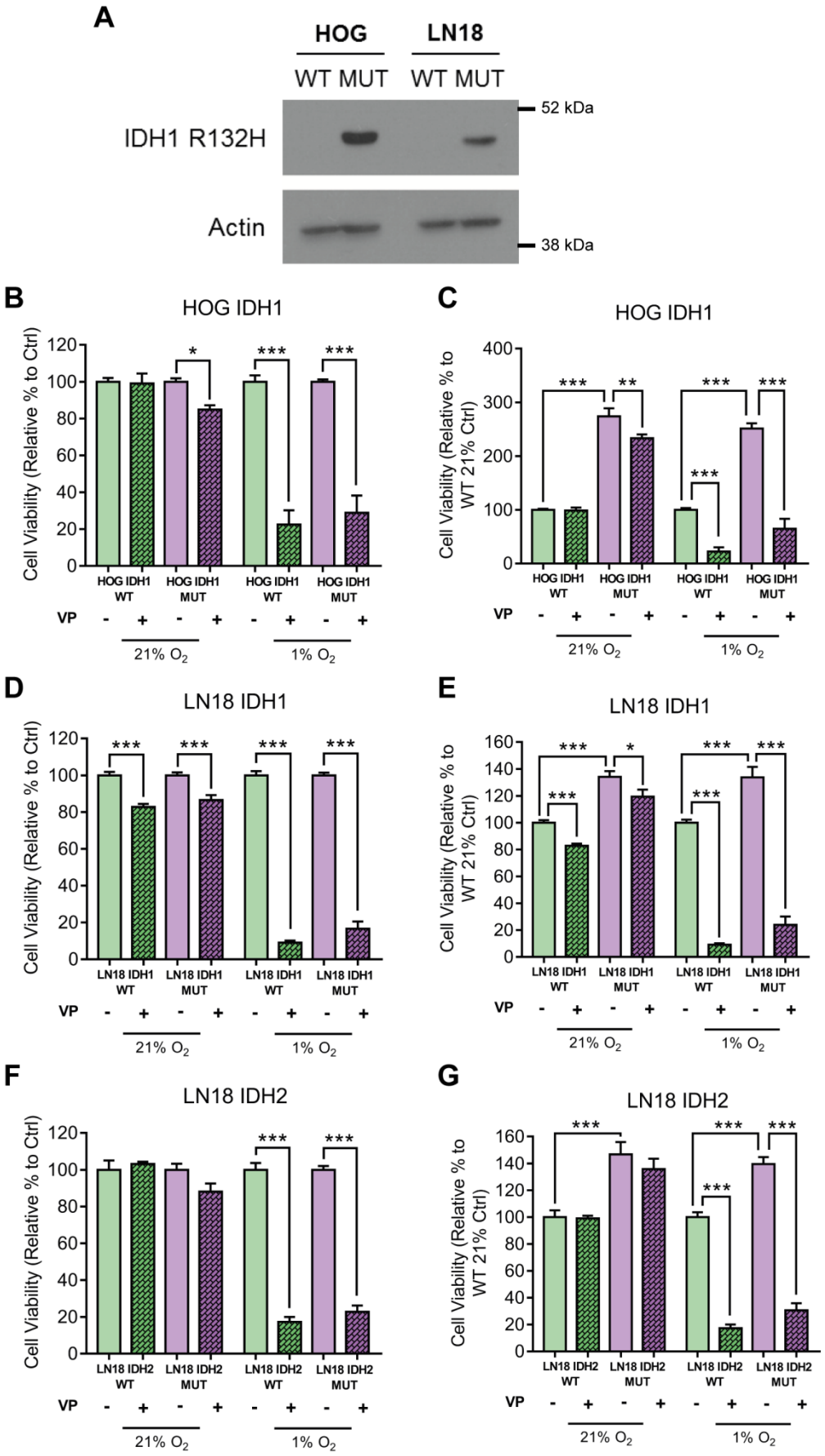
A
HOG
LN18
WT MUT
WT MUT
IDH1 R132H
52 kDa
Actin
38 kDa
B
HOG IDH1
Cell Viability (Relative % to Ctrl)
HOG IDH1 WT
HOG IDH1 MUT
VP
21% O2
1% O2
C
HOG IDH1
Cell Viability (Relative % to WT 21% Ctrl)
D
LN18 IDH1
E
LN18 IDH1
F
LN18 IDH2
G
LN18 IDH2

Figure 4.5 VP significantly reduces cell viability in IDH1 and IDH2 WT and MUT cells. (A) Representative western blot confirming the presence of the mutant IDH1 (R132H) protein in both the HOG and LN18 IDH1 MUT but not WT glioma cell lines. (B) Cell viability was measured via SRB in both HOG IDH1 WT and MUT cells following treatment with either vehicle (0.1% DMSO) or 5 μM VP for 24 h in 21% and 1% O_2. VP was seen to significantly reduce cell viability in hypoxia but also in the IDH1 MUT in normoxia. Viability was normalised to the control for each cell line in each oxygen tension. (C) Cell viability data was also normalised to the HOG IDH1 WT cell line showing that the IDH1 MUT cells proliferated considerably more in both oxygen tensions. (D) VP also increased cell death in hypoxia in LN18 IDH1 WT and MUT cells with some sensitisation also seen under normoxic conditions. (E) Normalisation to the LN18 IDH1 WT control cells in both oxygen tensions again show that the IDH1 mutation permitted increased proliferation. (F) LN18 IDH2 WT and MUT cells also showed VP-induced cell killing in hypoxic conditions. (G) Normalisation to the LN18 IDH2 WT control cells show that IDH2 MUT cells grew significantly more under both normoxia and hypoxia. Analysis was performed in technical triplicate, in 3 independent experiments. Error bars represent ± S.E.M. Significance was determined by one-way ANOVA, Tukey post-hoc analysis. * $p<0.05$, ** $p<0.01$ *** $p<0.001$.

4.2.3. VP reduces spheroid volume and causes destabilisation over time

To assess whether VP kills hypoxic cells in a more physiologically relevant *in vitro* model, U87 and U343 cells were cultured as 3D spheroids. After seeding, cells were cultured in the presence of 1-10 μM VP for 24 and 48 hours (Figure 4.6A, B). The average spheroid diameter was seen to be significantly reduced in a dose-dependent manner over 24 and 48 hours (Figure 4.6C, D). It was also clear that higher concentrations of VP (10 μM), restricted normal spheroid formation (Figure 4.6A, B).

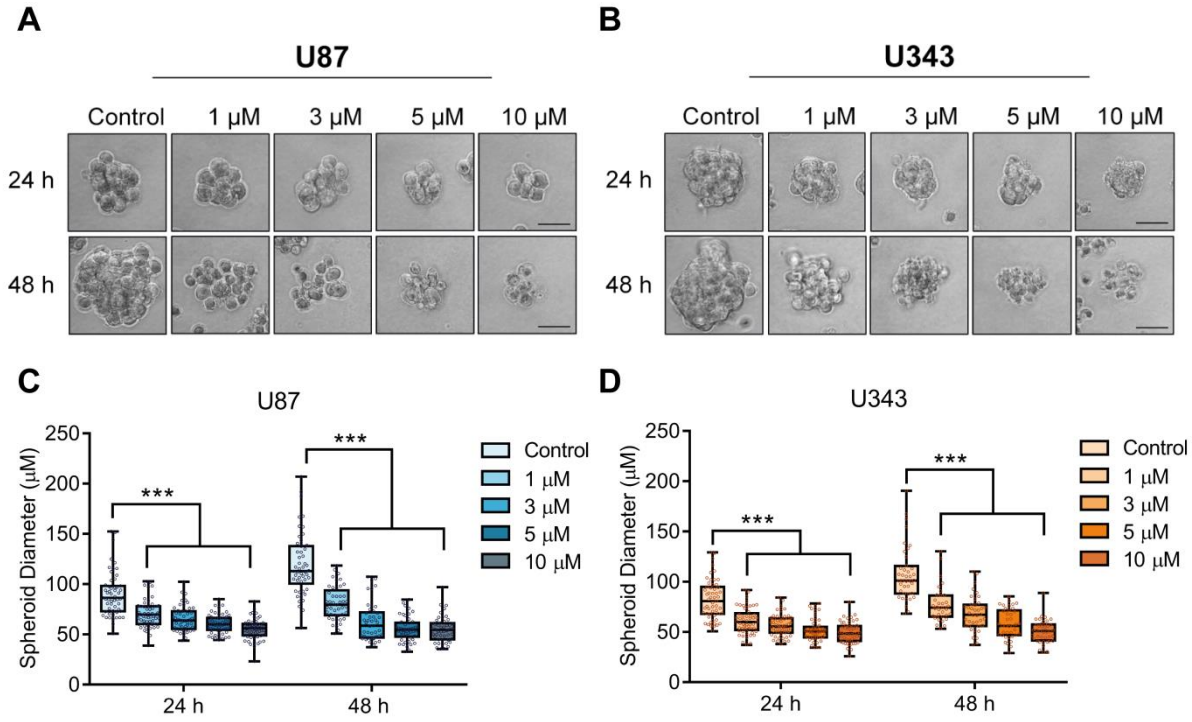

Figure 4.6 VP reduces proliferation and formation of glioma spheroids. U87 and U343 cells were grown as spheroids in the presence of either vehicle (0.2% DMSO) or 1-10 µM VP for 24 and 48 h after which the spheroid diameter was recorded. Representative images of U87 (A) and U343 (B) show a prominent reduction in spheroid size with increasing concentrations of VP. Additionally, spheroids formation appears to be altered due to the looser, less spherical appearance upon VP treatment. (C) and (D) Spheroid diameter was recorded from both U87 and U343 spheroids respectively, and was seen to be significantly reduced in all conditions following both 24 and 48 h VP treatment. Between 55-60 and 45-50 U87 and 50-55 and 35-40 U343 spheroids were analysed for each condition for both 24 and 48 h respectively. All experiments were conducted in biological triplicate. Scale bar represents 100 µm. Data is presented as box-and-whisker (min-max). Significance is determined by two-way ANOVA with Tukey post-hoc test. *** $p<0.001$.

When spheroids were incubated for a longer period of one week in the presence of VP, spheroids were unable to proliferate which was evident by the drastic reduction in size compared to the vehicle control (Figure 4.7A). To assess whether VP interfered with spheroid stability, cells were left to form spheroids for one week before the addition of 5 µM VP to the culture medium for a further 7 days. Spheroids were imaged over the course of treatment and it is evident that VP caused destabilisation of U87 and U343 spheroids due to the loss of spherical appearance and increased detachment of cells

which corresponded with a greater number of single cells present within the culture medium (Figure 4.7B, C).

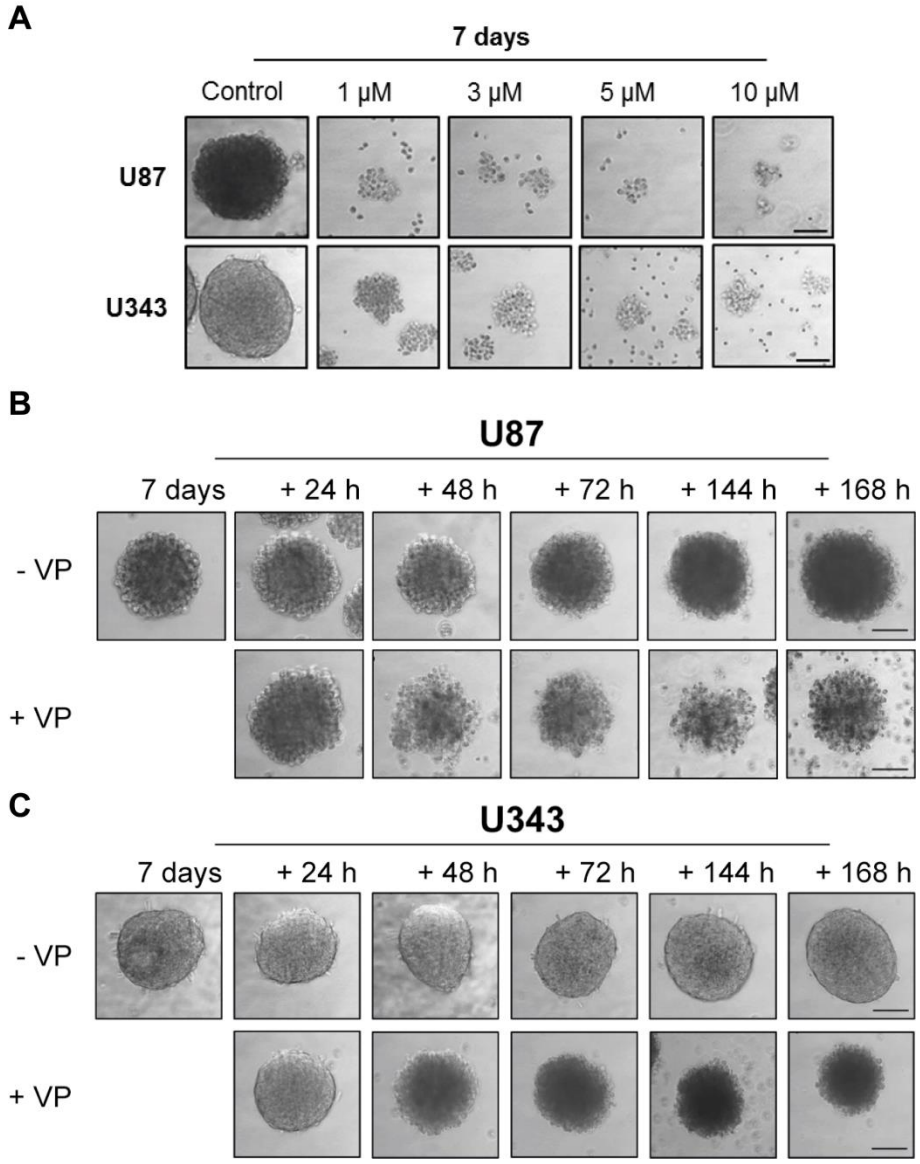

Figure 4.7 Destabilisation of glioma spheroids occurs following long-term VP treatment. (A) U87 and U343 spheroids were incubated for 7 days in the presence of vehicle (0.2% DMSO) or 1-10 μM VP. It is clear that compared to the vehicle control, spheroids are considerably smaller with significantly less cells comprising the spheroid. With higher concentrations (5-10 μM), the spheroids appear to have not properly formed, with a lot singular cells present. (B) and (C) U87 and U343 cells were first left to form spheroids over 7 days before being treated with 5 μM VP for an additional 7 days. Compared to the vehicle control spheroids, it is clear that VP causes the spheroids to destabilise and lose the cell-cell connections needed to form compact spheroids. Experiments were conducted in biological duplicate. Scale bar represents 100 μm.

4.2.4. VP rapidly induces changes in cell morphology

Anti-cancer treatments in the clinic are most often given over a shorter period than the VP treatments used above. It was therefore investigated whether VP could induce cell death within a more clinically relevant treatment window of 1-8 hours in both normoxic and hypoxic conditions, after which cells were processed via ICC and stained for YAP1 expression (Figure 4.8A, B). Alterations in gross cell morphology were apparent even after 1 hour VP treatment in both cell lines and was exacerbated with longer treatment time. Visually, the cells appeared to be undergoing cell-death processes even at this early time point, with characteristics present such as increased membrane blebbing and vacuolisation. In control cells, YAP1 was seen to be ubiquitously expressed in the cytoplasm, where the inactive phosphorylated form is understood to reside (Figure 4.8A, B). However upon VP addition, YAP1 is seen to progressively re-localise from the cytoplasm to being prominently expressed near the plasma membrane.

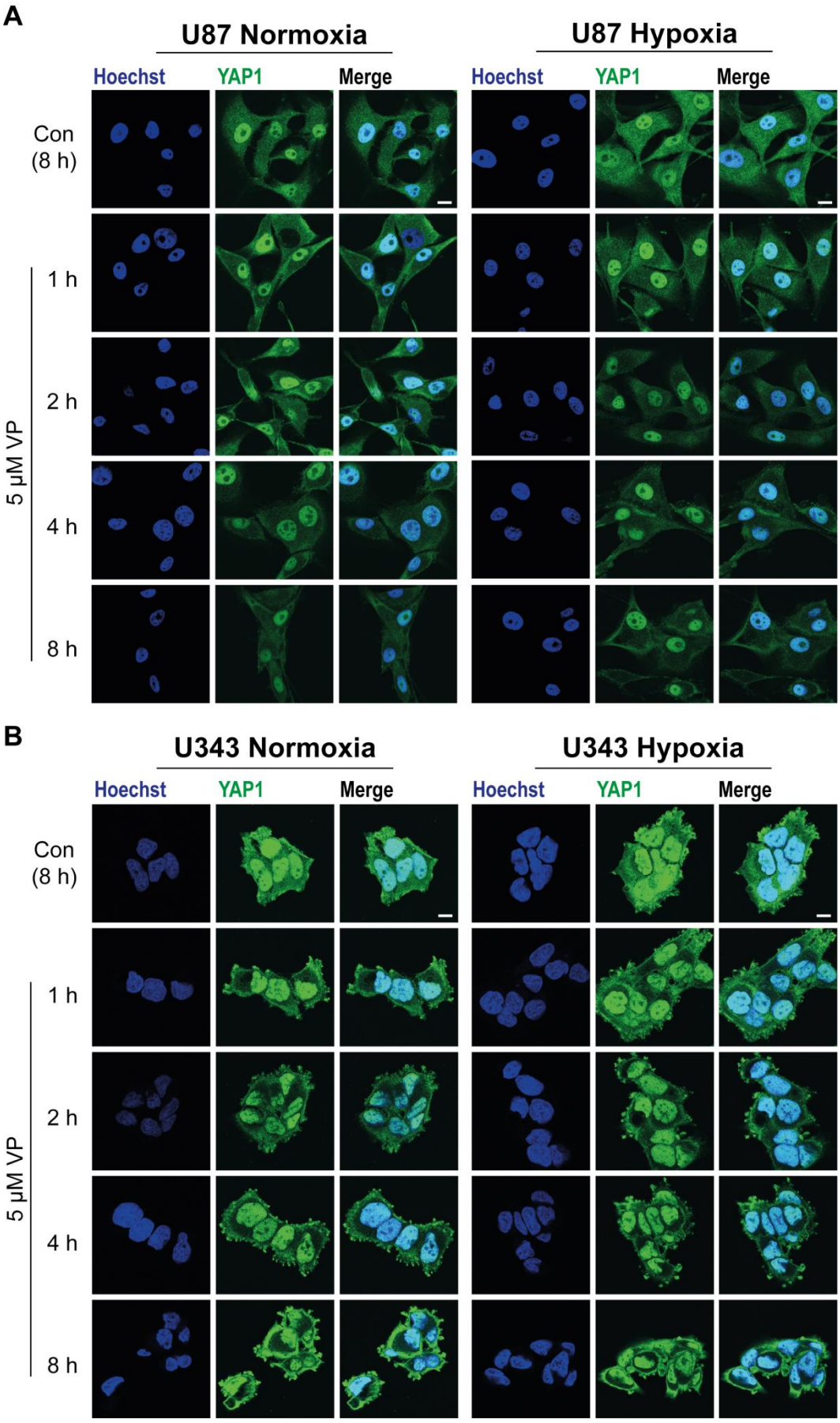
A
U87 Normoxia
U87 Hypoxia
Hoechst
YAP1
Merge
Hoechst
YAP1
Merge
Con
(8 h)
5 μM VP
1 h
2 h
4 h
8 h
B
U343 Normoxia
U343 Hypoxia
Hoechst
YAP1
Merge
Hoechst
YAP1
Merge
Con
(8 h)
5 μM VP
1 h
2 h
4 h
8 h

Figure 4.8 VP induces morphological changes in glioma cells. U87 (A) and U343 (B) cells were treated with 5 μM VP for 1-8 h in both 21% and 1% O_2. Cells were fixed at each stated time-point and processed via ICC and imaged via confocal microscopy. Cells were stained with YAP1 and Hoechst to distinguish the cell nucleus. Cellular morphology altered in VP treated cells as early as 1 h post-treatment compared to the control (Con). YAP1 relocalised from the cytoplasm to the plasma membrane with increasing time. Cells also appeared to have undergone significant cell death processes by 8 h post-treatment. Images are representative of 3 independent experiments. Scale bar represents 10 μm.

As previously described, the cellular localisation of YAP1 is critical to its function, with active YAP1 believed to residue in the cell nucleus where, as a transcriptional co-activator, it is free to bind with transcription factor binding partners to synergistically transcribe downstream target genes[143]. Quantitative analysis of YAP1 nuclear staining shows that YAP1 fluorescence is significantly increased in both U87 and U343 cells following 4 hours of hypoxia suggesting increased YAP1 activity in hypoxia (Figure 4.9A, B). This effect was also apparent after 8 hours hypoxia in U87 cells although was not observed in U343 cells (Figure 4.9C, D). Upon addition of VP however, YAP1 nuclear fluorescence was seen to reduce in all conditions, implying that not only could VP potentially inhibit YAP activity it could also alter its localisation or inhibit its expression.

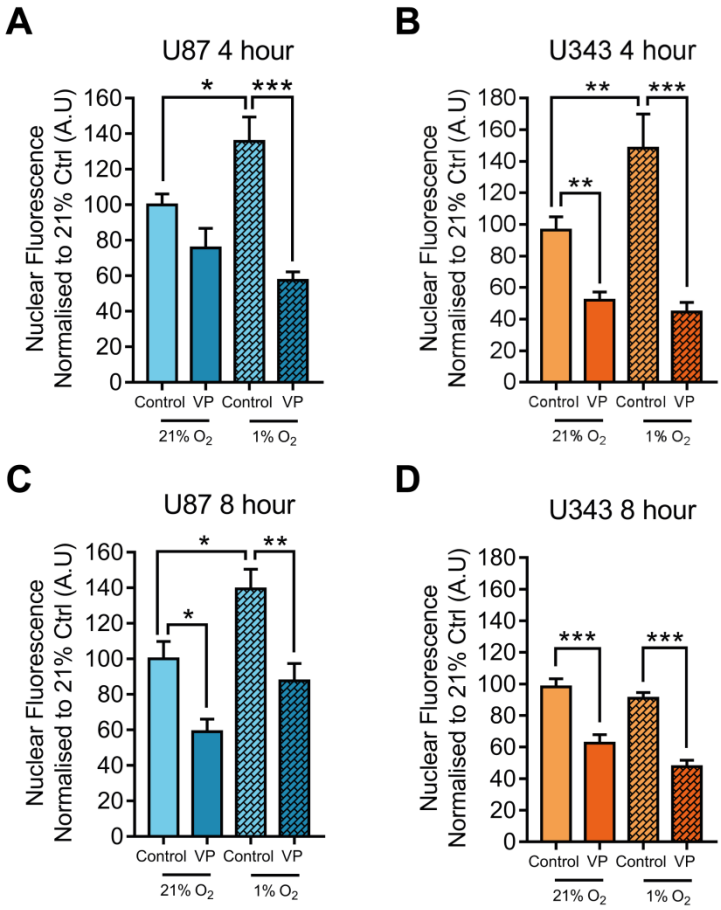

Figure 4.9 YAP1 expression is increased in hypoxia and reduced upon VP treatment. Nuclear YAP1 fluorescence was quantitatively analysed in both U87 and U343 cells 4 and 8 h post-treatment with 5 μM VP. YAP1 nuclear expression was seen to significantly increase in hypoxia after 4 h in both U87 (A) and U343 (B) cells but only in U87 (C) and not U343 (D) cells 8 h post VP treatment. VP was seen to reduce YAP1 nuclear expression compared to control cells in all oxygen conditions in both glioma cell lines 4 and 8 h post-treatment. All experiments were conducted in biological triplicate (except U343 4 h in biological duplicate). 2-4 images were analysed per condition, per experiment. Error bars represent ± S.E.M. Significance is determined by one-way ANOVA, with Tukey post-hoc analysis. * $p<0.05$, ** $p<0.01$, *** $p<0.001$.

To further investigate this, U87 and U343 cells were treated with 5 μM VP in both normoxic and hypoxic conditions for 4 hours, after which cells were lysed. Protein expression of YAP1, and its downstream target CTGF, was subsequently investigated via western blotting (Figure 4.10A). Unexpectedly, YAP1 and CTGF expression remained unchanged upon exposure to VP in both oxygen conditions indicating that despite attenuated YAP1 nuclear fluorescence with VP treatment, overall YAP protein

expression remains unaffected. To investigate whether VP could induce changes in YAP expression over a longer treatment period, cells were treated for 24 and 48 hours under normoxic conditions (Figure 4.10B). Long-term expression under hypoxic conditions could not be determined due to rapid VP-induced hypoxic cell death. Again, YAP1 and CTGF expression remained unchanged upon VP treatment suggesting VP to potentially exhibit YAP-independent effects in glioma cells within this time period.

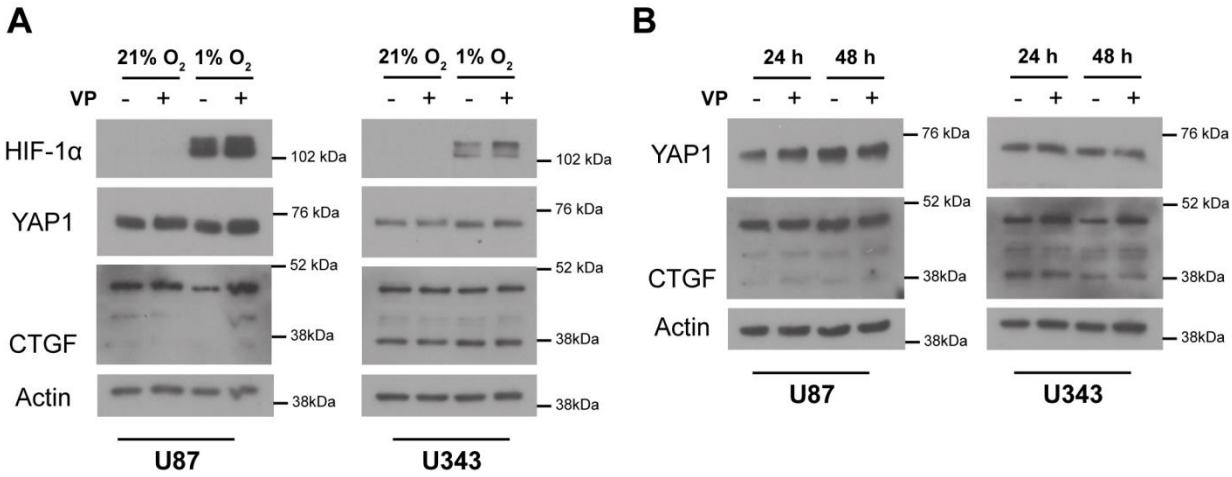

Figure 4.10 YAP1 protein expression is unchanged upon VP treatment. (A) Expression of YAP1 and YAP-target CTGF were assessed in both U87 and U343 cells following exposure to 5 μM VP for 4 h in both 21% and 1% O_2. Successful induction of hypoxia was observed through increased stabilisation of HIF-1α. YAP1 and CTGF expression levels remained unchanged following VP treatment. CTGF expression is denoted by the lower band and was incredibly low in U87 cells. (B) U87 and U343 cells were treated with and without 5 μM VP for 24 and 48 h under normoxic conditions. Again, VP did not induce any changes in protein expression of both YAP1 or CTGF. Blots are representative of 2 (4 h) and 1 (24-48 h) biological experiments.

4.2.5. Exposure to ambient light during VP treatment increases sensitivity

Since VP can induce cell death processes almost immediately following exposure, a more clinically relevant VP treatment time of 4 hours was chosen. To confirm that hypoxic glioma cells were indeed dying with VP treatment within this treatment window, cells were treated with VP for 4 hours after which they are incubated in normal medium without VP for the remaining 20 hours in both normoxic and hypoxic conditions (Figure

4.11A, B). Interestingly, despite the shorter treatment time of 4 hours, hypoxic cell death was still apparent in both cell lines indicating that VP induces early cell death mechanisms which cannot be prevented upon removal of the drug. Furthermore, due to the light-sensitivity of VP, experiments involving VP were conducted in the dark however if these cells were exposed to ambient light during the removal of VP, normoxic cells were significantly sensitised to VP treatment (Figure 4.11C, D). It should also be noted that despite VP being capable of inducing cell death after 4 hours, in hypoxia the killing was further increased if the cells had been exposed to VP for the complete treatment time of 24 hours thus indicating that to achieve almost complete cell death a longer treatment time is required.

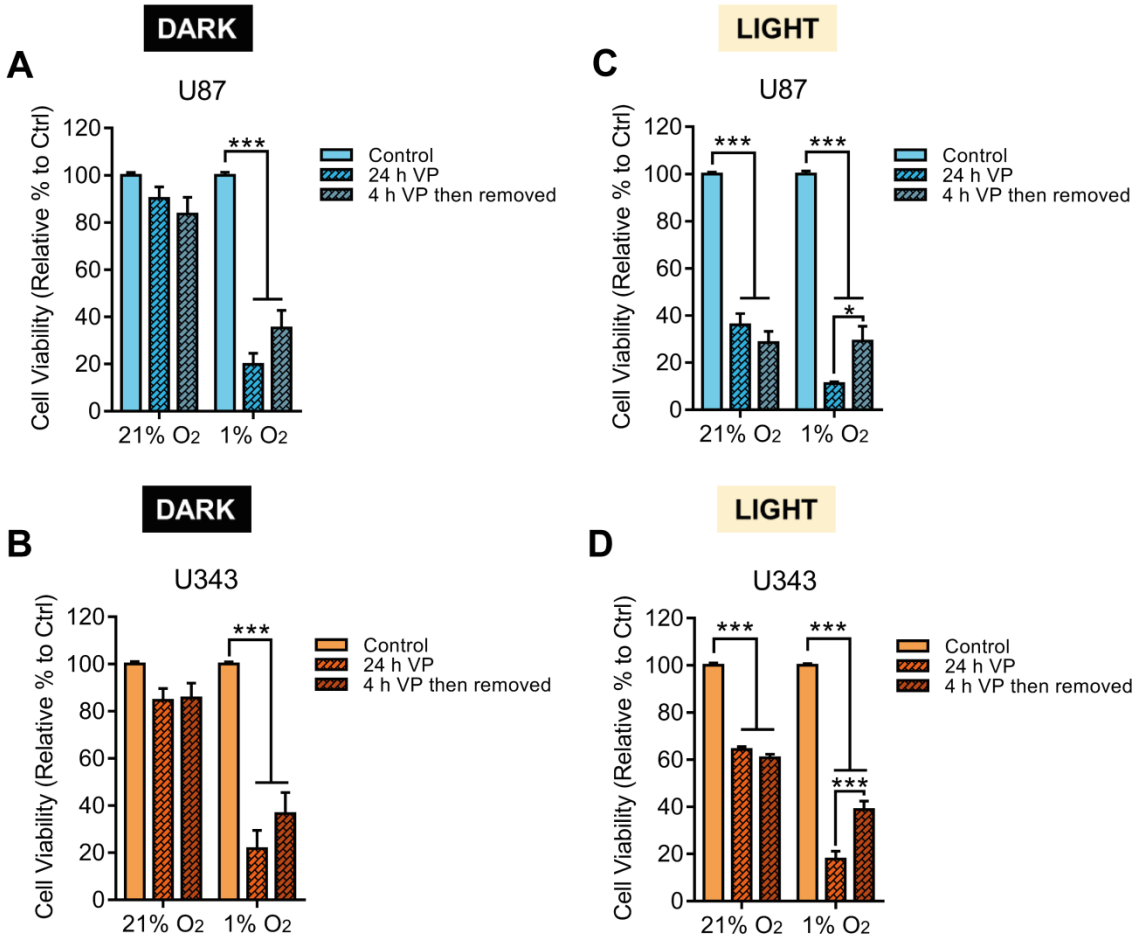

Figure 4.11 VP sensitises cells to death if exposed to ambient light during treatment. Cell viability was measured via SRB following treatment with vehicle (0.1% DMSO) or 5 μM VP for 4 h after which VP was removed and cells incubated in media for 20 h or 5 μM VP for 24 h. Cell viability of U87 (A) and U343 (B) cells which had remained obscured from ambient light during changing of the media after 4 h VP treatment. VP was still able to significantly induce cell death after 4 h treatment to levels similarly achieved with 24 h. Interestingly, if cells were exposed to light during changing of the media following 4 h treatment, VP also caused a significant reduction in cell viability under normoxic conditions in both U87 (C) and U343 (D) cells. Treatment was normalised to the control for each oxygen tension. Experiments were conducted in 3-4 biological experiments, in technical triplicate/quadruplicate. Error bars represent ± S.E.M. Significance is determined by two-way ANOVA, with Tukey post-hoc analysis. * $p<0.05$, *** $p<0.001$.

4.2.6. Global expression of tumour suppressor and YAP binding partner, p73 is increased following VP exposure

Now defined as a potent oncogene, YAP has been previously identified to exhibit many roles in the growth and survival of malignant cells. However its effects are largely reliant

on the cellular and microenvironmental context, as previously discussed. Under certain situations YAP has been identified to exhibit tumour suppressive qualities such as switching its transcription factor binding partners from the favoured TEAD family that promote cell survival, to other transcription factors such as p73, which act to transcribe genes linked to the induction of cell death. To examine if YAP was exhibiting this role during VP-induced cell death, the expression of YAP transcription factor binding partner and p53-related protein, p73 was investigated through ICC (Figure 4.12A, B). Evidently, a large increase in p73 expression was seen following 4 hour exposure to VP which was exacerbated with a longer treatment time of 8 hours. Increased p73 expression was apparent in both normoxic and hypoxic conditions, although was more prominently increased under hypoxic conditions. Co-localisation of YAP1 and p73 protein was also witnessed and seen to be enhanced in hypoxia, suggesting potential increased interaction of these two binding partners under these conditions.

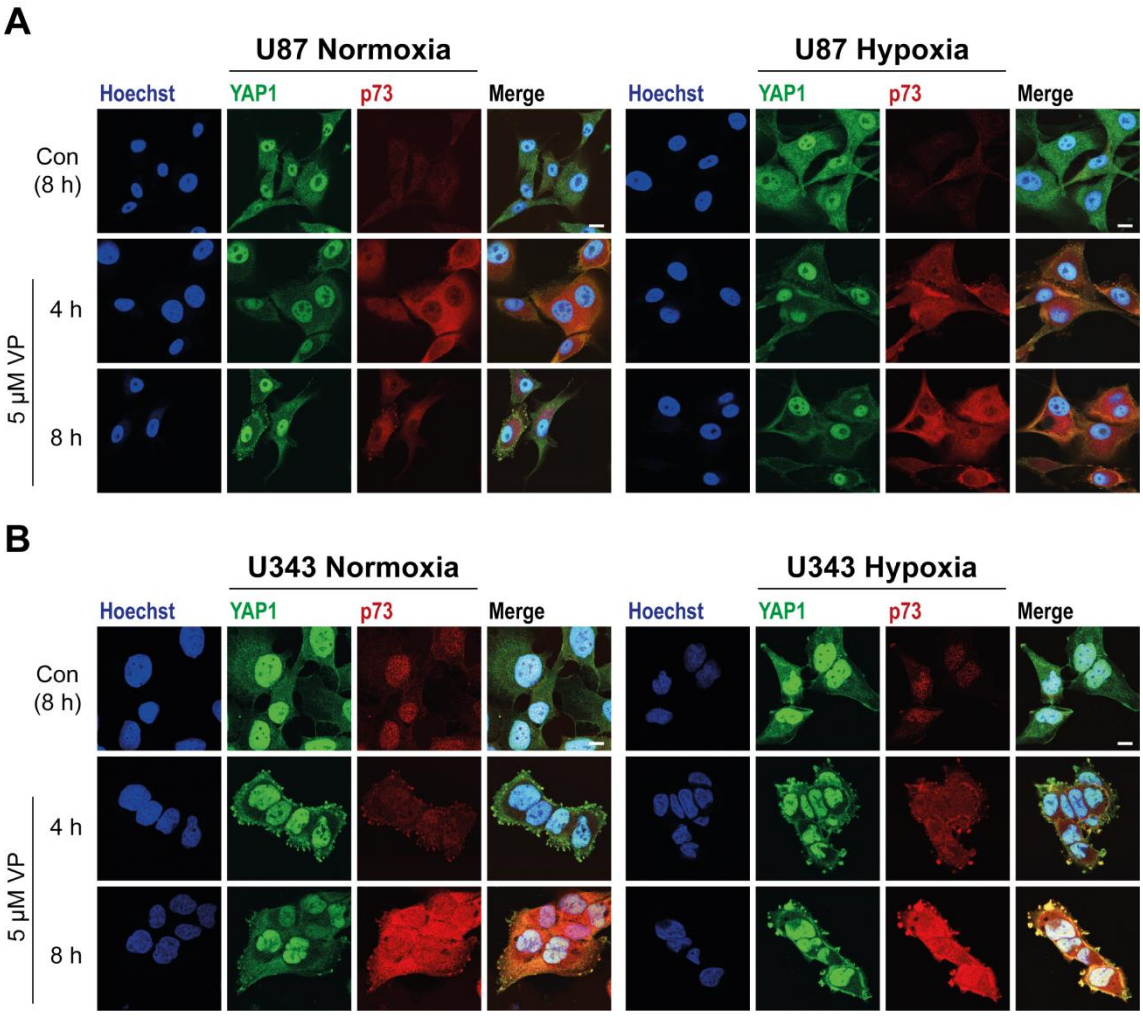

Figure 4.12 Expression of p73 is significantly increased following VP treatment. U87 (A) and U343 (B) cells were treated with either vehicle (0.1% DMSO; Con) or 5 µM VP for 4 and 8 h in both 21% (normoxia) and 1% (hypoxia) O_2. Cells were then processed via ICC and imaged via confocal microscopy. Expression of apoptotic protein p73 is dramatically increased upon VP treatment, which is enhanced under hypoxic conditions. Images are representative of 3 independent experiments. Scale bar represents 10 µm.

For further investigation of this potential interaction, U343 cells were treated with VP for 4 hours in hypoxia then subjected to co-immunoprecipitation using YAP1 coated agarose beads. Western blotting was then used to determine whether p73 could be detected through binding to YAP1 protein. Unexpectedly, no binding of p73 to YAP1 was exhibited (Figure 4.13A) suggesting that despite the significantly increased p73 expression, this event was potentially unrelated to YAP activity.

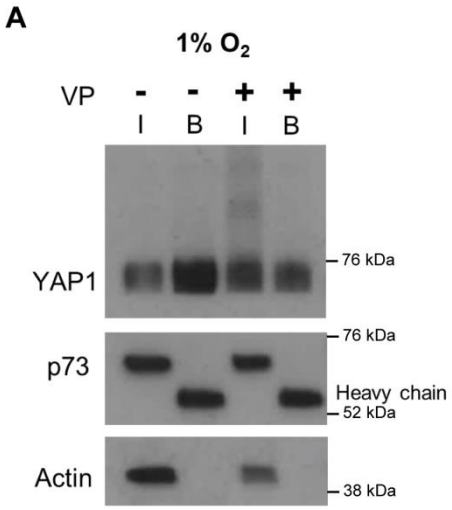

Figure 4.13 YAP1 does not bind partner p73 upon VP treatment in hypoxia, despite increased expression. (A) U343 cells were treated with either vehicle (DMSO) or 5 μM VP for 4 h under 1% O_2 after which lysates were subject to co-immunoprecipitation with YAP1-conjugated agarose beads for 3 h. Protein from the lysate (*I*) and those bound to the agarose beads (*B*) were subject to western blotting and probed for both YAP1 and p73 expression. It is clear that p73 did not bind with YAP1 in hypoxic conditions, with or without VP treatment. Experiments were conducted in biological triplicate.

4.2.7. VP-induced hypoxic cell death is YAP-independent

As VP has been characterised as a YAP inhibitor, we wanted to confirm that the hypoxia-specific cell death induced by VP treatment was through this mechanism. We therefore knocked down expression of YAP1, its paralog TAZ, and both proteins in U87 and U343 glioma cell lines. Western blot analysis confirmed that successful knockdown of these proteins was achieved (Figure 4.14A). Cell viability was then measured following 5 μM VP treatment for 24 hours in both normoxic and hypoxic conditions (Figure 4.14B, C). Surprisingly, VP was still able to induce significant cell death in hypoxia despite knockdown of YAP, TAZ and both YAP and TAZ suggesting that this VP-induced hypoxic cell death is YAP1-independent. Additionally, results in chapter three (Figure 3.10) show that knockdown of YAP, TAZ and YAP and TAZ was able to reduce cell proliferation but was not sufficient to induce hypoxic cell death, therefore unable to phenocopy the hypoxic-specific killing induced by VP.

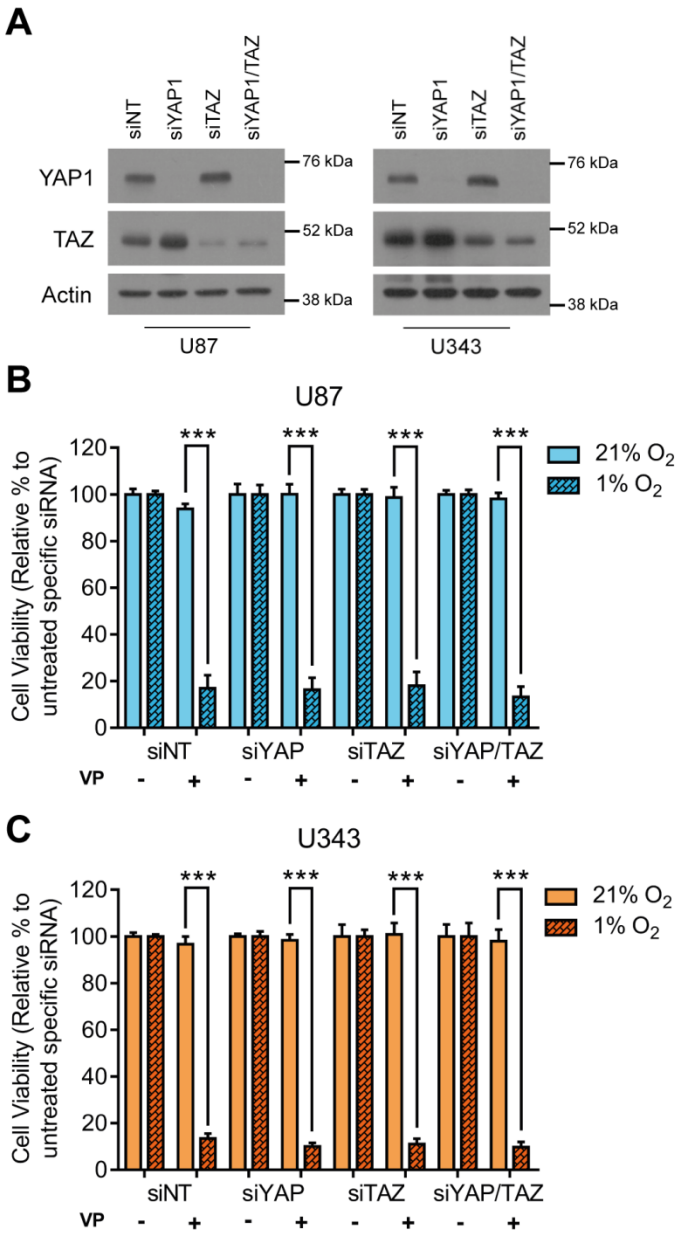

Figure 4.14 Hypoxic VP-induced cell death is YAP-independent. (A) Western blot showing successful knockdown of YAP (siYAP), TAZ (siTAZ) and both YAP and TAZ (siYAP/TAZ) 72 h post-transfection with 25 nM siRNA. Non-targeting siRNA (siNT) is used as a control. (B) and (C) U87 and U343 cells were treated with 5 μM VP 48 h post-transfection, for 24 h in both 21% and 1% O_2. VP still caused a significant reduction in cell viability despite knockdown of YAP, TAZ and both YAP and TAZ indicating that hypoxic VP-induced cell death is likely to be through a YAP-independent mechanism. Viability was determined via SRB assay with each condition normalised to each untreated siRNA control for each oxygen tension. Experiments were conducted in technical duplicate/triplicate in 3 independent experiments. Error bars represent ± S.E.M. Significance is determined by two-way ANOVA, Tukey post-hoc analysis. *** $p<0.001$.

It has recently been suggested that VP could act independently of YAP1, inducing cell death by forming cross-linked oligomers with p62, also known as sequestosome 1 (SQSTM1), which acts to recognise toxic cellular aggregates and target them to the autophagosome for degradation[268]. Aggregation of p62 consequently impairs this function and so toxic protein aggregates accumulate eventually causing proteotoxicity and cell death[268]. To see whether VP caused an increase in these protein aggregates in glioma cells, p62 expression was investigated following 4 hour VP treatment (Figure 4.15A, B). It is clear that basal expression of p62 was high in normoxic control cells and did not increase upon VP exposure. p62 was observed to form more aggregates with VP treatment although these results were not clear enough to conclude that this was a major mechanism of VP-induced cell death in hypoxia.

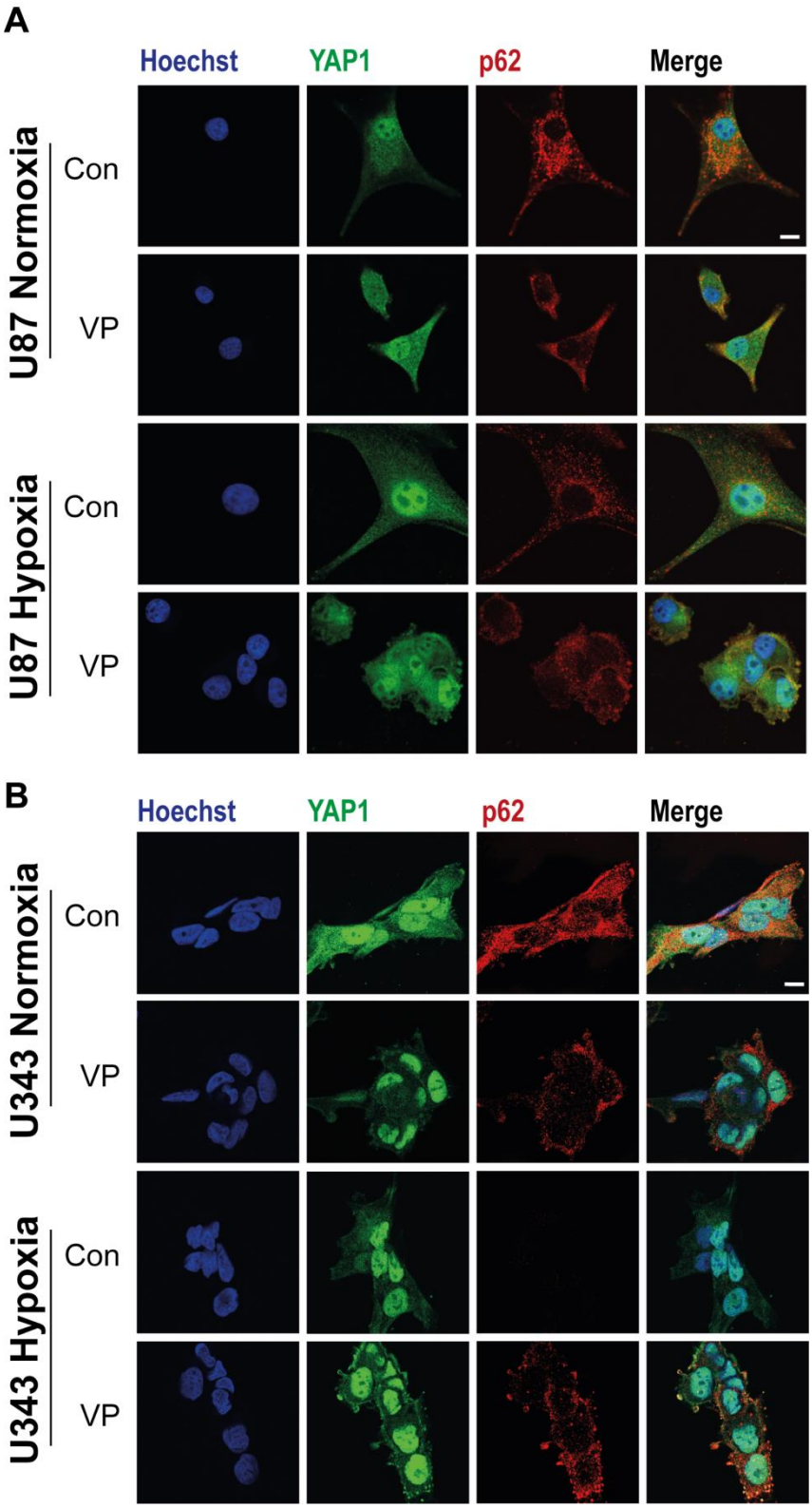

Figure 4.15 VP reduces p62 expression. U87(A) and U343 (B) cells were treated with VP for 4 h before stained for YAP1 and p62 expression. High p62 expression was observed in normoxic control cells in both the U87 and U343 cell lines. VP treatment however attenuated p62 expression but potentially induced aggregation. Experiments were conducted in biological duplicate. Scale bar represents 10 μm.

4.2.8. Stabilisation of HIF-1α only partially sensitises glioma cells to VP in normoxia

Due to VP-induced cell death occurring only under hypoxic conditions, this potential selective mechanism was further investigated. As previously described, hypoxia inducible transcription factor HIF-1α is considered to a central regulator of the adaptive cellular response to hypoxia. Stabilisation of HIF can be pharmacologically induced under normoxic conditions through the addition of the α-KG-like molecule DMOG, which acts as a PHD and FIH inhibitor[269,270]. DMOG was therefore used to assess whether mimicking hypoxic conditions under normoxia could sensitise normoxic cells to VP-induced cell death (Figure 4.16A, B). Intriguingly, addition of DMOG was seen to partially but significantly sensitise the cells to VP, although the effect was smaller in U343 cells. Western blots were used to confirm that DMOG-induced HIF-1α stabilisation under normoxia, and was comparable to expression levels seen in hypoxia (Figure 4.16C).

To further implore this concept, U87 cells were transfected with a plasmid to express a triple mutant form of HIF-1α (HIF1αTM), which is mutated on every residue that confers the sensitivity to oxygen tension through hydroxylation (P402, P564 and N803), and is therefore stable under normoxia[213]. Although stabilisation levels reached were not as high as with application of DMOG, overexpression of HIF1αTM caused a small, but significant, sensitisation to VP treatment in normoxia (Figure 4.16D, E). Despite the increased sensitisation, normoxic HIF-1α stabilisation was not enough to completely phenocopy the VP-induced cell death observed under hypoxic conditions, suggesting that other mechanisms were also involved.

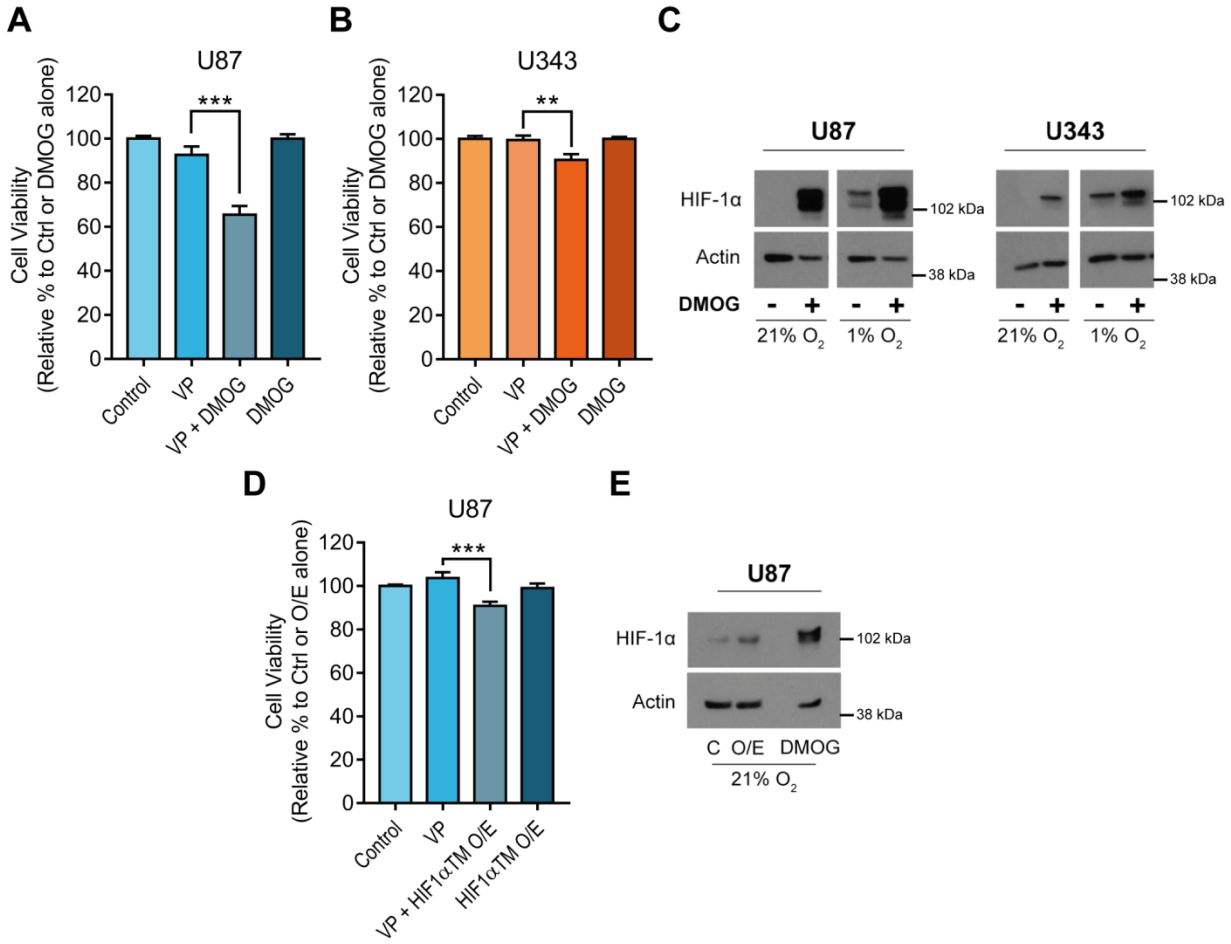

Figure 4.16 Normoxic glioma cells are sensitised to VP upon stabilisation of HIF-1α. U87 (A) and U343 (B) cells were treated overnight (14-16 h) with either vehicle or 1 mM DMOG prior to treatment with 5 μM VP for 4 h in 21% O_2. It is clear that upon stabilisation of HIF-1α in normoxia, cells became significantly more sensitive to VP treatment. Cell viability was measured via SRB assay and results were normalised to either control or untreated DMOG alone. (C) Representative western blots show increased HIF-1α stabilisation and hence protein expression in normoxia upon DMOG treatment. Protein extracted under hypoxia (1% O_2) is shown as a comparison. (D) A mutant form of HIF-1α (HIF1αTM) was over-expressed (O/E) in U87 cells to stabilise HIF-1α expression under normoxic conditions. Cells were treated 48 h post-transfection with 5 μM VP for 4 h in 21% O_2 after which cell viability was measured via SRB. Viability was significantly reduced upon HIF-1α overexpression, although the effect was not as great as when cells were treated with the chemical DMOG. (E) Western blot showing increased expression of HIF-1α with overexpression of the mutant form HIF1αTM. Protein extracted from cells treated with 1 mM DMOG for 20 h is shown as a comparison. Experiments were conducted in technical duplicate/triplicate in 3 independent experiments. Error bars represent ± S.E.M. Significance is determined by one-way ANOVA, Tukey post-hoc analysis. ** $p<0.01$, *** $p<0.001$.

As an alternative approach, siRNA was employed to knockdown HIF-1α in hypoxia to assess whether HIF-1α was required for VP to induce cell death. Surprisingly, despite dramatic reduction in HIF-1α protein, VP was still able to mediate hypoxic cell death (Figure 4.17A-C). This suggests that an additional aspect of hypoxic biology is likely the major determinant for hypoxic sensitisation to VP.

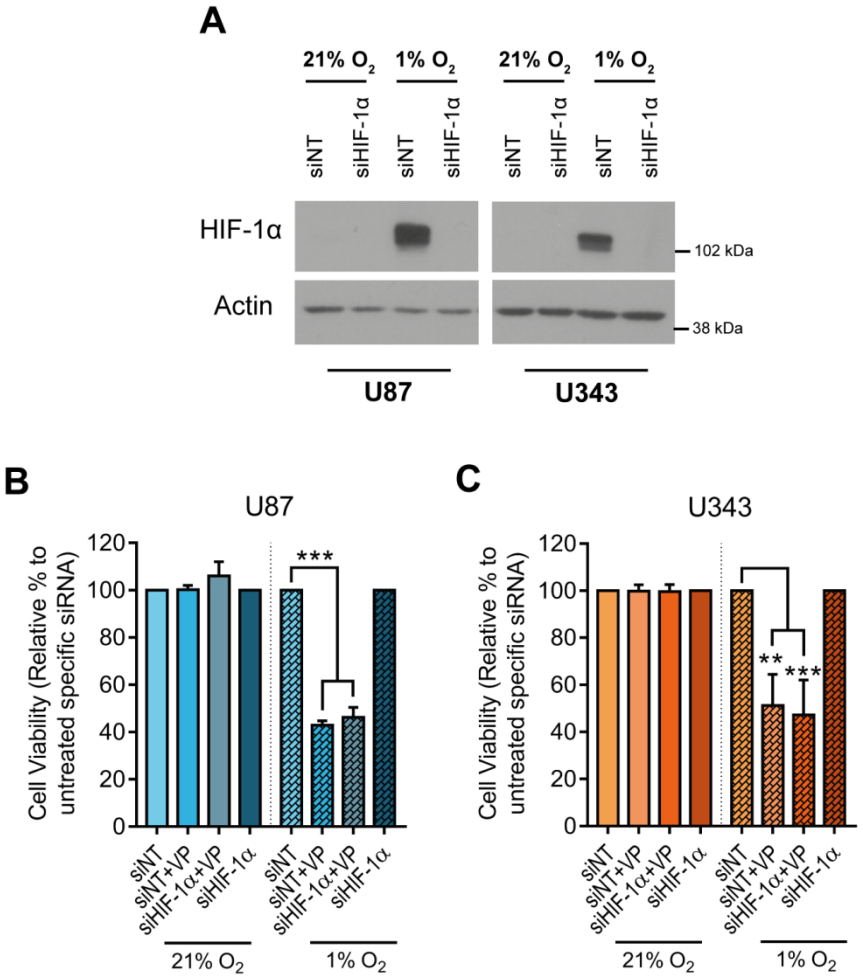

Figure 4.17 VP-induced hypoxic cell death despite knockdown of HIF-1α. Cells were subjected to 48 h siRNA knockdown of HIF-1α before 5 μM VP treatment in both normoxia and hypoxia for 24 h. (A) Representative western blot showing knockdown of HIF-1α. (B) U87 and U343 (C) cell viability analysis shows that despite successful knockdown of HIF-1α, VP could still induce hypoxic cell death. Experiments were conducted in biological triplicate. Data is presented as ± S.E.M. Significance is determined by two-way ANOVA, Tukey post-hoc analysis. * $p<0.05$, *** $p<0.001$.

4.2.9. VP-mediated hypoxic cell death is partially preventable by pharmacological inhibitors of cell death

To better define how exposure to VP caused hypoxic cell death in glioma cells, pharmacological inhibitors of different cell death processes were employed in an attempt to pinpoint the mechanism of VP-induced hypoxic cell death. Firstly, a few investigations had previously suggested that VP could induce apoptosis and so the pan-caspase and apoptosis inhibitor, Z-VAD-FMK was used. Cells were treated with 5 μM VP in the presence and absence of the caspase-inhibitor for 8 hours before assessing caspase-mediated cell death using Annexin V/PI staining and flow cytometry. The viable U87 cell population was measured and was significantly reduced upon VP addition in hypoxia (Figure 4.18A). Furthermore, addition of Z-VAD-FMK alongside VP was unable to significantly restore cell viability. Upon closer examination, it was apparent that upon VP treatment for 8 hours, the cells exhibited increased PI staining, reminiscent of necrotic rather than apoptotic cells (Figure 4.18B, C). To confirm that this necrosis was not as a result of a longer treatment time and thus missing early apoptotic mechanisms, cells were VP-treated for 4 hours (Figure 4.18D). Again, cells were seen to have pronounced staining for PI over Annexin V, implying that they were not passing through earlier apoptotic stages before undergoing necrosis. These results were also recapitulated in the U343 glioma cell line (Figure 4.19A-D).

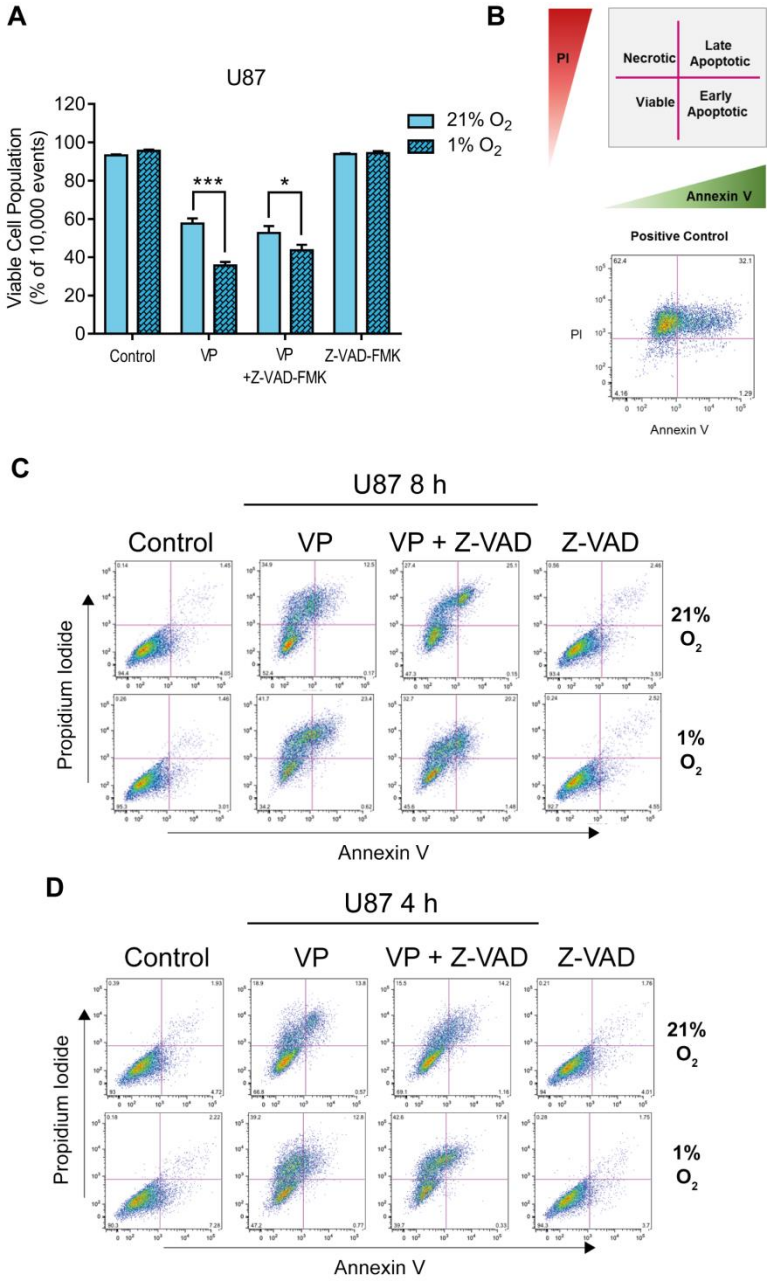

Figure 4.18 VP-induced cell death cannot be inhibited by Z-VAD-FMK in U87 cells. U87 (A) cells were pre-treated with 20 μM Z-VAD-FMK (Z-VAD) prior to being treated with 5 μM VP for 8 h in both 21% and 1% O_2. Cells were then dual stained with Annexin V and PI and the viable cell population measured via flow cytometry. No significant rescue in cell viability upon Z-VAD-FMK treatment was observed suggesting that cell death is not predominately through apoptosis. (B) Representative flow plot of H_2O_2 positive control to increase confidence in gating parameters. (C) Representative flow cytometry plots show that upon 8 h VP treatment cells have a significantly higher proportion of PI staining to Annexin V, indicating that these cells could be necrotic rather than apoptotic. (D) Flow plots of U87 cells treated for 4 h with VP and Z-VAD-FMK show that even with a shorter treatment time, these cells do not seem to pass through early apoptosis, which is normally indicated by high Annexin V, low PI staining. Data is from 4 biological experiments and 1 experiment for 4 h. Data is presented as ± S.E.M. Significance is determined by two-way ANOVA, Tukey post-hoc analysis. * $p<0.05$, *** $p<0.001$.

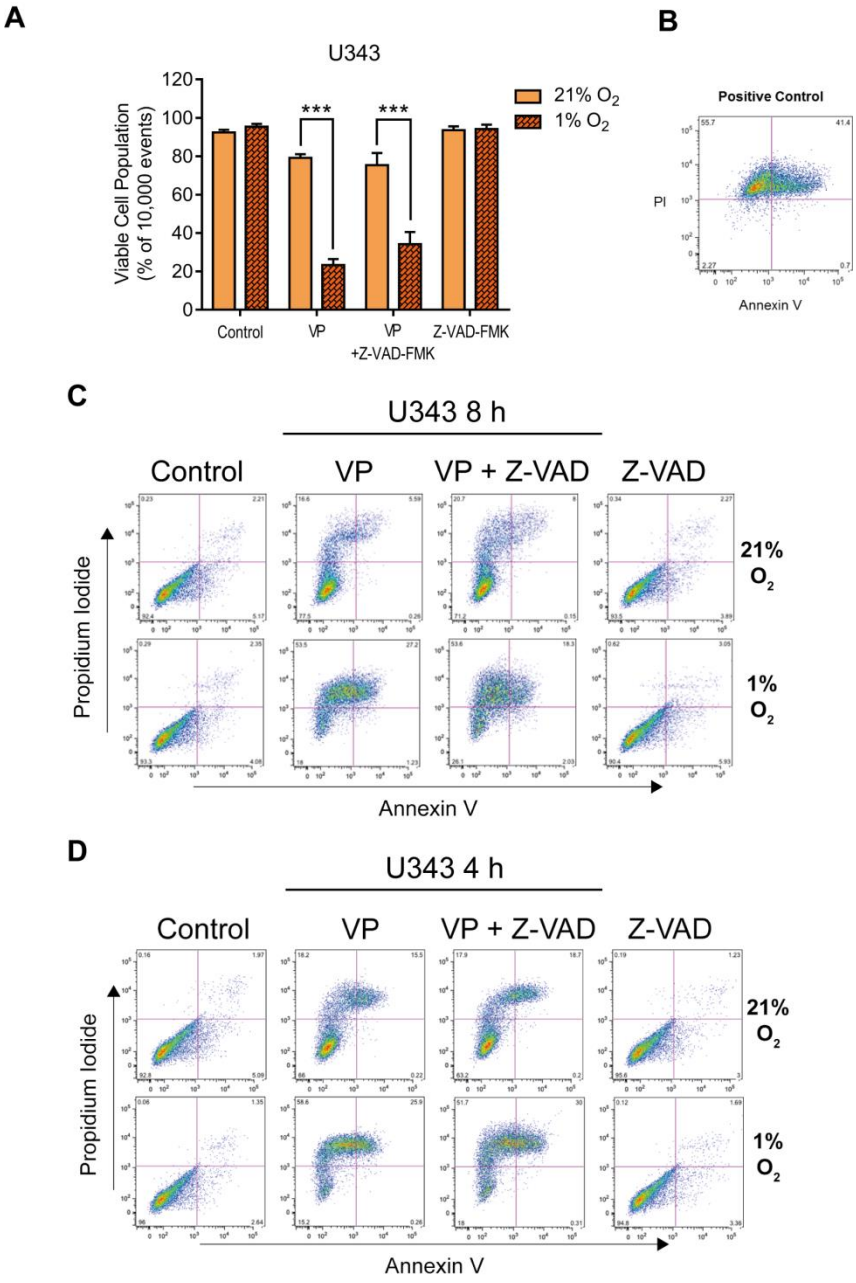

Figure 4.19 VP-induced cell death cannot be inhibited by Z-VAD-FMK in U343 cells. U343 (A) cells were pre-treated with 20 μM Z-VAD-FMK (Z-VAD) prior to being treated with 5 μM VP for 8 h in both 21% and 1% O_2. Cells were then dual stained with Annexin V and PI and the viable cell population was measured via flow cytometry. There was no significant rescue in cell viability upon Z-VAD-FMK treatment, suggesting that the mechanism of cell death is not predominately through apoptosis. (B) Representative flow plot of H_2O_2 positive control to increase confidence in gating parameters (C) Representative flow cytometry plots show that upon 8 h VP treatment cells have a significantly higher proportion of PI staining to Annexin V, indicating that these cells could be necrotic rather than apoptotic. (D) Flow plots of U87 cells treated for 4 h with VP and Z-VAD-FMK show that even with a shorter treatment time, these cells do not seem to pass through early apoptosis, which is normally indicated by high Annexin V, low PI staining. Data is from 3 biological experiments and 1 experiment for 4 h. Data is presented as ± S.E.M. Significance is determined by two-way ANOVA, Tukey post-hoc analysis. *** $p<0.001$.

Cell viability was alternatively measured through SRB analyses 24 hour post-treatment with VP and Z-VAD-FMK (Figure 4.20A, B). Cell viability was seen to partially increase upon co-treatment with Z-VAD-FMK in the U87 cell line however remained unchanged in the U343 cells implying different cell death pathways could potentially be utilised in the different cell lines.

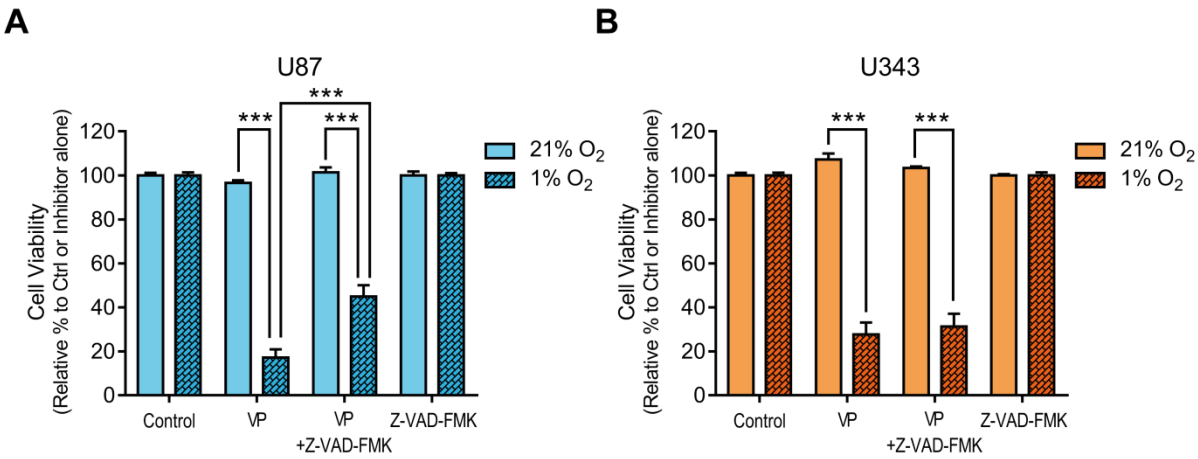

Figure 4.20 Z-VAD-FMK can partially rescue VP-induced death in U87 cells over 24 hours. U87 (A) and U343 (B) cells were treated with either vehicle (0.1% DMSO), 5 μM VP, 5 μM VP and 20 μM Z-VAD-FMK or 20 μM Z-VAD-FMK alone for 24 h in 21% and 1% O_2. Cell viability was significantly higher in U87 cells co-treated with VP and Z-VAD-FMK in hypoxia compared to VP alone. This rescue in viability was not seen in the U343 cells however suggesting that VP may affect different pathways in the different cell lines. Cell viability was measured via SRB and normalised to the control or Z-VAD-FMK alone for each oxygen tension. Experiments were conducted in technical triplicate/quadruplicate in 3 biological experiments. Data is presented as ± S.E.M. Significance is determined by two-way ANOVA, Tukey post-hoc analysis. *** $p<0.001$.

Immunocytochemistry analysis was further conducted to see whether Z-VAD-FMK could prevent the gross alterations seen in cell morphology upon VP treatment (Figure 4.21A, B). Unsurprisingly from the results obtained from the cell viability data, Z-VAD-FMK was unable to prevent the cell death and progressive relocalisation of YAP protein to the plasma membrane witnessed upon VP exposure.

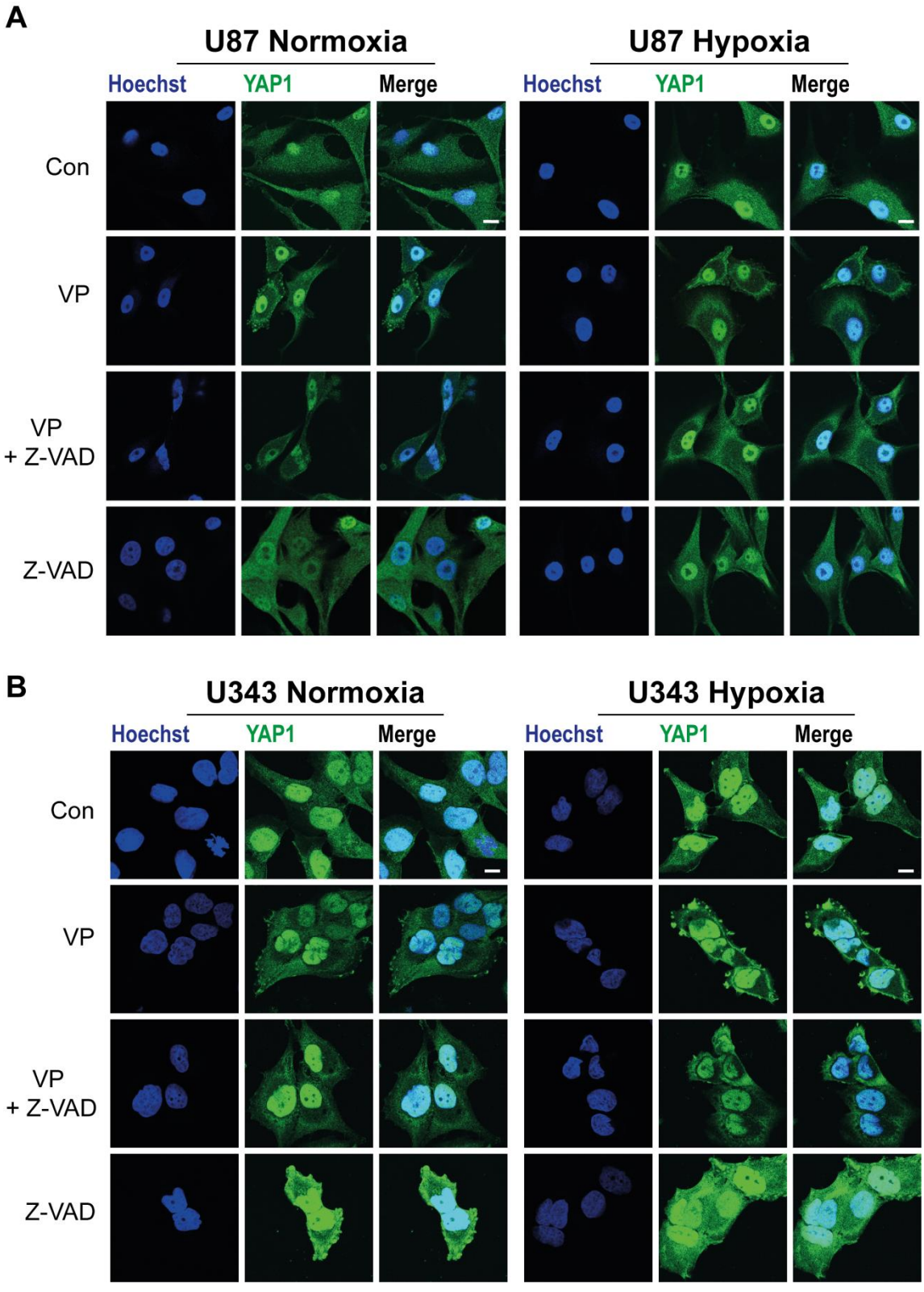
A
U87 Normoxia
U87 Hypoxia
Hoechst
YAP1
Merge
Hoechst
YAP1
Merge
Con
VP
VP
+ Z-VAD
Z-VAD
B
U343 Normoxia
U343 Hypoxia
Hoechst
YAP1
Merge
Hoechst
YAP1
Merge
Con
VP
VP
+ Z-VAD
Z-VAD

Figure 4.21 VP-induced changes in glioma cell morphology could not be prevented upon addition of Z-VAD-FMK. U87 (A) and U343 (B) cells were treated with either vehicle (0.1% DMSO; Con), 5 μM VP, 5 μM VP and 20 μM Z-VAD-FMK or 20 μM Z-VAD-FMK alone for 8 h in 21% and 1% O_2. It is clear that even upon addition of the caspase inhibitor, the cells were under significant stress and were dying following VP treatment again indicating that apoptosis was likely not the main mechanism of VP-induced cell death. Images are representative of 3 biological experiments. Scale bar represents 10 μm.

Since apoptosis was concluded to not be the main driver of VP-induced hypoxic cell death, additional cell death inhibitors inhibiting the activity of calpain and cathepsins (ALLN), calcium-mediated cell death occurring through opening of the mitochondrial permeability transition pore (mPTP; CsA) and also death domain receptor interacting protein kinase (RIPK)-dependent necrosis (Nec-1) were employed (Figure 4.22A, B). All of these inhibitors however were unable to prevent VP-induced hypoxic cell death although ALLN and CsA did induce a small sensitisation to VP under normoxic conditions (Figure 4.22C, D).

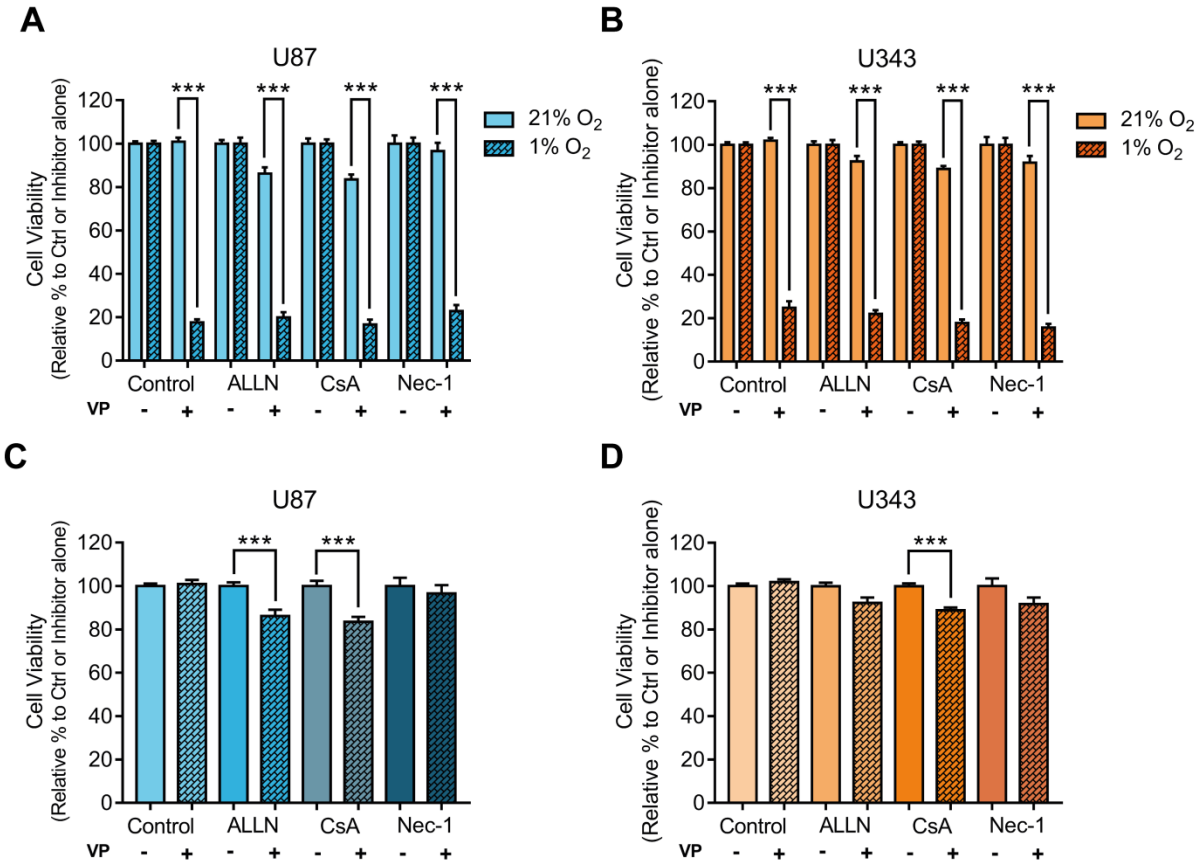

Figure 4.22 Hypoxic VP-induced cell death of glioma cells could not be prevented by alternative inhibitors of cell death. Cell viability of U87 (A) and U343 (B) cells was measured via SRB assay following 24 h treatment in 21% and 1% O_2 of either vehicle (0.1% DMSO) or 5 μM VP with and without the presence of alternative cell death inhibitors; 10 μM ALLN (Calpain/Cathepsin inhibitor), 15 μM CsA (mitochondrial cyclophillin D inhibitor) and 50 μM Nec-1 (inhibitor of RIP-kinase dependent necrosis. It is clear that VP-induced hypoxic cell death could not be prevented. Cell viability was normalised to either the control or the relevant untreated inhibitor for each oxygen tension. (C) and (D) Data normalised to the normoxic control for each inhibitor showed that ALLN in the U87 cells and CsA in both the U87 and U343s partially sensitised glioma cells to 5 μM VP treatment over 24h in 21% O_2. Experiments were conducted in technical quadruplicate in 5 (U87) and 6 (U343) biological experiments. Nec-1 data was conducted in 3 (U87) and 4 (U343) independent experiments. Data is presented as ± S.E.M. Significance is determined by two-way ANOVA, Tukey post-hoc analysis. *** $p<0.001$.

Next, cells were co-treated with VP and inhibitors against p53-mediated cell death (PFT-α) and autophagy (CQ) in order to elucidate the mechanism of cell death. Again, these inhibitors provided no protection against VP-induced hypoxic cell death in either of the glioma cell lines indicating that perhaps a non-traditional or regulated mechanism of cell death was being utilised (Figure 4.23A-D).

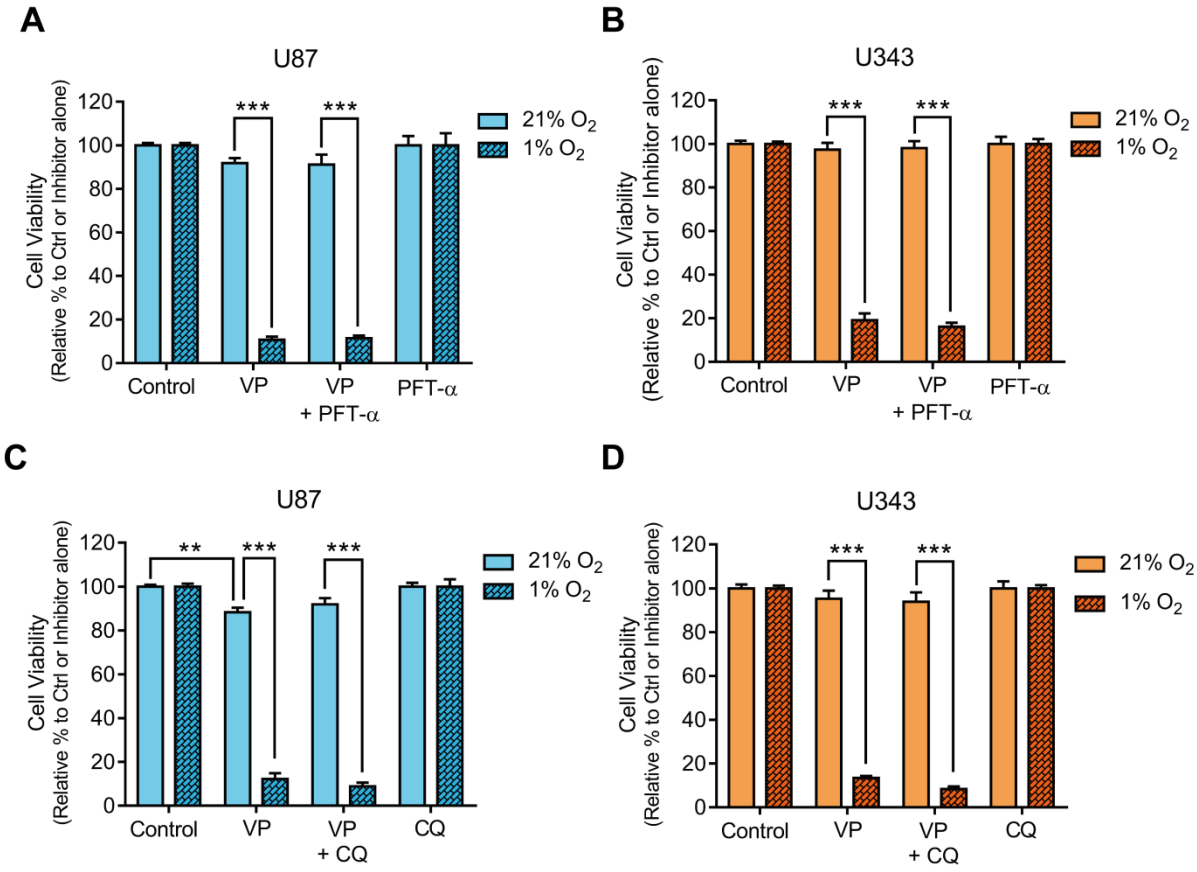

Figure 4.23 Inhibiting p53-mediated cell death and autophagy did not prevent VP-induced cell death in hypoxia. Cells were treated with p53/p73 inhibitor PFT-α (30 μM) alongside 5 μM VP for 24 h in both 21% and 1% O_2. SRB analysis shows that VP was still able to induce significant cell death in hypoxia in both U87 (A) and U343 (B) cells. Cells were also treated with autophagy inhibitor, CQ (10 μM) in combination with 5 μM VP for 24 h and was seen to not prevent hypoxic VP-induced cell death in either U87 (C) or U343 (D) cells. Data is normalised to the control or inhibitor alone for each oxygen tension. Experiments were conducted in technical triplicate in 3-4 independent experiments. Data is presented as ± S.E.M. Significance is determined by two-way ANOVA, Tukey post-hoc analysis. ** $p<0.01$, *** $p<0.001$.

4.2.10. Cellular vacuolisation is a prominent characteristic of VP-induced cell death

Cytoplasmic vacuolisation has recently become of interest in the mechanism of cell death, although has yet to be attributed to any one particular form. Evidence does suggest however that presence of the vacuoles could be associated with increased cellular stress from a range of stress inducers, affecting intracellular organelles such as

the ER[271,272]. It was noted that upon VP exposure, cytoplasmic vacuolisation was induced and was particularly amplified in both vacuole number and size under hypoxic conditions. These large vacuoles were apparent by both bright-field (Figure 4.24A) and confocal microscopy (Figure 4.24B) in both of the cell lines.

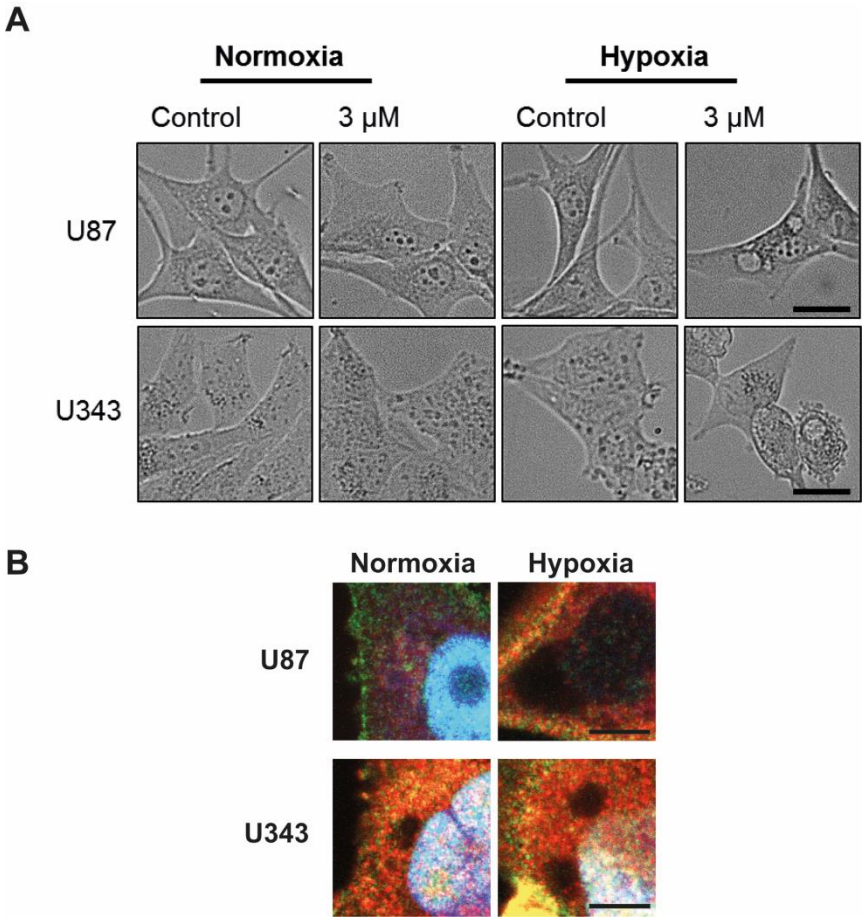

Figure 4.24 VP induces cytoplasmic vacuolisation. (A) Large vacuoles can be seen in cells treated with 3 μM VP for 24 h but only in 1% O_2. Images were taken at 20x objective. Scale bar represents 25 μm. (B) Cells imaged using confocal microscopy also show presence of cytoplasmic vacuoles upon 5 μM VP for 8 h. Vacuolisation is enhanced under hypoxic (1% O_2) conditions compared to normoxia (21% O_2). Scale bar represents 5 μm.

To further investigate whether VP was indeed increasing cellular stress, in particular ER stress, cells were stained with an ER stress marker CRT following 4 hour VP treatment (Figure 4.25A, B). Exposure to VP was seen to cause an increase in ER stress, which was exacerbated under hypoxic conditions due to the pronounced increase in CRT expression.

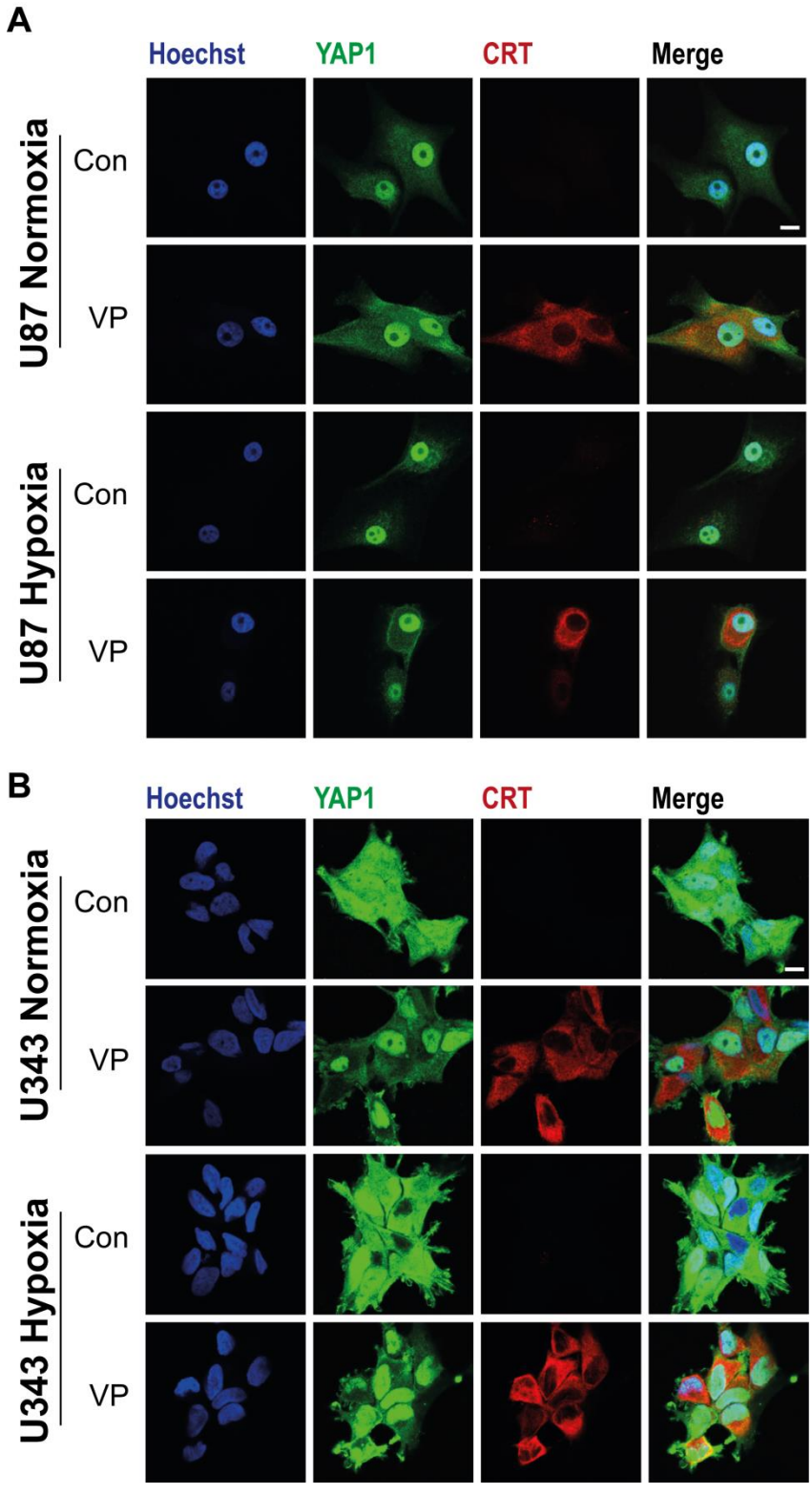

Figure 4.25 ER stress is significantly increased upon VP treatment and is enhanced in hypoxia. U87 (A) and U343 (B) cells were treated with 5 μM VP for 2 h in both 21% and 1% O_2 after which cells were fixed and stained with Hoechst, YAP1 and ER stress marker, CRT. CRT expression was seen to dramatically increase upon VP treatment compared to the control and was enhanced under hypoxic conditions. Images are representative of 3 biological experiments. Scale bar 10 μm.

Since this suggested that ER stress may play a role in VP-mediated cell death, cells were treated with an inhibitor of the ER-associated protein degradation pathway (ERAD), Eer1, to see whether this inhibition could rescue hypoxic cell viability post VP exposure. Immunocytochemistry showed that Eer1 unfortunately could not rescue cell death or vacuolisation of the cell in hypoxia (Figure 4.26A) although at a higher concentration, Eer1 was able to partially increase cell viability when co-incubated alongside VP (Figure 4.26B, C). This rescue in viability was again not complete, suggesting that there could still be other factors playing a role in VP-induced hypoxic cell death.

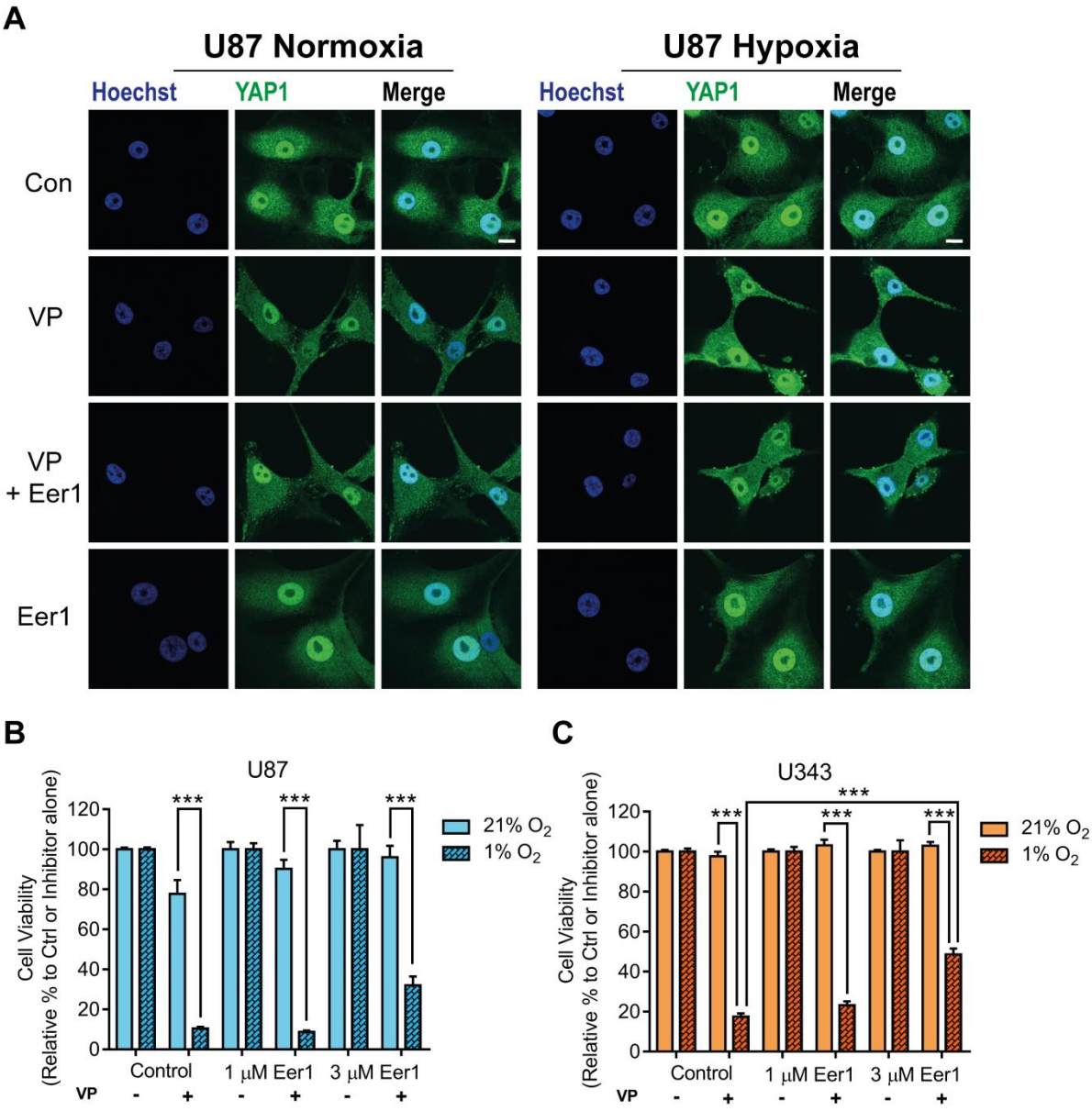

Figure 4.26 ERAD inhibitor Eer1 causes partial rescue of cell viability following VP treatment in hypoxia. (A) U87 cells were treated with 1 μM Eer1 alongside 5 μM VP for 4 h in both 21% and 1% O_2, after which cells were fixed and stained with Hoechst and YAP1 for confocal microscopy. Eer1 did not appear to inhibit the cells from dying in hypoxia compared to VP treated cells. Images are from 1 independent experiment. Cell viability of U87 (B) and U343 (C) cells was also measured via SRB analyses following co-treatment of 1 μM and 3 μM Eer1 with 5 μM VP for 24 h in both 21% and 1% O_2. Co-treatment with 3 μM Eer1 and VP caused a significant increase in cell viability in hypoxia in U343 cells and a small increase but non-significant in the U87 cells compared to VP-treated cells. Data is normalised to the control or inhibitor alone for each oxygen tension. Experiments were conducted in technical triplicate in 3-4 independent experiments. Data is presented as ± S.E.M. Significance is determined by two-way ANOVA, Tukey post-hoc analysis. *** $p<0.001$. Scale bar represents 10 μm.

4.2.11. Increased ROS production and DNA oxidation suggests VP significantly increases cellular oxidative stress

Cells are known to undergo oxidative stress when perturbations in the normal redox homeostasis are induced through the increased generation of ROS such as superoxide anions, hydrogen peroxide and the highly reactive hydroxyl radicals. These radicals can attack many biological molecules such as DNA, lipids and proteins, eventually leading to destruction of the cell and ultimately cell death. Since VP is a known photosensitiser and can generate ROS after photoactivation, the question was raised as to whether VP can exert the same mechanism and induce oxidative stress in the absence of light.

Cells were therefore treated with VP and the presence, or increase in 8-hydroxydeoxyguanosine (8-OHdG), a marker of ROS-induced DNA oxidation, was assessed. We observed that 8-OHdG staining was dramatically increased in both normoxia and hypoxia (Figure 4.27A, B), but that it was more pronounced under hypoxic conditions in U87 cells compared to normoxia. Conversely, ROS-induced damage as a result of VP treatment in the U343 cells was lower in hypoxia. Basal levels of DNA oxidation under 1% O_2 however was already higher in this cell line implying some differences between cell lines in the sensitivity to oxidative stress under hypoxic conditions. This is also highlighted by the differential sensitivity to the positive control, H_2O_2, with the U343 cells exhibiting a decreased sensitivity.

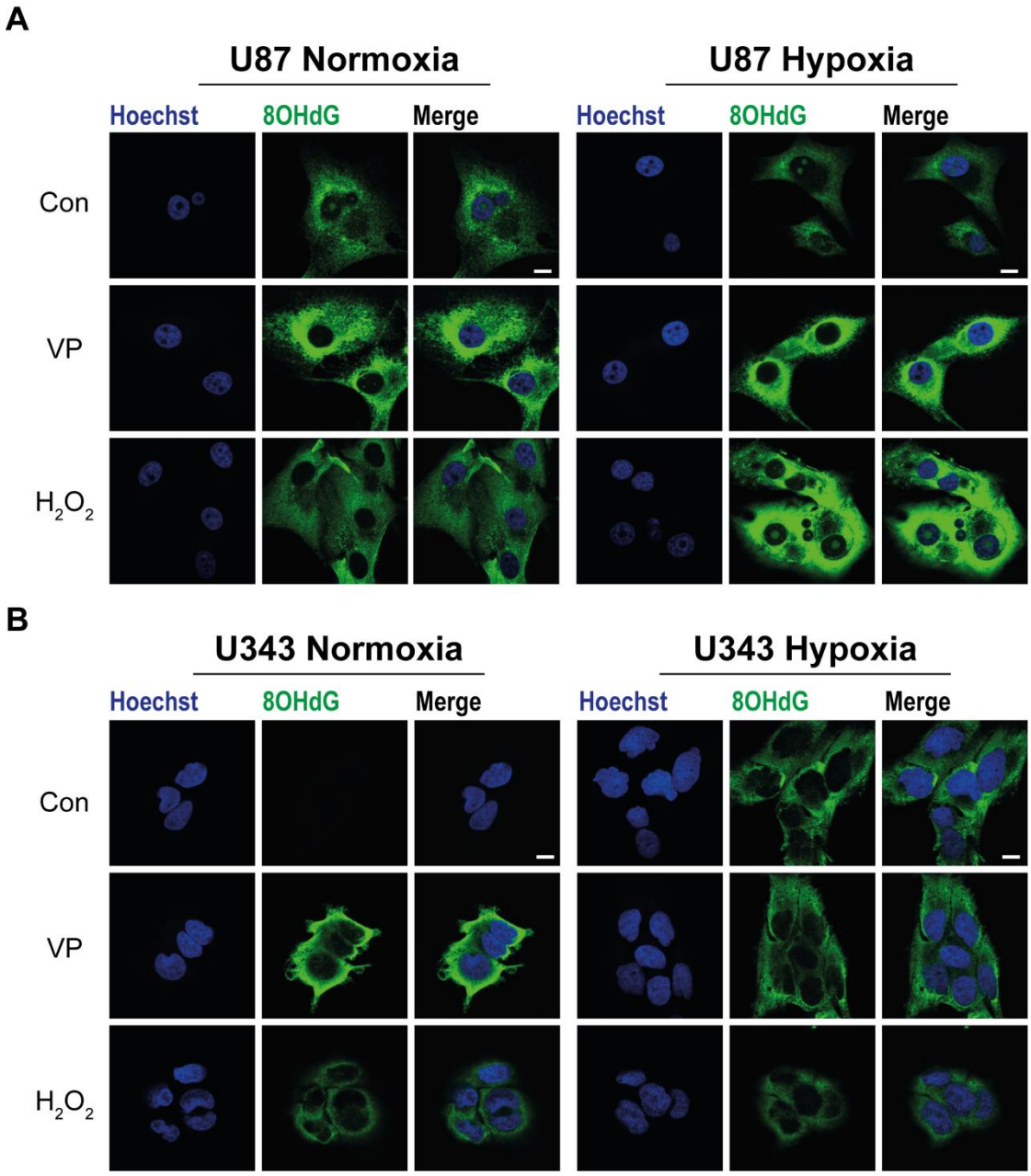

Figure 4.27 VP causes a significant increase in DNA oxidation. U87 (A) and U343 (B) were treated with 5 μM VP for 2 h in 21% and 1% O_2 after which cells were fixed and stained with DNA oxidation marker, 8-OHdG. DNA oxidation was seen to be markedly increased after VP treatment compared to control in both normoxic and hypoxic conditions. H_2O_2 (100 μM) was used as a positive control. Images are representative of 4 independent experiments. Scale bar 10 μm.

Production of ROS was measured using a DCFDA assay and was seen to be significantly increased upon VP exposure in the immortalised U87 and U343 cell lines as well as in the primary GBM cells, T1 and T2 (Figure 4.28A-D). Interestingly, when cells

were first pre-treated and then co-treated alongside VP with the free radical scavenger TEMPOL, this increase in ROS production could be reversed to levels lower than the control. H_2O_2 treatment, which was used as a positive control, confirmed that TEMPOL could indeed inhibit ROS production. Furthermore, it should be noted that in the T1 GBM cells, H_2O_2 did not generate a significant increase in ROS production suggesting that this therapy-resistant GBM line required a higher concentration of H_2O_2 to generate a response. ROS levels were also measured in the U343 cells under hypoxic conditions and again the same trend was observed with VP significantly increasing ROS production (Figure 4.28E). When levels were normalised to the normoxic control, it is clear that ROS levels were significantly elevated under hypoxia and were further exacerbated upon VP exposure (Figure 4.28F). Interestingly, treatment with related porphyrin PPIX did not increase ROS production in both normoxia and hypoxia when compared to the control (Figure 4.28G).

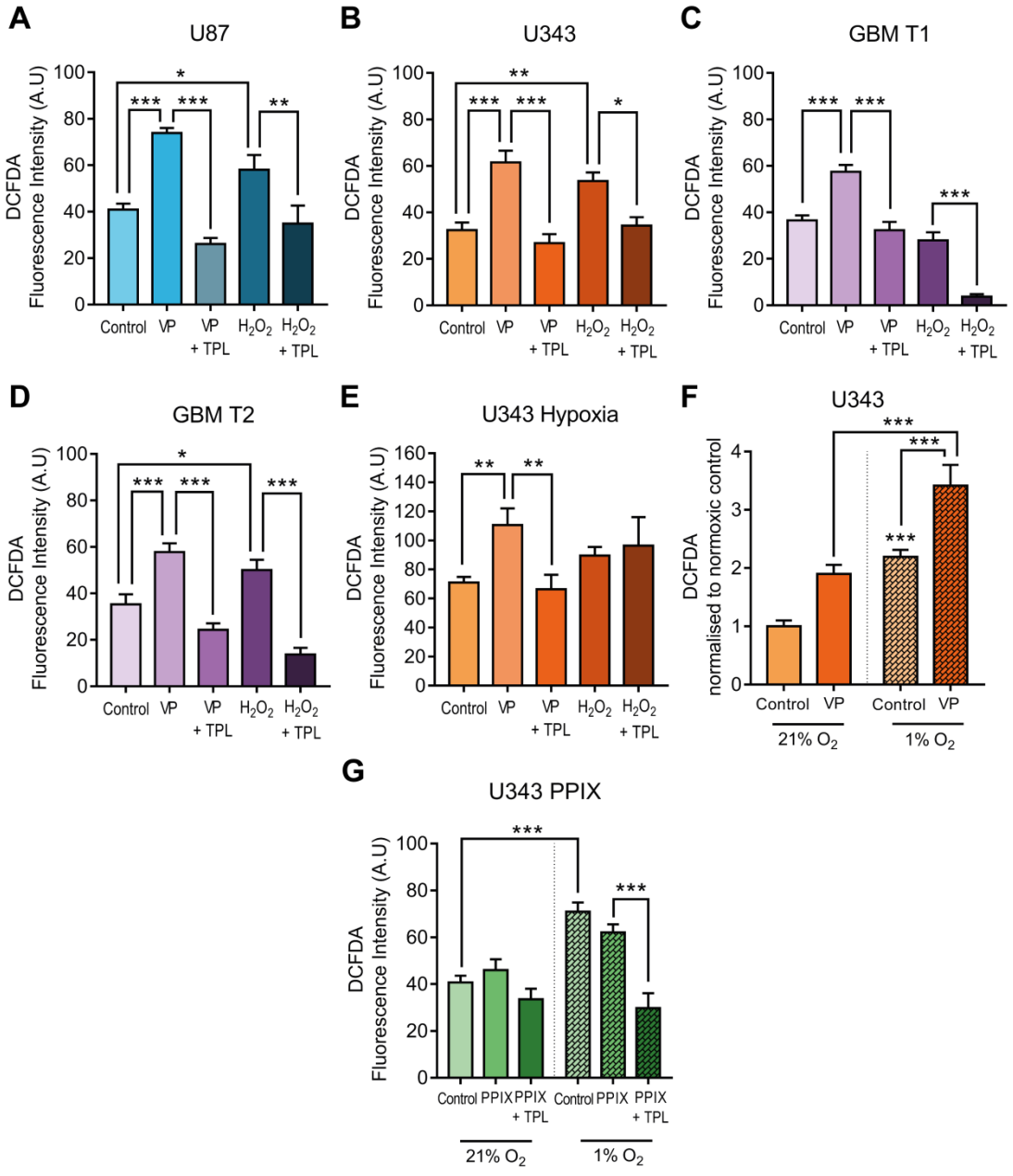

Figure 4.28 VP increases ROS which can be prevented upon treatment with TEMPOL. Cells were treated with 5 μM VP for 2 h in 21% O_2 followed by overlay of 2x DCFDA (20 μM final concentration) 45 min before treatment endpoint after which fluorescence was measured at 520 nm. DCFDA fluorescence was significantly increased upon VP treatment in U87 (A), U343 (B) and GBM lines T1 (C) and T2 (D). This increase could be prevented if cells were co-treated with 3 mM TEMPOL (TPL; 2 h pre-treatment). H_2O_2 (50 μM, 2 h) was used as a positive control for ROS production. (E) U343 cells were treated with VP in hypoxia for 2 h. ROS levels were also significantly increased following VP treatment, which could be reduced when co-treated with TEMPOL. (F) DCFDA fluorescence values from both U343 normoxia and hypoxia were normalised to the normoxic control and were increased in hypoxia, which is significantly increased upon the addition of VP. (G) PPIX however did not induce ROS production in normoxia or hypoxia. Experiments were conducted in technical quadruplicate in 3 independent experiments. Data is presented as ± S.E.M. Significance is determined by one-way ANOVA, Tukey post-hoc analysis. * p<0.05, ** p<0.01, *** p<0.001.

Cell viability following 24 hour VP treatment in the presence of anti-oxidant TEMPOL was also measured (Figure 4.29A, B). TEMPOL treatment was seen to significantly increase hypoxic cell viability after VP exposure, which was most pronounced in the U343 cells. Although the viability was improved, the VP-mediated hypoxic cell death could not be completely reversed in either cell line suggesting again that the mode of cell death induced by VP is multifactorial.

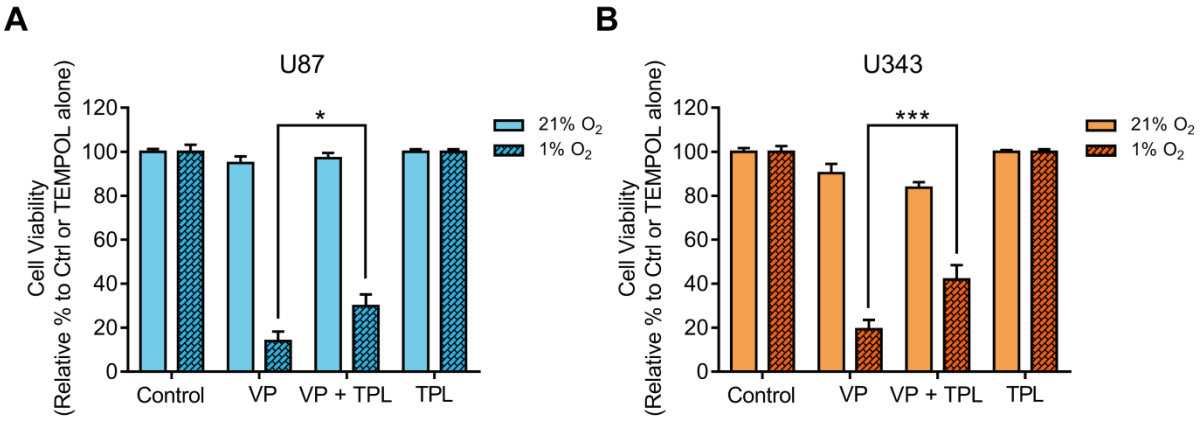

Figure 4.29 VP- induced cell death in hypoxia can be significantly reduced upon co-treatment with TEMPOL. Cell viability of U87 (A) and U343 (B) cells determined by SRB analyses following treatment with either vehicle (0.1% DMSO), 5 μM VP, 5 μM VP+ 3mM TEMPOL (TPL) or 3 mM TEMPOL alone for 24 h in both 21% and 1% O_2. Cell viability was significantly increased when cells were co-treated with TEMPOL. Experiments were conducted in technical quadruplicate in 3 independent experiments. Data is presented as ± S.E.M. Significance is determined by two-way ANOVA, Tukey post-hoc analysis. * $p<0.05$, *** $p<0.001$.

4.2.12. VP avidly binds ferric iron

Noting that VP is structurally similar to porphyrins, such as PPIX (Figure 4.4A), which are capable of metal complexation, the mode of action of VP was hypothesised to be through binding of free iron resulting in a Fenton-like mechanism to generate hydroxyl radicals that perturbed cellular redox homeostasis.

Firstly, the absorbance spectrum of VP was measured in the UV/visible spectrum after being diluted in either distilled H_2O or methanol. The absorbance spectrum was seen to be most prominent when diluted in methanol and so this was then chosen as the diluent for further experiments (Figure 4.30A). To keep the absorbance values in a suitable range of 0-1 (arbitrary units), the concentration of VP most appropriate for experiments was found to be 30 μM (Figure 4.30B).

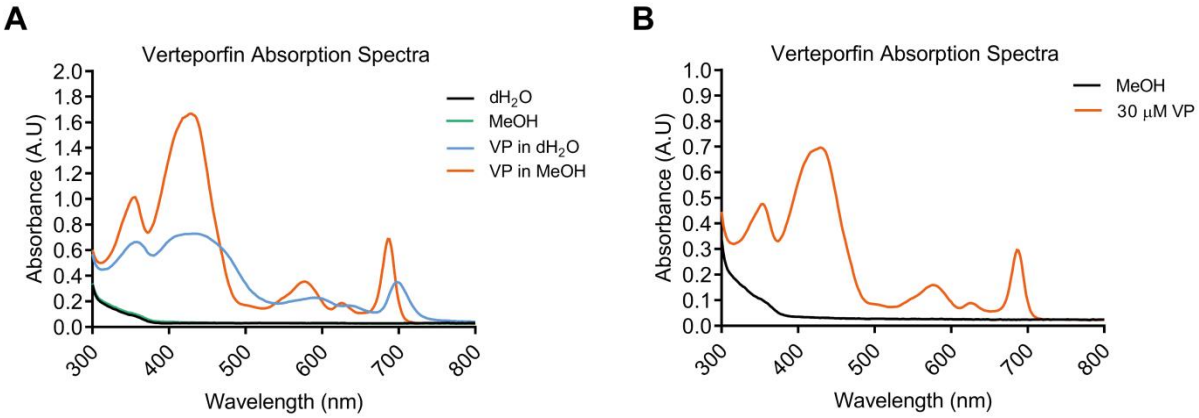

Figure 4.30 VP absorption spectra profile. (A) VP was diluted in either dH_2O or MeOH to a concentration of 75 μM and its absorption spectra measured in the UV/Vis range (300-800 nm). It is clear that using methanol as a diluent produces a cleaner absorption spectra for VP. (B) Absorption spectra of 30 μM VP in the UV/visible range diluted in MeOH.

Next, 30 μM VP was incubated in the presence or absence of ferric iron (Fe^{3+}; 3-500 μM) and the absorbance spectra measured immediately. Upon increasing concentrations of ferric iron, the absorbance spectra was seen to shift; evident by an increase absorption around 430 nm as well as shifts in the peaks around 600 and 700 nm indicating potential iron binding (Figure 4.31). As previously mentioned, VP is currently used clinically in the treatment of AMD as a photosensitiser during PDT. The PDT laser activation point of VP is around 685-690 nm and so closer inspection of the spectra around this activation point shows that addition of ferric iron caused a dramatic shift in the spectra (Figure 4.31B). Upon increasing ferric iron concentrations of 30 μM and above, the absorbance peak

shifts from 686 nm towards 670 nm, and is accompanied with a decrease in absorbance, strongly suggesting that VP is indeed binding iron resulting in a change of structure and hence alterations in absorbance profile.

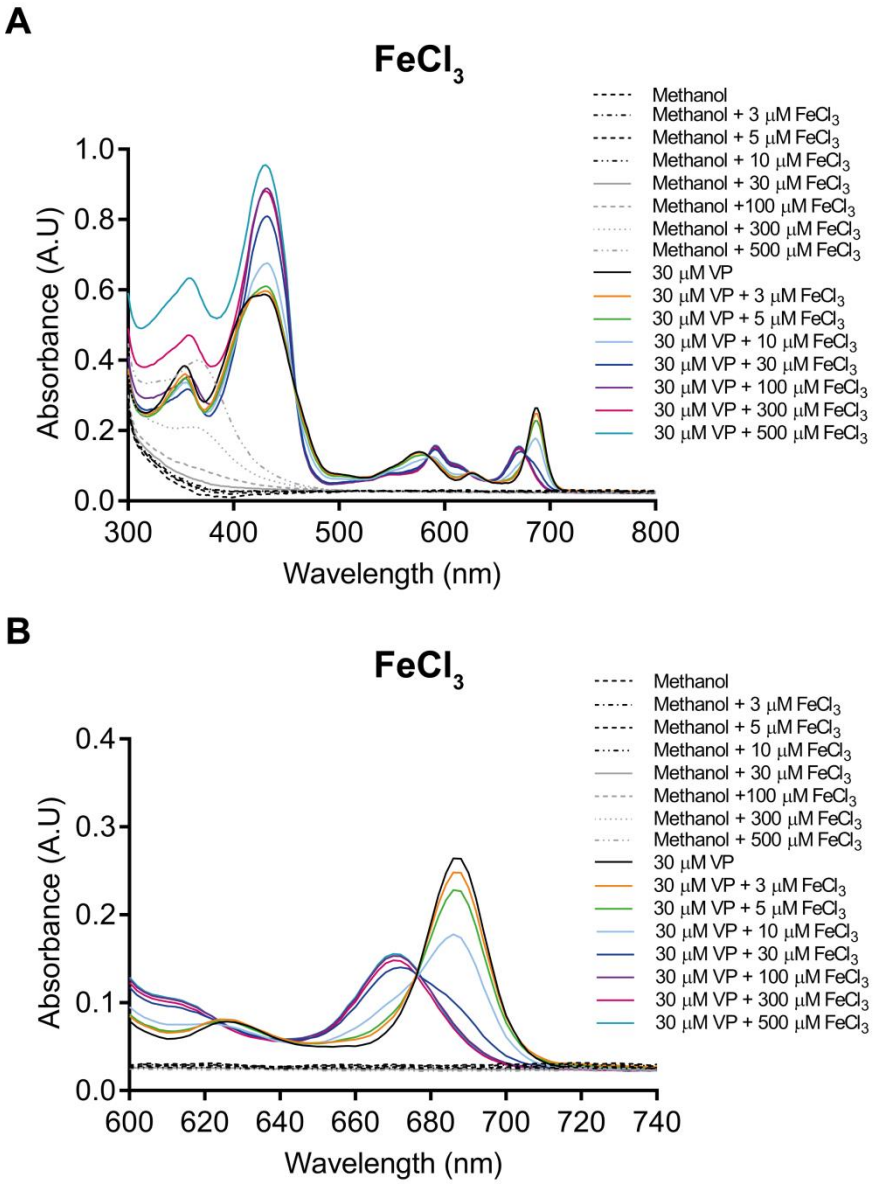

Figure 4.31 VP rapidly binds ferric chloride. (A) Increasing concentrations of ferric chloride ($FeCl_3/Fe^{3+}$; 3-500 μM) was added to 30 μM VP diluted in MeOH. Absorption spectra were then measured being 300-800 nm, 1 min following combination. There is a distinctive shift in VP absorption spectra as well as a dramatic increase in absorbance around 430 nm with increasing concentrations of iron indicating binding. (B) A closer look around the VP photodynamic therapy activation point at 686 nm shows a progressive shift towards 670 nm and a reduction in absorbance with increasing concentrations of ferric chloride. Graphs are representative of experiments conducted in biological triplicate.

Further investigations into whether the iron oxidation state was important for VP binding employed the same approach as above, but in the presence or absence of ferrous iron (Fe^{2+}; 3-500 μM). The absorbance profiles generated did not show the same alterations as was seen upon ferric iron addition (Figure 4.32) – while ferrous iron induced a slight increase in absorption around 430 nm, few differences were seen around the PDT activation peak (Figure 4.32B). Higher concentrations of ferrous iron appeared to cause a small shift in the spectra with a decrease in absorbance around 686 nm, although this was not enough to shift the spectra as significantly as observed with ferric ions.

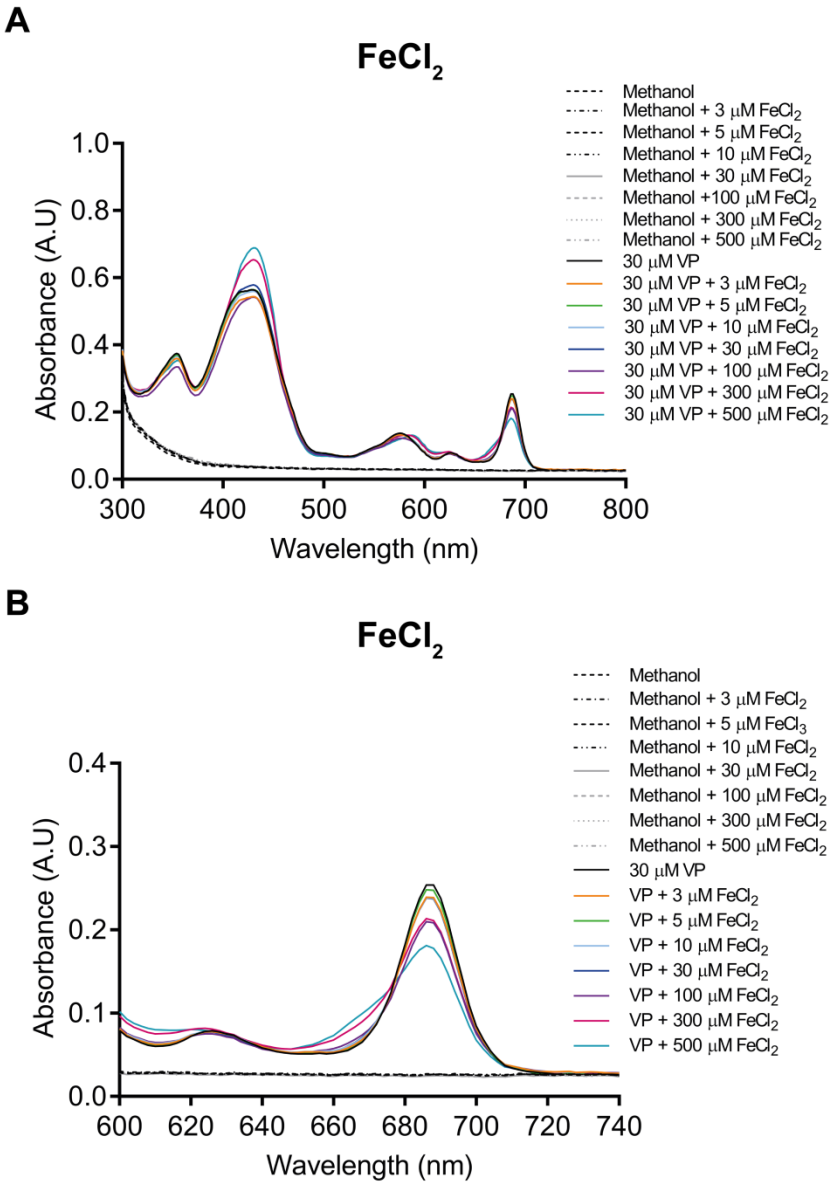

Figure 4.32 VP does not bind ferrous chloride as rapidly as ferric chloride. (A) Increasing concentrations of ferrous chloride ($FeCl_2/Fe^{2+}$; 3-500 μM) was added to 30 μM VP diluted in MeOH. Absorption spectra were then measured being 300-800 nm, 1 min following combination. A slight change in absorbance is seen around 430 and 686 nm however only at higher concentrations. (B) A closer look at the absorbance peak at 686 nm shows a lack of shift towards 670 nm which was apparent with $FeCl_3$. There is a slight change however but only with higher concentrations (300 and 500 μM). Graphs are representative of experiments conducted in biological triplicate.

Absorbance spectra profiles were also generated for the addition of other metal ions, zinc ($ZnCl_2$; Zn^{2+}) and magnesium ($MgCl_2$; Mg^{2+}), to VP. As with ferrous iron, these metal ions did not induce the significant alterations in the VP absorbance spectra (Figure

4.33A-D). Furthermore, spectral analysis of ferric iron and VP showed that binding was capable in both normoxic and hypoxic conditions (Figure 4.33E).

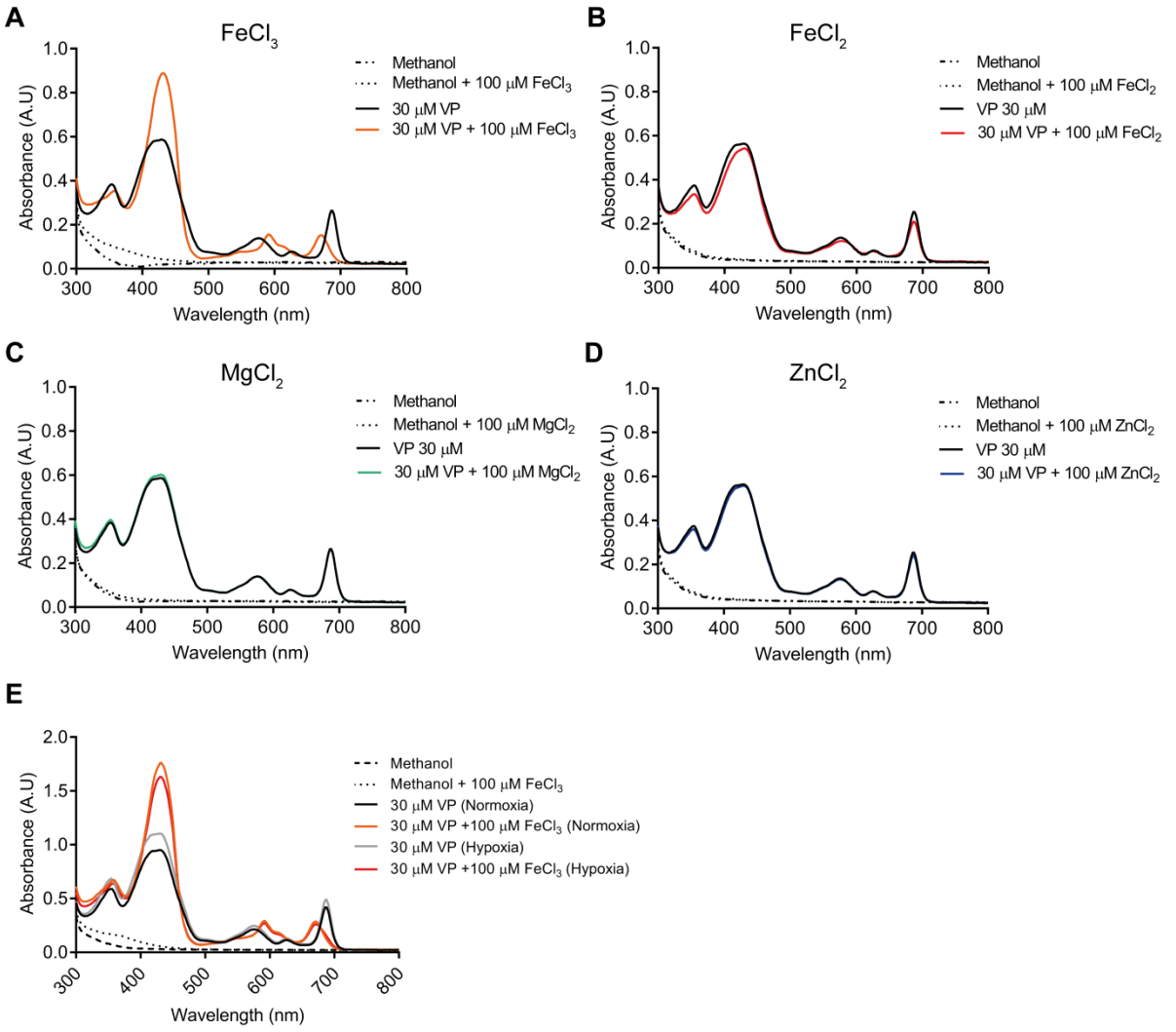

Figure 4.33 VP does not immediately bind metal chlorides, magnesium and zinc. Absorption was measured in the UV/Vis range 1 min after 30 µM VP was added to 100 µM ferric chloride ($FeCl_3$; A), ferrous chloride ($FeCl_2$; B), magnesium chloride ($MgCl_2$; C) and zinc chloride ($ZnCl_2$; D). Only addition of ferric chloride was able to alter the absorption spectra of VP. (E) Binding of $FeCl_3$ was similar in hypoxia to that of normoxia. Graphs are representative of experiments conducted in biological triplicate.

It was still possible however that other ions would bind over a longer time period. To investigate this, first-order binding kinetics curves were generated from calculating the ratio in absorbance at 670 and 686 nm, demonstrative of the largest spectral shift (Figure

4.34A-C). VP was added to a range of concentrations of $FeCl_3$, $FeCl_2$, $ZnCl_2$ and $MgCl_2$ and absorbance values were taken immediately and after 8 and 24 hours. Corroborating previous data, ferric iron showed immediate complexation to VP. Additionally, both ferrous iron and zinc also showed complexation to VP, albeit over a slower timescale, with no apparent immediate spectral alterations however significant changes observed after 8 and 24 hours. On the contrary, magnesium did not induce any spectral changes even after 24 hour incubation, indicating no VP complex formation.

These observations were then validated by MS, which again shows VP able to complex with ferric iron, ferrous iron and zinc but not magnesium (Figure 4.34D). These data also indicate 1:1 binding stoichiometry for the three complexes, with two pyrrole units deprotonated in each case which is consistent with the macrocycle acting as a tetradentate chelating ligand (as interpreted from raw spectra in Appendix 2). Together these data suggest VP can bind free iron, potentially leading to increased oxidative stress.

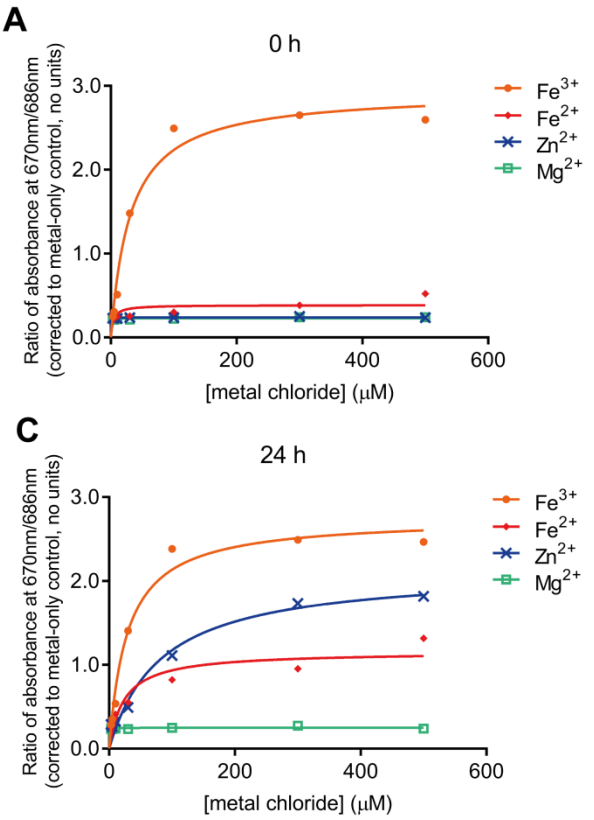

D

Metal Ion	Predicted Formula	Calculated *m/z*	Observed *m/z*
Fe^{2+}	$C_{41}H_{40}FeN_4O_8$	772.22	772.02
Fe^{3+}	$C_{41}H_{40}FeN_4O_8$	772.22	772.02
Mg^{2+}	$C_{41}H_{40}MgN_4O_8$	740.27	No Peak Detected
Zn^{2+}	$C_{41}H_{40}ZnN_4O_8$	780.21	780.02

Figure 4.34 VP can bind ferrous and zinc chloride but only over time. Increasing concentrations of ferric, ferrous, magnesium and zinc chloride (3-500 μM) were added to VP (30 μM) diluted in methanol. VP absorption spectra was then measured 1 min (A), 8 (B) and 24 h (C) following combination. First order binding kinetic graphs were then generated by calculating the ratio of absorbance at 670/686 nm. It is clear that VP can immediately and avidly bind ferric chloride. VP can also bind ferrous and zinc chloride but only after 8 h which was increased after 24 h. VP did not bind magnesium chloride at all as there is no change across all time points. (D) Mass spectrometry was conducted in collaboration with Prof. J. Tucker's research group in the School of Chemistry, UoB. Data showed that VP bound Fe^{3+}, Fe^{2+} and Zn^{2+} but not Mg^{2+}, supporting the spectrophotometry data. *m/z* denotes mass to charge ratio.

4.3. Discussion

Despite some small improvements in patient survival over the past two decades, gliomas remain incurable. The standard treatment for these patients has remained the same regardless of tumour mutational status, heterogeneity or therapy-resistance. Current treatments do not or are unable to take into account some of the most significant aspects of glioma biology such as widespread hypoxia, which is a major determinant for treatment failure. Identifying therapies that address the tumour microenvironment could be a way of universally targeting the tumour as a whole rather than designing individual treatments around the stratification of patients based on mutational status.

As previously reported, the transcriptional co-activator YAP may play an important role in hypoxic biology. Results presented in chapter three, demonstrate hypoxia to be an upstream regulator of YAP in glioma, increasing its gene expression as well as downstream activity. Abnormal YAP activation has been linked to tumorigenesis in many cancers, inducing chemoresistance and promoting tumour invasion, migration and progression. Therefore, investigations were conducted into whether the YAP inhibitor, VP could be repurposed as a novel treatment for suppressing glioma growth and progression.

4.3.1. VP suppresses glioma cell proliferation

VP has been previously reported to supress YAP oncogenic ability through interference of the YAP-TEAD interaction thereby downregulating transcription of proliferative target genes such as *CTGF*, *CYR61* and *axl*, causing suppression of cell proliferation[153,158]. In corroboration with previous investigations in other cancer types, initial experiments showed VP to inhibit glioma cell growth in a dose-dependent manner (Figure 4.2)[158-160].

These results are also in agreement with a recent study by Al-Moujahed *et al*., who showed VP to selectively inhibit growth of LN-229 and SNB-19 glioma cell lines through downregulation of YAP-TEAD target genes under normoxic conditions[161]. This paper also suggests VP to reduce cell viability, measured through a MTT assay, when cells were treated with increasing concentrations of VP (2 and 10 µg/ml) over 3 and 6 days. However, it is not made clear whether this reduction in viability is a result of cell death or a result of suppression of proliferation since this assay cannot easily distinguish between the two. In this present study, images were taken of VP treated cells after 72 and 96 hours, clearly showing that under these conditions, glioma cells remain viable following VP exposure, and that a reduction in cell number (analysed through SRB assay which measures cell protein content) is a result of a reduced proliferation rate (Figure 4.1C and 4.2C).

4.3.2. VP induces cell death under hypoxic conditions

Hypoxia, as previously described, has been shown to enhance YAP's role as a transcriptional coactivator and thus has been closely linked to increased proliferation and survival of malignant cells. Since YAP inhibitor VP demonstrated significantly reduced cell proliferation capacity under normoxic conditions, the question was raised as to whether VP could induce enhanced growth suppression under conditions that mimicked the hypoxic glioma microenvironment. This study provides evidence for the first time, that VP can selectively kill hypoxic glioma cells – which was confirmed through cell imaging – rather than suppressing hypoxic cell proliferation (Figure 4.3). Despite previous research demonstrating VP to induce a reduction in cell viability under normoxic conditions in other cancers, normoxic glioma cells in this study remained viable at a VP concentration which could induce death under hypoxic conditions. These results suggest however that

this discrepancy may well lie in the careful exclusion of light from experiments, which increases normoxic cell death.

Adherent monolayer cell culture has undoubtedly been invaluable in the process of drug discovery and elucidation of both physiological and pathophysiological cellular mechanisms. However, it has come under some scrutiny as to whether these 2D cultures can accurately represent the complexity of *in vivo* biology. Culturing cells in 3D as cellular aggregates, commonly known as spheroids, provides a more biologically relevant model as it allows spatial and temporal organisation of cell growth as well as generation of a nutrient, metabolite and oxygen gradient across the spheroid which is reminiscent of *in vivo* tumours[273].

U87 and U343 cells were subsequently grown as spheroids to assess the relationship of VP and cell proliferation and death in a more physiologically relevant model. VP treatment significantly attenuated spheroid size and growth in a dose-dependent manner if cells were exposed during spheroid formation (Figure 4.6). Furthermore, VP exposure destabilised the integrity of the surface layer of fully formed spheroids, leading to detachment of cells and spheroid destabilisation. Proliferating cells are known to preferentially locate on the outermost layers of spheroids and therefore are easily accessible for VP to potentially suppress YAP activity and lead to decreased growth[274]. These observations are supported by Fisher *et al*., who showed that VP was capable of suppressing formation of melanoma spheroids and through prolonged treatment, caused complete spheroid destruction, which was associated with a downregulation in YAP/TAZ expression[164].

In addition to VP, the structurally-related porphyrin PPIX was also previously shown to disrupt the physical interaction between YAP and TEAD[153]. In this investigation, glioma cells were treated with PPIX and an additional derivative ZnPP, to uncover whether it was a characteristic of porphyrins in general that could elicit this hypoxia-selective cell killing (Figure 4.4). Surprisingly, VP was the only porphyrin member to induce glioma cell death, which was corroborated in the melanoma cell line, A375. This selectivity could be a result of VP displaying a stronger inhibitory phenotype since PPIX has been previously reported to exhibit weaker inhibitory properties compared to VP[153]. In support of this, Wang *et al*., also reported that VP treatment of endometrial cancer cell lines induced a dose and time-dependent decrease in YAP protein expression that upon PPIX treatment remained unchanged[275]. Additionally, although a structural derivative of PPIX, VP has distinctive structural modifications such as the addition of a propionic acid methyl ester and a cyclohexadiene ring bearing two methanoic acid methyl esters[264] (Figure 4.35). Due to the difference in ability of inducing cell death between the compounds, a number of chemical analogs of VP could be therefore generated to identify what specific structural properties are required for hypoxic cell killing.

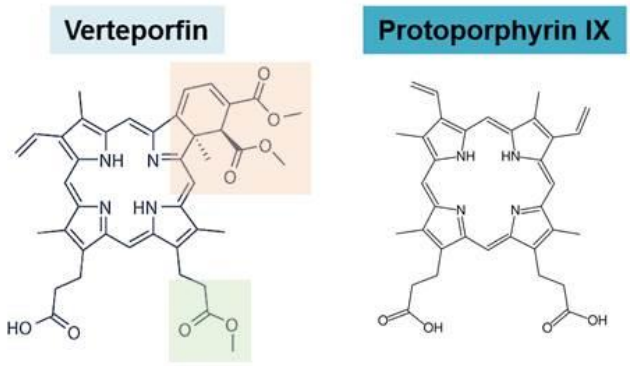

Figure 4.35 Chemical additions to VP.. Structurally derived from PPIX, VP has two main chemical modifications – addition of a cyclohexadiene ring bearing two methanoic acid methyl esters (orange) and a propionic acid methyl ester (green).

Novel GBM cell lines derived from a patient biopsy were generated in order to test whether VP sensitivity could be observed in a cell system more closely linked to 'real' tumours. After treatment with VP *in vitro*, it was observed that both T1 and T2 GBM lines were sensitive to VP in hypoxia (Figure 4.4). This is a key result, as the area of the original tumour from which the T1 cell line was derived had been resistant to conventional therapy (TMZ + fractionated 54 Gy radiation), while T2 cells had demonstrated therapy responsiveness. The results presented in this chapter therefore suggest that VP-mediated cell killing is independent of normal resistance mechanisms observed in GBM, and may reduce the rate of relapse and progression. Previous research has shown that YAP-inhibition through VP (in normoxia) can re-sensitise resistant cells to drugs such as cisplatin, erlotinib and paclitaxel as well as improving effectiveness of radiation treatments[162,163]. VP therefore has the potential to not only be employed as a mono-therapy in the selective killing of hypoxic cells in cancer but could be introduced as part of a combination therapy to enhance treatment sensitivity in therapy-resistant tumours. Unfortunately, at least 50% of TMZ-treated patients exhibit resistance so future experiments should investigate whether there is a synergistic

relationship between VP and TMZ and whether this provides any improvement in TMZ-resistant patient survival[276].

4.3.3. VP induces rapid changes in cell morphology and is sensitive to ambient light

We also investigated whether VP could be used at a more clinically relevant treatment period, showing that hypoxic-induced cell death was a rapid process that was initiated within the first hour of exposure (Figure 4.8). These observations were also supported by cell viability assays showing that 4 hour VP exposure followed by removal of the drug for the remaining 20 hours was adequate to induce significant cell death under hypoxic conditions (Figure 4.11A, B). This data additionally supports evidence by Zhang *et al.,* showing that washout of VP following treatment did not restore cell proliferation in colon cancer cells[165]. Normoxic sensitivity was also apparent in this study if cells were exposed to ambient light during the media replacement following 4 hour treatment, showing that photo-activation of VP can also increase the sensitivity of glioma cells to cell death under normoxic conditions (Figure 4.11C, D).

Hypoxic induction of nuclear YAP expression was apparent after 4 hours hypoxia (Figure 4.9A, B); again supporting evidence presented in chapter three showing hypoxic upregulation of YAP in glioma cells. However, U343 cells failed to recapitulate this observation following 8 hours hypoxia suggesting that despite increased gene expression (Figure 3.2), these cells have differential protein expression. This is also supported by the minimal increase in YAP1 protein expression observed following 8 hours hypoxia (Figure 3.6), possibly due to an increased basal level of YAP1. VP attenuated YAP1 nuclear expression and localisation (immunofluorescence) in this study,

which was enhanced under hypoxic conditions, suggesting VP not only as an inhibitor of YAP activity but also of its expression. This observation is supported by previous research showing VP to dramatically reduce YAP protein expression[164,275] as well as its downstream targets CTGF, CYR61, axl, survivin and OCT4[158,161]. Although ICC showed a reduction in YAP1 nuclear fluorescence in this study, analysis of protein expression by western blot provides contradictory evidence as YAP1 and CTGF expression remained unchanged upon 4-48 hour VP exposure (Figure 4.10). The disparity in results could be due to protein being extracted from the whole cell for western blotting compared to selective analysis of just nuclear fluorescence in ICC. This would therefore suggest that global YAP expression may not alter within that time period however YAP could undergo relocation from the nucleus upon VP exposure. Cellular fractionation techniques could therefore be employed to determine YAP expression in the different subcellular fractions upon VP treatment to see if this supports the ICC data. Furthermore, VP concentrations used in the literature can range from 3 μM for 24 hours to 1 μM for 6 days, with some studies even using concentrations of 20 and 40 μM[162,164,277]. Therefore, alterations in YAP expression appear to be cell line specific and also dependent on dose and treatment time and so for VP to influence YAP expression in these glioma cells, a higher concentration or longer exposure time could be required. Conversely, due to the rapid induction of hypoxic cytotoxicity and unchanged YAP activity with this concentration of VP (5 μM), it is likely that VP is acting either in a YAP-independent fashion or independent of YAP-TEAD suppression to induce cell death. It should be noted however that the peak concentration of VP found in AMD patient plasma after a 10 minute infusion of 6-12 mg/m^2 body surface area is approximately between 2-5 μM and so within the range predominately used in this investigation[278].

4.3.4. Expression of YAP-binding partner p73 is increased upon VP exposure but does not lead to increased YAP-p73 interaction

p73, identified to be a structural and functional homolog of p53, is involved in tumour suppression and through direct association with YAP can enhance co-activation and transcription of target genes such as *BBC3* to induce apoptosis[143,279]. As it has been previously discussed, YAP is known to exhibit differential selectivity in transcription factor binding partner dependent on cellular and microenvironmental context. Since VP has been described to suppress the pro-proliferative YAP-TEAD interaction, the question was asked whether this interference could encourage YAP to switch its binding partner to favour p73, therefore inducing cell death. Results showed VP to dramatically increase p73 expression upon exposure, which was enhanced under hypoxic conditions (Figure 4.12). Increased p73 expression however does not correlate to increased activity and consequently YAP1 did not appear to interact with p73 in co-immunoprecipitation analysis (Figure 4.13). As previously discussed, this investigation showed VP to reduce YAP1 nuclear fluorescence but not total YAP1 protein implying potential protein relocalisation. Previous research has shown that 14-3-3 binding proteins are significantly upregulated following VP treatment, consequently sequestering YAP in the cytoplasm[275]. Cellular localisation is critically important for p73 and YAP as sequestered cytoplasmic YAP is inactive as it can no longer co-activate gene transcription in the nucleus. Intriguingly, VP induced a widespread cytoplasmic expression of p73 which is contradictory for it to function as a nuclear co-activator in the induction of apoptosis. Cytoplasmic localisation of p73 has however previously been observed although its importance remains to be elucidated[280,281]. Nuclear exclusion of p73 could be a potential negative regulatory mechanism to limit its transcriptional activity since its nuclear import and export has previously been shown to be tightly controlled [282]. However, cytoplasmic

localisation could enable a novel function for this protein, as it has been proposed that p73 may have a cytoplasmic function which can occur independently to its transcriptional regulation of apoptosis. The WW-domain-containing oxidoreductase (Wwox) protein has been identified as a tumour suppressor and has been shown to potently sequester and co-localise with p73 in the cytoplasm[283]. This resulting interaction competitively inhibits co-activation of p73 by YAP as YAP and Wwox compete for binding to the proline-rich PPxY motif of p73[279,284,285]. Subsequent sequestration and binding of cytoplasmic p73 has shown to markedly enhance the pro-apoptotic function of Wwox, enabling a pro-apoptotic function of p73 which is independent of its transcriptional activity[283,284,286]. Due to the dramatic VP-induced p73 expression and decreased nuclear localisation of YAP1 in this study, this cytoplasmic function of p73 could be of importance in VP-induced cell death. To investigate whether VP-mediated cell death could be suppressed through reduction in p73 expression, siRNA targeting p73 was used however successful knockdown could not be achieved (data not shown). Further investigations into the relationship between YAP, p73 and Wwox upon VP treatment are therefore imperative. Furthermore, the distinct splice variants of p73, TA-p73 and ΔN-p73, have also been proposed as a regulatory mechanism, allowing p73 to exhibit both pro- and anti-apoptotic activity respectively[287,288]. Therefore, a closer look is required as to whether VP can influence which p73 isoform is expressed and whether this significant VP-induced increase in p73 expression is directly associated with the VP-induced cell death observed in these glioma cells.

4.3.5. VP-induced hypoxic cell death is YAP-independent

The data in this study suggest that VP can induce cell death very rapidly in glioma cells – within 1 hour of exposure. These results therefore raised the question as to whether it

was possible for YAP to orchestrate this process, given that changes in YAP-mediated gene expression would be expected to act over a longer period. To investigate this, YAP, its paralog TAZ, and both proteins were silenced in glioma cells before exposure to VP (Figure 4.14). Despite significant knockdown of these proteins, VP was still able to induce hypoxic cell death indicating, along with the unchanged YAP target gene expression levels, that this process was YAP-independent. A question was raised however that potentially other YAP isoforms, such as YAP1-2, could still be present and inhibited upon VP treatment however the YAP1 siRNA used specifically targets the YAP1 gene and was therefore, based on the siRNA target sequences (Appendix 1), expected to silence all nine YAP1 protein coding isoforms.

Despite numerous studies highlighting VP to inhibit YAP oncogenic activity through YAP-TEAD suppression, it has emerged in recent years that VP also exhibits significant 'off-target' effects. Research conducted by both Zhang *et al*., and Konstantinou *et al*., have shown VP to induce proteotoxicity through formation of high-molecular weight protein oligomers, such as that of p62 protein, which cannot be successfully cleared through proteasomal and autophagic pathways, thereby resulting in cellular toxicity[165,289]. The function of p62 ensures proper turnover of potentially harmful proteins by targeting these toxic aggregates for autophagy, consequently promoting cell survival[268]. However, abnormal aggregation and increased sequestration of p62 and other cross-linked proteins leads to proteotoxicity-induced apoptosis. VP has been previously identified to significantly increase p62 aggregation in colorectal cancer lines and tumours, with p62 becoming increasing localised to the perinuclear region of the cell[165]. Expression of p62 was therefore investigated in this study, but was observed to decrease as opposed to

increase upon VP treatment suggesting that this mechanism might not be relevant in glioma (Figure 4.15).

Originally proposed as a light-independent effect of VP, Konstantinou *et al*., have suggested that VP does indeed need to be light activated to induce these high-molecular weight protein complexes, and that although most studies involving VP are conducted in the dark, often post-treatment processes such as cell lysis and western blotting are conducted in the light. The authors show that this ambient light exposure post-lysis is sufficient to activate VP, inducing its photochemical properties and formation of these protein oligomers through increased cross-linking as a result of increased free radical generation[289]. It should be noted that in this study, cells were shielded from ambient light during treatment although when harvested for western blotting, cells were lysed and run in the light. That being the case, VP was unable to induce changes in protein expression of YAP or its downstream targets suggesting that in this investigation, VP exhibited YAP-independent effects despite potential post-lysis light-activation of VP. It should be noted that more consideration should be taken when reporting light-dependent and independent effects of VP, with studies being more explicit in stating the light conditions of experiments; something which is not currently done. Additionally, when studying light-independent effects, samples should not only be shielded from light during the treatment period but during all downstream processing.

4.3.6. VP-mediated hypoxic cell death is HIF-1α independent

This study has demonstrated that VP can selectively induce cell death under hypoxic but not normoxic conditions. These results therefore raised the question as to what hypoxia-responsive mechanism was responsible for influencing this selective sensitivity. Hypoxia

results in numerous alterations in cell phenotype some of which are mediated through hypoxia-induced activity of the HIF-1 transcription factor, often entitled the master regulator of hypoxia[135,290]. Other phenotypic changes however can be directly triggered through the reduced oxygen availability such as disturbances in mitochondrial activity and increased generation of ROS. Results from chapter three support the few investigations which show hypoxia-mediated upregulation of YAP expression and activity through increased nuclear localisation, thereby promoting tumour survival[131,134,135,229]. Previous attempts to elucidate this relationship uncovered the presence of a nuclear YAP-HIF-1α or TAZ-HIF-1α complex that stimulated TEAD transcriptional activity and whose activity was enhanced under hypoxic conditions[134]. VP has been recently identified to inhibit formation of this YAP-HIF-1α complex, independent of TEAD activity[277]. HIF-1-dependent effects on VP-induced cell death were therefore investigated via pharmacological stabilisation of HIF-1α in normoxia as well as over-expression of a HIF-1α mutant resistant to normoxic degradation[213] (Figure 4.16). Induction of HIF-1α partially sensitised cells to VP, although the effect did not approach the level observed under 1% O_2. Since it had also been shown that VP was capable of inducing cell death independent of YAP function, it could explain why only partial sensitivity was seen with HIF-1α stabilisation in normoxic conditions as there are other participating hypoxia-responsive mechanisms independent of the putative YAP-HIF-1α relationship. Knockdown of HIF-1α confirmed that the VP-induced cell death observed in this study appears to be YAP- and HIF-1-independent, as VP was still able to induce cell death in hypoxia even in the absence of HIF-1α (Figure 4.17). Although HIF-1α stabilisation was capable of partially sensitising cells to VP-cell death in this study, the greatest effect was observed with DMOG treatment suggesting that DMOG could potentially exhibit other off-target effects, contributing to cell death. This partial sensitivity also suggests that there

are clearly additional mechanisms which have a greater precedence in VP-induced cell death and are exacerbated under low oxygen conditions.

4.3.7. Traditional cell death inhibitors only partially prevent VP-mediated hypoxic cell death

To further elucidate the mode of VP-induced hypoxic cell death in glioma cells, a number of pharmacological inhibitors of cell death were employed. Previous papers have suggested in various cancer models that VP induces cell death through apoptosis both *in vivo* and *in vitro,* although it is unclear whether this induction is light-dependent or independent[159,166,291]. Glioma cell lines were therefore treated with VP in the presence and absence of a cell-permeable pan-caspase inhibitor, Z-VAD-FMK. Despite previous research demonstrating that VP induces apoptosis, it was found here to not be the predominant mode of cell death, assessed through incapability of Z-VAD-FMK in preventing VP-induced cell death (Figure 4.18-4.21). Although a small rescue in cell viability was observed in the U87 cells upon Z-VAD-FMK addition, Annexin V-PI cell viability assays demonstrated cells to have minimal Annexin V staining but increased PI uptake, which is indicative of a disrupted plasma membrane therefore suggesting an alternative form of cell death, such as necrosis[292,293]. Since apoptosis can be executed as rapidly as 4 hours, a shorter VP-treatment time was investigated in case the cells exhibited early-apoptotic mechanisms before necrosis. However, even at these timepoints, increased uptake of PI was still predominant over Annexin V staining. This was also corroborated by the fact that traditional morphological hallmarks of apoptosis such as nuclear fragmentation or shrinkage were not apparent in these cells (Figure 4.21). From the use of Z-VAD-FMK, the data suggests VP cell death is not predominately

through caspase-dependent apoptosis however it does not rule out other caspase-independent apoptotic and alternative mechanisms of cell death.

Once regarded to be a chaotic, unprogrammed mode of cell death, research has uncovered necrosis to be an alternative and often tightly-regulated mechanism of death; also known as necroptosis. Nec-1 is a potent allosteric inhibitor of RIPK1, inhibiting the formation of the necrosome and subsequent activation of necroptosis[294,295]. Surprisingly, contrary to research showing VP and PDT to induce tissue necrosis[156], VP-induced hypoxic cell death could not be prevented in the presence of Nec-1, indicating that other mechanisms are at play (Figure 4.22). Apoptosis, necrosis and autophagy were once believed to be distinct individual death mechanisms, with apoptosis being the most favoured by the cell; however it is now understood that there is considerable cross-talk between these modes of cell death. Research has uncovered evidence that these pathways are often regulated by the same stimuli and can even share downstream initiator and effector molecules[296]. With this in mind, cells were also treated with the inhibitor ALLN, which prevents activation of calpains – known to play a role in caspase-independent apoptosis and necrosis – and cathepsins – believed to be a part of autophagic cell death[296,297] (Figure 4.22). Again, VP-induced cell death could not be prevented upon addition of this inhibitor. A number of modes of cell death induce, as part of their process, opening of the mPTP, mitochondrial swelling, dissipation of the mitochondrial inner transmembrane potential and release of apoptogenic molecules into the cytosol[261,298]. Cyclophillin D, (CyP-D) is an essential component of this membrane pore playing a vital role in channel opening and can be potently inhibited by the compound CsA[299,300]. Interestingly, Belzacq *et al*., have also shown VP to act on the mPTP inducing cell death, although light-activation was required[261]. Glioma cells were

therefore treated with VP in the presence of CsA to investigate whether inhibiting mPTP opening could prevent VP-induced cell death (Figure 4.22). In this system however, hypoxia-specific cell death could not be inhibited upon VP exposure. Finally, inhibitors against p53/p73 mediated and autophagic cell death, PFT-α[301] and CQ[302], were employed although neither could prevent VP cell death under hypoxic conditions (Figure 4.23). From use of these various inhibitors, the data suggest that VP-induced cell death is multifactorial and likely based on a biochemical, rather than a signalling, response. It should be noted however, as previously mentioned, that there is convergence of these cell death mechanisms and evidence to suggest that treating cells with one cell death inhibitor can often push cells towards utilising an alternative mode of cell death. Nec-1 has recently been identified to also inhibit apoptosis in addition to necroptosis and conversely Z-VAD-FMK can also induce expression of the necroptosis effector RIPK1[298]. To increase confidence in confirming the mode of VP-induced cell death in glioma cells, a combination of inhibitors should be employed upon VP exposure and a further look at molecular initiators and effectors such as BCL2 proteins and cytochrome *c* release could confirm that these regulated mechanisms of cell death are not involved.

4.3.8. Hypoxia exacerbates VP-induced cellular vacuolisation and ER stress

A significant phenotype observed as a result of VP exposure was cellular vacuolisation, which was exacerbated under hypoxic conditions (Figure 4.24). Vacuolisation is a hallmark of non-apoptotic or caspase-independent cell death pathways such as autophagy, methuosis, oncosis, paraptosis and also necroptosis[271]. It is believed that irreversible vacuolisation can arise in cytopathological conditions as a result of cytotoxic stimuli, significantly affecting the Golgi apparatus, the endosomal-lysosomal compartment as well as the ER[272]. However, it remains undetermined whether these

vacuoles play a role in cell survival under stress conditions or whether they are connected to cell death. The ER was therefore investigated to determine whether VP-induced vacuolisation could be a result of increased stress to this organelle. VP exposure significantly increased ER stress, which was determined through expression of CRT; an ER-residing molecular chaperone involved in the correct folding of glycosylated proteins and regulation of calcium homeostasis and is subsequently known to be significantly upregulated under conditions of ER stress[303]. ER stress was additionally observed to be amplified under hypoxic conditions (Figure 4.25). Previous studies have suggested that increased ER stress can increase cell vacuolisation leading to a disruption in the ERAD pathway[272]. Under normal conditions, the ERAD pathway is part of a quality control network ensuring correct folding and processing of proteins to prevent toxic aggregates of misfolded proteins from accumulating in the cell[304]; pathologies that are observed in neurodegeneration diseases such as Parkinson's and Alzheimer's disease[304,305]. When this pathway is disrupted, misfolded proteins can amass in the ER, increasing ER stress and inducing the UPR which quickly acts to restore the physiological balance by halting protein translation, degrading misfolded proteins as well as increasing expression of chaperones for increased protein folding[306,307]. However, if UPR is not completed either rapidly or successfully, then the cell is targeted for cell death[306,307]. Eer1 is a known inhibitor of the p97/VCP cytosolic AAA+ ATPase which retrotranslocates misfolded substrates from the ER to the cytoplasm for subsequent proteasomal degradation[308,309]. Eer1-mediated ERAD inhibition has therefore shown to increase ER stress due to the accumulation of protein aggregates, driving the cells to die[307,309,310]. This is contrary to the response observed in this investigation, as Eer1 treatment partially rescued cell viability following VP exposure (Figure 4.26). This differing response to Eer1 inhibition could be due to a dose- and time-dependent effect

as Wang *et al*., have shown that by disrupting ERAD, it increases the time for the cell to correct misfolded proteins before targeted degradation, allowing the cell to survive longer before potential induction of UPR and cell death[311]. Additionally, the observations in this study are also supported by Shah *et al*., who showed Eer1 to induce EMT and increase cell migration and invasion for a period before induction of cell death, which was eventually induced through prolonged inhibition of p97/VCP[312]. Mild activation of the UPR has also been shown to promote cancer progression as it can improve ER function[309]. It therefore appears that there is a fine balance in the regulation of this pathway in that brief inhibition of ERAD can actually alleviate ER stress promoting cell survival however sustained ERAD inhibition over a matter of days causes excessive ER stress, resulting in cell death. Furthermore, the concentration of Eer1 used should be further investigated as it could have opposing effects with lower doses causing partial ERAD inhibition and mild UPR response allowing cell survival, whereas higher doses could induce full ERAD inhibition exacerbating ER stress, and thereby forcing the decision of cell to die. With respect to VP treatment, it suggests that mild UPR activation during VP treatment was able to partially prevent VP-induced cell death indicating that VP does indeed trigger ER stress and potential protein aggregation which could therefore instigate cell death mechanisms.

4.3.9. VP induces significant cellular stress through increased production of ROS

Tight regulation of redox homeostasis is crucial for maintaining both healthy and malignant cell survival and as previously discussed, there is a close relationship between ER stress and oxidative stress. During excessive ROS production, these highly reactive oxygenated molecules, particularly the hydroxyl radical OH•, can attack and cause

oxidation of DNA, protein and lipids[202]. VP, as previously discussed, is a photosensitiser and when activated by light has been shown to generate cytotoxic free radicals, predominately singlet oxygen – much like other physiological porphyrin molecules – exerting damage to the surrounding tissue[154,155]. To investigate whether VP could induce oxidative stress, in addition to ER stress in the absence of light-activation, markers of oxidative stress were analysed. VP was seen to induce a significant increase in DNA oxidation, observed through increased presence of 8-OHdG and significantly increased DCF fluorescence (Figure 4.27-4.28). ROS production upon VP exposure was also observed in this investigation to be significantly exacerbated under hypoxic conditions; a known stimulator of ROS production[313]. Although VP induces ROS in normoxic conditions, it appears that cell death could be selectively induced in hypoxia since these cells already exhibit a higher basal level of ROS production. Therefore, amplifying ROS generation under these sensitive conditions is sufficient to tip the balance towards causing excessive cellular damage consequently driving the cells to initiate cell death driven by apoptotic or necrotic mechanisms. Furthermore, related-porphyrin PPIX did not significantly increase ROS production in both normoxia and hypoxia, again providing evidence that VP-induced death in hypoxia is explicit to this porphyrin and potentially through exacerbated ROS production (Figure 4.28).

Attenuation of ROS production was observed upon the addition of general redox-cycling TEMPOL, which is capable of catalysing O_2^- to H_2O_2, facilitate detoxification of H_2O_2 to H_2O as well as inhibiting Fenton chemistry and subsequent generation of OH• radicals from H_2O_2[314](Figure 4.28). TEMPOL was also capable of partially inhibiting VP-induced hypoxic cell death indicating, as previously mentioned, that there are other mechanisms contributing to VP-induced cell death and inhibition of one mechanism is not enough to

fully rescue cell viability (Figure 4.29). Further experiments could involve using a combination of ROS and cell death inhibitors and over-expressing endogenous antioxidant mechanisms such as catalase to see if this can increase cell viability over exogenously applied antioxidants.

4.3.10. VP can bind intracellular iron for use in potential Fenton-like chemistry to exacerbate ROS production

Iron is vital for cellular metabolism as in addition to playing a central role in oxygen transport, cellular respiration and DNA synthesis, it forms the active site of numerous redox-active enzymes enabling these reactions to occur[315,316]. Under physiological conditions, iron homeostasis is tightly-regulated in its uptake, storage and release. Iron metabolism is known to be disrupted in cancer with tumours exhibiting enhanced iron dependence resulting in increased iron uptake which contributes to increased tumour survival[316,317]. GBM, along with other cancers, has shown in addition to increased iron uptake, to increase expression of iron-storage protein ferritin which subsequently allows higher sequestration and storage of intracellular iron[317,318]. Paradoxically, iron dysregulation resulting in the excess of free iron can be toxic to the cell due to its role in the generation of highly reactive hydroxyl radicals from H_2O_2 in the Fenton reaction[319]. This increased ROS, as previously mentioned, could be at first beneficial for cancer progression as low levels can amplify various survival pathways, such as the Akt/mTOR pathway, however once ROS accumulate in excessive amounts it can instigate cell death[316].

Porphyrins are known to bind to metals to form complexes, with the metal ion usually possessing a charge of 2^+ or 3^+. Due to the similarity in structure of VP with other

porphyrins, it was hypothesised that VP would also be capable of binding transition metals. The precise mechanism of how VP generates ROS, particularly in the absence of light-activation, is not known and so it was further hypothesised that the mode of action could be through iron catalysing the Fenton reaction. Results show that VP is indeed capable of complexing with ferric (Fe^{3+}), ferrous (Fe^{2+}) and zinc (Zn^{2+}) ions however not magnesium (Mg^{2+}) (Figure 4.31-4.34). It was found that VP did not bind magnesium – considering that Mg^{2+} is a biologically relevant ion and porphyrins are capable of binding magnesium, this is a significant result[320]. Instead, ferric iron was the predominant metal species which bound to VP, with ferrous and zinc only binding over a longer period of 24 hours (Figure 4.34). Mass spectrometry data indicated that VP was acting as a tetradentate chelating ligand forming a coordination complex with the metal ions. It could be hypothesised that VP is predominately chelating ferric iron, which can then elicit Fenton-like redox cycling, which would therefore exacerbate ROS production. The toxicity of H_2O_2 is dependent on its reaction with ferrous iron to generate the highly reactive OH• through the Fenton reaction, as previously discussed. It is now accepted that the ferrous iron needed for this reaction can be generated from the reduction of ferric iron by superoxide anions, in the iron-catalysed Haber-Weiss reaction (now referred to as Fenton-like chemistry)[321,322]:

$$Fenton - Like\ Reaction:\ Fe^{3+} + O_2^{-} \rightarrow Fe^{2+} + H_2O_2$$

Starke and Farber have shown that both ferric iron and superoxide ions were required for the H_2O_2-induced cell death of hepatocytes *in vitro*[323]. Theoretically, VP could bind ferric iron to initiate increased redox cycling as reduction of Fe^{3+} upon the presence of superoxide anions generates Fe^{2+} which consequently produces reactive OH• and Fe^{3+}

which could again bind VP therefore perpetuating the ROS pool. Due to the nature of the tetradentate complex, the planar structure could also lead to exposure of the iron centre making it easily accessible for reduction by superoxide anions. Haem is another iron-coordinated porphyrin and ROS have been shown to randomly attack the carbon methene bridges situated in the tetrapyrrole rings subsequently generating pyrrole products and the release of iron, supporting this theory of iron cycling[324]. Furthermore, hypoxia is a known reducing environment and so could exacerbate the reduction of the Fe^{3+}-VP complex to produce ferrous ions thereby amplifying ROS production which could contribute to the VP-induced hypoxic cell death observed in glioma cells[325]. Ascorbate is another reducing agent known to reduce ferric compounds to ferrous and interestingly has been shown to enhance the toxicity of VP[326].

This observation could therefore shed some light on the potential mechanism of VP-induced ROS generation. Further experiments are required to elucidate the chemistry of this reaction to fully understand the mechanism of VP preferentially binding ferric iron. Cyclic voltammetry experiments could therefore be applied to investigate this potential iron redox cycling. Furthermore, it is important to investigate the effect of iron chelation on the activity of VP, since it could be hypothesised that upon diminished presence of iron, VP would potentially lose its activity. The structural modifications of VP should also be further investigated as addition of the cyclohexadiene ring and additional propionic acid methyl ester are likely affecting the reactivity of VP within the cells as PPIX and ZnPP were not capable of inducing cell death at the same concentration. Iron stores are known to be elevated in highly metabolic areas such as the brain and consequently gliomas are known to have increased ferritin expression[315,318]. VP therapy could therefore be beneficial for targeting these malignant cells as high levels of iron could

therefore increase cell death through increased activity of VP. Thus, iron content and release should be analysed in these glioma cells to strengthen this hypothesis.

4.4. Summary

The data presented in this chapter clearly outline VP as an attractive target for further clinical investigation as a novel treatment for glioma. Results show that VP is capable of not only reducing glioma cell proliferation but is capable of inducing cell death in the most highly therapy-resistant hypoxic subset of tumour cells. Hypoxic cells represent a significant clinical challenge and therapies that can modulate this resistance or directly kill hypoxic cells may significantly improve patient outcomes in a number of tumours types, not just glioma. Investigations into the mechanism of VP uncovered YAP-independent effects which were likely induced through increased ER and oxidative stress, exacerbating the production of ROS. Although VP was capable of inducing these processes under normoxic conditions, ROS was significantly amplified in cells already stressed under hypoxia therefore pushing the cells 'over the edge' towards cell death. Additionally, VP was discovered to bind transition metals, in particular ferric iron; an unprecedented finding that sheds some light on the potential mechanism of VP generated ROS production. Further investigations are therefore warranted to accurately identify how this drug can be used clinically such as identifying the appropriate therapeutic dose and treatment window as well as potential methods of drug delivery. In summary, these data propose the enormous potential of this clinically available and FDA-approved therapeutic, VP to be repurposed to target a significant hypoxic population of highly resistant and aggressive cells in gliomas.

Chapter 5:

Concluding remarks

5.1. Significance and aims of investigation

Advancements in prevention, detection and treatment over the last 40 years have significantly transformed cancer healthcare[327] – at least 78% of melanoma, prostate and breast cancer patients now survive 10-years or more post-diagnosis[328]. However there are a few cancers that are consistently lagging behind, with little improvement in survival seen over the past decade[328]. Lung, pancreatic, oesophageal and brain cancers share a significantly poor 10-year survival rate of between 1-14% and as such are considered as cancers of a substantial unmet need[327,328].

Gliomas, an aggressive type of brain tumour, invade deep into the surrounding healthy brain consequently making successful treatment incredibly challenging[259]. The severe hypoxic nature of glioma adds further complications to therapeutic efficacy as hypoxia limits efficient drug delivery as well as increasing resistance to both chemo and radiotherapy[97]. As such, these patients cannot be successively cured by existing therapies and prognosis remains unrelentingly poor. Therapies that target both the hypoxic tumour microenvironment and pathways that regulate glioma growth and progression in this environment have significant potential to improve patient survival. This thesis therefore aimed to characterise the potential hypoxic and metabolic relationship with YAP/TAZ signalling in glioma; a pathway strongly associated with induction of the cancer phenotype. Furthermore, this research highlights the significant repurposing potential of an inhibitor of this signalling pathway, identifying a possible novel therapeutic for hypoxic and therapy-resistant gliomas.

5.2. Hypoxia influences YAP/TAZ signalling in glioma

The Hippo pathway has become of interest in cancer research due to its strong association with tumorigenesis, with increased activity of its downstream effectors YAP/TAZ leading to enhanced tumour growth, invasion, metastasis and therapy resistance in many cancers[136]. Regulation of YAP/TAZ signalling is incredibly complex however has recently been associated with hypoxia in a model of breast cancer[131]. This research demonstrates for the first time that hypoxia also influences YAP/TAZ signalling in glioma. Results confirm that hypoxia (1% O_2) induces a significant upregulation of YAP1 mRNA, concomitant with an increase in expression of YAP-target genes, *CTGF*, *CYR61* and *BBC3* across four glioma cell lines. A hypoxia-induced increase in CTGF protein expression was also observed alongside enhanced nuclear YAP1 localisation, both of which imply that YAP1 transcriptional co-activation activity is increased as a result of hypoxia. Together, these data suggest that hypoxic induction of YAP/TAZ signalling in glioma could be to confer a survival advantage through increased transcription of pro-proliferative genes, such as *CTGF*, to sustain tumour cell proliferation in a hostile microenvironment.

YAP/TAZ signalling was also amplified under hypoxia in two novel GBM lines. Interestingly, these two lines, despite originating from the same tumour specimen, had exhibited differential sensitivity to chemoradiation treatment. T1 cells were derived from an area of tumour recurrence that had progressed significantly post-treatment, and was thus believed to be therapy-resistant, whereas T2 cells were harvested from an area of the tumour which had not progressed post-treatment, and was therefore considered therapy-responsive. Both p-YAP and YAP1 expression were observed to be considerably higher in T1 cells compared to T2 cells, indicating amplified YAP signalling in the

therapy-resistant cells. Since increased YAP expression and activity has been previously associated with chemoresistance in other cancers, it suggests a potential reason for this upregulation in the tumour cells. However, further experimentation will be required to test whether this increased YAP signalling does in fact confer resistance to current chemotherapeutic agents *in vitro*.

This investigation provides a solid basis to suggest that suppressing YAP/TAZ signalling could potentially be a valuable therapeutic opportunity, particularly in hypoxic tumours as well as for patients with limited treatment options as a result of high therapy resistance. There are however, a few limitations to this study which should be addressed in future research. For instance, while established cell lines have been invaluable to cancer research and drug discovery, it should be acknowledged that there are potential limitations to their use in this investigation. For example, genomic instability and serial passage and culture of cell lines can induce both genotypic and phenotypic variation over time[329]. Therefore, these cell lines may not adequately represent the primary tumour from which they originated and could therefore lead to potential differences in experimental results. Furthermore, the *in vitro* cell culture environment is dissimilar to the original tumour, omitting potential crucial interactions with surrounding cell types as well as altering cell morphology, gene expression and behaviour of signalling pathways[329]. These established cell lines do however provide an *in vitro* model which can be used easily and rapidly in a controlled and reproducible fashion, and alongside adequate measures such as cell line authentication and low passage cultures, allow detailed pre-clinical investigations which should then be further tested in more appropriate *in vivo* models[330].

This investigation demonstrated that hypoxia induced YAP/TAZ signalling, however it was assessed in established 2D cultures *in vitro*. Although this provides a good initial understanding of this relationship, as previously mentioned, a more meaningful pre-clinical assessment may be achieved through investigation of the hypoxic regulation of YAP/TAZ signalling using a GBM spheroid model or *in vivo* using patient-derived xenografts; both of which more faithfully recapitulate the key features and microenvironment of the tumour[331]. Nevertheless, hypoxia was observed to enhance YAP expression in primary cells derived from a GBM tumour, which were cultured long-term under hypoxic conditions. Upregulation of YAP/TAZ expression and signalling should therefore be further examined using more primary cell lines as well in those derived from both LGG and HGG patients to establish whether there are any differences between malignancy grades and whether this hypoxic upregulation of YAP/TAZ signalling could be a contributing factor to this progression.

5.3. YAP/TAZ support glucose and glutamine metabolism in glioma

It has long been established that cancer cells rewire their metabolism to fuel the increased energetic demand and generation of new biomass required to sustain uncontrolled tumour proliferation[239]. Hypoxia-induced signalling further remodels these metabolic pathways to increase tumour survival within a hostile microenvironment, promoting a malignant phenotype[192]. Since aberrant YAP/TAZ signalling often plays a significant role in these tumour phenotypes and as this study showed hypoxia to induce YAP/TAZ signalling in glioma, it was investigated whether YAP/TAZ could directly influence aspects of hypoxic metabolism in this system. Using metabolic-tracing and siRNA approaches, the preliminary research presented in this thesis establishes for the

first time an important role for YAP/TAZ in both glucose and glutamine metabolism in glioma.

Metabolic tracing analysis identified knockdown of YAP/TAZ to significantly reduce *de novo* serine synthesis and alter the metabolism of pyruvate by the cell; sustaining PC activity under hypoxia to support anaplerosis. Continued mitochondrial pyruvate oxidation in hypoxia, along with reduced activity of the SSP attenuating anti-oxidant capacity, could potentially lead to enhanced ROS accumulation, which could theoretically culminate in reduced cell survival. Furthermore, the results demonstrate that YAP/TAZ depletion significantly affected oxidative glutamine metabolism, decreasing both the anaplerotic metabolism and potentially ATP-generation fuelled by glutamine. The total carbon contribution from both glucose and glutamine were calculated for various metabolites, with results illustrating that reductions in YAP/TAZ expression clearly reduced the cell's ability to utilise glutamine in the generation of metabolites crucial for cellular growth such as aspartate, independently of oxygen tension. These data correlate with a significant reduction in cell proliferation observed upon YAP/TAZ knockdown, suggesting the possibility that YAP/TAZ are required to support various biosynthetic pathways that generate precursors for protein and nucleic acids synthesis as well as modulating cellular antioxidant capacity to promote tumour growth and survival[221].

The data presented provides a clear picture of the metabolic processes influenced by YAP/TAZ, although it is restricted in that these data only illustrate the percentage carbon contribution from glucose and glutamine and do not take into account absolute metabolite concentrations, which could vary significantly. For future improvement of this study, these values should be incorporated as well as measuring metabolite uptake and

excretion rates to investigate metabolic flux. Furthermore, this relationship would need to be characterised in other established and primary glioma cell lines. Glioma cells form only part of the tumour mass, which is also made up of other cell types such as microglia and endothelial cells. The role of YAP/TAZ in determining the metabolic relationship between these multiple cell types would be key to defining the nature of this signalling pathway in glioma aetiology[71]. Finally, more in-depth metabolic tracing needs to be conducted using other relevant nutrient tracers such as acetate and fatty acids as well as investigation into the expression of the various biosynthetic enzymes to gain a fuller understanding of the relationship between YAP/TAZ and hypoxic glioma metabolism.

These data do however provide preliminary evidence to suggest that disrupting YAP/TAZ expression and transcriptional co-activator activity, particularly in hypoxia, could be a valuable target for therapeutic development since both pro-survival signalling and metabolism can be targeted in combination to reduce glioma growth and progression.

5.4. VP induces hypoxia specific cell death showing potential as a novel therapeutic for glioma

As suppression of YAP/TAZ signalling in hypoxic glioma cells was identified to be a potentially valuable therapeutic opportunity, the effect of VP – a previously identified YAP inhibitor – on malignant cell growth and survival was investigated. VP is a particularly attractive agent as, if effective, it has the potential to be rapidly repurposed to treat gliomas, as well as other hypoxic tumours. The results presented in this thesis demonstrated VP to be a potent suppressor of glioma cell proliferation, corroborating previous research determining VP to attenuate tumour growth through suppression of YAP-TEAD activity[158,159,161]. Strikingly, when glioma cells were treated with VP under

hypoxic conditions, VP was observed to induce significant cell death. This observation was also recapitulated in a more biologically relevant spheroid model. A significant finding was the ability of VP to induce cell death in both the therapy-resistant (T1) and therapy-sensitive (T2) primary GBM cells, suggesting that hypoxia-specific VP-mediated cell killing is independent of normal resistance mechanisms observed in GBM, and therefore may also reduce the rate of relapse and progression. VP has the potential therefore to not only be employed as a mono-therapy in the selective killing of hypoxic cells in cancer but could also be introduced as part of a combination therapy to enhance treatment sensitivity in therapy-resistant tumours, given that the radiotherapy element of the current therapeutic regime is highly sensitive to oxygen tension. As previously discussed, higher doses of radiation are required in hypoxic areas of tumours to instigate significant ROS- induced damage. Since VP significantly increased ROS levels and selectively killed hypoxic glioma cells in this investigation, it could be suggested that combined radiotherapy and VP treatment could therefore reduce the dosage of radiation required in hypoxic cells to initiate the same cell death effect and potentially improve time to recurrence by eliminating more of the hypoxic, therapy-resistant cells that instigate tumour relapse. Promising results have been recently demonstrated in clinical trials investigating the combination of poly (ADP-ribose) polymerase (PARP) inhibitors such as olaparib and chemotherapy in the treatment of glioma. It therefore may also be beneficial to incorporate VP given its specificity with hypoxia, and its mode of action (ROS generation), which would be expected to increase the rate of DNA damage in hypoxia and make the cells more susceptible to PARP inhibition[332,333].

In this investigation, the activity of VP in inducing hypoxic cell death was interestingly discovered to be YAP-independent and instead through significant exacerbation of

oxidative and ER stress under hypoxia. The precise mechanism of VP-induced cell death remains to be fully elucidated, although this thesis presents evidence to suggest that this increased ROS production is generated through the ability of VP to bind to iron – a surprisingly novel finding given the well-known iron binding characteristics of the porphyrin family of molecules. This investigation provides a promising pre-clinical assessment for repurposing VP that could also be extended to the treatment of hypoxic tumours. It should be noted, however, that the hypoxia-activated prodrug tirapazamine, which similarly elicits release of cytotoxic radicals, while demonstrating excellent clinical efficacy *in vitro*, in phase III trials demonstrated no clinical benefit[97,334]. Importantly though, retrospective analysis of the data showed that no measurement of hypoxia was undertaken before or during the trial and thus the patients that would most benefit were not identified prospectively[97]. Further research and appropriately designed trials are clearly required in an *in vivo* setting to determine whether VP will exhibit clinical efficacy.

A promising characteristic of VP is that it has been shown to be selectively taken up by malignant cells through LDLs, providing further treatment specificity[155]. Furthermore, LDLs are known to be increased in hypoxia, suggesting potential increased VP uptake by hypoxic cells which may contribute towards this selective cell death observed under these conditions[335]. Theoretically, it could also suggest that if VP cellular uptake is indeed increased in hypoxia, then possibly a significantly lower concentration of VP is required to induce cell death compared with normoxia – although it should be noted that cell death was not observed in normoxic conditions in this investigation (up to 10 μM VP). Future experiments could therefore quantitatively measure VP uptake by normoxic and hypoxic cells to investigate this hypothesis. It also should be noted that VP is a benzoporphyrin derivative, derived from the structure of PPIX[155]. As previously

mentioned, oral administration of exogenous 5-ALA to aid surgical resection of HGG tumours, results in subsequent conversion and tumour-specific accumulation of PPIX, which is known to be well tolerated by patients[44,45,336]. This therefore suggests that VP, being so structurally similar to PPIX, could be predicted to exhibit the same selective uptake, and potentially tolerability, in HGG.

Promisingly, VP has shown to induce minimal side-effects in patients during its use in PDT, as well as sparing normoxic cells from death, despite being given through an intravenous route rather than topically[155]. With respect to further studies here, the effect of VP would have to be investigated at physiological oxygen concentrations (~4.6% O_2) as well as in healthy brain cells to determine any potential adverse side-effects when treating glioma. Despite this, the additional benefit of using VP proposed in this investigation is that not only does VP induce cell death in hypoxia, it also suppresses cell proliferation in normoxic conditions, and so could be used to target this population of tumour cells as well.

A difficulty in using VP as a glioma therapeutic could arise however in establishing how and when to employ VP as a treatment. One of the frequently encountered problems when treating gliomas – accessibility through the BBB – is unlikely to be an issue with VP, given that it is lipophilic. However, delivery of VP to the hypoxic tumour areas may still prove challenging. Theoretically, VP could be injected or delivered in slow-release coated beads when the patient undergoes tumour biopsy or resection. This could also benefit the hypoxic tumour cells which are inevitably left behind and are known to cause tumour recurrence and relapse. The effect of VP combined with the current standard treatment for glioma (TMZ + ionising radiation) should also be investigated due to VP's

ability to significant induce ROS, particularly under hypoxic conditions where these current treatments exhibit limited efficacy. It could be predicted that VP would improve sensitivity and response to both TMZ and radiation in hypoxia since they are themselves ROS inducing treatments, as previously discussed, and addition of VP would therefore significantly amplify this ROS-induced damage and subsequent cell death. Supporting evidence in PC9 lung cancer cells has shown that VP synergises with both cisplatin and radiation treatment, significantly improving both treatment sensitivity and increasing cell death[162]. This therefore provides promising evidence that VP could also exhibit a similar effect alongside standard TMZ and radiation treatment for glioma and could also significantly improve their efficacy in hypoxia. Further studies are therefore inevitably required to determine the most effective treatment modality and regime.

Together, the data in this thesis establishes the importance of hypoxic and metabolic regulation of YAP/TAZ signalling in glioma to support tumour growth and proliferation. Furthermore, this research also highlights the significant potential for the clinically available and FDA-approved therapeutic VP, to be repurposed to treat glioma, as it targets hypoxic glioma cells specifically, which may significantly improve patient survival.

List of references:

1 CRUK.. *What is cancer?*, <https://www.cancerresearchuk.org/about-cancer/what-is-cancer> (2018). (23.09.18).

2 CRUK. *Cancer mortality statistics*, <https://www.cancerresearchuk.org/health-professional/cancer-statistics/mortality> (2018). (23.09.18).

3 CRUK.. *Brain, other CNS and intracranial tumours statistics*, <https://www.cancerresearchuk.org/health-professional/cancer-statistics/statistics-by-cancer-type/brain-other-cns-and-intracranial-tumours> (2018) (23.09.18)..

4 D'Amico, R. S., Englander, Z. K., Canoll, P. & Bruce, J. N. Extent of Resection in Glioma-A Review of the Cutting Edge. *World Neurosurg* **103**, 538-549, doi:10.1016/j.wneu.2017.04.041 (2017).

5 Xia, L., Fang, C., Chen, G. & Sun, C. Relationship between the extent of resection and the survival of patients with low-grade gliomas: a systematic review and meta-analysis. *BMC Cancer* **18**, 48, doi:10.1186/s12885-017-3909-x (2018).

6 Stupp, R. *et al.* Radiotherapy plus concomitant and adjuvant temozolomide for glioblastoma. *New England Journal of Medicine* **352**, 987-996 (2005).

7 McNamara, M. G., Sahebjam, S. & Mason, W. P. Emerging Biomarkers in Glioblastoma. *Cancers* **5**, 1103-1119 (2013).

8 Furnari, F. B. *et al.* Malignant astrocytic glioma: genetics, biology, and paths to treatment. *Genes & development* **21**, 2683-2710, doi:10.1101/gad.1596707 (2007).

9 Louis, D. N. *et al.* The 2007 WHO classification of tumours of the central nervous system. *Acta neuropathologica* **114**, 97-109 (2007).

10 Nupponen, N. N. & Joensuu, H. Molecular pathology of gliomas. *Current Diagnostic Pathology* **12**, 394-402 (2006).

11 Louis, D. N. *et al.* The 2016 World Health Organization Classification of Tumors of the Central Nervous System: a summary. *Acta Neuropathol* **131**, 803-820, doi:10.1007/s00401-016-1545-1 (2016).

12 Kleihues, P. *et al.* The WHO classification of tumors of the nervous system. *Journal of Neuropathology & Experimental Neurology* **61**, 215-225 (2002).

13 Rong, Y., Durden, D. L., Van Meir, E. G. & Brat, D. J. 'Pseudopalisading'necrosis in glioblastoma: a familiar morphologic feature that links vascular pathology, hypoxia, and angiogenesis. *Journal of Neuropathology & Experimental Neurology* **65**, 529-539 (2006).

14 Hartmann, C. *et al.* Molecular markers in low-grade gliomas: predictive or prognostic? *Clinical Cancer Research* **17**, 4588-4599 (2011).

15 Claus, E. B. *et al.* Survival and low-grade glioma: the emergence of genetic information. *Neurosurg Focus* **38**, E6, doi:10.3171/2014.10.FOCUS12367 (2015).

16 Omuro, A. & DeAngelis, L. M. Glioblastoma and other malignant gliomas: a clinical review. *JAMA* **310**, 1842-1850 (2013).

17 Ohgaki, H. & Kleihues, P. The definition of primary and secondary glioblastoma. *Clinical Cancer Research* **19**, 764-772 (2013).

18 Olar, A. & Aldape, K. D. Using the molecular classification of glioblastoma to inform personalized treatment. *The Journal of pathology* **232**, 165-177 (2014).

19 Bonavia, R., Cavenee, W. K. & Furnari, F. B. Heterogeneity maintenance in glioblastoma: a social network. *Cancer research* **71**, 4055-4060 (2011).
20 Gerlinger, M. *et al.* Intratumor heterogeneity and branched evolution revealed by multiregion sequencing. *New England Journal of Medicine* **366**, 883-892 (2012).
21 Riemenschneider, M. J., Jeuken, J. W., Wesseling, P. & Reifenberger, G. Molecular diagnostics of gliomas: state of the art. *Acta neuropathologica* **120**, 567-584 (2010).
22 Huse, J. T. *et al.* Where are we now? And where are we going? A report from the Accelerate Brain Cancer Cure (ABC2) Low-grade Glioma Research Workshop. *Neuro-oncology* **16**, 173-178, doi:10.1093/neuonc/not229 (2014).
23 McLendon, R. *et al.* Comprehensive genomic characterization defines human glioblastoma genes and core pathways. *Nature* **455**, 1061-1068 (2008).
24 Verhaak, R. G. *et al.* Integrated Genomic Analysis Identifies Clinically Relevant Subtypes of Glioblastoma Characterized by Abnormalities in< i> PDGFRA</i>,< i> IDH1</i>,< i> EGFR</i>, and< i> NF1</i>. *Cancer cell* **17**, 98-110 (2010).
25 Nobusawa, S., Watanabe, T., Kleihues, P. & Ohgaki, H. IDH1 mutations as molecular signature and predictive factor of secondary glioblastomas. *Clinical Cancer Research* **15**, 6002-6007 (2009).
26 Hartmann, C. *et al.* Long-Term Survival in Primary Glioblastoma With Versus Without Isocitrate Dehydrogenase Mutations. *Clinical Cancer Research* **19**, 5146-5157 (2013).
27 Yan, H. *et al.* IDH1 and IDH2 mutations in gliomas. *New England Journal of Medicine* **360**, 765-773 (2009).
28 Szerlip, N. J. *et al.* Intratumoral heterogeneity of receptor tyrosine kinases EGFR and PDGFRA amplification in glioblastoma defines subpopulations with distinct growth factor response. *Proceedings of the National Academy of Sciences* **109**, 3041-3046 (2012).
29 Van Meir, E. G. *et al.* Exciting New Advances in Neuro-Oncology: The Avenue to a Cure for Malignant Glioma. *CA: a cancer journal for clinicians* **60**, 166-193 (2010).
30 Inda, M.-d.-M., Bonavia, R. & Seoane, J. Glioblastoma Multiforme: A Look Inside Its Heterogeneous Nature. *Cancers* **6**, 226-239 (2014).
31 Sottoriva, A. *et al.* Intratumor heterogeneity in human glioblastoma reflects cancer evolutionary dynamics. *Proceedings of the National Academy of Sciences* **110**, 4009-4014 (2013).
32 Houillier, C. *et al.* IDH1 or IDH2 mutations predict longer survival and response to temozolomide in low-grade gliomas. *Neurology* **75**, 1560-1566 (2010).
33 Parsons, D. W. *et al.* An integrated genomic analysis of human glioblastoma multiforme. *Science* **321**, 1807-1812 (2008).
34 Hartmann, C. *et al.* Type and frequency of IDH1 and IDH2 mutations are related to astrocytic and oligodendroglial differentiation and age: a study of 1,010 diffuse gliomas. *Acta neuropathologica* **118**, 469-474 (2009).
35 Frezza, C., Tennant, D. A. & Gottlieb, E. IDH1 mutations in gliomas: when an enzyme loses its grip. *Cancer cell* **17**, 7-9 (2010).

36 Rakheja, D., Medeiros, L. J., Bevan, S. & Chen, W. The emerging role of d-2-hydroxyglutarate as an oncometabolite in hematolymphoid and central nervous system neoplasms. *Front Oncol* **3**, 169, doi:10.3389/fonc.2013.00169 (2013).
37 Dang, L. *et al.* Cancer-associated IDH1 mutations produce 2-hydroxyglutarate. *Nature* **462**, 739-744 (2009).
38 Mondesir, J., Willekens, C., Touat, M. & de Botton, S. IDH1 and IDH2 mutations as novel therapeutic targets: current perspectives. *J Blood Med* **7**, 171-180, doi:10.2147/JBM.S70716 (2016).
39 Claes, A., Idema, A. J. & Wesseling, P. Diffuse glioma growth: a guerilla war. *Acta neuropathologica* **114**, 443-458 (2007).
40 Dandy, W. E. Removal of right cerebral hemisphere for certain tumors with hemiplegia: Preliminary report. *Journal of the American Medical Association* **90**, 823-825, doi:10.1001/jama.1928.02690380007003 (1928).
41 Bougnaud, S. *et al.* Molecular crosstalk between tumour and brain parenchyma instructs histopathological features in glioblastoma. *Oncotarget* **7**, 31955-31971, doi:10.18632/oncotarget.7454 (2016).
42 Pignatti, F. *et al.* Prognostic factors for survival in adult patients with cerebral low-grade glioma. *Journal of Clinical Oncology* **20**, 2076-2084 (2002).
43 NICE. *Brain tumours (primary) and brain metastases in adults*, <https://www.nice.org.uk/guidance/ng99> (2018). (23.09.18).
44 Ferraro, N. *et al.* The role of 5-aminolevulinic acid in brain tumor surgery: a systematic review. *Neurosurg Rev* **39**, 545-555, doi:10.1007/s10143-015-0695-2 (2016).
45 Johansson, A. *et al.* 5-Aminolevulinic acid-induced protoporphyrin IX levels in tissue of human malignant brain tumors. *Photochem Photobiol* **86**, 1373-1378, doi:10.1111/j.1751-1097.2010.00799.x (2010).
46 Stepp, H. *et al.* ALA and malignant glioma: fluorescence-guided resection and photodynamic treatment. *J Environ Pathol Toxicol Oncol* **26**, 157-164 (2007).
47 Weller, M. *et al.* European Association for Neuro-Oncology (EANO) guideline on the diagnosis and treatment of adult astrocytic and oligodendroglial gliomas. *Lancet Oncol* **18**, e315-e329, doi:10.1016/S1470-2045(17)30194-8 (2017).
48 Gzell, C., Back, M., Wheeler, H., Bailey, D. & Foote, M. Radiotherapy in Glioblastoma: the Past, the Present and the Future. *Clin Oncol (R Coll Radiol)* **29**, 15-25, doi:10.1016/j.clon.2016.09.015 (2017).
49 Walker, M. D. *et al.* Evaluation of BCNU and/or radiotherapy in the treatment of anaplastic gliomas. A cooperative clinical trial. *J Neurosurg* **49**, 333-343, doi:10.3171/jns.1978.49.3.0333 (1978).
50 Arvold, N. D. & Reardon, D. A. Treatment options and outcomes for glioblastoma in the elderly patient. *Clin Interv Aging* **9**, 357-367, doi:10.2147/CIA.S44259 (2014).
51 Cancer, L. (2014).
52 Mann, J., Ramakrishna, R., Magge, R. & Wernicke, A. G. Advances in Radiotherapy for Glioblastoma. *Front Neurol* **8**, 748, doi:10.3389/fneur.2017.00748 (2017).

53 Royal College of Radiologists. *Radiotherapy dose fractionation, second edition* <https://www.rcr.ac.uk/system/files/publication/field_publication_files/bfco163_dose_fractionation_2nd_ed_march2017.pdf> (2016). (04.02.19).
54 Keime-Guibert, F. *et al.* Radiotherapy for glioblastoma in the elderly. *N Engl J Med* **356**, 1527-1535, doi:10.1056/NEJMoa065901 (2007).
55 Stupp, R., van den Bent, M. J. & Hegi, M. E. Optimal role of temozolomide in the treatment of malignant gliomas. *Current neurology and neuroscience reports* **5**, 198-206 (2005).
56 Hegi, M. E. *et al.* MGMT gene silencing and benefit from temozolomide in glioblastoma. *New England Journal of Medicine* **352**, 997-1003 (2005).
57 Kitange, G. J. *et al.* Induction of MGMT expression is associated with temozolomide resistance in glioblastoma xenografts. *Neuro-oncology* **11**, 281-291 (2009).
58 Ramirez, Y. P., Weatherbee, J. L., Wheelhouse, R. T. & Ross, A. H. Glioblastoma Multiforme Therapy and Mechanisms of Resistance. *Pharmaceuticals* **6**, 1475-1506 (2013).
59 Shergalis, A., Bankhead, A., Luesakul, U., Muangsin, N. & Neamati, N. Current Challenges and Opportunities in Treating Glioblastoma. *Pharmacol Rev* **70**, 412-445, doi:10.1124/pr.117.014944 (2018).
60 Davis, M. E. Glioblastoma: Overview of Disease and Treatment. *Clin J Oncol Nurs* **20**, S2-8, doi:10.1188/16.CJON.S1.2-8 (2016).
61 Narita, Y. Bevacizumab for glioblastoma. *Ther Clin Risk Manag* **11**, 1759-1765, doi:10.2147/TCRM.S58289 (2015).
62 Wang, Y., Schmid-Bindert, G. & Zhou, C. Erlotinib in the treatment of advanced non-small cell lung cancer: an update for clinicians. *Ther Adv Med Oncol* **4**, 19-29, doi:10.1177/1758834011427927 (2012).
63 Raizer, J. J. *et al.* A phase II trial of erlotinib in patients with recurrent malignant gliomas and nonprogressive glioblastoma multiforme postradiation therapy. *Neuro Oncol* **12**, 95-103, doi:10.1093/neuonc/nop015 (2010).
64 Mun, E. J., Babiker, H. M., Weinberg, U., Kirson, E. D. & Von Hoff, D. D. Tumor-Treating Fields: A Fourth Modality in Cancer Treatment. *Clin Cancer Res* **24**, 266-275, doi:10.1158/1078-0432.CCR-17-1117 (2018).
65 Brown, N. F., Carter, T. J., Ottaviani, D. & Mulholland, P. Harnessing the immune system in glioblastoma. *Br J Cancer* **119**, 1171-1181, doi:10.1038/s41416-018-0258-8 (2018).
66 Sager, O. *et al.* A concise review of immunotherapy for glioblastoma. (2018).
67 McGranahan, T., Li, G. & Nagpal, S. History and current state of immunotherapy in glioma and brain metastasis. *Ther Adv Med Oncol* **9**, 347-368, doi:10.1177/1758834017693750 (2017).
68 Liau, L. M. *et al.* First results on survival from a large Phase 3 clinical trial of an autologous dendritic cell vaccine in newly diagnosed glioblastoma. *J Transl Med* **16**, 142, doi:10.1186/s12967-018-1507-6 (2018).
69 Sarkaria, J. N. *et al.* Is the blood-brain barrier really disrupted in all glioblastomas? A critical assessment of existing clinical data. *Neuro Oncol* **20**, 184-191, doi:10.1093/neuonc/nox175 (2018).
70 Yu, B. *et al.* Measuring tumor cycling hypoxia and angiogenesis using a side-firing fiber optic probe. *Journal of biophotonics* **7**, 552-564, doi:10.1002/jbio.201200187 (2014).

71 Eales, K. L., Hollinshead, K. E. & Tennant, D. A. Hypoxia and metabolic adaptation of cancer cells. *Oncogenesis* **5**, e190, doi:10.1038/oncsis.2015.50 (2016).
72 Semenza, G. L. Hypoxia-inducible factors: mediators of cancer progression and targets for cancer therapy. *Trends in pharmacological sciences* **33**, 207-214, doi:10.1016/j.tips.2012.01.005 (2012).
73 Semenza, G. L. Regulation of metabolism by hypoxia-inducible factor 1. *Cold Spring Harb Symp Quant Biol* **76**, 347-353, doi:10.1101/sqb.2011.76.010678 (2011).
74 Epstein, A. C. *et al.* C. elegans EGL-9 and mammalian homologs define a family of dioxygenases that regulate HIF by prolyl hydroxylation. *Cell* **107**, 43-54 (2001).
75 Bruick, R. K. & McKnight, S. L. A conserved family of prolyl-4-hydroxylases that modify HIF. *Science* **294**, 1337-1340, doi:10.1126/science.1066373 (2001).
76 Kaelin, W. G. & Ratcliffe, P. J. Oxygen sensing by metazoans: the central role of the HIF hydroxylase pathway. *Mol Cell* **30**, 393-402, doi:10.1016/j.molcel.2008.04.009 (2008).
77 Mahon, P. C., Hirota, K. & Semenza, G. L. FIH-1: a novel protein that interacts with HIF-1alpha and VHL to mediate repression of HIF-1 transcriptional activity. *Genes & development* **15**, 2675-2686, doi:10.1101/gad.924501 (2001).
78 Lando, D., Peet, D. J., Whelan, D. A., Gorman, J. J. & Whitelaw, M. L. Asparagine hydroxylation of the HIF transactivation domain a hypoxic switch. *Science* **295**, 858-861, doi:10.1126/science.1068592 (2002).
79 Koivunen, P., Hirsilä, M., Günzler, V., Kivirikko, K. I. & Myllyharju, J. Catalytic properties of the asparaginyl hydroxylase (FIH) in the oxygen sensing pathway are distinct from those of its prolyl 4-hydroxylases. *J Biol Chem* **279**, 9899-9904, doi:10.1074/jbc.M312254200 (2004).
80 Vaupel, P. The role of hypoxia-induced factors in tumor progression. *Oncologist* **9 Suppl 5**, 10-17, doi:10.1634/theoncologist.9-90005-10 (2004).
81 Semenza, G. L. *et al.* Hypoxia response elements in the aldolase A, enolase 1, and lactate dehydrogenase A gene promoters contain essential binding sites for hypoxia-inducible factor 1. *J Biol Chem* **271**, 32529-32537 (1996).
82 Keith, B., Johnson, R. S. & Simon, M. C. HIF1α and HIF2α: sibling rivalry in hypoxic tumour growth and progression. *Nature reviews. Cancer* **12**, 9-22, doi:10.1038/nrc3183 (2011).
83 Mole, D. R. *et al.* Genome-wide association of hypoxia-inducible factor (HIF)-1alpha and HIF-2alpha DNA binding with expression profiling of hypoxia-inducible transcripts. *J Biol Chem* **284**, 16767-16775, doi:10.1074/jbc.M901790200 (2009).
84 Carroll, V. A. & Ashcroft, M. Targeting the molecular basis for tumour hypoxia. *Expert Rev Mol Med* **7**, 1-16, doi:10.1017/S1462399405009117 (2005).
85 Vaupel, P. & Mayer, A. Hypoxia in cancer: significance and impact on clinical outcome. *Cancer Metastasis Rev* **26**, 225-239, doi:10.1007/s10555-007-9055-1 (2007).

86 Semenza, G. L. HIF-1 mediates metabolic responses to intratumoral hypoxia and oncogenic mutations. *J Clin Invest* **123**, 3664-3671, doi:10.1172/JCI67230 (2013).
87 Kaur, B. *et al.* Hypoxia and the hypoxia-inducible-factor pathway in glioma growth and angiogenesis. *Neuro Oncol* **7**, 134-153, doi:10.1215/S1152851704001115 (2005).
88 Paolicchi, E. *et al.* Targeting hypoxic response for cancer therapy. *Oncotarget* **7**, 13464-13478, doi:10.18632/oncotarget.7229 (2016).
89 Ryan, H. E. *et al.* Hypoxia-inducible factor-1alpha is a positive factor in solid tumor growth. *Cancer Res* **60**, 4010-4015 (2000).
90 Maxwell, P. H. *et al.* Hypoxia-inducible factor-1 modulates gene expression in solid tumors and influences both angiogenesis and tumor growth. *Proc Natl Acad Sci U S A* **94**, 8104-8109 (1997).
91 Tennant, D. A. *et al.* Reactivating HIF prolyl hydroxylases under hypoxia results in metabolic catastrophe and cell death. *Oncogene* **28**, 4009-4021, doi:10.1038/onc.2009.250 (2009).
92 Latif, F. *et al.* Identification of the von Hippel-Lindau disease tumor suppressor gene. *Science* **260**, 1317-1320 (1993).
93 Rathmell, W. K. & Chen, S. VHL inactivation in renal cell carcinoma: implications for diagnosis, prognosis and treatment. *Expert Rev Anticancer Ther* **8**, 63-73, doi:10.1586/14737140.8.1.63 (2008).
94 Laurenti, G. & Tennant, D. A. Isocitrate dehydrogenase (IDH), succinate dehydrogenase (SDH), fumarate hydratase (FH): three players for one phenotype in cancer? *Biochem Soc Trans* **44**, 1111-1116, doi:10.1042/BST20160099 (2016).
95 Kluckova, K. & Tennant, D. A. Metabolic implications of hypoxia and pseudohypoxia in pheochromocytoma and paraganglioma. *Cell Tissue Res* **372**, 367-378, doi:10.1007/s00441-018-2801-6 (2018).
96 Rampling, R., Cruickshank, G., Lewis, A. D., Fitzsimmons, S. A. & Workman, P. Direct measurement of pO2 distribution and bioreductive enzymes in human malignant brain tumors. *Int J Radiat Oncol Biol Phys* **29**, 427-431 (1994).
97 Hammond, E. M. *et al.* The meaning, measurement and modification of hypoxia in the laboratory and the clinic. *Clin Oncol (R Coll Radiol)* **26**, 277-288, doi:10.1016/j.clon.2014.02.002 (2014).
98 Harrison, L. B., Chadha, M., Hill, R. J., Hu, K. & Shasha, D. Impact of tumor hypoxia and anemia on radiation therapy outcomes. *Oncologist* **7**, 492-508 (2002).
99 Rockwell, S., Dobrucki, I. T., Kim, E. Y., Marrison, S. T. & Vu, V. T. Hypoxia and radiation therapy: past history, ongoing research, and future promise. *Curr Mol Med* **9**, 442-458 (2009).
100 Harrison, L. & Blackwell, K. Hypoxia and anemia: factors in decreased sensitivity to radiation therapy and chemotherapy? *Oncologist* **9 Suppl 5**, 31-40, doi:10.1634/theoncologist.9-90005-31 (2004).
101 Huang, W. J., Chen, W. W. & Zhang, X. Glioblastoma multiforme: Effect of hypoxia and hypoxia inducible factors on therapeutic approaches. *Oncol Lett* **12**, 2283-2288, doi:10.3892/ol.2016.4952 (2016).

102 Mo, J. S., Park, H. W. & Guan, K. L. The Hippo signaling pathway in stem cell biology and cancer. *EMBO reports* (2014).
103 Tumaneng, K., Russell, R. C. & Guan, K.-L. Organ size control by Hippo and TOR pathways. *Current Biology* **22**, R368-R379 (2012).
104 Ma, Y., Yang, Y., Wang, F., Wei, Q. & Qin, H. Hippo-YAP signaling pathway: A new paradigm for cancer therapy. *International Journal of Cancer* (2014).
105 Nishio, M., Otsubo, K., Maehama, T., Mimori, K. & Suzuki, A. Capturing the mammalian Hippo: elucidating its role in cancer. *Cancer science* **104**, 1271-1277 (2013).
106 Pan, D. The hippo signaling pathway in development and cancer. *Developmental cell* **19**, 491-505 (2010).
107 Zhao, B., Tumaneng, K. & Guan, K.-L. The Hippo pathway in organ size control, tissue regeneration and stem cell self-renewal. *Nature cell biology* **13**, 877-883 (2011).
108 Dong, J. *et al.* Elucidation of a universal size-control mechanism in Drosophila and mammals. *Cell* **130**, 1120-1133, doi:10.1016/j.cell.2007.07.019 (2007).
109 Gaffney, C. J. *et al.* Identification, basic characterization and evolutionary analysis of differentially spliced mRNA isoforms of human YAP1 gene. *Gene* **509**, 215-222 (2012).
110 Porazinski, S. & Ladomery, M. Alternative Splicing in the Hippo Pathway-Implications for Disease and Potential Therapeutic Targets. *Genes (Basel)* **9**, doi:10.3390/genes9030161 (2018).
111 Hong, W. & Guan, K. L. The YAP and TAZ transcription co-activators: key downstream effectors of the mammalian Hippo pathway. *Semin Cell Dev Biol* **23**, 785-793, doi:10.1016/j.semcdb.2012.05.004 (2012).
112 Varelas, X. The Hippo pathway effectors TAZ and YAP in development, homeostasis and disease. *Development* **141**, 1614-1626 (2014).
113 O'Neill, E., Rushworth, L., Baccarini, M. & Kolch, W. Role of the kinase MST2 in suppression of apoptosis by the proto-oncogene product Raf-1. *Science* **306**, 2267-2270 (2004).
114 Barron, D. A. & Kagey, J. D. The role of the Hippo pathway in human disease and tumorigenesis. *Clinical and translational medicine* **3**, 25 (2014).
115 Park, H. W. & Guan, K. L. Regulation of the Hippo pathway and implications for anticancer drug development. *Trends in pharmacological sciences* **34**, 581-589, doi:10.1016/j.tips.2013.08.006 (2013).
116 Guo, X. & Zhao, B. Integration of mechanical and chemical signals by YAP and TAZ transcription coactivators. *Cell Biosci* **3**, 33 (2013).
117 Li, Z. *et al.* Structural insights into the YAP and TEAD complex. *Genes & development* **24**, 235-240 (2010).
118 Pobbati, A. V. & Hong, W. Emerging roles of TEAD transcription factors and its coactivators in cancers. *Cancer Biol Ther* **14**, 390-398, doi:10.4161/cbt.23788 (2013).
119 Fausti, F., Di Agostino, S., Sacconi, A., Strano, S. & Blandino, G. Hippo and RASSF1A pathways: a growing Affair. *Molecular biology international* **2012** (2012).
120 Bertini, E., Oka, T., Sudol, M., Strano, S. & Blandino, G. YAP: at the crossroad between transformation and tumor suppression. *Cell Cycle* **8**, 49-57, doi:10.4161/cc.8.1.7259 (2009).

121 Matallanas, D., Romano, D., Hamilton, G., Kolch, W. & O'Neill, E. A Hippo in the ointment. *Cell Cycle* **7**, 879-884 (2008).
122 van der Weyden, L. *et al.* Loss of rassf1a synergizes with deregulated runx2 signaling in tumorigenesis. *Cancer research* **72**, 3817-3827 (2012).
123 Ehmer, U. & Sage, J. Control of Proliferation and Cancer Growth by the Hippo Signaling Pathway. *Mol Cancer Res* **14**, 127-140, doi:10.1158/1541-7786.MCR-15-0305 (2016).
124 Meng, Z., Moroishi, T. & Guan, K. L. Mechanisms of Hippo pathway regulation. *Genes & development* **30**, 1-17, doi:10.1101/gad.274027.115 (2016).
125 Schlegelmilch, K. *et al.* Yap1 acts downstream of α-catenin to control epidermal proliferation. *Cell* **144**, 782-795 (2011).
126 Piccolo, S., Dupont, S. & Cordenonsi, M. The biology of YAP/TAZ: hippo signaling and beyond. *Physiol Rev* **94**, 1287-1312, doi:10.1152/physrev.00005.2014 (2014).
127 Dupont, S. *et al.* Role of YAP/TAZ in mechanotransduction. *Nature* **474**, 179-183 (2011).
128 Aragona, M. *et al.* A mechanical checkpoint controls multicellular growth through YAP/TAZ regulation by actin-processing factors. *Cell* **154**, 1047-1059 (2013).
129 Codelia, V. A. & Irvine, K. D. Hippo signaling goes long range. *Cell* **150**, 669-670 (2012).
130 Hansen, C. G., Moroishi, T. & Guan, K. L. YAP and TAZ: a nexus for Hippo signaling and beyond. *Trends Cell Biol* **25**, 499-513, doi:10.1016/j.tcb.2015.05.002 (2015).
131 Ma, B. *et al.* Hypoxia regulates Hippo signalling through the SIAH2 ubiquitin E3 ligase. *Nat Cell Biol* **17**, 95-103, doi:10.1038/ncb3073 (2015).
132 Nakayama, K., Qi, J. & Ronai, Z. The ubiquitin ligase Siah2 and the hypoxia response. *Mol Cancer Res* **7**, 443-451, doi:10.1158/1541-7786.MCR-08-0458 (2009).
133 Xiang, L. *et al.* Hypoxia-inducible factor 1 mediates TAZ expression and nuclear localization to induce the breast cancer stem cell phenotype. *Oncotarget* **5**, 12509-12527, doi:10.18632/oncotarget.2997 (2014).
134 Xiang, L. *et al.* HIF-1α and TAZ serve as reciprocal co-activators in human breast cancer cells. *Oncotarget* **6**, 11768-11778, doi:10.18632/oncotarget.4190 (2015).
135 Dai, X. Y. *et al.* Nuclear translocation and activation of YAP by hypoxia contributes to the chemoresistance of SN38 in hepatocellular carcinoma cells. *Oncotarget* **7**, 6933-6947, doi:10.18632/oncotarget.6903 (2016).
136 Plouffe, S. W., Hong, A. W. & Guan, K. L. Disease implications of the Hippo/YAP pathway. *Trends Mol Med* **21**, 212-222, doi:10.1016/j.molmed.2015.01.003 (2015).
137 Lorenzetto, E. *et al.* YAP1 acts as oncogenic target of 11q22 amplification in multiple cancer subtypes. *Oncotarget* (2014).
138 Zanconato, F., Cordenonsi, M. & Piccolo, S. YAP/TAZ at the Roots of Cancer. *Cancer Cell* **29**, 783-803, doi:10.1016/j.ccell.2016.05.005 (2016).
139 Hao, J. *et al.* Role of Hippo signaling in cancer stem cells. *Journal of cellular physiology* **229**, 266-270 (2014).

140 Zhao, J. *et al.* Effect of YAP1 silencing on esophageal cancer. *Onco Targets Ther* **9**, 3137-3146, doi:10.2147/OTT.S102338 (2016).
141 Lee, T. F. *et al.* YAP1 is essential for tumor growth and is a potential therapeutic target for EGFR-dependent lung adenocarcinomas. *Oncotarget* **8**, 89539-89551, doi:10.18632/oncotarget.19647 (2017).
142 Yang, Z. *et al.* Knockdown of YAP1 inhibits the proliferation of osteosarcoma cells in vitro and in vivo. *Oncol Rep* **32**, 1265-1272, doi:10.3892/or.2014.3305 (2014).
143 Moroishi, T., Hansen, C. G. & Guan, K. L. The emerging roles of YAP and TAZ in cancer. *Nature reviews. Cancer* **15**, 73-79, doi:10.1038/nrc3876 (2015).
144 Sun, Z. *et al.* Prognostic Value of Yes-Associated Protein 1 (YAP1) in Various Cancers: A Meta-Analysis. *PLoS One* **10**, e0135119, doi:10.1371/journal.pone.0135119 (2015).
145 Lamar, J. M. *et al.* The Hippo pathway target, YAP, promotes metastasis through its TEAD-interaction domain. *Proceedings of the National Academy of Sciences* **109**, E2441-E2450 (2012).
146 Fullenkamp, C. A. *et al.* TAZ and YAP are frequently activated oncoproteins in sarcomas. *Oncotarget* **7**, 30094-30108, doi:10.18632/oncotarget.8979 (2016).
147 Jeong, W. *et al.* Activation of YAP1 Is Associated with Poor Prognosis and Response to Taxanes in Ovarian Cancer. *Anticancer research* **34**, 811-817 (2014).
148 Song, S. *et al.* Hippo coactivator YAP1 upregulates SOX9 and endows stem-like properties to esophageal cancer cells. *Cancer research*, canres. 3569.2013 (2014).
149 Orr, B. A. *et al.* Yes-associated protein 1 is widely expressed in human brain tumors and promotes glioblastoma growth. *J Neuropathol Exp Neurol* **70**, 568-577, doi:10.1097/NEN.0b013e31821ff8d8 (2011).
150 Zhang, H. *et al.* Expression and significance of Hippo/YAP signaling in glioma progression. *Tumour Biol*, doi:10.1007/s13277-016-5318-1 (2016).
151 Xie, D. *et al.* Levels of expression of CYR61 and CTGF are prognostic for tumor progression and survival of individuals with gliomas. *Clin Cancer Res* **10**, 2072-2081 (2004).
152 Zhang, Y. *et al.* YAP Promotes Migration and Invasion of Human Glioma Cells. *J Mol Neurosci*, doi:10.1007/s12031-017-1018-6 (2018).
153 Liu-Chittenden, Y. *et al.* Genetic and pharmacological disruption of the TEAD-YAP complex suppresses the oncogenic activity of YAP. *Genes & development* **26**, 1300-1305, doi:10.1101/gad.192856.112 (2012).
154 Scott, L. J. & Goa, K. L. Verteporfin. *Drugs Aging* **16**, 139-146; discussion 147-138 (2000).
155 Schmidt-Erfurth, U. & Hasan, T. Mechanisms of action of photodynamic therapy with verteporfin for the treatment of age-related macular degeneration. *Surv Ophthalmol* **45**, 195-214 (2000).
156 Huggett, M. T. *et al.* Phase I/II study of verteporfin photodynamic therapy in locally advanced pancreatic cancer. *Br J Cancer* **110**, 1698-1704, doi:10.1038/bjc.2014.95 (2014).

157 Ratkay, L. G., Waterfield, J. D. & Hunt, D. W. Photodynamic therapy in immune (non-oncological) disorders: focus on benzoporphyrin derivatives. *BioDrugs* **14**, 127-135 (2000).
158 Brodowska, K. *et al.* The clinically used photosensitizer Verteporfin (VP) inhibits YAP-TEAD and human retinoblastoma cell growth in vitro without light activation. *Exp Eye Res* **124**, 67-73, doi:10.1016/j.exer.2014.04.011 (2014).
159 Wei, H. *et al.* Verteporfin suppresses cell survival, angiogenesis and vasculogenic mimicry of pancreatic ductal adenocarcinoma via disrupting the YAP-TEAD complex. *Cancer Sci* **108**, 478-487, doi:10.1111/cas.13138 (2017).
160 Feng, J. *et al.* Verteporfin, a suppressor of YAP-TEAD complex, presents promising antitumor properties on ovarian cancer. *Onco Targets Ther* **9**, 5371-5381, doi:10.2147/OTT.S109979 (2016).
161 Al-Moujahed, A. *et al.* Verteporfin inhibits growth of human glioma in vitro without light activation. *Sci Rep* **7**, 7602, doi:10.1038/s41598-017-07632-8 (2017).
162 Cheng, H. *et al.* Functional genomics screen identifies YAP1 as a key determinant to enhance treatment sensitivity in lung cancer cells. *Oncotarget* **7**, 28976-28988, doi:10.18632/oncotarget.6721 (2016).
163 Pan, W. *et al.* Verteporfin can Reverse the Paclitaxel Resistance Induced by YAP Over-Expression in HCT-8/T Cells without Photoactivation through Inhibiting YAP Expression. *Cell Physiol Biochem* **39**, 481-490, doi:10.1159/000445640 (2016).
164 Fisher, M. L., Grun, D., Adhikary, G., Xu, W. & Eckert, R. L. Inhibition of YAP function overcomes BRAF inhibitor resistance in melanoma cancer stem cells. *Oncotarget* **8**, 110257-110272, doi:10.18632/oncotarget.22628 (2017).
165 Zhang, H. *et al.* Tumor-selective proteotoxicity of verteporfin inhibits colon cancer progression independently of YAP1. *Sci Signal* **8**, ra98, doi:10.1126/scisignal.aac5418 (2015).
166 Dasari, V. R. *et al.* Verteporfin exhibits YAP-independent anti-proliferative and cytotoxic effects in endometrial cancer cells. *Oncotarget* **8**, 28628-28640, doi:10.18632/oncotarget.15614 (2017).
167 Hanahan, D. & Weinberg, R. A. Hallmarks of cancer: the next generation. *Cell* **144**, 646-674, doi:10.1016/j.cell.2011.02.013 (2011).
168 Cairns, R. A., Harris, I. S. & Mak, T. W. Regulation of cancer cell metabolism. *Nature reviews. Cancer* **11**, 85-95, doi:10.1038/nrc2981 (2011).
169 Warburg, O., Wind, F. & Negelein, E. J. T. J. o. g. p. The metabolism of tumors in the body. **8**, 519 (1927).
170 Warburg, O. J. T. J. o. C. R. The metabolism of carcinoma cells. **9**, 148-163 (1925).
171 Vander Heiden, M. G., Cantley, L. C. & Thompson, C. B. Understanding the Warburg effect: the metabolic requirements of cell proliferation. *Science* **324**, 1029-1033, doi:10.1126/science.1160809 (2009).
172 Gillies, R. J., Robey, I. & Gatenby, R. A. Causes and consequences of increased glucose metabolism of cancers. *J Nucl Med* **49 Suppl 2**, 24S-42S, doi:10.2967/jnumed.107.047258 (2008).
173 WARBURG, O. On the origin of cancer cells. *Science* **123**, 309-314 (1956).

174 Guppy, M., Greiner, E. & Brand, K. The role of the Crabtree effect and an endogenous fuel in the energy metabolism of resting and proliferating thymocytes. *Eur J Biochem* **212**, 95-99 (1993).
175 Tennant, D. A., Durán, R. V., Boulahbel, H. & Gottlieb, E. Metabolic transformation in cancer. *Carcinogenesis* **30**, 1269-1280, doi:10.1093/carcin/bgp070 (2009).
176 Hosios, A. M. *et al.* Amino Acids Rather than Glucose Account for the Majority of Cell Mass in Proliferating Mammalian Cells. *Dev Cell* **36**, 540-549, doi:10.1016/j.devcel.2016.02.012 (2016).
177 DeBerardinis, R. J. & Chandel, N. S. Fundamentals of cancer metabolism. *Sci Adv* **2**, e1600200, doi:10.1126/sciadv.1600200 (2016).
178 Cantor, J. R. & Sabatini, D. M. Cancer cell metabolism: one hallmark, many faces. *Cancer Discov* **2**, 881-898, doi:10.1158/2159-8290.CD-12-0345 (2012).
179 Gray, L. R., Tompkins, S. C. & Taylor, E. B. Regulation of pyruvate metabolism and human disease. *Cell Mol Life Sci* **71**, 2577-2604, doi:10.1007/s00018-013-1539-2 (2014).
180 Cheng, T. *et al.* Pyruvate carboxylase is required for glutamine-independent growth of tumor cells. *Proc Natl Acad Sci U S A* **108**, 8674-8679, doi:10.1073/pnas.1016627108 (2011).
181 Sullivan, L. B. *et al.* Aspartate is an endogenous metabolic limitation for tumour growth. *Nature cell biology* **20**, 782-788, doi:10.1038/s41556-018-0125-0 (2018).
182 Garcia-Bermudez, J. *et al.* Aspartate is a limiting metabolite for cancer cell proliferation under hypoxia and in tumours. *Nature cell biology* **20**, 775-781, doi:10.1038/s41556-018-0118-z (2018).
183 Wise, D. R. & Thompson, C. B. Glutamine addiction: a new therapeutic target in cancer. *Trends Biochem Sci* **35**, 427-433, doi:10.1016/j.tibs.2010.05.003 (2010).
184 McGivan, J. D. & Bungard, C. I. The transport of glutamine into mammalian cells. *Front Biosci* **12**, 874-882 (2007).
185 Forman, H. J., Zhang, H. & Rinna, A. Glutathione: overview of its protective roles, measurement, and biosynthesis. *Mol Aspects Med* **30**, 1-12, doi:10.1016/j.mam.2008.08.006 (2009).
186 Altman, B. J., Stine, Z. E. & Dang, C. V. From Krebs to clinic: glutamine metabolism to cancer therapy. *Nature reviews. Cancer* **16**, 749, doi:10.1038/nrc.2016.114 (2016).
187 Enzo, E. *et al.* Aerobic glycolysis tunes YAP/TAZ transcriptional activity. *EMBO J* **34**, 1349-1370, doi:10.15252/embj.201490379 (2015).
188 Santinon, G. *et al.* dNTP metabolism links mechanical cues and YAP/TAZ to cell growth and oncogene-induced senescence. *EMBO J* **37**, doi:10.15252/embj.201797780 (2018).
189 Cox, A. G. *et al.* Yap reprograms glutamine metabolism to increase nucleotide biosynthesis and enable liver growth. *Nature cell biology* **18**, 886-896, doi:10.1038/ncb3389 (2016).
190 Bertero, T. *et al.* Vascular stiffness mechanoactivates YAP/TAZ-dependent glutaminolysis to drive pulmonary hypertension. *J Clin Invest* **126**, 3313-3335, doi:10.1172/JCI86387 (2016).

191 Du, K. *et al.* Hedgehog-YAP Signaling Pathway Regulates Glutaminolysis to Control Activation of Hepatic Stellate Cells. *Gastroenterology* **154**, 1465-1479.e1413, doi:10.1053/j.gastro.2017.12.022 (2018).
192 Kim, J. W., Gao, P. & Dang, C. V. Effects of hypoxia on tumor metabolism. *Cancer Metastasis Rev* **26**, 291-298, doi:10.1007/s10555-007-9060-4 (2007).
193 Marín-Hernández, A., Gallardo-Pérez, J. C., Ralph, S. J., Rodríguez-Enríquez, S. & Moreno-Sánchez, R. HIF-1alpha modulates energy metabolism in cancer cells by inducing over-expression of specific glycolytic isoforms. *Mini Rev Med Chem* **9**, 1084-1101 (2009).
194 Ullah, M. S., Davies, A. J. & Halestrap, A. P. The plasma membrane lactate transporter MCT4, but not MCT1, is up-regulated by hypoxia through a HIF-1alpha-dependent mechanism. *J Biol Chem* **281**, 9030-9037, doi:10.1074/jbc.M511397200 (2006).
195 Kim, J. W., Tchernyshyov, I., Semenza, G. L. & Dang, C. V. HIF-1-mediated expression of pyruvate dehydrogenase kinase: a metabolic switch required for cellular adaptation to hypoxia. *Cell Metab* **3**, 177-185, doi:10.1016/j.cmet.2006.02.002 (2006).
196 Golias, T. *et al.* Hypoxic repression of pyruvate dehydrogenase activity is necessary for metabolic reprogramming and growth of model tumours. *Sci Rep* **6**, 31146, doi:10.1038/srep31146 (2016).
197 Fendt, S. M. *et al.* Reductive glutamine metabolism is a function of the α-ketoglutarate to citrate ratio in cells. *Nat Commun* **4**, 2236, doi:10.1038/ncomms3236 (2013).
198 Metallo, C. M. *et al.* Reductive glutamine metabolism by IDH1 mediates lipogenesis under hypoxia. *Nature* **481**, 380-384, doi:10.1038/nature10602 (2011).
199 Wong, B. W., Marsch, E., Treps, L., Baes, M. & Carmeliet, P. Endothelial cell metabolism in health and disease: impact of hypoxia. *EMBO J* **36**, 2187-2203, doi:10.15252/embj.201696150 (2017).
200 Reuter, S., Gupta, S. C., Chaturvedi, M. M. & Aggarwal, B. B. Oxidative stress, inflammation, and cancer: how are they linked? *Free Radic Biol Med* **49**, 1603-1616, doi:10.1016/j.freeradbiomed.2010.09.006 (2010).
201 Sies, H., Berndt, C. & Jones, D. P. Oxidative Stress. *Annu Rev Biochem* **86**, 715-748, doi:10.1146/annurev-biochem-061516-045037 (2017).
202 Schieber, M. & Chandel, N. S. ROS function in redox signaling and oxidative stress. *Curr Biol* **24**, R453-462, doi:10.1016/j.cub.2014.03.034 (2014).
203 Pisoschi, A. M. & Pop, A. The role of antioxidants in the chemistry of oxidative stress: A review. *Eur J Med Chem* **97**, 55-74, doi:10.1016/j.ejmech.2015.04.040 (2015).
204 Tafani, M. *et al.* The Interplay of Reactive Oxygen Species, Hypoxia, Inflammation, and Sirtuins in Cancer Initiation and Progression. *Oxid Med Cell Longev* **2016**, 3907147, doi:10.1155/2016/3907147 (2016).
205 Salazar-Ramiro, A. *et al.* Role of Redox Status in Development of Glioblastoma. *Front Immunol* **7**, 156, doi:10.3389/fimmu.2016.00156 (2016).
206 Cao, S. S. & Kaufman, R. J. Endoplasmic reticulum stress and oxidative stress in cell fate decision and human disease. *Antioxid Redox Signal* **21**, 396-413, doi:10.1089/ars.2014.5851 (2014).

207 Malhotra, J. D. *et al.* Antioxidants reduce endoplasmic reticulum stress and improve protein secretion. *Proc Natl Acad Sci U S A* **105**, 18525-18530, doi:10.1073/pnas.0809677105 (2008).
208 Reitman, Z. J. *et al.* Profiling the effects of isocitrate dehydrogenase 1 and 2 mutations on the cellular metabolome. *Proc Natl Acad Sci U S A* **108**, 3270-3275, doi:10.1073/pnas.1019393108 (2011).
209 Hollinshead, K. E. R. *et al.* Oncogenic IDH1 Mutations Promote Enhanced Proline Synthesis through PYCR1 to Support the Maintenance of Mitochondrial Redox Homeostasis. *Cell Rep* **22**, 3107-3114, doi:10.1016/j.celrep.2018.02.084 (2018).
210 Yuhas, J. M., Li, A. P., Martinez, A. O. & Ladman, A. J. A simplified method for production and growth of multicellular tumor spheroids. *Cancer Research* **37**, 3639-3643 (1977).
211 Schindelin, J. *et al.* Fiji: an open-source platform for biological-image analysis. *Nat Methods* **9**, 676-682, doi:10.1038/nmeth.2019 (2012).
212 Fitzpatrick, M. *Measuring cell fluorescence using Image J* <https://theolb.readthedocs.io/en/latest/imaging/measuring-cell-fluorescence-using-imagej.html> (2014). (23.09.18).
213 Hu, C. J., Sataur, A., Wang, L., Chen, H. & Simon, M. C. The N-terminal transactivation domain confers target gene specificity of hypoxia-inducible factors HIF-1alpha and HIF-2alpha. *Mol Biol Cell* **18**, 4528-4542, doi:10.1091/mbc.E06-05-0419 (2007).
214 Jang, C., Chen, L. & Rabinowitz, J. D. Metabolomics and Isotope Tracing. *Cell* **173**, 822-837, doi:10.1016/j.cell.2018.03.055 (2018).
215 Antoniewicz, M. R. A guide to. *Exp Mol Med* **50**, 19, doi:10.1038/s12276-018-0060-y (2018).
216 Zhang, J. *et al.* 13C isotope-assisted methods for quantifying glutamine metabolism in cancer cells. *Methods Enzymol* **542**, 369-389, doi:10.1016/B978-0-12-416618-9.00019-4 (2014).
217 Buescher, J. M. *et al.* A roadmap for interpreting (13)C metabolite labeling patterns from cells. *Curr Opin Biotechnol* **34**, 189-201, doi:10.1016/j.copbio.2015.02.003 (2015).
218 Hiller, K. *et al.* MetaboliteDetector: comprehensive analysis tool for targeted and nontargeted GC/MS based metabolome analysis. *Anal Chem* **81**, 3429-3439, doi:10.1021/ac802689c (2009).
219 Wlodkowic, D., Telford, W., Skommer, J. & Darzynkiewicz, Z. Apoptosis and beyond: cytometry in studies of programmed cell death. *Methods Cell Biol* **103**, 55-98, doi:10.1016/B978-0-12-385493-3.00004-8 (2011).
220 Figueroa, D., Asaduzzaman, M. & Young, F. Real time monitoring and quantification of reactive oxygen species in breast cancer cell line MCF-7 by 2',7'-dichlorofluorescin diacetate (DCFDA) assay. *J Pharmacol Toxicol Methods* **94**, 26-33, doi:10.1016/j.vascn.2018.03.007 (2018).
221 Mattaini, K. R., Sullivan, M. R. & Vander Heiden, M. G. The importance of serine metabolism in cancer. *J Cell Biol* **214**, 249-257, doi:10.1083/jcb.201604085 (2016).
222 Yang, M. & Vousden, K. H. Serine and one-carbon metabolism in cancer. *Nature reviews. Cancer* **16**, 650-662, doi:10.1038/nrc.2016.81 (2016).

223 Amelio, I., Cutruzzolá, F., Antonov, A., Agostini, M. & Melino, G. Serine and glycine metabolism in cancer. *Trends Biochem Sci* **39**, 191-198, doi:10.1016/j.tibs.2014.02.004 (2014).
224 Hensley, C. T., Wasti, A. T. & DeBerardinis, R. J. Glutamine and cancer: cell biology, physiology, and clinical opportunities. *J Clin Invest* **123**, 3678-3684, doi:10.1172/JCI69600 (2013).
225 Tanner, J. J., Fendt, S. M. & Becker, D. F. The Proline Cycle As a Potential Cancer Therapy Target. *Biochemistry* **57**, 3433-3444, doi:10.1021/acs.biochem.8b00215 (2018).
226 Brown, J. M. & Wilson, W. R. Exploiting tumour hypoxia in cancer treatment. *Nature reviews. Cancer* **4**, 437-447, doi:10.1038/nrc1367 (2004).
227 Li, P., Zhou, C., Xu, L. & Xiao, H. Hypoxia enhances stemness of cancer stem cells in glioblastoma: an in vitro study. *Int J Med Sci* **10**, 399-407, doi:10.7150/ijms.5407 (2013).
228 Swinson, D. E. & O'Byrne, K. J. Interactions between hypoxia and epidermal growth factor receptor in non-small-cell lung cancer. *Clin Lung Cancer* **7**, 250-256, doi:10.3816/CLC.2006.n.002 (2006).
229 Yan, L., Cai, Q. & Xu, Y. Hypoxic conditions differentially regulate TAZ and YAP in cancer cells. *Arch Biochem Biophys* **562**, 31-36, doi:10.1016/j.abb.2014.07.024 (2014).
230 Chittaranjan, S. *et al.* Mutations in CIC and IDH1 cooperatively regulate 2-hydroxyglutarate levels and cell clonogenicity. *Oncotarget* **5**, 7960-7979, doi:10.18632/oncotarget.2401 (2014).
231 Xu, W. *et al.* Oncometabolite 2-hydroxyglutarate is a competitive inhibitor of α-ketoglutarate-dependent dioxygenases. *Cancer Cell* **19**, 17-30, doi:10.1016/j.ccr.2010.12.014 (2011).
232 Ploumakis, A. & Coleman, M. L. OH, the Places You'll Go! Hydroxylation, Gene Expression, and Cancer. *Mol Cell* **58**, 729-741, doi:10.1016/j.molcel.2015.05.026 (2015).
233 Xia, Y., Zhang, Y. L., Yu, C., Chang, T. & Fan, H. Y. YAP/TEAD co-activator regulated pluripotency and chemoresistance in ovarian cancer initiated cells. *PLoS One* **9**, e109575, doi:10.1371/journal.pone.0109575 (2014).
234 He, C. *et al.* The Hippo/YAP pathway interacts with EGFR signaling and HPV oncoproteins to regulate cervical cancer progression. *EMBO Mol Med* **7**, 1426-1449, doi:10.15252/emmm.201404976 (2015).
235 Wang, C. *et al.* Knockdown of yes-associated protein inhibits proliferation and downregulates large tumor suppressor 1 expression in MHCC97H human hepatocellular carcinoma cells. *Mol Med Rep* **11**, 4101-4108, doi:10.3892/mmr.2015.3257 (2015).
236 Lu, T., Sun, L. & Zhu, X. Yes-associated protein enhances proliferation and attenuates sensitivity to cisplatin in human gastric cancer cells. *Biomed Pharmacother* **105**, 1269-1275, doi:10.1016/j.biopha.2018.06.031 (2018).
237 Yang, R. *et al.* The Hippo transducer TAZ promotes cell proliferation and tumor formation of glioblastoma cells through EGFR pathway. *Oncotarget* **7**, 36255-36265, doi:10.18632/oncotarget.9199 (2016).
238 Finch-Edmondson, M. L. *et al.* TAZ Protein Accumulation Is Negatively Regulated by YAP Abundance in Mammalian Cells. *J Biol Chem* **290**, 27928-27938, doi:10.1074/jbc.M115.692285 (2015).

239 Liberti, M. V. & Locasale, J. W. The Warburg Effect: How Does it Benefit Cancer Cells? *Trends Biochem Sci* **41**, 211-218, doi:10.1016/j.tibs.2015.12.001 (2016).
240 Dong, W., Keibler, M. A. & Stephanopoulos, G. Review of metabolic pathways activated in cancer cells as determined through isotopic labeling and network analysis. *Metab Eng* **43**, 113-124, doi:10.1016/j.ymben.2017.02.002 (2017).
241 Newman, A. C. & Maddocks, O. D. K. Serine and Functional Metabolites in Cancer. *Trends Cell Biol* **27**, 645-657, doi:10.1016/j.tcb.2017.05.001 (2017).
242 Samanta, D. *et al.* PHGDH Expression Is Required for Mitochondrial Redox Homeostasis, Breast Cancer Stem Cell Maintenance, and Lung Metastasis. *Cancer Res* **76**, 4430-4442, doi:10.1158/0008-5472.CAN-16-0530 (2016).
243 Semenza, G. L. Hypoxia-inducible factors: coupling glucose metabolism and redox regulation with induction of the breast cancer stem cell phenotype. *EMBO J* **36**, 252-259, doi:10.15252/embj.201695204 (2017).
244 Ye, J. *et al.* Pyruvate kinase M2 promotes de novo serine synthesis to sustain mTORC1 activity and cell proliferation. *Proc Natl Acad Sci U S A* **109**, 6904-6909, doi:10.1073/pnas.1204176109 (2012).
245 Yang, W. *et al.* EGFR-induced and PKCε monoubiquitylation-dependent NF-κB activation upregulates PKM2 expression and promotes tumorigenesis. *Mol Cell* **48**, 771-784, doi:10.1016/j.molcel.2012.09.028 (2012).
246 Shi, Y. *et al.* Nuclear EGFR-PKM2 axis induces cancer stem cell-like characteristics in irradiation-resistant cells. *Cancer Lett* **422**, 81-93, doi:10.1016/j.canlet.2018.02.028 (2018).
247 Luo, W. *et al.* Pyruvate kinase M2 is a PHD3-stimulated coactivator for hypoxia-inducible factor 1. *Cell* **145**, 732-744, doi:10.1016/j.cell.2011.03.054 (2011).
248 Yang, C. S. *et al.* Glutamine-utilizing transaminases are a metabolic vulnerability of TAZ/YAP-activated cancer cells. *EMBO Rep* **19**, doi:10.15252/embr.201643577 (2018).
249 Labuschagne, C. F., van den Broek, N. J., Mackay, G. M., Vousden, K. H. & Maddocks, O. D. Serine, but not glycine, supports one-carbon metabolism and proliferation of cancer cells. *Cell Rep* **7**, 1248-1258, doi:10.1016/j.celrep.2014.04.045 (2014).
250 Maddocks, O. D. K. *et al.* Modulating the therapeutic response of tumours to dietary serine and glycine starvation. *Nature* **544**, 372-376, doi:10.1038/nature22056 (2017).
251 Rong, Y. *et al.* Lactate dehydrogenase A is overexpressed in pancreatic cancer and promotes the growth of pancreatic cancer cells. *Tumour Biol* **34**, 1523-1530, doi:10.1007/s13277-013-0679-1 (2013).
252 Le, A. *et al.* Inhibition of lactate dehydrogenase A induces oxidative stress and inhibits tumor progression. *Proc Natl Acad Sci U S A* **107**, 2037-2042, doi:10.1073/pnas.0914433107 (2010).
253 Still, E. R. & Yuneva, M. O. Hopefully devoted to Q: targeting glutamine addiction in cancer. *Br J Cancer* **116**, 1375-1381, doi:10.1038/bjc.2017.113 (2017).
254 Yuneva, M. O. *et al.* The metabolic profile of tumors depends on both the responsible genetic lesion and tissue type. *Cell metabolism* **15**, 157-170, doi:10.1016/j.cmet.2011.12.015 (2012).

255 Huang, F., Zhang, Q., Ma, H., Lv, Q. & Zhang, T. Expression of glutaminase is upregulated in colorectal cancer and of clinical significance. *Int J Clin Exp Pathol* **7**, 1093-1100 (2014).
256 Sullivan, L. B. *et al.* Supporting Aspartate Biosynthesis Is an Essential Function of Respiration in Proliferating Cells. *Cell* **162**, 552-563, doi:10.1016/j.cell.2015.07.017 (2015).
257 Smith, R. J. & Phang, J. M. The importance of ornithine as a precursor for proline in mammalian cells. *J Cell Physiol* **98**, 475-481, doi:10.1002/jcp.1040980306 (1979).
258 Rohwer, N. & Cramer, T. Hypoxia-mediated drug resistance: novel insights on the functional interaction of HIFs and cell death pathways. *Drug Resist Updat* **14**, 191-201, doi:10.1016/j.drup.2011.03.001 (2011).
259 Maher, E. A. *et al.* Malignant glioma: genetics and biology of a grave matter. *Genes & development* **15**, 1311-1333, doi:10.1101/gad.891601 (2001).
260 Newlands, E. S., Stevens, M. F., Wedge, S. R., Wheelhouse, R. T. & Brock, C. Temozolomide: a review of its discovery, chemical properties, pre-clinical development and clinical trials. *Cancer Treat Rev* **23**, 35-61 (1997).
261 Belzacq, A. S. *et al.* Apoptosis induction by the photosensitizer verteporfin: identification of mitochondrial adenine nucleotide translocator as a critical target. *Cancer Res* **61**, 1260-1264 (2001).
262 Chen, M. *et al.* Verteporfin Inhibits Cell Proliferation and Induces Apoptosis in Human Leukemia NB4 Cells without Light Activation. *Int J Med Sci* **14**, 1031-1039, doi:10.7150/ijms.19682 (2017).
263 Borovikova, L. V. *et al.* Vagus nerve stimulation attenuates the systemic inflammatory response to endotoxin. *Nature* **405**, 458-462 (2000).
264 Donohue, E. *et al.* Inhibition of autophagosome formation by the benzoporphyrin derivative verteporfin. *J Biol Chem* **286**, 7290-7300, doi:10.1074/jbc.M110.139915 (2011).
265 Sleire, L. *et al.* Drug repurposing in cancer. *Pharmacol Res* **124**, 74-91, doi:10.1016/j.phrs.2017.07.013 (2017).
266 Palumbo, A. *et al.* Thalidomide for treatment of multiple myeloma: 10 years later. *Blood* **111**, 3968-3977, doi:10.1182/blood-2007-10-117457 (2008).
267 Chae, Y. K. *et al.* Repurposing metformin for cancer treatment: current clinical studies. *Oncotarget* **7**, 40767-40780, doi:10.18632/oncotarget.8194 (2016).
268 Rusten, T. E. & Stenmark, H. p62, an autophagy hero or culprit? *Nature cell biology* **12**, 207-209, doi:10.1038/ncb0310-207 (2010).
269 Jaakkola, P. *et al.* Targeting of HIF-alpha to the von Hippel-Lindau ubiquitylation complex by O2-regulated prolyl hydroxylation. *Science* **292**, 468-472, doi:10.1126/science.1059796 (2001).
270 Milkiewicz, M., Pugh, C. W. & Egginton, S. Inhibition of endogenous HIF inactivation induces angiogenesis in ischaemic skeletal muscles of mice. *J Physiol* **560**, 21-26, doi:10.1113/jphysiol.2004.069757 (2004).
271 Maltese, W. A. & Overmeyer, J. H. Methuosis: nonapoptotic cell death associated with vacuolization of macropinosome and endosome compartments. *Am J Pathol* **184**, 1630-1642, doi:10.1016/j.ajpath.2014.02.028 (2014).

272 Shubin, A. V., Demidyuk, I. V., Komissarov, A. A., Rafieva, L. M. & Kostrov, S. V. Cytoplasmic vacuolization in cell death and survival. *Oncotarget* **7**, 55863-55889, doi:10.18632/oncotarget.10150 (2016).
273 Bates, R. C., Edwards, N. S. & Yates, J. D. Spheroids and cell survival. *Critical reviews in oncology/hematology* **36**, 61-74 (2000).
274 Molla, A., Couvet, M. & Coll, J. L. Unsuccessful mitosis in multicellular tumour spheroids. *Oncotarget* **8**, 28769-28784, doi:10.18632/oncotarget.15673 (2017).
275 Wang, C. *et al.* Verteporfin inhibits YAP function through up-regulating 14-3-3σ sequestering YAP in the cytoplasm. *Am J Cancer Res* **6**, 27-37 (2016).
276 Lee, S. Y. Temozolomide resistance in glioblastoma multiforme. *Genes & Diseases* **3**, 198-210 (2016).
277 Chen, R. *et al.* High mobility group protein B1 controls liver cancer initiation through yes-associated protein -dependent aerobic glycolysis. *Hepatology* **67**, 1823-1841, doi:10.1002/hep.29663 (2018).
278 European Medicines Agency. *Visudyne*, <http://www.ema.europa.eu/docs/en_GB/document_library/EPAR_-_Product_Information/human/000305/WC500052407.pdf> (2018) (23.09.18).
279 Strano, S. *et al.* Physical interaction with Yes-associated protein enhances p73 transcriptional activity. *J Biol Chem* **276**, 15164-15173, doi:10.1074/jbc.M010484200 (2001).
280 Dobbelstein, M., Strano, S., Roth, J. & Blandino, G. p73-induced apoptosis: a question of compartments and cooperation. *Biochem Biophys Res Commun* **331**, 688-693, doi:10.1016/j.bbrc.2005.03.155 (2005).
281 Nekulová, M., Zitterbart, K., Sterba, J. & Veselská, R. Analysis of the intracellular localization of p73 N-terminal protein isoforms TAp73 and ΔNp73 in medulloblastoma cell lines. *J Mol Histol* **41**, 267-275, doi:10.1007/s10735-010-9288-0 (2010).
282 Inoue, T., Stuart, J., Leno, R. & Maki, C. G. Nuclear import and export signals in control of the p53-related protein p73. *J Biol Chem* **277**, 15053-15060, doi:10.1074/jbc.M200248200 (2002).
283 Aqeilan, R. I. *et al.* Functional association between Wwox tumor suppressor protein and p73, a p53 homolog. *Proc Natl Acad Sci U S A* **101**, 4401-4406, doi:10.1073/pnas.0400805101 (2004).
284 Salah, Z., Aqeilan, R. & Huebner, K. WWOX gene and gene product: tumor suppression through specific protein interactions. *Future Oncol* **6**, 249-259, doi:10.2217/fon.09.152 (2010).
285 Reuven, N., Shanzer, M. & Shaul, Y. Tyrosine phosphorylation of WW proteins. *Exp Biol Med (Maywood)* **240**, 375-382, doi:10.1177/1535370214565991 (2015).
286 Yoon, M. K., Ha, J. H., Lee, M. S. & Chi, S. W. Structure and apoptotic function of p73. *BMB Rep* **48**, 81-90 (2015).
287 Maisse, C., Guerrieri, P. & Melino, G. p73 and p63 protein stability: the way to regulate function? *Biochem Pharmacol* **66**, 1555-1561 (2003).
288 Ramadan, S. *et al.* p73 induces apoptosis by different mechanisms. *Biochem Biophys Res Commun* **331**, 713-717, doi:10.1016/j.bbrc.2005.03.156 (2005).

289 Konstantinou, E. K. *et al.* Verteporfin-induced formation of protein cross-linked oligomers and high molecular weight complexes is mediated by light and leads to cell toxicity. *Sci Rep* **7**, 46581, doi:10.1038/srep46581 (2017).
290 Semenza, G. L. Hypoxia-inducible factor 1: master regulator of O2 homeostasis. *Curr Opin Genet Dev* **8**, 588-594 (1998).
291 Chiou, J. F., Wang, Y. H., Jou, M. J., Liu, T. Z. & Shiau, C. Y. Verteporfin-photoinduced apoptosis in HepG2 cells mediated by reactive oxygen and nitrogen species intermediates. *Free Radic Res* **44**, 155-170, doi:10.3109/10715760903380458 (2010).
292 Degterev, A. & Yuan, J. Expansion and evolution of cell death programmes. *Nat Rev Mol Cell Biol* **9**, 378-390, doi:10.1038/nrm2393 (2008).
293 Golstein, P. & Kroemer, G. Cell death by necrosis: towards a molecular definition. *Trends Biochem Sci* **32**, 37-43, doi:10.1016/j.tibs.2006.11.001 (2007).
294 Degterev, A. *et al.* Chemical inhibitor of nonapoptotic cell death with therapeutic potential for ischemic brain injury. *Nat Chem Biol* **1**, 112-119, doi:10.1038/nchembio711 (2005).
295 Degterev, A. *et al.* Identification of RIP1 kinase as a specific cellular target of necrostatins. *Nat Chem Biol* **4**, 313-321, doi:10.1038/nchembio.83 (2008).
296 Nikoletopoulou, V., Markaki, M., Palikaras, K. & Tavernarakis, N. Crosstalk between apoptosis, necrosis and autophagy. *Biochim Biophys Acta* **1833**, 3448-3459, doi:10.1016/j.bbamcr.2013.06.001 (2013).
297 Storr, S. J., Carragher, N. O., Frame, M. C., Parr, T. & Martin, S. G. The calpain system and cancer. *Nature reviews. Cancer* **11**, 364-374, doi:10.1038/nrc3050 (2011).
298 Chen, S. *et al.* Critical contribution of RIPK1 mediated mitochondrial dysfunction and oxidative stress to compression-induced rat nucleus pulposus cells necroptosis and apoptosis. *Apoptosis*, doi:10.1007/s10495-018-1455-x (2018).
299 Crompton, M., Ellinger, H. & Costi, A. Inhibition by cyclosporin A of a Ca2+-dependent pore in heart mitochondria activated by inorganic phosphate and oxidative stress. *The Biochemical journal* **255**, 357-360 (1988).
300 Rao, V. K., Carlson, E. A. & Yan, S. S. Mitochondrial permeability transition pore is a potential drug target for neurodegeneration. *Biochim Biophys Acta* **1842**, 1267-1272, doi:10.1016/j.bbadis.2013.09.003 (2014).
301 Davidson, W. *et al.* Inhibition of p73 function by Pifithrin-alpha as revealed by studies in zebrafish embryos. *Cell Cycle* **7**, 1224-1230, doi:10.4161/cc.7.9.5786 (2008).
302 Redmann, M. *et al.* Inhibition of autophagy with bafilomycin and chloroquine decreases mitochondrial quality and bioenergetic function in primary neurons. *Redox Biol* **11**, 73-81, doi:10.1016/j.redox.2016.11.004 (2017).
303 Fucikova, J. *et al.* Relevance of the chaperone-like protein calreticulin for the biological behavior and clinical outcome of cancer. *Immunol Lett* **193**, 25-34, doi:10.1016/j.imlet.2017.11.006 (2018).
304 Meusser, B., Hirsch, C., Jarosch, E. & Sommer, T. ERAD: the long road to destruction. *Nature cell biology* **7**, 766-772, doi:10.1038/ncb0805-766 (2005).

305 Hirabayashi, M. *et al.* VCP/p97 in abnormal protein aggregates, cytoplasmic vacuoles, and cell death, phenotypes relevant to neurodegeneration. *Cell Death Differ* **8**, 977-984, doi:10.1038/sj.cdd.4400907 (2001).
306 McKibbin, C. *et al.* Inhibition of protein translocation at the endoplasmic reticulum promotes activation of the unfolded protein response. *The Biochemical journal* **442**, 639-648, doi:10.1042/BJ20111220 (2012).
307 Auner, H. W. *et al.* Combined inhibition of p97 and the proteasome causes lethal disruption of the secretory apparatus in multiple myeloma cells. *PLoS One* **8**, e74415, doi:10.1371/journal.pone.0074415 (2013).
308 Wang, Q., Li, L. & Ye, Y. Inhibition of p97-dependent protein degradation by Eeyarestatin I. *J Biol Chem* **283**, 7445-7454, doi:10.1074/jbc.M708347200 (2008).
309 Wang, Q. *et al.* The ERAD inhibitor Eeyarestatin I is a bifunctional compound with a membrane-binding domain and a p97/VCP inhibitory group. *PLoS One* **5**, e15479, doi:10.1371/journal.pone.0015479 (2010).
310 Wang, Q. *et al.* ERAD inhibitors integrate ER stress with an epigenetic mechanism to activate BH3-only protein NOXA in cancer cells. *Proc Natl Acad Sci U S A* **106**, 2200-2205, doi:10.1073/pnas.0807611106 (2009).
311 Wang, F., Song, W., Brancati, G. & Segatori, L. Inhibition of endoplasmic reticulum-associated degradation rescues native folding in loss of function protein misfolding diseases. *J Biol Chem* **286**, 43454-43464, doi:10.1074/jbc.M111.274332 (2011).
312 Shah, P. P. & Beverly, L. J. Regulation of VCP/p97 demonstrates the critical balance between cell death and epithelial-mesenchymal transition (EMT) downstream of ER stress. *Oncotarget* **6**, 17725-17737, doi:10.18632/oncotarget.3918 (2015).
313 Duranteau, J., Chandel, N. S., Kulisz, A., Shao, Z. & Schumacker, P. T. Intracellular signaling by reactive oxygen species during hypoxia in cardiomyocytes. *J Biol Chem* **273**, 11619-11624 (1998).
314 Wilcox, C. S. Effects of tempol and redox-cycling nitroxides in models of oxidative stress. *Pharmacol Ther* **126**, 119-145, doi:10.1016/j.pharmthera.2010.01.003 (2010).
315 Piñero, D. J. & Connor, J. R. Iron in the brain: an important contributor in normal and diseased states. *The Neuroscientist* **6**, 435-453 (2000).
316 Bystrom, L. M., Guzman, M. L. & Rivella, S. Iron and reactive oxygen species: friends or foes of cancer cells? *Antioxid Redox Signal* **20**, 1917-1924, doi:10.1089/ars.2012.5014 (2014).
317 Manz, D. H., Blanchette, N. L., Paul, B. T., Torti, F. M. & Torti, S. V. Iron and cancer: recent insights. *Ann N Y Acad Sci* **1368**, 149-161, doi:10.1111/nyas.13008 (2016).
318 Schonberg, D. L. *et al.* Preferential Iron Trafficking Characterizes Glioblastoma Stem-like Cells. *Cancer Cell* **28**, 441-455, doi:10.1016/j.ccell.2015.09.002 (2015).
319 Torti, S. V. & Torti, F. M. Iron and cancer: more ore to be mined. *Nature reviews. Cancer* **13**, 342-355, doi:10.1038/nrc3495 (2013).
320 Borah, K. D. & Bhuyan, J. Magnesium porphyrins with relevance to chlorophylls. *Dalton Trans* **46**, 6497-6509, doi:10.1039/c7dt00823f (2017).

321 Kehrer, J. P. The Haber-Weiss reaction and mechanisms of toxicity. *Toxicology* **149**, 43-50 (2000).
322 Ensing, B., Buda, F. & Baerends, E. J. Fenton-like Chemistry in Water: Oxidation Catalysis by Fe(III) and H2O2. *The Journal of Physical Chemistry A* **107**, 5722-5731, doi:10.1021/jp0267149 (2003).
323 Starke, P. E. & Farber, J. L. Ferric iron and superoxide ions are required for the killing of cultured hepatocytes by hydrogen peroxide. Evidence for the participation of hydroxyl radicals formed by an iron-catalyzed Haber-Weiss reaction. *J Biol Chem* **260**, 10099-10104 (1985).
324 Nagababu, E. & Rifkind, J. M. Heme degradation by reactive oxygen species. *Antioxid Redox Signal* **6**, 967-978, doi:10.1089/ars.2004.6.967 (2004).
325 Chen, H. & Shi, H. A reducing environment stabilizes HIF-2alpha in SH-SY5Y cells under hypoxic conditions. *FEBS Lett* **582**, 3899-3902, doi:10.1016/j.febslet.2008.10.031 (2008).
326 Kramarenko, G. G., Wilke, W. W., Dayal, D., Buettner, G. R. & Schafer, F. Q. Ascorbate enhances the toxicity of the photodynamic action of Verteporfin in HL-60 cells. *Free Radic Biol Med* **40**, 1615-1627, doi:10.1016/j.freeradbiomed.2005.12.027 (2006).
327 CRUK. *Tackle cancers with substantial unmet need: our research strategy*<https://www.cancerresearchuk.org/funding-for-researchers/our-research-strategy/tackle-cancers-with-substantial-unmet-need> (2018). (23.09.18).
328 CRUK. *Cancer survival for common cancers*, <https://www.cancerresearchuk.org/health-professional/cancer-statistics/survival/common-cancers-compared#heading-Two> (2018). (23.09.18).
329 Ferreira, D., Adega, F. & Chaves, R. *Oncogenomics and cancer proteomics-novel approaches in biomarkers discovery and therapeutic targets in cancer* Intech, (2013).
330 Lenting, K., Verhaak, R., Ter Laan, M., Wesseling, P. & Leenders, W. Glioma: experimental models and reality. *Acta Neuropathol* **133**, 263-282, doi:10.1007/s00401-017-1671-4 (2017).
331 Gomez-Roman, N., Stevenson, K., Gilmour, L., Hamilton, G. & Chalmers, A. J. A novel 3D human glioblastoma cell culture system for modeling drug and radiation responses. *Neuro Oncol* **19**, 229-241, doi:10.1093/neuonc/now164 (2017).
332 Chalmers, A. J. Overcoming resistance of glioblastoma to conventional cytotoxic therapies by the addition of PARP inhibitors. *Anticancer Agents Med Chem* **10**, 520-533 (2010).
333 Halford, S. E. R. *et al.* Results of the OPARATIC trial: A phase I dose escalation study of olaparib in combination with temozolomide (TMZ) in patients with relapsed glioblastoma (GBM). *Journal of Clinical Oncology* **35**, 2022-2022, doi:10.1200/JCO.2017.35.15_suppl.2022 (2017).
334 Kling, J. Hypoxia-activated prodrugs forge ahead in cancer. *Nat Biotechnol* **30**, 381, doi:10.1038/nbt0512-381 (2012).
335 Castellano, J. *et al.* Hypoxia stimulates low-density lipoprotein receptor-related protein-1 expression through hypoxia-inducible factor-1α in human vascular

smooth muscle cells. *Arterioscler Thromb Vasc Biol* **31**, 1411-1420, doi:10.1161/ATVBAHA.111.225490 (2011).

336 Hadjipanayis, C. G., Widhalm, G. & Stummer, W. What is the Surgical Benefit of Utilizing 5-Aminolevulinic Acid for Fluorescence-Guided Surgery of Malignant Gliomas? *Neurosurgery* **77**, 663-673, doi:10.1227/NEU.0000000000000929 (2015).

Appendices:

Materials and Methods:

Appendix 1- Target sequences for ON-TARGETplus Human YAP1 and TAZ (WWTR1) siRNA.

Raw Data:

Appendix 2-

Spectra from MS metal ion binding experiment (Figure 3.36D) conducted by Mr. E. Wilkinson and The School of Chemistry, UoB.

Appendix 1- Target sequences for ON-TARGETplus Human YAP1 (A) and TAZ (WWTR1; B) siRNA.

A

L-012200-00-0005, ON-TARGETplus Human YAP1 (10413) siRNA - SMARTpool, 5 nmol

ON-TARGETplus SMARTpool siRNA J-012200-05, YAP1	
Target Sequence:	GCACCUAUCACUCUCGAGA
Mol. Wt.	Ext. Coeff.
13,444.9 (g/mol)	367,659 (L/mol·cm)
ON-TARGETplus SMARTpool siRNA J-012200-06, YAP1	
Target Sequence:	UGAGAACAAUGACGACCAA
Mol. Wt.	Ext. Coeff.
13,414.7 (g/mol)	374,957 (L/mol·cm)
ON-TARGETplus SMARTpool siRNA J-012200-07, YAP1	
Target Sequence:	GGUCAGAGAUACUUCUUAA
Mol. Wt.	Ext. Coeff.
13,399.8 (g/mol)	382,611 (L/mol·cm)
ON-TARGETplus SMARTpool siRNA J-012200-08, YAP1	
Target Sequence:	CCACCAAGCUAGAUAAAGA
Mol. Wt.	Ext. Coeff.
13,414.9 (g/mol)	375,046 (L/mol·cm)

B

L-016083-00-0005, ON-TARGETplus Human WWTR1 (25937) siRNA - SMARTpool, 5 nmol

ON-TARGETplus SMARTpool siRNA J-016083-05, WWTR1	
Target Sequence:	CCGCAGGGCUCAUGAGUAU
Mol. Wt.	Ext. Coeff.
13,459.8 (g/mol)	361,429 (L/mol·cm)
ON-TARGETplus SMARTpool siRNA J-016083-06, WWTR1	
Target Sequence:	GGACAAACACCCAUGAACA
Mol. Wt.	Ext. Coeff.
13,429.9 (g/mol)	369,617 (L/mol·cm)
ON-TARGETplus SMARTpool siRNA J-016083-07, WWTR1	
Target Sequence:	AGGAACAAACGUUGACUUA
Mol. Wt.	Ext. Coeff.
13,399.9 (g/mol)	380,564 (L/mol·cm)
ON-TARGETplus SMARTpool siRNA J-016083-08, WWTR1	
Target Sequence:	CCAAAUCUCGUGAUGAAUC
Mol. Wt.	Ext. Coeff.
13,414.9 (g/mol)	375,936 (L/mol·cm)

Appendix 2- Spectra from MS metal ion binding experiment (Figure 4.34D).

VP and $FeCl_3$

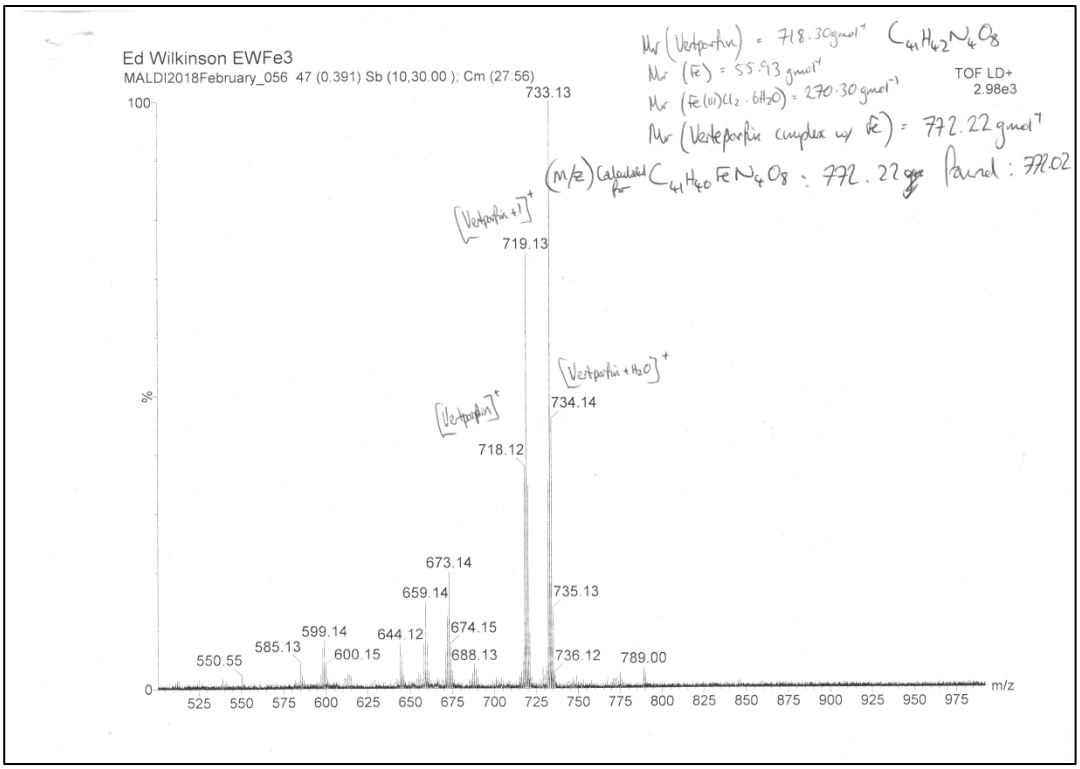

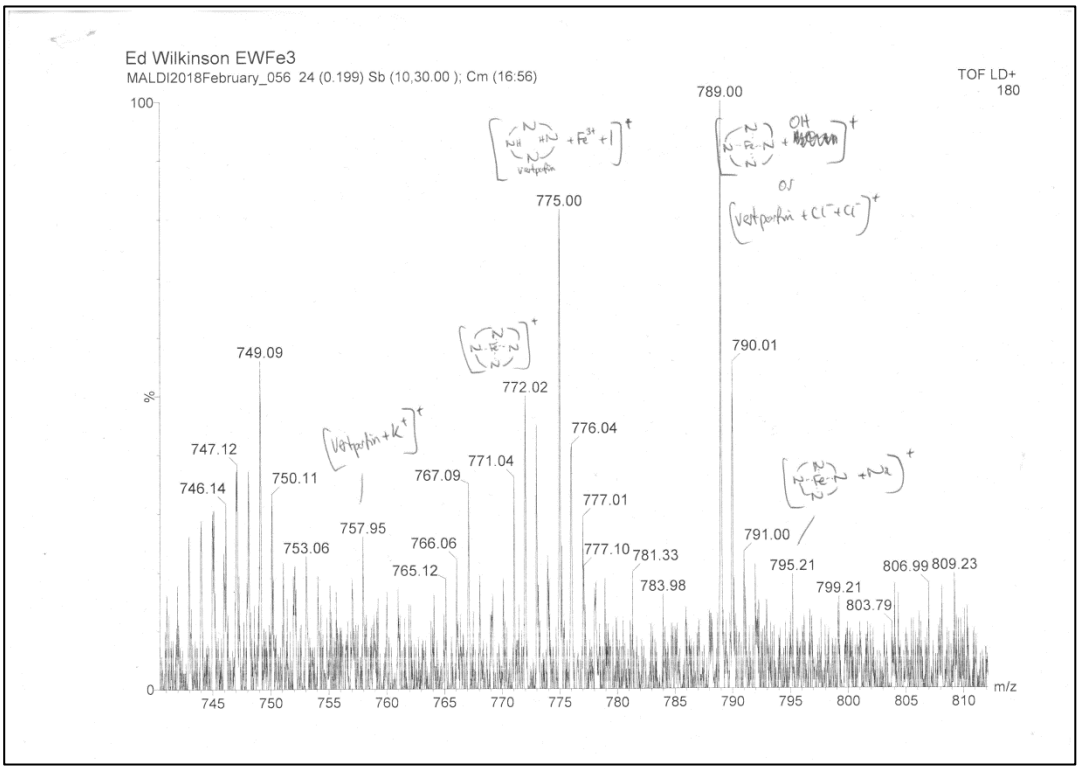

VP and $FeCl_2$

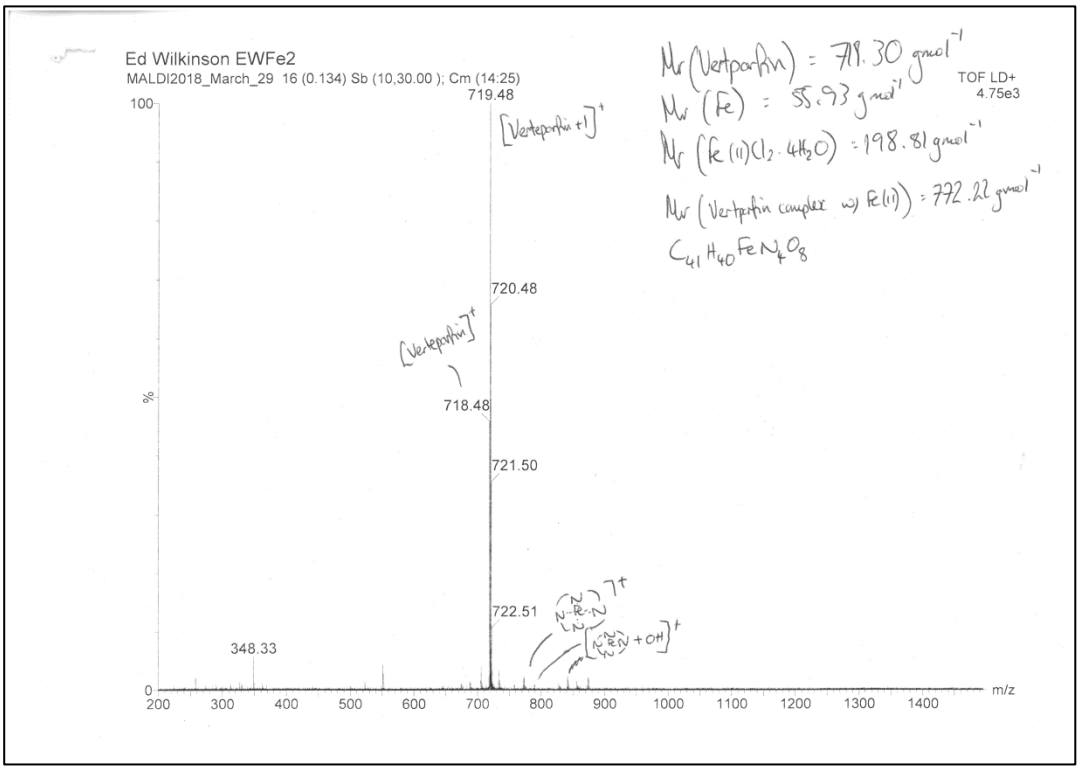
Ed Wilkinson EWFe2
MALDI2018_March_29 16 (0.134) Sb (10,30.00); Cm (14:25)
TOF LD+
4.75e3
719.48
[Verteporfin+1]+
720.48
[Verteporfin]+
718.48
721.50
722.51
348.33
100
%
0
200
300
400
500
600
700
800
900
1000
1100
1200
1300
1400
m/z
Mr (Verteporfin) = 719.30 gmol-1
Mr (Fe) = 55.93 gmol-1
Mr (Fe(II)Cl2.4H2O) = 198.81 gmol-1
Mr (Verteporfin complex w) Fe(II)) = 772.22 gmol-1
C41H40FeN4O8

VP and $ZnCl_2$

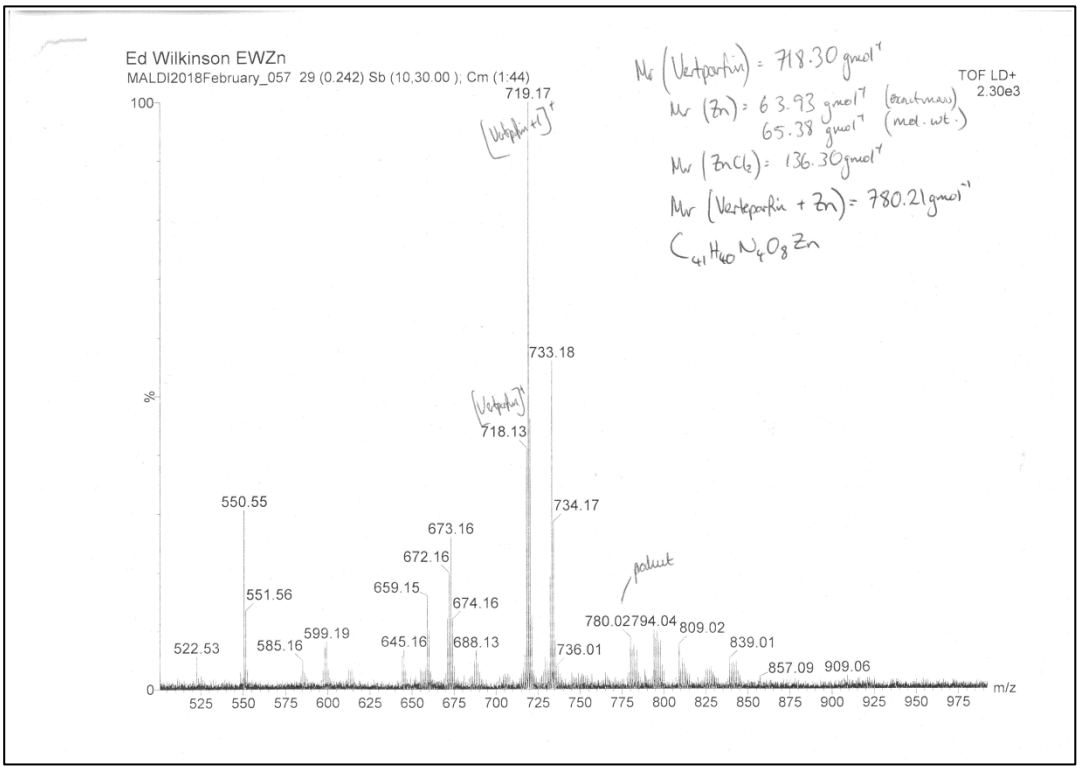
Ed Wilkinson EWZn
MALDI2018February_057 29 (0.242) Sb (10,30.00); Cm (1:44)
TOF LD+
2.30e3
719.17
733.18
718.13
734.17
550.55
673.16
672.16
659.15
674.16
551.56
599.19
585.16
645.16
688.13
522.53
736.01
780.02
794.04
809.02
839.01
857.09
909.06
product
m/z

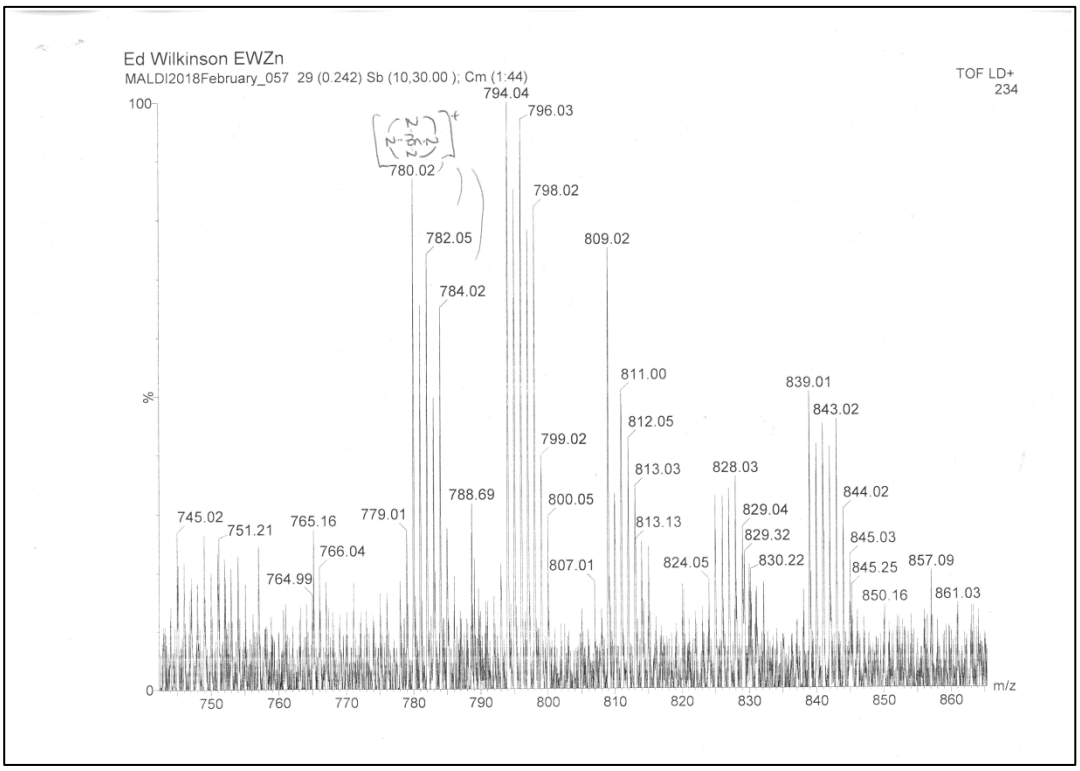
Ed Wilkinson EWZn
MALDI2018February_057 29 (0.242) Sb (10,30.00); Cm (1:44)
TOF LD+
234
794.04
796.03
780.02
798.02
782.05
809.02
784.02
811.00
839.01
812.05
843.02
799.02
813.03
828.03
844.02
788.69
800.05
829.04
813.13
745.02
751.21
765.16
779.01
829.32
845.03
766.04
807.01
824.05
830.22
845.25
857.09
764.99
850.16
861.03
m/z

VP and $MgCl_2$

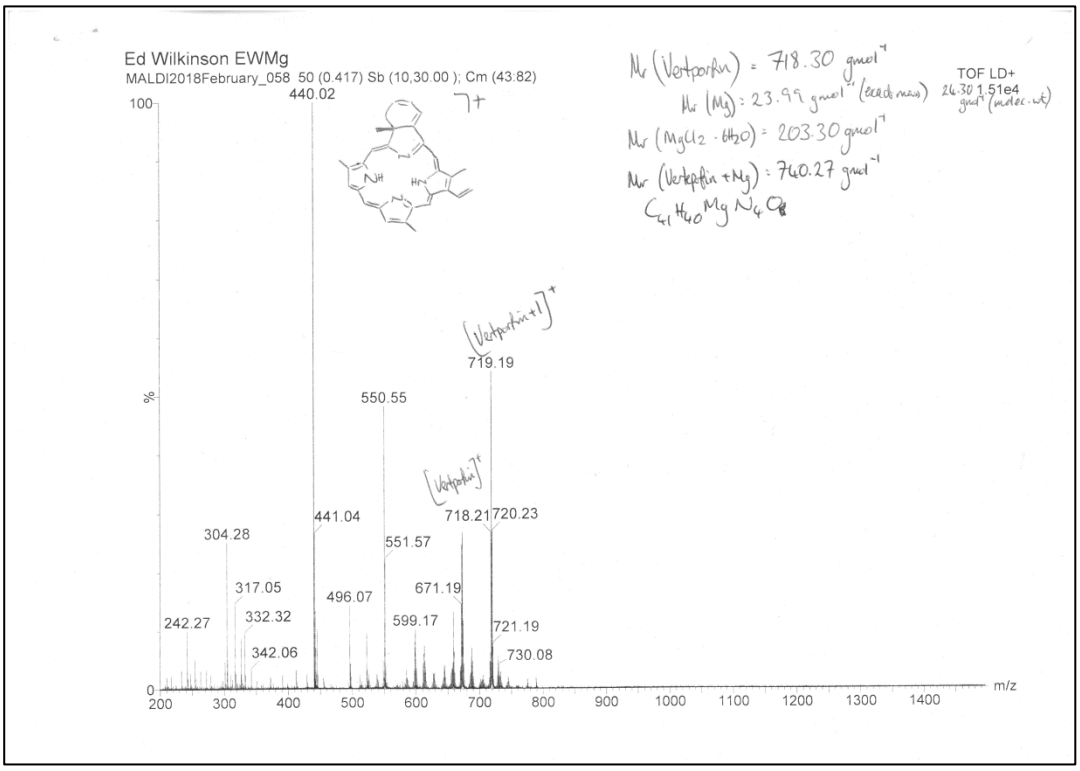
Ed Wilkinson EWMg
MALDI2018February_058 50 (0.417) Sb (10,30.00); Cm (43:82)
TOF LD+
440.02
719.19
550.55
441.04
718.21
720.23
551.57
304.28
317.05
496.07
671.19
242.27
332.32
599.17
721.19
342.06
730.08
m/z
Mr (Verteporfin) = 718.30 gmol⁻¹
Mr (Mg) = 23.99 gmol⁻¹ (exact mass)
Mr (MgCl2 · 6H2O) = 203.30 gmol⁻¹
Mr (Verteporfin + Mg) = 740.27 gmol⁻¹
C41 H40 Mg N4 O8

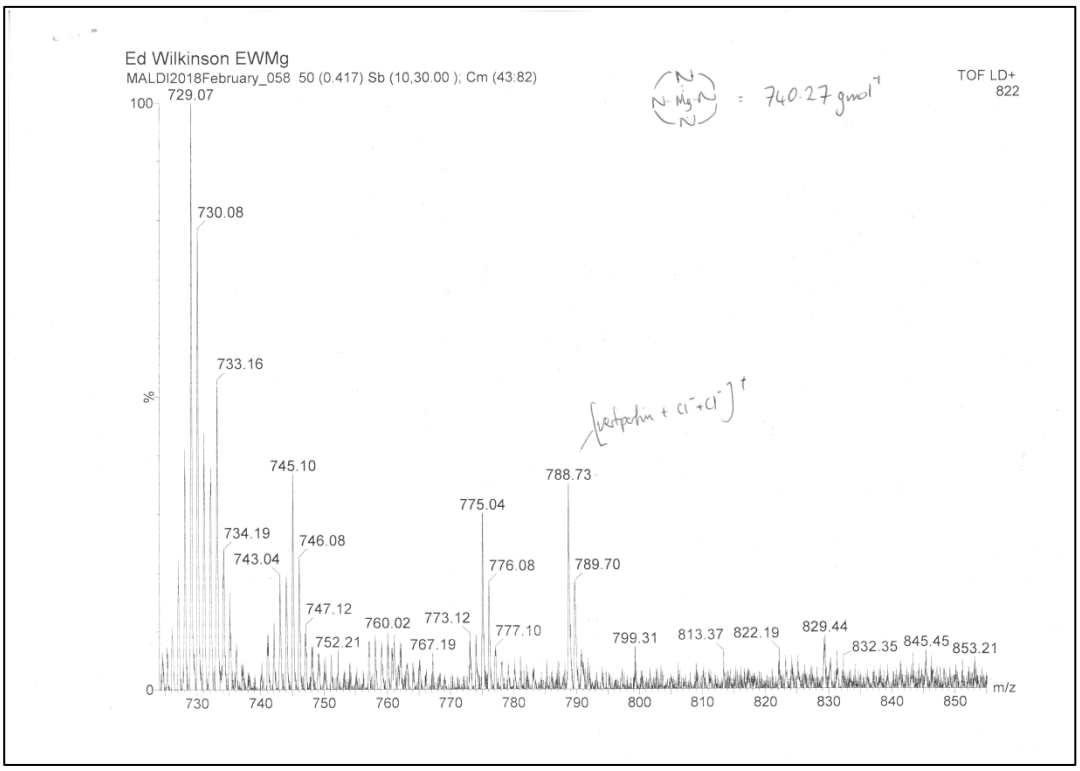
Ed Wilkinson EWMg
MALDI2018February_058 50 (0.417) Sb (10,30.00); Cm (43:82)
TOF LD+
822
= 740.27 gmol⁻¹
729.07
730.08
733.16
745.10
788.73
775.04
734.19
746.08
743.04
776.08
789.70
747.12
760.02
773.12
752.21
767.19
777.10
799.31
813.37
822.19
829.44
832.35
845.45
853.21
m/z